THÈSE

En vue de l'obtention du

DOCTORAT DE L'UNIVERSITÉ DE TOULOUSE

Délivré par *l'Université Toulouse III - Paul Sabatier*
Discipline ou spécialité : *Océanographie Spatiale*

Présentée et soutenue par *William Llovel*
Le *6 Décembre 2010*

Titre : *"Hausse du niveau de la mer et impact du changement climatique global"*

JURY
Nick Hall (Président du jury)
Sabrina Speich (Rapporteur)
Sabine Arnault (Rapporteur)
Serge Planton (Examinateur)
CK Shum (Examinateur)
Anny Cazenave (Directrice de thèse)

Ecole doctorale : *SDU2E*
Unité de recherche : *LEGOS UMR 5566*
Directeur(s) de Thèse : *Anny Cazenave*
Rapporteurs : *Voir JURY*

Remerciements

Bien évidemment, je tiens à remercier ma directrice de thèse Anny Cazenave pour m'avoir fait confiance et surtout pour m'avoir confié un sujet de thèse particulièrement passionnant au sein d'une équipe dynamique et mondialement reconnue. Anny m'a fait partager sa large culture et sa passion pour la science, son enthousiasme et j'ai énormément appris au cours de cette thèse, je l'en remercie grandement.

Je tiens aussi à remercier les deux partenaires qui ont cofinancé ma thèse par le biais d'une bourse BDI/Région : le CNRS et la Région Midi-Pyrénées.

Mon travail de doctorat s'est déroulé au sein de l'équipe GOHS (Géophysique, Océanographie et Hydrologie Spatiales) du LEGOS, sur le site de l'Observatoire Midi-Pyrénées à Toulouse. Parmi l'ensemble de l'équipe GOHS, que je remercie de m'avoir accueillie, je voudrais remercier chaleureusement Alix Lombard pour m'avoir initié aux études du niveau de la mer. Je veux également remercier Mélanie Becker et Benoît Meyssignac avec lesquels j'ai toujours travaillé dans une très bonne humeur.

Je veux également remercier mes collègues « modélisateurs » David Salas-y-Mélia du CNRM et Philippe Rogel du CERFACS pour m'avoir fourni plusieurs sorties de modèles et de réanalyses océaniques mais aussi pour m'avoir beaucoup appris sur cette science qui m'été totalement inconnue auparavant.

Mes remerciements vont également à ma famille et à mes amis et plus particulièrement aux thésards de l'observatoire que j'ai fréquenté pendant mes 3 années de thèse. Un grand merci à mon ami « Boutch » avec qui j'ai partagé le bureau D108 pendant toutes ces années, pour ces pauses café ponctuées de beaucoup de joie et de franches rigolades.

Table des matières

1 Introduction **1**

2 Les variations du niveau de la mer : des temps géologiques aux dernières décennies **5**
2.1 Les variations du niveau de la mer dans le passé 5
2.1.1 Au cours des temps géologiques 5
2.1.2 Les cycles glaciaire-interglaciaires du Quaternaire 6
2.2 Les variations du niveau de la mer : la période post-industrielle . 10
2.2.1 Les marégraphes : observations des variations séculaires du niveau de la mer 10
2.2.2 L'altimétrie spatiale : observations synoptiques à haute précision du niveau de la mer 14
2.3 Les projections futures du niveau de la mer 19
2.3.1 Rappel des résultats du dernier rapport de l'IPCC de 2007 19
2.3.2 Les projections futures du niveau de la mer 20

3 Les causes des variations du niveau de la mer en moyenne globale **23**
3.1 Les différentes contributions affectant le niveau de la mer pour les dernières décennies 23
3.2 La contribution de l'expansion thermique aux variations du niveau de la mer 24
3.2.1 Définition et généralité 24
3.2.2 Le calcul de l'expansion thermique 25
3.2.3 Les données hydrographiques 26
3.3 La fonte des glaces continentales : apports d'eaux douces aux océans 28
3.3.1 Les glaciers de montagne et les petites calottes polaires . . 29
3.3.2 Les calottes polaires : Antarctique et Groenland 31
3.4 Bilans du niveau de la mer des dernières décennies d'après le rapport de l'IPCC (2007) 33

4 Les variations du niveau de la mer des années récentes aux dernières décennies **37**
4.1 La contribution du niveau de la mer stérique 38
4.2 La contribution du signal massique de l'océan : études des données de GRACE 40
4.2.1 La mission spatiale GRACE 41
4.2.2 Le signal massique des océans 43
4.2.3 Le rebond post-glaciaire 43
4.2.4 Bilans de masse des calottes polaires 46
4.2.5 Variabilité interannuelle et régionale du niveau de la mer sur la période 2002-2009 à partir des données d'altimétrie spatiale, des flotteurs Argo et de la gravimétrie spatiale GRACE : résumé de l'article publié dans le journal « Ocean Dynamics » 47
4.3 La contribution des eaux continentales 62
4.3.1 Généralités 62
4.3.2 Les années récentes : La contribution des eaux continentales en moyenne globale à la hausse du niveau de la mer sur la période 2002-2009 : article publié dans le journal « Comptes rendus de l'Académie des Sciences » 65
4.3.3 Variabilité interannuelle des eaux continentales : études sur les périodes : 2002-2009, 1993-2003 et 1950-1995. Article publié dans le journal « Global and Planetary Change ». 78
4.4 Bilans du niveau de la mer en moyenne globale 93
4.4.1 Synthèse des différentes contributions aux variations du niveau de la mer sur les périodes 1993-2009 et 2003-2009 93
4.4.2 Résumé d'un article de revue sur les contributions et les bilans du niveau de la mer : « Contemporary Sea Level Rise », article publié dans le journal « Annual Review of Marine Science » 97

5 Les variations régionales du niveau de la mer **129**
5.1 Période altimétrique : observations du niveau des mers entre 1993 et 2010 129
5.2 Les causes de la variabilité régionale du niveau de la mer : la composante thermostérique 130
5.3 Interprétation du signal résiduel entre les variations observées du niveau de la mer et l'expansion thermique des océans : les différences régionales 133
5.4 La variabilité régionale du niveau de la mer des dernières décennies 138
5.4.1 Les méthodes de reconstruction 138
5.4.2 Résultats 142

5.4.3 Analyses en composantes principales : détermination des principaux modes de variabilité des vitesses du niveau de la mer reconstruit sur 1950-2003 145
5.4.4 La cartographie régionale du niveau de la mer thermostérique et ses principaux modes de variabilité 149
5.4.5 Résumé de l'article : « Reconstruction à deux dimensions du niveau de la mer passé (1950-2003) à partir de données marégraphiques et d'un modèle de circulation générale d'océan », publié dans le journal « Climate of the Past » . . 153
5.4.6 Les modèles climatiques couplés : comparaisons du niveau de la mer reconstruit sur les 5 dernières décennies avec le modèle CNRM-CM3 165

6 Conclusion **169**

Bibliographie **173**

A Annexe : Article *Berge-Nguyen et al.* **[2008] : « Le niveau de la mer reconstruit sur les 50 dernières années en utilisant le niveau de la mer thermostérique, les données marégraphiques, l'altimétrie spatiale et les sorties d'une réanalyses océanique » , publié dans le journal « Global and Planetary Change »** **185**

B Annexe : Article *Cazenave et al.* **[2009] : « Le bilan du niveau de la mer sur la période récente 2003-2008 : une réévaluation à partir des données de gravimétrie spatiale GRACE, d'altimétrie spatiale et des flotteurs Argo », publié dans le journal « Global and Planetary Change »** **201**

C Annexe : Article *Becker et al.* **[2010] : « Le comportement hydrologique récent de la région des grands lacs d'Afrique de l'est déduit des données GRACE, de l'altimétrie spatiale et des précipitations », publié dans le journal « Comptes Rendus Géoscience »** **209**

Publications

W. Llovel, A. Cazenave, P. Rogel, A. Lombard, and M.B. Nguyen, Two-dimensional reconstruction of past sea level (1950-2003) from tide gauge data and an Ocean General Circulation Model, *Climate of the Past*, vol. 5, pp. 217-227, **2009**,

W. Llovel, M. Becker, A. Cazenave, J. Cretaux, and G. Ramillien, Global land water storage change from GRACE over 2002-2009 ; Inference on sea level, *Comptes Rendus Geoscience*, vol. 342, pp. 179-188, **2010a**.

W. Llovel, S. Guinehut, A. Cazenave, Regional and interannual variability in sea level over 2002-2009 based on satellite altimetry, Argo float data and GRACE ocean mass, *Ocean Dynamics*, vol. 60, pp. 1193-1204, **2010b**.

W. Llovel, M. Becker, A. Cazenave, S. Jevrejeva, R. Alkama, B. Decharme, H. Douville, M. Ablain and B. Beckley, Terrestrial waters and sea level variations on interannual time scale, *Global and Planetary Change*, vol. 75, pp. 76-82, **2011**.

B. Meyssignac, F. M. Calafat, S. Somot, V. Rupolo, P.Stocchi, **W.Llovel**, A. Cazenave, R. Morrow, Two-dimensional reconstruction of the Mediterranean sea level over 1970-2006 from tide gauge data and regional ocean circulation model outputs, *Ocean Dynamics*, soumis.

Marta Marcos, Francesc M. Calafat, **William Llovel**, Damia Gomis and Benoit Meyssignac, Regional distribution of steric and mass contributions to sea level changes, *Global and Planetary Change*, en revision.

A. Cazenave and **W. Llovel**, Contemporary Sea Level Rise, *Annual Review of Marine Science*, vol. 2, pp. 145-173, **2010**.

L. Xavier, M. Becker, A. Cazenave, L. Longuevergne, **W. Llovel** and O.C. Rotunno, Interannual variability in water storage over 2003-2008 in the Amazon Basin from GRACE space gravimetry, in situ river level and precipitation data, *Remote Sensing of Environment*, vol. 114, pp. 1629-1637, **2010**.

M. Becker, **W. Llovel**, A. Cazenave, A. Guntner, and J. Cretaux, Recent hydrological behavior of the East African great lakes region inferred from GRACE,

satellite altimetry and rainfall observations, *Comptes Rendus Geoscience*, vol. 342, pp. 223-233, **2010**.

A. Cazenave, K. Dominh, S. Guinehut, E. Berthier, **W. Llovel**, G. Ramillien, M. Ablain, and G. Larnicol, Sea level budget over 2003-2008 : A reevaluation from GRACE space gravimetry, satellite altimetry and Argo, *Global and Planetary Change*, vol. 65, pp. 83-88, **2009**.

M. Berge-Nguyen, A. Cazenave, A. Lombard, **W. Llovel**, J. Viarre and J. Cretaux, Reconstruction of past decades sea level using thermosteric sea level, tide gauge, satellite altimetry and ocean reanalysis data, *Global and Planetary Change*, vol. 62, pp. 1-13, **2008**.

A. Cazenave, A. Lombard and **W. Llovel**, Present-day sea level rise : A synthesis, *Comptes Rendus Geoscience*, vol. 340, pp. 761-770, **2008**.

Chapitre 1

Introduction

Durant l'histoire de la Terre, le niveau de la mer a évolué sur des échelles de temps diverses. En effet, il y a -20 000 ans, lors du dernier maximum glaciaire, le niveau de la mer était 120 mètres plus bas qu'aujourd'hui et l'hémisphère nord était en partie recouvert de glace d'après les études basées sur les observations géologiques. A la suite de la fonte de ces calottes de glace, le niveau de la mer a monté et il s'est stabilisé il y a -6 000 ans. Dès lors, le niveau moyen global de la mer a peu varié et a augmenté avec une vitesse faible de l'ordre de 0.7 mm/an.

A partir du XX^{ème} siècle, les observations marégraphiques ont pris le relais pour observer les variations du niveau de la mer. Ces instruments étant fixés le long des côtes, ils ne nous renseignent que sur les variations côtières du niveau de la mer. Au cours du XX^{ème} siècle, ces instruments enregistrent une hausse de 1.8 mm/an soit une valeur bien supérieure à celle des siècle passés. Et, depuis le début des années 1990, les observations des satellites altimétriques Topex/Poséïdon, Jason-1 et Jason-2 indiquent une élévation en moyenne globale du niveau de la mer égale à 3.3 mm/an.

De nos jours, les populations vivent en grande partie sur les zones côtières. Ainsi, des variations même faibles du niveau de la mer peuvent avoir des conséquences importantes tant sur les habitants que sur les activités économiques. De ce fait, les études des variations du niveau de la mer et de ses causes (réchauffement de l'océan, fonte actuelle des glaces continentales) sont d'une importance capitale dans le contexte du réchauffement climatique global. Le dernier rapport de l'IPCC-AR4 (2007) (Intergovernmental Panel on Climate Change, GIEC en français) fournit une synthèse complète les différentes contri-

butions à la hausse observée du niveau de la mer sur les périodes 1961-2003 et 1993-2003. Sur la période des dernières décennies (1961-2003), la somme des contributions climatiques expliquent 1.1 +/- 0.5 mm/an sur les 1.8 +/- 0.5 mm/an observés. Donc, le bilan reste encore ouvert. Pour la période plus récente, 1993-2003, les diverses contributions climatiques expliquent 2.8 +/- 0.7 mm/an des 3.1 +/- 0.7 mm/an observés. Dans ce cas, le bilan du niveau de la mer est *quasiment* fermé compte tenu des incertitudes associées. Néanmoins, de nombreuses questions restent en suspens : assiste-t-on à une accélération de la hausse observée du niveau de la mer et de ses contributions climatiques ? Peut-on totalement expliquer la hausse observée du niveau de la mer ?

Les satellites altimétriques Topex/Poséïdon, Jason-1 et Jason-2 surveillent en permanence les variations du niveau de la mer depuis presque 2 décennies maintenant. Ces données sont précieuses pour les études des variations en moyenne globale mais aussi de la variabilité régionale du niveau marin. Depuis peu, diverses observations, tant *in situ* que spatiales, ont permis de mieux quantifier les différentes contributions climatiques impliquées dans la hausse observée du niveau de la mer, telles que l'expansion thermique de l'eau de mer dûe au réchauffement des océans, la fonte des glaciers de montagne et des calottes polaires, et les variations du stock d'eau continentale. Mon travail de thèse contribue à comprendre les différentes contributions climatiques à la hausse observée du niveau de la mer pour les années récentes, non seulement pour étudier le bilan mais aussi pour comprendre la variabilité régionale du niveau de la mer des dernières décennies.

Ma thèse s'articule en quatre chapitres.

Le premier chapitre fournit une introduction générale sur les variations passées du niveau de la mer. Après une courte introduction basée sur les interactions entre changements climatiques et les variations du niveau de la mer aux échelles de temps géologiques, nous nous intéressons tout particulièrement au XX^{ème} siècle et aux moyens d'observations dont nous disposons à ce jour.

Le deuxième chapitre est consacré à l'étude et à la compréhension des causes de la hausse observée du niveau, c'est-à-dire l'expansion thermique et les variations de masse de l'océan sur la période 1993-2003. Nous résumons

les résultats du dernier rapport de l'IPCC-AR4 (2007). De plus, nous faisons état des derniers résultats publiés récemment.

Le troisième chapitre décrit les principaux résultats obtenus pendant cette thèse sur les causes de la hausse observée du niveau de la mer en moyenne globale à partir de 2003. Dans ce chapitre, nous détaillons les causes de la hausse observée du niveau de la mer, en particulier le niveau de la mer stérique (somme des effets de température et salinité de l'océan), les apports d'eau douce dûs à la fonte actuelle des calottes polaires et des glaciers de montagne, et les variations des eaux continentales. Enfin, nous étudions le bilan du niveau de la mer (comparaison entre observations et causes) entre 1993 et 2009 (période altimétrique totale) et 2003-2009 (années récentes).

Enfin, le dernier chapitre est consacré à l'étude de la variabilité régionale du niveau de la mer des dernières décennies. Tout d'abord, nous étudions les causes de la variabilité régionale du niveau de la mer observé. Nous interprétons ensuite la cartographie régionale des vitesses du signal résiduel entre le niveau de la mer observé et la niveau de la mer thermostérique sur la période altimétrique totale. Dans la seconde partie de ce chapitre, nous nous intéressons sur les taux de variation du niveau de la mer des 5 dernières décennies, à l'aide d'une méthode de reconstruction du niveau marin combinant différentes sources de données telles que les enregistrements marégraphiques et les sorties de modèles numériques de circulation générale des océans. Les cartographies des vitesses de variation du niveau de la mer reconstruit sont comparées à la composante thermostérique observée à partir de données hydrographiques *in situ* et aux sorties d'un modèle climatique couplé. Enfin, les principaux modes de variabilité de tous ces paramètres océanographiques sont analysés.

Chapitre 2

Les variations du niveau de la mer : des temps géologiques aux dernières décennies

2.1 Les variations du niveau de la mer dans le passé

2.1.1 Au cours des temps géologiques

Le niveau de la mer a évolué de façon plus ou moins rapide sur des échelles de temps variées en réponse à différents facteurs. Ainsi, sur des échelles de temps géologiques (plusieurs centaines de millions d'années), les variations du niveau de la mer sont principalement dûes aux mouvements de la croûte terrestre. Ces mouvements contrôlent la forme des bassins océaniques par des phénomènes de subduction des plaques océaniques, de collision des continents, d'ouverture de nouveaux océans et de formation des dorsales océaniques. Les marges continentales enregistrent les variations des lignes de côte et ainsi du niveau de la mer. Une autre contribution à ce niveau de la mer élevé résulte du taux de CO_2 atmosphérique plus important qu'aujourd'hui (avec donc un climat plus chaud).

A ces échelles de temps, les variations du niveau de la mer ont pu être reconstruites à partir de l'analyse des roches sédimentaires, en utilisant une technique de stratigraphie séquentielle (*Vail et al.* [1977]). La figure 2.1 montre

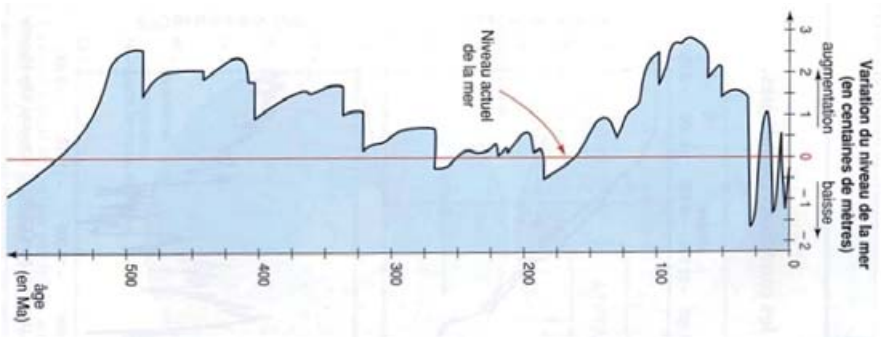

FIG. 2.1 – Variations du niveau de la mer depuis 600 millions d'années (*Vail et al.* [1977], la courbe rouge représente le niveau actuel de la mer.

les variations passées depuis 600 millions d'années (*Vail et al.* [1977]). Ces auteurs ont montré que le niveau marin a beaucoup varié au cours de cette période géologique. Ainsi, le niveau de la mer a atteint jusqu'à 200-300 mètres de plus que le niveau actuel, toutefois avec en moyenne un niveau de la mer plus haut qu'aujourd'hui.

2.1.2 Les cycles glaciaire-interglaciaires du Quaternaire

Sur les échelles temporelles allant de quelques milliers d'années à plusieurs centaines de milliers d'années, les variations du niveau marin sont principalement expliquées par les échanges de masses d'eaux entre les continents et les océans via les variations de volume des glaces continentales. Les variations du stock de glace sont intimement liées à celles de l'insolation solaire reçue dans les régions de haute latitude au cours de l'année, en réponse aux variations périodiques de l'orbite (principalement l'excentricité), de l'obliquité et de la précession de la Terre (cycles de Milankovitch, 1938), mais aussi à la présence de continents près des pôles. Au cours de cette période (depuis environ deux millions d'années), on dénombre 17 cycles glaciaires et interglaciaires, associés successivement à des périodes chaudes (équivalentes aux conditions actuelles) et froides (hémisphère nord englacé et niveau de la mer bas).

L'étude des paléoclimats repose sur les analyses des carottes glaciaires et sédimentaires basées sur différentes techniques. Les calottes polaires sont des archives climatiques d'une très grande valeur. En effet, les bulles d'air piégées dans les carottes de glace permettent de déterminer la composition de l'atmosphère passée et notamment la teneur en gaz à effet de serre. Un lien étroit a été mis en évidence entre les paramètres climatiques tels que la température, la teneur en gaz carbonique et en méthane de l'atmosphère (*Petit et al.* [1999];

Raynaud et al. [2005]). La figure 2.2 montre les variations de ces trois paramètres climatiques sur les dernières 450 000 années. Durant une période froide, la température est inférieure de 8°C (par rapport à la moyenne) et la concentration en gaz carbonique est réduite d'un tiers tandis que celle du méthane de moitié. Cette figure met en évidence les fluctuations passées du climat alternant des cycles chauds et froids.

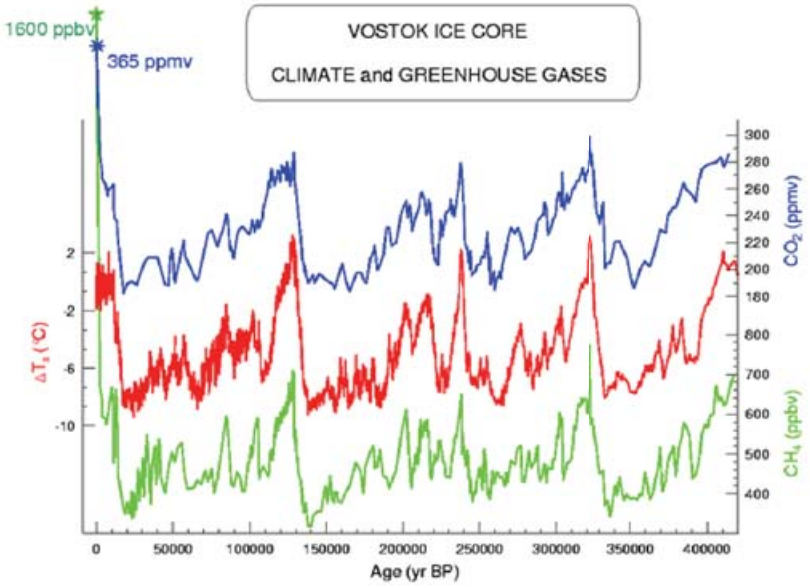

FIG. 2.2 – Evolutions au cours des derniers 450 000 ans de la teneur en CO_2 (courbe bleue), en CH_4 (courbe verte) et de la température (par rapport à la moyenne, courbe rouge) en Antarctique déduites de l'analyse des carottes glaciaires de Vostok (*Petit et al.* [1999]; *Raynaud et al.* [2005]) et EPICA (*community members* [2004])

Les analyses isotopiques, notamment le rapport O^{18}/O^{16} contenu dans les bulles d'air des carottes glaciaires, ont permis de reconstruire les variations de température de l'atmosphère et ainsi, les variations passées du climat. La concentration isotopique lourd O^{18} dépend directement de la température ambiante de l'atmosphère de l'époque à laquelle la glace s'est formée.

Les foraminifères, organismes unicellulaires marins, sont d'une aide précieuse pour les reconstructions paléo-océanographiques. Ces organismes sont nombreux dans tous les océans et mers du globe. De plus, ils sont sensibles aux conditions climatiques. Ils fixent le carbonate dans leur squelette ce qui permet de déterminer la composition isotopique de l'eau grâce au rapport

O^{18}/O^{16} et ainsi, d'en déduire la température ambiante dans laquelle ils ont développé leur coquille (*Emiliani* [1955]).

L'analyse du rapport O^{18}/O^{16} des foraminifères benthiques (vivant au fond des océans) reflète en première approximation uniquement les variations de la composition isotopique de l'eau de mer. L'hypothèse principale est que la température du fond est considérée comme constante. Lors d'une période glaciaire, l'accumulation de glaces pauvres en O^{18} aux pôles a pour conséquence un enrichissement de l'eau de mer en O^{18}. De ce fait, les variations O^{18}/O^{16} des foraminifères benthiques informent alors sur les variations du volume des calottes polaires, et permettent donc de calculer les variations du niveau de la mer équivalent. *Shackleton* [2000] a montré qu'une variation de 0.01% du rapport isotopique O^{18}/O^{16} des squelettes des foraminifères correspond à une hausse de 10m du niveau de la mer.

Les récifs coralliens sont aussi très sensibles aux variations de l'environnement, car ils vivent à quelques mètres sous la surface de la mer. Ces structures sont de très bons indicateurs des variations passées du niveau marin depuis le dernier maximum glaciaire il y a environ -20 000 ans. L'analyse du rapport isotopique O^{18}/O^{16} de la composition des squelettes des coraux permet de déterminer la température de l'eau à un moment précis dans le passé, et avec une datation précise d'en déduire les variations du niveau de la mer associées (*Pirazzoli* [1996]).

Il y a environ 20 000 ans, lors du dernier maximum glaciaire du Quaternaire, le niveau de la mer était 120 mètres plus bas qu'aujourd'hui. Lors de la fonte des grandes calottes polaires, le niveau de la mer a monté pour se stabiliser vers -7000 ans. Durant l'Holocène, le niveau de la mer a peu varié. La figure 2.3 représente l'évolution de niveau de la mer durant le Quaternaire et l'Holocène (*Fleming et al.* [1998]; *Milne et al.* [2005]).

Les études géologiques tentent de comprendre le caractère cyclique des dépôts sédimentaires observés *quasiment* partout sur Terre. La théorie la plus robuste montre que cet aspect cyclique est la réponse principale des processus de déposition dûs aux élévations et baisses du niveau de la mer. Sur les roches, les géologues voient l'enregistrement des époques où le niveau de la mer était étonnamment bas, alternant avec des époques où il était bien plus haut qu'aujourd'hui. A la dernière glaciation, il y a environ 20 000 ans, des centaines de milliers de kilomètres cubes de glace étaient empilées sur les continents formant ainsi de grandes calottes polaires. Le littoral était plus loin par rapport à

aujourd'hui et donc, les dépôts sédimentaires se formaient dans une zone bien plus en retrait.

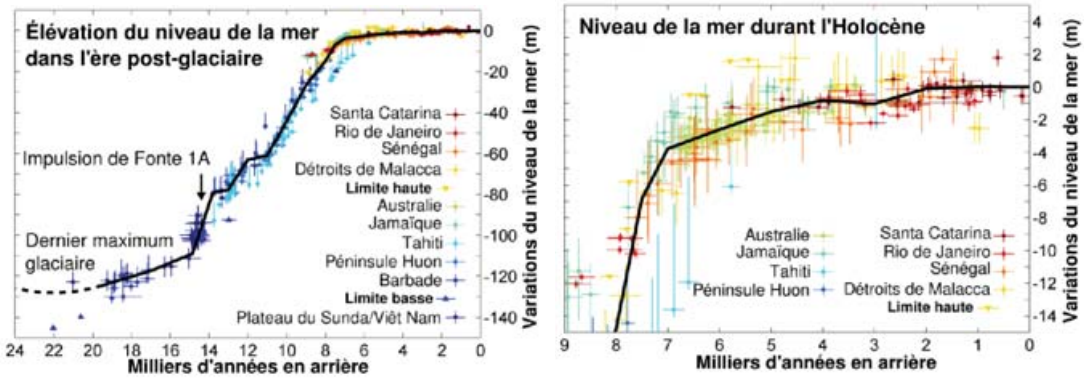

(a) Niveau de la mer durant le Quaternaire (b) Niveau de la mer durant l'Holocène

FIG. 2.3 – Estimations des variations du niveau de la mer durant le Quaternaire et l'Holocène basées sur des études sédimentaires (*Fleming et al.* [1998]; *Milne et al.* [2005])

Les indicateurs paléoclimatiques s'accordent sur le fait que le niveau de la mer durant l'Holocène supérieur connait une forte hausse entre -20 000 et -7 000 ans à une vitesse moyenne de 10 mm/an. Cette hausse est liée à une réponse de l'augmentation rapide de la température moyenne de l'atmosphère et à la désintégration de larges calottes de glaces continentales. Ensuite, le niveau de la mer continue à s'élever mais bien plus lentement. Durant les derniers 1 000 ans et avant le XX^{ème} siècle, la vitesse moyenne de la hausse du niveau de la mer serait inférieure à 0.7 mm/an (*Lambeck et al.* [2002]; *Miller et al.* [2009]).

Aux échelles de temps plus courtes (inférieures à 1 000 ans), les variations du niveau de la mer sont intimement liées aux changements climatiques, soit d'origine naturelle soit d'origine anthropique. Il parait donc extrêmement important de comprendre les mécanismes de cette interaction et d'estimer correctement les causes afin d'être capable de prédire la hausse future du niveau de la mer dûe au réchauffement climatique global et son impact sur les zones côtières. Pour cela, nous avons aujourd'hui accès à des systèmes d'observations précis et complémentaires du niveau de la mer.

2.2 Les variations du niveau de la mer : la période post-industrielle

Pour le XX^{ème} siècle et les deux dernières décennies, nous disposons de deux principaux moyens d'observation du niveau de la mer : les marégraphes et les satellites altimétriques. Les enregistrements marégraphiques disponibles depuis environ un siècle permettent d'étudier les variations à long terme du niveau de la mer (variations multi-décennales). Cependant, étant principalement fixés à la côte, ces instruments mesurent un niveau de la mer relatif. Il est donc nécessaire de corriger ces données des mouvements verticaux de la croûte afin d'avoir accès aux données absolues. Les satellites altimétriques, quant à eux, fournissent des observations globales du niveau de la mer depuis environ 17 ans maintenant. Contrairement aux marégraphes, les altimètres embarqués sur les satellites mesurent directement le niveau de la mer absolu par rapport au centre de masse de la Terre. Au cours de ce paragraphe, ces deux types d'observation sont détaillés.

2.2.1 Les marégraphes : observations des variations séculaires du niveau de la mer

Les mesures des marégraphes historiques sont utilisées pour étudier les variations du niveau de la mer durant le siècle passé. Les premières mesures marégraphiques remontent au XVIII^{ème} siècle. Ces enregistrements fournissent de longues séries temporelles très précieuses pour l'estimation des variations à long terme du niveau de la mer. Malheureusement, une vingtaine de stations seulement fournissent des données au cours du XX^{ème} siècle et, ces dernières sont situées principalement dans l'hémisphère nord le long des côtes d'Europe et d'Amérique du Nord (d'où, une résolution spatiale des données marégraphiques très limitée).

Principe de la mesure marégraphique : mesure du niveau de la mer relatif

Au XVIII^{ème} siècle, les premières mesures étaient effectuées à partir de lecture de hauteurs d'eau à l'aide d'une échelle de marée, simple mire graduée en bois fixée à un quai. Dès le XIX^{ème} siècle, une nouvelle génération de marégraphe a vu le jour : les marégraphes mécaniques à flotteur. Le principe est très simple et repose sur le déplacement du flotteur dans un puits de tran-

quillisation, grâce auquel, les oscillations de courtes périodes de la surface de la mer sont filtrées. Les mouvements verticaux sont par la suite transmis par un système mécanique à un stylo qui enregistre les mouvements analogiquement sur un rouleau de papier : le marégramme. Depuis, les techniques ont évolué et se sont modernisées. Il existe maintenant des marégraphes à ultrasons qui mesurent le temps de propagation aller/retour d'une onde acoustique émise au-dessus du plan d'eau, tandis que les marégraphes à pression mesurent la pression exercée par la colonne fluide au-dessus de l'appareil immergé. Quelle que soit la technique utilisée, les marégraphes mesurent le niveau instantané de la mer par rapport à un niveau de référence local. Cette référence locale est définie par rapport à des repères matériels au voisinage immédiat du socle de l'instrument, appelé repère de marée. Ces repères assurent la continuité et la cohérence des observations du niveau de la mer, notamment lorsque celles-ci sont effectuées par plusieurs marégraphes au cours du temps. Effectivement, la continuité des enregistrements marégraphiques est un paramètre crucial pour l'étude des variations à long terme du niveau de la mer.

Les estimations les plus récentes de la hausse séculaire observée du niveau marin déduites des enregistrements marégraphiques sont de l'ordre de 1.5 à 2 mm/an au cours du XX^{ème}. Les différentes estimations réalisées sont basées sur l'analyse des données historiques du Permanent Service for Mean Sea Level (PSMSL, *Woodworth and Player* [2003]).

Les premières estimations furent basées sur l'utilisation d'un jeu de 27 enregistrements marégraphiques, regroupés en 10 régions. Ces 27 marégraphes furent choisis pour leur longueur temporelle supérieure à 70 ans dans le but d'estimer précisément la hausse séculaire du niveau de la mer (*Douglas* [2001]; *Peltier* [2001]). La vitesse de la hausse en moyenne globale du niveau de la mer était estimée à 1.71 +/- 0.5 mm/an, d'après *Douglas* [2001], et de 1.84 +/- 0.35 mm/an après correction de l'effet du rebond post-glaciaire par le modèle ICE-4G/VM2 d'après *Peltier* [2001].

Sur le même sujet, *Holgate and Woodworth* [2004] estiment que la hausse du niveau moyen global côtier est égale à 1.7 +/- 0.2 mm/an entre 1948 et 2002. Ces auteurs ont pris en compte 177 séries marégraphiques, divisées en 13 régions et corrigées du rebond post-glaciaire en utilisant le modèle ICE-4G (*Peltier* [2001]). Dans une étude plus récente, *Holgate* [2007] estime, à partir de

9 marégraphes, une hausse de 1.74 +/- 0.16 mm/an du niveau moyen global des mers au cours du XX^{ème} siècle.

Une autre étude (*Jevrejeva et al.* [2006]) estime une hausse du niveau de la mer de 1.8 mm/an sur le XX^{ème} siècle à partir de 1023 enregistrements marégraphiques. Afin de ne pas donner trop de poids aux régions sur échantillonnées, ces auteurs calculent des stations dites « virtuelles » (moyenne des marégraphes d'une même zone géographique), soient 12 au total, pour évaluer le niveau moyen global de la mer.

En revanche, l'analyse de *Church et al.* [2004] est différente des autres car elle combine les séries temporelles marégraphiques aux données altimétriques de Topex/Poseidon. Cette méthode de « reconstruction » sera développée par la suite dans le chapitre 5. Ces auteurs estiment, quant à eux, une hausse séculaire du niveau moyen global des océans égale à 1.8 +/- 0.3 mm/an sur le XX^{ème}siècle.

Le problème récurrent dans l'analyse des données marégraphiques est la pollution de ces enregistrements due aux mouvements verticaux de la croûte terrestre. Ces mouvements doivent être corrigés dans les données marégraphiques. Malheureusement, lors des précédentes études, les seules corrections appliquées aux marégraphes étaient les mouvements verticaux induits par le rebond post-glaciaire. Cependant, il existe d'autres causes géophysiques provoquant des mouvements du niveau de la mer relatif et donc des erreurs de mesure. Néanmoins, pour pallier ces problèmes, les données de Global Positionning System (GPS) sont utilisées afin de corriger au mieux les mouvements de la croûte aux sites marégraphiques. Ainsi, en corrigeant les séries temporelles marégraphiques, les études récentes montrent une hausse en moyenne globale du niveau de la mer égale à 1.61 +/- 0.19 mm/an d'après *Woppelmann et al.* [2009].

Le tableau 2.1 répertorie les études récentes réalisées à partir des données marégraphiques afin d'estimer la hausse séculaire du niveau de la mer sur les dernières décennies et le siècle passé. Toutes ces études convergent pour une hausse *quasi* constante aux alentours de 1.7 - 1.8 mm/an d'élévation en moyenne globale sur le XX^{ème} siècle.

La figure 2.4 montre l'évolution en moyenne globale du niveau de la mer basée sur les enregistrements marégraphiques d'après les études de *Church et al.* [2004] (courbe rouge), *Jevrejeva et al.* [2006] courbe bleue et *Holgate and Woodworth* [2004] (courbe noire). Mise à part la hausse de 1.8 mm/an décelée

Auteurs	Tendance (mm/an)	Période
Church et al. [2001]	1 - 2	20^{e} siècle
Peltier [2001]	1.84 +/- 0.35	20^{e} siècle
Douglas [2001]	1.71 +/- 0.5	20^{e} siècle
Douglas and Peltier [2002]	1.5 - 2	20^{e} siècle
Church et al. [2004]	1.8 +/- 0.3	1950 - 2000
Holgate and Woodworth [2004]	1.7 +/- 0.2	1948 - 2002
Jevrejeva et al. [2006]	1.8	20^{e} siècle
Holgate [2007]	1.74 +/- 0.16	20^{e} siècle
Woppelmann et al. [2009]	1.61 +/- 0.19	20^{e} siècle

TAB. 2.1 – Estimations récentes de la hausse observée du niveau marin au cours du XX^{ème} siècle, basées sur l'analyse des données marégraphiques.

sur le siècle passé, ces courbes révèlent une forte variabilité interannuelle du niveau de la mer observé.

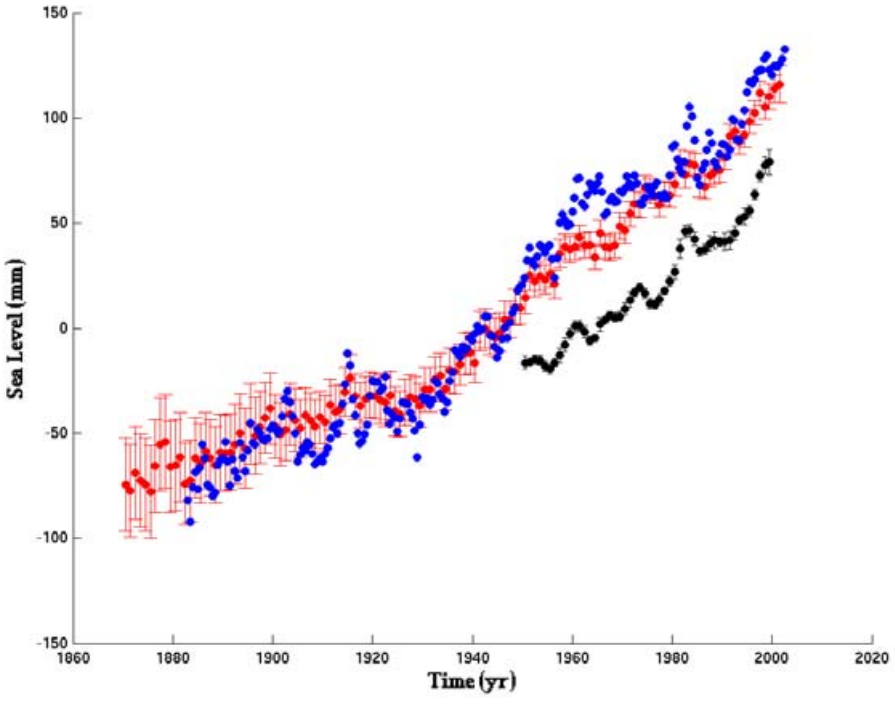

FIG. 2.4 – Evolution du niveau de la mer basée sur les données marégraphiques au cours du XX^{ème} siècle (Courbe rouge : *Church and White* [2006]), courbe bleue : *Jevrejeva et al.* [2006], courbe noire : *Holgate and Woodworth* [2004]). Les signaux saisonniers à 1 an et 6 mois ont été retirés de ces courbes.

2.2.2 L'altimétrie spatiale : observations synoptiques à haute précision du niveau de la mer

Depuis environ 17 ans maintenant, avec les missions altimétriques de haute précision, principalement Topex/Poséïdon (lancé en août 1992), ses successeurs Jason-1 (lancé en décembre 2001) et Jason-2 (lancé en Juin 2008), la hauteur de la surface des océans est mesurée avec une très grande précision de l'ordre de 1 à 2 cm en variations absolues du niveau de la mer, et avec une couverture *quasi* complète du domaine océanique (entre +/- 66° de latitude) ce qui permet d'en déduire l'évolution du niveau de la mer avec une précision de l'ordre de quelques dixièmes de millimètre par an.

Principe de la mesure altimétrique : mesure du niveau de la mer absolu

Un radar altimètre embarqué à bord d'un satellite émet un signal à très haute fréquence (plus de 1700 impulsions par seconde) à la verticale de celui-ci en direction du sol et reçoit en retour l'écho réfléchi par la surface de la mer. L'analyse de l'écho permet d'extraire une mesure très précise du temps de trajet aller-retour entre le satellite et la surface de la mer, mais aussi de la hauteur des vagues et de la vitesse du vent. Le temps d'aller-retour est ensuite transformé en distance par simple multiplication avec la vitesse de la lumière, vitesse à laquelle se propagent les ondes électromagnétiques émises. En moyennant sur une seconde les distances estimées, on obtient une mesure très précise de la distance satellite-océan. Toutefois les ondes électromagnétiques peuvent être ralenties pendant leur traversée de l'atmosphère, cet effet étant lié aux taux taux de sècheresse, d'humidité, et d'ionisation. Une fois appliquées les corrections nécessaires pour prendre en compte ces phénomènes physiques, la distance finale (distance R), satellite-surface de l'océan, est estimée avec une précision de 1 à 2 centimètres (figure 2.5).

L'objectif final étant de mesurer le niveau de la mer par rapport à un référentiel terrestre, il est nécessaire de connaître de manière indépendante avec une très grande précision la trajectoire du satellite sur son orbite, soit sa position en latitude, longitude, et son altitude exacte.

Pour l'étude des océans, on utilise principalement les observations du niveau de la mer issues de Topex/Poseidon (T/P), Jason-1 (J1) et Jason-2 (J2). Ces satellites volent à une altitude de 1336 km sur une orbite inclinée à 66° par rapport à l'axe nord-sud de la Terre. De ce fait la couverture est limitée à 66° nord et sud en latitude. Son orbite est dite répétitive, c'est-à-dire que le

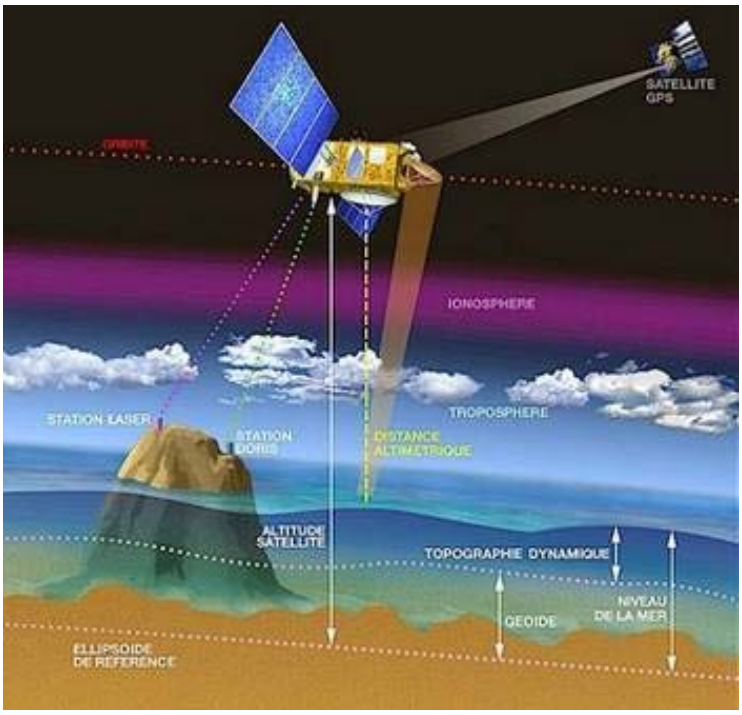

FIG. 2.5 – Principe de la mesure altimétrique

satellite repasse sur les mêmes points au sol tous les 10 jours, offrant ainsi un échantillonnage homogène de la surface du globe pendant cette même période.

Ces satellites sont localisés à l'aide de plusieurs méthodes. T/P, J1 et J2 sont localisés par le système DORIS (Détermination d'orbite et de radiopositionnement intégrés par satellite), le GPS et les stations laser. Ce système repose sur un réseau de balises au sol émettant en direction des satellites. Environ 50 balises sont actuellement en fonctionnement de par le monde. Un tel réseau permet de connaître très précisément, par analyse de l'effet Doppler, la vitesse du satellite sur son orbite (voir figure 2.5). En s'appuyant ensuite sur des modèles dynamiques d'orbitographie, on déduit de cette vitesse la trajectoire exacte du satellite, soit sa position et sa vitesse par rapport à la Terre.

Cette position est calculée par rapport à une surface de référence arbitraire, un ellipsoïde (voir figure 2.5). Cet ellipsoïde de référence correspond à une forme élémentaire de la Terre, une « sphère » aplatie aux deux pôles.

L'altitude du satellite au dessus de l'ellipsoïde de référence (distance S) est calculée avec une précision supérieure à 2,5 centimètres de variance sur un cycle.

On utilise aussi les données du satellite ENVISAT. Ce satellite a été lancé le 1er mars 2002 sur une orbite inclinée à 102° et de répétitivité de 35 jours.

Le niveau des océans s'obtient par le calcul d'une différence entre l'orbite du satellite et la distance altimétrique (avec cependant toutes les corrections nécessaires) :

Niveau de la mer = S - R

Le niveau des océans SSH (Sea Surface Height) représente plusieurs effets combinés :

- la surface que la mer aurait en absence de toutes perturbations (vent, marées, courants, etc.). Cette surface appelée géoïde reflète les variations de gravité liées aux différences de masses et de densité importantes du fond marin et de la structure interne de la Terre. Ainsi une zone de roches denses, liée par exemple à la présence d'un volcan sous-marin, déforme le niveau de la mer de plusieurs dizaines de mètres, faisant apparaître une « bosse » sur le géoïde.

- la circulation océanique appelée encore topographie dynamique. La circulation océanique qui comprend une partie permanente stationnaire (circulation permanente liée à la rotation de la Terre, aux vents permanents, etc.) et une partie fortement variable (liée aux vents, à la variabilité saisonnière, etc.), représente des amplitudes de l'ordre du mètre en moyenne.

Pour accéder au seul effet de la topographie dynamique, il suffirait de retrancher la hauteur du géoïde à la hauteur du niveau de la mer. En pratique, le géoïde n'est pas connu avec suffisamment de précision, et c'est donc le niveau moyen de la mer (géoïde plus circulation permanente) qui est retranché au niveau de la mer, donnant ainsi l'accès à la partie variable du signal océanique.

Le niveau de la mer en moyenne globale

Un apport majeur de l'altimétrie spatiale est la mesure du niveau moyen des mers. Pour cela, on calcule, pour chaque cycle, la moyenne géographique des hauteurs de mer déduites de l'altimétrie spatiale. La figure 2.6 représente la courbe du niveau moyen global de la mer entre 1992 et 2009. La hausse

observée sur cette période est égale à 3 mm/an. Cette valeur doit être corrigée du rebond post-glaciaire dû à la fonte des anciennes calottes polaires du Quaternaire (voir discussion dans le paragraphe 4.2.3). Cette valeur compte pour -0.3 mm/an et doit être retranchée de l'estimation de la vitesse de hausse du niveau moyen global de la mer. Ainsi, la hausse observée est égale à 3.3 mm/an sur la période 1993-2009 (*Cazenave and Llovel* [2010]).

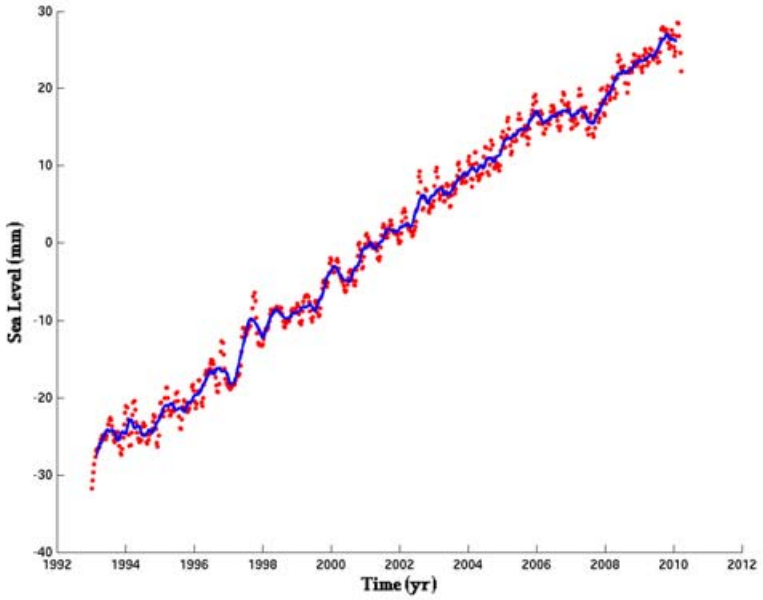

FIG. 2.6 – Variations du niveau moyen global de la mer calculées à partir des données altimétriques de Topex/Poseidon, Jason-1 et Jason-2 sur la période 1993-2009 (source AVISO : CLS-LEGOS)

L'incertitude associée à cette estimation est égale à environ 0.4 mm/an comme le résume le tableau 2.2 (*Ablain et al.* [2009]). En effet, lors du traitement des données altimétriques, les signaux bruts sont corrigés des erreurs liées au positionnement (orbite), à la traversée de l'atmosphère (troposphère sèche et humide), aux biais liés à l'état de la mer et au vent de surface des océans et des erreurs de métrologie liées à l'utilisation de différents radiomètres de Topex/Poséïdon, Jason-1 et Jason-2.

Sources d'erreur	minimum (mm/an)	maximum (mm/an)
Orbite	0.10	0.15
Troposphère humide (Radiomètre)	0.20	0.30
Troposphère sèche	0.05	0.10
Biais d'état de la mer (vent de surface)	0.10	0.25
Biais entre Topex A, Topex B et Jason	0.1	0.25
Somme quadratique des erreurs	0.32	0.44

TAB. 2.2 – Tableau des erreurs associées au calcul des tendances de la moyenne globale du niveau de la mer par altimétrie spatiale (*Ablain et al.* [2009])

D'autres groupes de recherche mettent aussi régulièrement à jour la série temporelle altimétrique. Ainsi, la figure 2.7 montre les courbes du niveau moyen de la mer obtenues par le groupe de l'Université du Colorado (courbe rouge, *Nerem et al.* [2006]), par le groupe du Goddard Space Flight Center (GSFC/NASA, *Beckley et al.* [2010]) et enfin par le groupe de Collecte et Localisation par Satellite (CLS, *Ablain et al.* [2009]). Les vitesses de hausse sont respectivement 3.06 mm/an, 2.95 mm/an et 3.01 mm/an (ces valeurs ne sont pas corrigées du rebond post-glaciaire). Nous notons une bonne cohérence entre ces diverses estimations de la hausse observée du niveau marin. Toutefois, la variabilité interannuelle présente des différences pour ces trois estimations.

La variabilité régionale du niveau de la mer

Un autre apport considérable de l'altimétrie spatiale est la cartographie des vitesses de variation du niveau de la mer. La figure 2.8 montre les vitesses calculées sur la période 1993-2009. Pour la première fois, et grâce à l'altimétrie spatiale, on voit que les variations du niveau de la mer ont une forte signature régionale (*Cazenave and Nerem* [2004]; *Cazenave and Llovel* [2010]). Malgré de longues séries temporelles, les marégraphes n'ont jamais pu mettre en évidence une telle variabilité du fait de leur couverture spatiale très limitée. Il était souvent admis jusqu'ici que le niveau de la mer s'élevait uniformément. Grâce à l'altimétrie, cette hypothèse est aujourd'hui invalide. En effet, la cartographie des vitesses du niveau de la mer montre que dans certaines parties des océans le niveau de la mer a atteint 3 à 5 fois la valeur de la moyenne globale (Océan Pacifique de l'Ouest, l'Océan Atlantique Nord). Dans d'autres régions, au contraire le niveau de la mer a baissé (Océan Pacifique de l'Est).

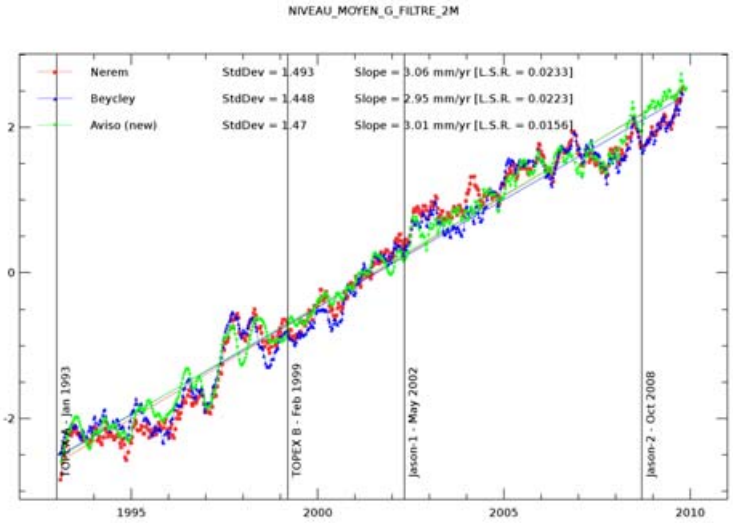

FIG. 2.7 – Variations du niveau moyen global de la mer sur la période 1993-2009 pour différents produits fournis par les groupes de recherche de l'Université du Colorado (courbe rouge, *Nerem et al.* [2006]), GSFC/NASA (courbe bleue, *Beckley et al.* [2010]) et CLS (courbe verte, *Ablain et al.* [2009]).

2.3 Les projections futures du niveau de la mer

2.3.1 Rappel des résultats du dernier rapport de l'IPCC de 2007

L'Intergovernment Panel on Climate Change (IPCC) - le Groupe d'experts Intergouvernemental sur l'Evolution du Climat (GIEC en français) - est un organisme créé en 1988 par l'Organisation Météorologique Mondiale (OMM) et le Programme des Nations Unies pour l'Environnement (PNUE) afin d'évaluer les informations scientifiques, techniques et socio-économiques qui sont nécessaires pour mieux comprendre les fondements scientifiques des risques liés au changement climatique d'origine anthropique, de cerner plus précisément les conséquences possibles de ce changement et d'envisager d'éventuelles stratégies d'adaptation et d'atténuation. Cet organisme n'a pas pour vocation de mener des travaux de recherche, en revanche ses évaluations sont principalement fondées sur des publications scientifiques internationales et techniques dont la valeur scientifique est largement reconnue. C'est dans cette optique qu'a été publié en 2007 le 4ème rapport de l'IPCC. Ici, nous nous intéresserons

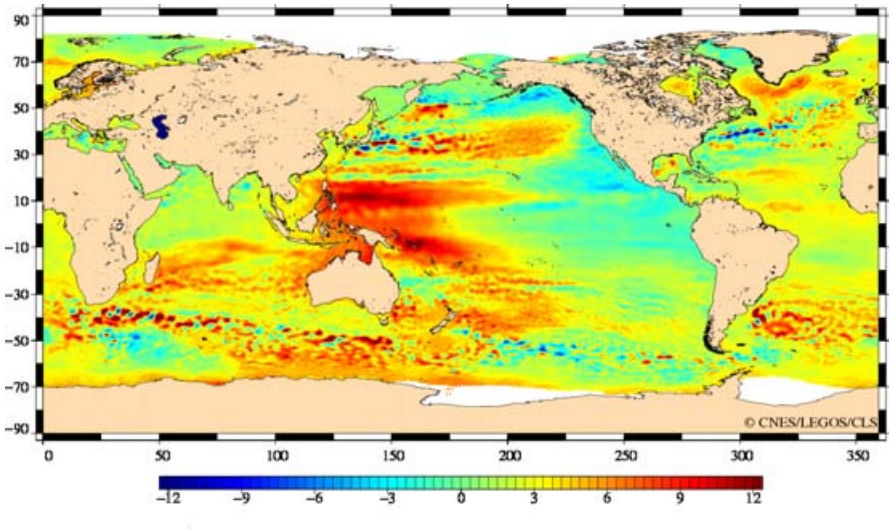

FIG. 2.8 – Cartographie des vitesses du niveau de la mer entre 1993 et 2009 d'après les observations des satellites Topex/Poseidon, Jason-1 et Jason-2 (*Cazenave and Llovel* [2010])

aux chapitres traitant de la problématique du niveau de la mer mais aussi aux études des glaces terrestres (*Bindoff et al.* [2007]; *Lemke et al.* [2007]).

2.3.2 Les projections futures du niveau de la mer

Lors de cet exercice de synthèse, les modèles climatiques ont estimé la hausse future du niveau de la mer jusqu'en 2100. La figure 2.9 résume les variations du niveau de la mer entre 1800 et 2100. Avant 1870, on estime que le niveau moyen de la mer à peu bougé (*Lambeck et al.* [2002]). A partir de 1870, les données marégraphiques nous renseignent sur l'élévation du niveau de la mer à partir d'observations *in situ* (courbe rouge). La courbe verte représente la courbe du niveau moyen global de la mer déduite grâce aux données d'altimétrie spatiale. Enfin, l'enveloppe bleue représente les différentes estimations réalisées à l'aide de modèles numériques couplés avec différents scénarios d'émissions futures de gaz à effet de serre. La moyenne des estimations des modèles suggère une hausse du niveau de la mer en moyenne globale de l'ordre de 40 cm avec une incertitude de 20 cm (dépendant de la dispersion des modèles et des différents scénarios considérés).

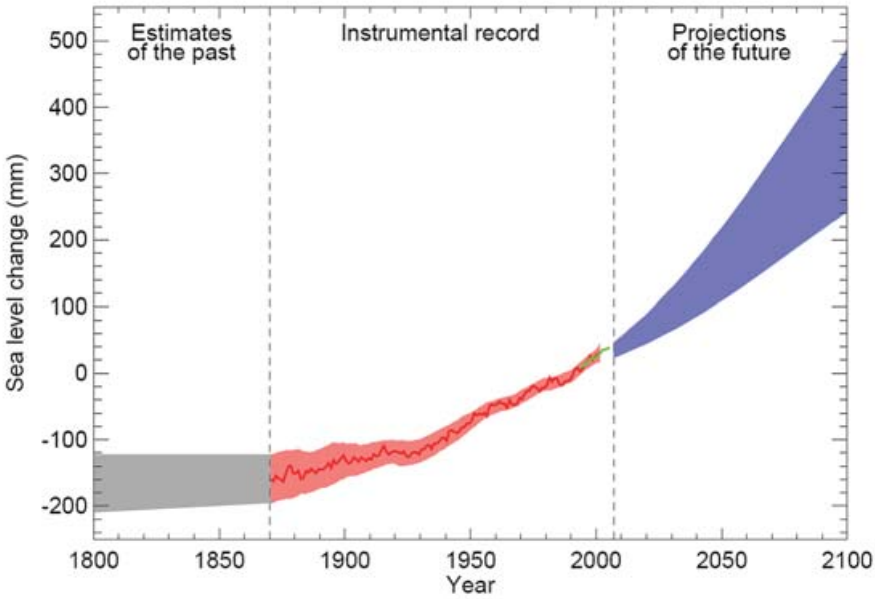

FIG. 2.9 – Evolution du niveau moyen global de la mer entre 1800 et 2100 (IPCC, 2007). La courbe grise représente les estimations faites à partir des études géologiques. La courbe rouge représente le niveau de la mer observé par les marégraphes (*Church et al.* [2004]). La courbe verte représente le niveau moyen global observé par altimétrie spatiale. Enfin, l'enveloppe bleue représente les estimations basées sur les modèles numériques climatiques de l'IPCC (2007).

Chapitre 3

Les causes des variations du niveau de la mer en moyenne globale

Dans ce chapitre, nous nous intéressons aux bilans de la hausse observée du niveau de la mer en moyenne globale. Dans un premier temps, nous établierons un état des connaissances des résultats publiés lors du dernier rapport de l'IPCC (2007) pour les diverses contributions au niveau de la mer. De plus, les avancés scientifiques majeures faites depuis la parution du dernier rapport de 2007 seront décrites.

3.1 Les différentes contributions affectant le niveau de la mer pour les dernières décennies

Aux échelles de temps interannuelles et décennales, les variations du niveau de la mer en moyenne globale sont expliquées par les variations du niveau de la mer stérique (variations de température et de salinité de la colonne fluide) mais aussi par les échanges des masses d'eaux entre les divers réservoirs terrestre (océans, atmosphère et réservoirs continentaux). L'équation suivante résume les contributions impliquées dans les variations actuelles du niveau de la mer.

$$\Delta H_{Total} = \Delta H_{Steric} + \Delta H_{Mass} \tag{3.1}$$

Dans cette équation, ΔH_{Total} représente les variations du niveau de la mer observé, ΔH_{Steric} les variations du niveau de la mer stérique et ΔH_{Mass} les

variations eustatiques des océans, principalement liées aux apports d'eaux douces des continents par la fonte des glaces continentales et les stocks d'eaux dans les bassins hydrologiques. Dans ce chapitre nous allons étudier les différents termes de l'équation 3.1 à l'aide de données *in situ*, spatiales et de modélisations numérique.

3.2 La contribution de l'expansion thermique aux variations du niveau de la mer

3.2.1 Définition et généralité

Comparés à l'atmosphère, les océans ont une capacité calorifique bien plus importante. *Levitus et al.* [2005] ont montré qu'une élévation de la température moyenne de l'océan de 0.1˚C correspondrait à un réchauffement moyen de l'atmosphère de 100˚C si toutefois toute la chaleur était intégralement transférée vers l'atmosphère. En effet, la quantité de chaleur, ou contenu thermique, contenue dans l'océan est liée à la température de la colonne fluide par la relation suivante :

$$H_o = C_{po} M_o \Delta T \tag{3.2}$$

où, C_{po} représente la capacité calorifique de l'eau de mer, M_o la masse totale des océans et ΔT la température.

La capacité calorifique de l'eau de mer est quatre fois supérieure à la capacité calorifique de l'air et la masse de l'océan est 300 fois plus grande que celle de l'atmosphère. Ainsi, la capacité thermique de l'océan est 1 200 fois supérieure à celle de l'atmosphère à élévation de température équivalente. Au cours des 50 dernières années, la quantité de chaleur stockée dans les océans est environ 20 fois supérieure à la quantité stockée dans l'atmosphère. La figure 3.1 compare le réchauffement total de la planète avec ses différents réservoirs (océans, atmosphère, continents et cryosphère) depuis 50 ans. Les océans stockent la plus grande partie de cette chaleur avec environ 85% du réchauffement total. Cette chaleur est principalement stockée dans les couches supérieures des océans où 50% concerne directement les 300 premiers mètres en moyenne globale. Ce constat est vrai pour les océans Pacifique et Indien.

Néanmoins, à cause de phénomènes de convection profonde, la couche s'étend jusqu'à 1 000 mètres de profondeur dans l'océan Atlantique.

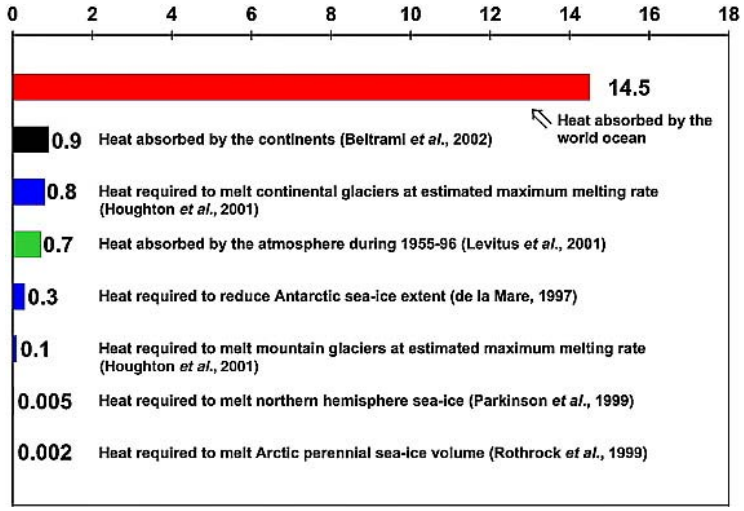

FIG. 3.1 – Bilan de chaleur pour divers réservoirs terrestre (valeurs en 10^{22} Joules) pour la période 1955-1998 (*Levitus et al.* [2005]).

Il existe une inertie de l'océan en relation avec sa capacité calorifique. Donc, ce dernier met un certain temps à atteindre un équilibre thermique de l'ordre de la saison pour les couches supérieures de l'océan, à plusieurs dizaines d'années pour les plus profondes. Ce phénomène est assez complexe. Ainsi, pour un même apport de chaleur les eaux chaudes de surface, qui sont très peu denses, (par exemple dans les régions équatoriales) auront plus tendance à se dilater que les eaux froides profondes, plus denses. Par conséquence, l'absorption de chaleur par l'océan et son transport par circulation à grande échelle génère une variabilité régionale importante du niveau de la mer.

3.2.2 Le calcul de l'expansion thermique

L'utilisation des « hauteurs stériques » en océanographie correspond à la composante du niveau de la mer due à la dilatation/contraction de la colonne d'eau sous l'effet des variations de température et de salinité de l'océan (*Antonov* [2002]). Le calcul de la hauteur stérique d'une colonne fluide est défini par l'équation suivante :

$$H(0, z_{ref}) = \int_0^{z_{ref}} \frac{\rho(z) - \rho_{ref}(z)}{\rho_{ref}(z)} dz \tag{3.3}$$

L'équation 3.3 correspond à l'élévation d'une colonne d'eau de densité $\rho(z)$ par rapport à la hauteur qu'aurait une colonne d'eau standard de densité de référence ρ_{ref} pour une température T=0°C et une salinité S=35PSU (Practical Salinity Unit).

La densité de l'eau de mer dépend non seulement de la température et de la salinité mais aussi de la pression, en d'autre terme, de la profondeur. L'équation d'état de l'eau de mer est de la forme : $\rho = \rho(T, S, P)$ (*Gill* [1982]) et elle permet de calculer la densité de l'eau de mer avec une précision de $3.10^{-5} g/cm^3$ (*Millero and Poisson* [1981]).

Le calcul de la hauteur stérique d'une colonne fluide nécessite le choix d'une profondeur de référence z_{ref}. Nous faisons comme hypothèse qu'à la profondeur z_{ref} (généralement 700 mètres pour les données hydrographiques *in situ* car au-delà les données sont très peu nombreuses), l'océan est au repos : on suppose ainsi qu'à cette profondeur la pression est constante.

3.2.3 Les données hydrographiques

Des données hydrographiques *in situ* de température et de salinité de l'océan ont été effectuées régulièrement à partir des années 1950. Dans un premier temps le long des routes des navires marchands puis, grâce aux missions océanographiques à l'aide de sondes CTD (Conductivity Temperature Depth), MBT (Mechanical BathyThermograph) et XBT (eXpendable BathyThermograph). Ces mesures sont complétées par des mesures issues de mouillages ainsi que des bouées dérivantes. Plus récemment, avec le déploiement de flotteurs profilant de subsurface dans le cadre du projet international Argo (Global Array of profiling floats, *Roemmich and Gilson* [2009]), la couverture des océans est maintenant *quasi* globale ce qui n'était pas le cas lors de l'acquisition des données hydrographiques réalisées par les navires.

C'est à partir des années 1990, avec le lancement des programmes internationaux WOCE (World Ocean Circulation Experiment), CLIVAR (Climate Variability and Predictability Experiment), TOGA (Tropical Ocean and Global Atmosphere) qu'une véritable synthèse globale des observations océaniques s'est mise en place pour établir des bases de données historiques de température et de

salinité de subsurface. Les bases de données se sont ainsi succédées au fil des années : la World Ocean Database 1994 (WOD94, *Levitus and Boyer* [1994]), la WOD98 (*Levitus et al.* [1998]), la WOD01 (*Conkright et al.* [2002]), la WOD05 (*Boyer et al.* [2005]) et plus récemment la WOD09 (*Levitus et al.* [2009]).

Dans cette dernière version, les données ont été corrigées de biais liés à la vitesse de chute des sondes XBT et MBT (*Levitus et al.* [2009]). En effet, ces sondes ne mesurent pas directement la profondeur mais la pression. De ce fait, la profondeur est calculée à partir de formules appelées « fall-rate equation » et du temps à partir duquel la sonde a pénétré dans la colonne d'eau. Il a été montré qu'il existe des erreurs systématiques liées à la détermination de la profondeur (*Gouretski and Koltermann* [2007]). De nombreuses études ont tenté recemment de corriger ces erreurs.

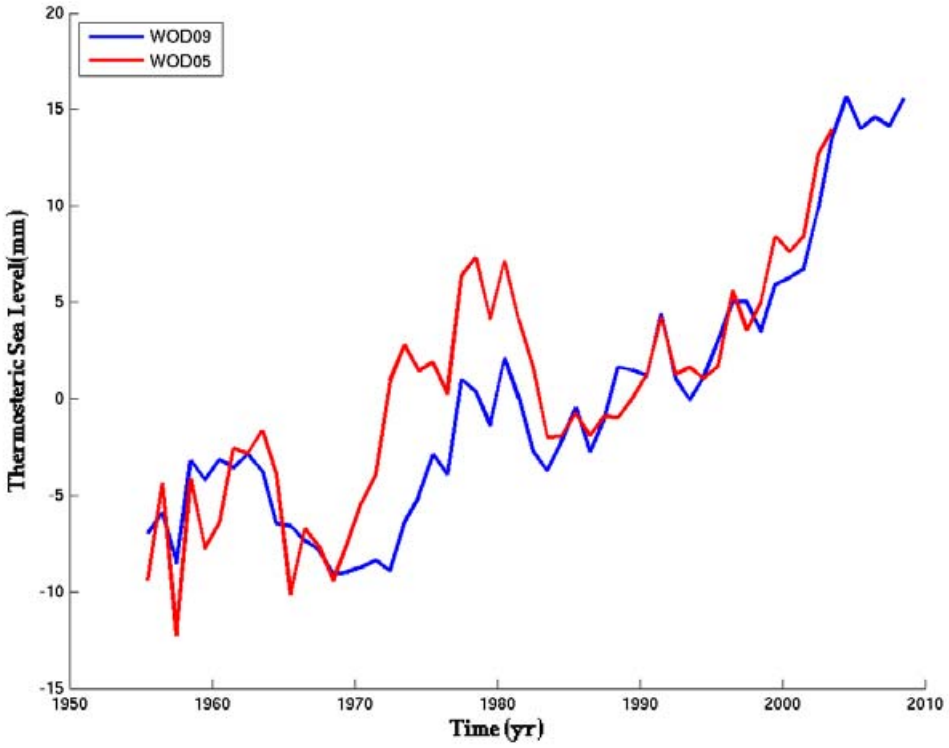

FIG. 3.2 – Evolutions de l'expansion thermique des océans déduites des bases de données hydrographiques WOD05 et WOD09.

D'après la figure 3.2 la nouvelle version du WOD09 montre une hausse *quasi* identique à celle déduite du WOD05 dans le niveau de la mer stérique en moyenne globale. La tendance est de l'ordre de 0.4 mm/an sur la période 1961-

2003. Néanmoins, la variabilité interannuelle est plus faible. La différence vient essentiellement de la correction de biais des données XBT (*Levitus et al.* [2009]).

Cependant, certaines parties des océans restent encore sous échantillonnées d'après les données WOD09 (*Levitus et al.* [2009]). La figure 3.3 montre la répartition géographique des données de subsurface pour le début de l'année 1999. L'Atlantique nord et le Pacifique nord restent bien échantillonnés tandis que l'océan Austral et l'océan Indien manquent terriblement de données pour estimer correctement la composante thermostérique de l'océan mondial.

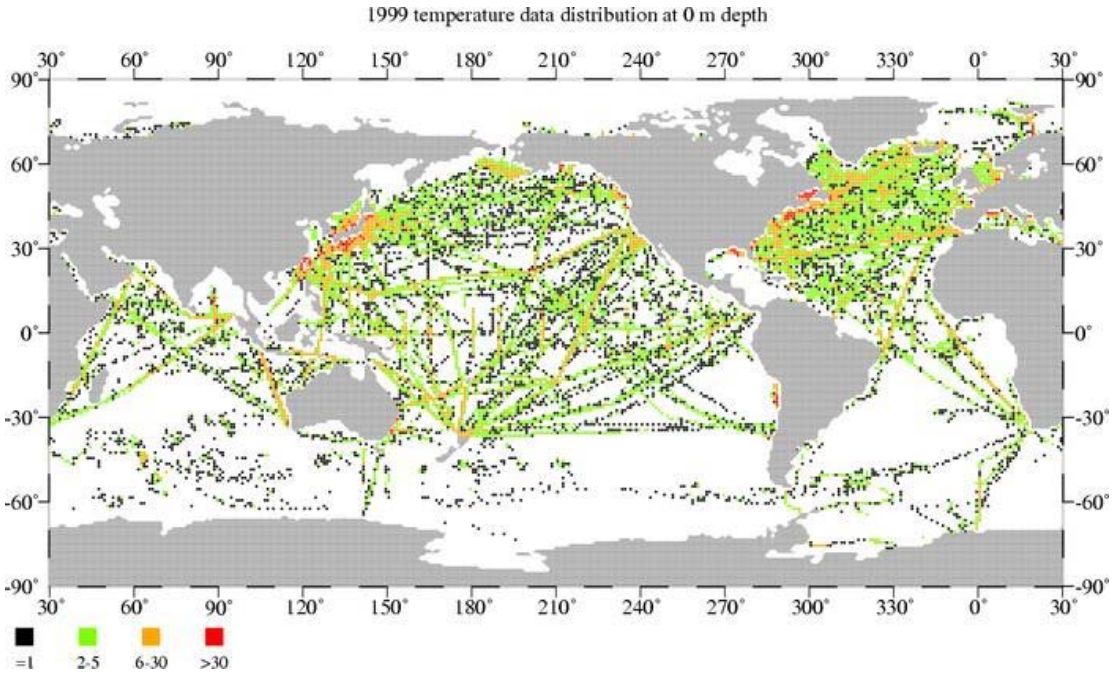

FIG. 3.3 – Distribution régionale de données de subsurface de la WOD09 pour le début de l'année 1999 (*Levitus et al.* [2009])

3.3 La fonte des glaces continentales : apports d'eaux douces aux océans

L'étude des glaces continentales est d'une importance majeure dans la compréhension du changement climatique global. En effet, les glaces continentales sont de très bons indicateurs du changement climatique global actuel.

Les différentes composantes qui peuvent influer sur les variations du niveau de la mer sont analysées par la suite.

3.3.1 Les glaciers de montagne et les petites calottes polaires

Les glaciers de montagne et les petites calottes polaires, autres que celles du Groenland et de l'Antarctique, constituent un réservoir d'eau douce qui peut contribuer à l'élévation du niveau de la mer. Bien que ces structures ne représentent que quelques pourcents de la glace totale de la Terre, la fonte de ces glaciers est une cause importante de la hausse observée du niveau marin depuis plusieurs années maintenant (*Lemke et al.* [2007]). Malheureusement, les mesures *in situ* restent sous échantillonnées à cause du grand nombre de glaciers et de leur inaccessibilité. La fonte intégrale des 150 000 glaciers et étendues de glace dans le monde impliquerait une hausse du niveau moyen des océans de 60 +/- 7 cm (d'après l'étude de *Radic and Hock* [2010]).

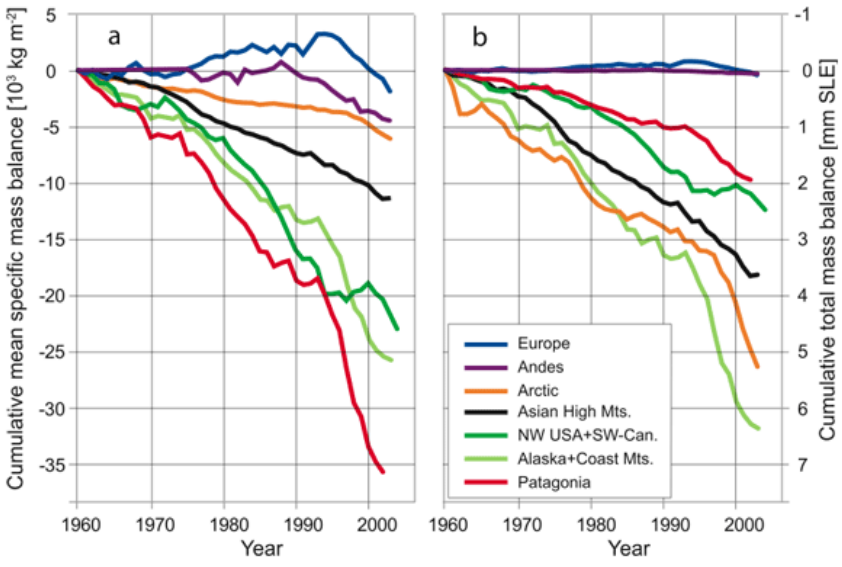

FIG. 3.4 – Bilans de masse des glaciers de montagne pour différentes régions du monde. (a) bilans de masse par unité de surface, (b) bilans de masse exprimés en niveau de la mer équivalent (IPCC, 2007), les valeurs sont normalisées par la surface totale des océans (SLE : Sea Level Equivalent)

Plusieurs études récentes ont cherché à estimer la contribution des glaciers de montagne (qui reculent à l'échelle planétaire) à l'élévation observée du niveau de la mer (*Dyurgerov and Meier* [2005]). La figure 3.4 montre les bilans de

masse pour chaque région, figure 3.4a, et la contribution du niveau de la mer observé, figure 3.4b pour les glaciers de montagne d'Europe, des Andes, d'Arctique, d'Asie, des USA et Canada, d'Alaska et de Patagonie sur la période 1960-2003. D'après ces courbes, à l'exception des glaciers d'Europe et des Andes - qui ont une contribution *quasi* nulle -, les glaciers de montagne perdent de la masse et ainsi participent à élever le niveau moyen global des océans, toutefois avec des vitesses plus ou moins élevées. Notons au passage que la plus grande contribution provient des glaciers de l'Alaska.

Le rapport de l'IPCC (2007) indique que la contribution des glaciers à la hausse observée du niveau de la mer compte pour 0.5 +/- 0.18 mm/an pour les décennies passées (1960-2003) et 0.77 +/- 0.22 mm/an pour les années plus récentes (1993-2003).

Récemment, la fonte des glaciers de montagne semble s'être accélérée (*Kaser et al.* [2006]; *Meier et al.* [2007]; *Cogley* [2009]). Depuis 2003, les récentes estimations prévoient une hausse du niveau marin due à la perte de masse des glaciers de l'ordre de 1.1 mm/an (*Meier et al.* [2007]; *Cogley* [2009]).

Une étude récente de *Hock et al.* [2009] réévalue la contribution des glaciers de montagne et des petites calottes polaires à la hausse observée du niveau de la mer sur la période 1960-2004. Ces auteurs estiment que cet apport contribue à une élévation du niveau de la mer de 0.51 +/- 0.29 mm/an sur cette même période d'étude. Pour palier le manque de données de terrain, ces auteurs utilisent un modèle numérique afin d'estimer les bilans de masse des zones où les données *in situ* sont manquantes. Avec cette nouvelle estimation, la contribution des glaciers de montagne et des petites calottes polaires expliqueraient environ 28% de la hausse totale observée du niveau marin contre les 23% du rapport de l'IPCC (2007) sur la période 1961-2003.

Une autre étude récente a réévalué la perte de masse des glaciers de montagne de l'Alaska uniquement sur la période 1962-2006 (*Berthier et al.* [2010]). Dans le rapport de l'IPCC (2007), il est estimé que l'Alaska est responsable d'un tiers de la contribution totale des glaciers de montagne (environ 0.5 mm/an) entre 1960 et 2003. Cette nouvelle étude montre l'apport important de l'imagerie spatiale haute résolution (SPOT5 notamment) pour mesurer l'évolution dynamique et volumétrique des glaciers. Ainsi, les auteurs estiment que la perte de masse des glaciers de montagne de l'Alaska contribue à élever le niveau des mers d'une valeur de 0.12 mm/an sur la période 1962-2006. Cette nou-

velle estimation est 32% plus faible que celle publiée dans le rapport de l'IPCC (2007).

Certaines études utilisant la gravimétrie spatiale (satellites GRACE) ont estimé la perte de masse des glaciers de l'Alaska. Cette perte est de l'ordre de -101 +/- 22 Gt/an (soit 0.28 +/- 0.06 mm/an en équivalent niveau de la mer, valeur normalisée par la surface totale des océans) sur la période d'avril 2002 à novembre 2005 (*Chen et al.* [2006a]). Une autre étude (*Luthcke et al.* [2008]) utilisant une autre catégorie de solutions GRACE (Gravity Recovery And Climate Experiment) ('MASCON' ; MASs CONcentration) démontre une perte de -71 +/- 6 Gt/an (soit 0.2 +/- 0.02 en équivalent niveau de la mer) entre juillet 2003 et juillet 2008 pour les glaciers de l'Alaska. Ces estimations concordent avec les études basées sur des données de lasers aéroportés : perte de -96 +/- 35 Gt/an (soit 0.26 +/- 0.1 mm/an en équivalent niveau de la mer) sur la période 1990 à 2001 (*Arendt et al.* [2002]).

3.3.2 Les calottes polaires : Antarctique et Groenland

Les modifications du bilan de masse des calottes polaires par fonte et par perte de masse sont d'un intérêt considérable dans le contexte du changement climatique global. De plus, la fonte occasionnée constitue une source d'échange d'eau avec les océans non négligeable. Notons que la fonte des glaces de mer (par exemple la banquise des régions du Pôle Nord) n'affecte pas le niveau de la mer, en raison du principe d'Archimède.

Grâce aux satellites, on suit depuis presque deux décennies, les variations des masses de glace du Groenland et de l'Antarctique. L'altimétrie spatiale permet de mesurer les variations d'altitude des calottes, donc d'en déduire la variation de leur masse. Avec une technique appelée « Interférométrie Radar ou InSAR », on peut estimer la vitesse d'écoulement des glaciers côtiers vers la mer, donc la quantité de glace déversée dans l'océan. Combinée à des mesures de bilan de masse en surface (précipitations neigeuses versus fonte en surface), on en déduit le bilan de masse total. Enfin, depuis 2002, la gravimétrie spatiale (mission GRACE), permet de mesurer directement les variations de la masse de glace des calottes. Le principe de la mission spatiale gravimétrique GRACE sera décris dans le paragraphe 4.2.1.

La synthèse de ces observations indique une perte de masse très marquée dans les régions côtières du sud du Groenland, de l'ordre de 150 milliards de

tonnes de glace par an sur la dernière décennie (avec une nette accélération au cours des années récentes) (Figure 3.5). Ces observations révèlent aussi une perte importante de masse de glace en Antarctique de l'ouest, en particulier dans le secteur de la mer d'Amundsen. On estime à environ 100 milliards de tonnes la masse de glace perdue par an en Antarctique de l'ouest. En revanche l'Antarctique de l'est est à peu près en équilibre (dans cette partie du continent, la perte de masse de glace des régions côtières est compensée par une accumulation des précipitations neigeuses dans les régions centrales d'altitude élevée.

On a observé une accélération importante depuis quelques années de la perte de masse de glace dans le sud du Groenland et en Antarctique de l'ouest. L'essentiel de la glace perdue se fait par écoulement très rapide des glaciers côtiers vers la mer et le déversement d'icebergs dans l'océan. Ce phénomène est particulièrement actif lorsque le socle rocheux à l'aval du glacier est situé sous le niveau de la mer. C'est le cas par exemple du glacier Jakobshavn Isbrae le plus grand glacier du Groenland situé sur la côte ouest de l'île, dont la vitesse d'écoulement a atteint près de 15 km/an ces dernières années. On commence tout juste à entrevoir les mécanismes à l'origine de ce phénomène. Le plus important est probablement lié au bilan des forces qui s'exercent à l'avant du glacier. A cause du réchauffement des eaux océaniques, la partie avant du glacier s'amincit et s'avère incapable de retenir l'écoulement de la glace en aval ; le glacier devient instable. En Antarctique on observe un phénomène identique en particulier là où les glaciers se terminent par une plateforme de glace. En fondant, celle-ci se désolidarise de la calotte, laissant libre cours à l'écoulement du glacier vers la mer. Au Groenland, un autre phénomène contribue à l'instabilité des glaciers (quoique de façon secondaire) : la fonte estivale en surface et la propagation de l'eau au travers de crevasses contribuent à lubrifier la base de la calotte et donc d'accélérer l'écoulement de la glace vers la mer.

La dynamique des calottes polaires est complexe et encore mal comprise. Nous ne savons pas si les phénomènes observés depuis quelques années vont s'atténuer ou au contraire s'emballer. L'observation depuis l'espace du comportement des calottes polaires est donc un objectif majeur.

La figure 3.5 illustre l'accélération de la perte de masse des calottes polaires du Groenland et de l'Antarctique décelée lors des deux dernières décennies basée à partir de données spatiales d'altimétrie, InSAR et de gravimétrie.

Le tableau 3.1 regroupe quelques unes des différentes estimations publiées ces dernières années, sur les bilans de masse des calottes polaires du Groenland et de l'Antarctique basées sur les données GRACE. Les estimations va-

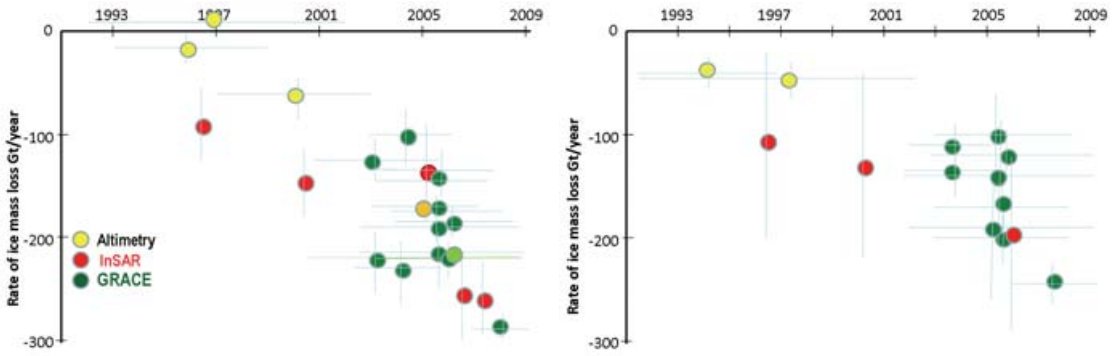

(a) Pertes de masse de la calotte du Groenland

(b) Perte de masse de la calotte de l'Antarctique

FIG. 3.5 – Compilation de résultats publiés sur la perte de masse des calottes polaires du Groenland (fig a) et de l'Antarctique (fig b) entre 1993 et 2009 basées sur l'interférométrie radar, l'altimétrie spatiale et la gravimétrie spatiale (d'après *Cazenave and Llovel* [2010]).

rient d'une étude sur l'autre. La première raison provient des périodes temporelles considérées. En effet, en plus d'être courtes, les périodes ne sont pas les mêmes et, de fait les estimations ne sont pas comparables. Par contre, comme le suggère de récentes études (*Velicogna* [2009]; *Chen et al.* [2009]), les données de GRACE semblent révèler une accélération de la perte de masse de la calotte de l'Antarctique. Ces études estiment une perte de masse de -104 Gt/an sur la période 2002-2006 bien plus importante que la perte de -246 Gt/an sur la période 2006-2009. Pour le Groenland, *Velicogna* [2009] montre que la perte de masse sur la période 2007-2009 est comprise entre -286 Gt/an comparée à la perte de masse de -137 sur la période 2002-2003.

3.4 Bilans du niveau de la mer des dernières décennies d'après le rapport de l'IPCC (2007)

Le bilan des différentes contributions climatiques à la hausse du niveau de la mer au cours des 50 dernières années est résumé dans le tableau 3.2.

Pour les 50 dernières années, la somme des différentes contributions climatiques à la hausse du niveau de la mer est de 1.1 +/- 0.5 mm/an. Au cours de la même période, les observations marégraphiques ont enregistré une élévation du niveau de la mer de 1.8 +/- 0.5 mm/an. Ainsi, les contributions climatiques

	Antarctique	Groenland	Période d'étude
Velicogna and Wahr [2006]	-	-227 +/- 33	2002-2006
Ramillien et al. [2006]	-129 +/- 15	-169 +/- 66	Jul. 2002 - Mar. 2005
Chen et al. [2006b,d]	-	-219 +/- 21	2002-2005
Luthcke et al. [2006]	-	-101 +/- 16	2003-2005
Velicogna [2009]	-143 +/- 73	-230 +/- 33	Avr. 2002 - Fev. 2009
Chen et al. [2009]	-190 +/- 77	-	Avr. 2002 - Jan. 2009
Wouters et al. [2008])	-	-179 +/- 25	Fev. 2003 - Jan. 2008

TAB. 3.1 – Estimations des pertes de masse (en Gt/an) des calottes polaires du Groenland et de l'Antarctique avec les périodes temporelles associées à chaque étude.

n'expliquent pas la totalité de la hausse observée du niveau marin. La partie non expliquée représente 0.7 +/- 0.7 mm/an.

Pour la période de 1993 à 2003, la somme des différentes contributions climatiques à la hausse observée du niveau de la mer est égale à 2.8 +/- 0.7 mm/an explique une très grande partie de la hausse observée du niveau de la mer par altimétrie spatiale de 3.1 +/- 0.7 mm/an. Il reste cependant une part non négligeable de 0.3 +/- 1.0 mm/an non expliquée par les contributions climatiques à la hausse du niveau marin.

Pour la période longue, 1961-2003, la somme des contributions climatiques n'expliquent pas totalement la hausse observée du niveau marin. Par contre, sur la période plus récente, entre 1993 et 2003, nous fermons le bilan du niveau de la mer en considérant les barres d'erreur assez importantes. Le challenge est maintenant de diminuer les incertitudes et ainsi, améliorer les estimations des différentes contributions climatiques à la hausse observée du niveau de la mer. Regardons maintenant l'élévation du niveau marin et ses composantes climatiques depuis 2003.

	1961-2003	1993-2003
Expansion thermique	0.42 +/- 0.14	1.6 +/- 0.5
Glaciers de montagne	0.50 +/- 0.18	0.77 +/- 0.22
Antarctique	0.05 +/- 0.12	0.21 +/- 0.35
Groenland	0.14 +/- 0.41	0.21 +/- 0.07
Somme	1.1 +/- 0.5	2.8 +/- 0.7
Niveau de la mer observé	1.8 +/- 0.5	3.1 +/- 0.7
Différence	0.7+/- 0.7	0.3 +/- 1.0

TAB. 3.2 – Bilan de la hausse du niveau marin entre 1961-2003 et 1993-2003 (IPCC, 2007)

Chapitre 4

Les variations du niveau de la mer des années récentes aux dernières décennies

Comme nous venons de le voir dans le chapitre précédent, le rapport de l'IPCC-AR4 (2007) indique que la vitesse de la hausse observée du niveau de la mer est égale à 3.1 mm/an en moyenne globale sur la période 1993-2003. Or, pour les années récentes, entre 2002 et 2008, le niveau de la mer continue de monter avec cependant une vitesse plus faible de l'ordre de 2.7 mm/an (mise à jour des travaux de Cazenave et al. [2009]). Notons toutefois que la vitesse d'élévation du niveau global des mers est égale à 3.2 +/- 0.4 mm/an sur la période totale 1993-2009 (mise à jours des travaux de Ablain et al. [2009]; Cazenave and Llovel [2010]). Nous allons maintenant analyser les différentes contributions qui font varier le niveau de la mer en moyenne globale et ensuite, établir des bilans du niveau de la mer pour les années récentes et entre 2002 et 2009, en termes de tendance. Dans ce chapitre, nous trouverons les articles publiés durant ce travail de thèse. Notamment, un premier article traitant de la variabilité régionale et en moyenne globale du niveau de la mer des années récentes (Llovel et al. [2010b]). Puis, nous trouverons un article sur la contribution des eaux continentales aux variations du niveau de la mer en moyenne globale (Llovel et al. [2010a]) et un autre article sur la contribution des eaux continentales sur les variations inter-annuelles du niveau de la mer (Llovel et al. [2011]). Puis, nous présenterons un article de revue sur le niveau de la mer et les bilans associés pour les années récentes (Cazenave and Llovel [2010]).

4.1 La contribution du niveau de la mer stérique

Le projet international Argo

Le début des années 2000 a été marqué par le commencement du déploiement des flotteurs profilant de subsurface du projet Argo. Pour la première fois l'acquisition de données de température et de salinité assure une couverture globale des océans jusqu'à 2000 mètres de profondeur. Le réseau a été déployé en intégralité et c'est maintenant plus de 3000 flotteurs qui dérivent au gré des courants. La fig 4.1 montre la distribution spatiale des profileurs pour le mois de mars 2010. La couverture spatiale est, de loin, meilleure que celle des données hydrographiques. Ce projet a permis d'améliorer l'échantillonnage des océans, surtout dans l'océan Austral.

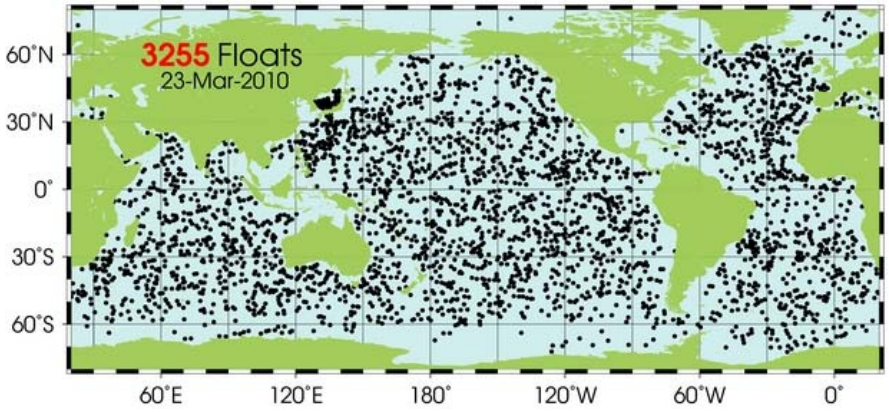

FIG. 4.1 – Distribution des flotteurs profilant Argo pour le mois de mars 2010.

Ces flotteurs sont équipés de balises Argos qui transmettent les données par satellite à un centre de réception en temps réel via le GTS (Global Telecommunication System). Le cycle d'une balise est schématisée par la figure 4.2. Le flotteur descend à 1000m où il dérive pendant environ 9 jours (parking depth). Puis, il plonge à 2000m et remonte à la surface en 6 heures. Durant cette remontée, le flotteur acquiert le profil de température et de salinité au point de la surface où celui-ci est géoréférencé par satellites. Ces enregistrements sont ensuite envoyés aux banques de données du projet afin d'être traités ultérieurement.

Dans notre estimation du contenu stérique de l'océan, nous nous sommes intéressés à traiter les données Argo fournies par différentes équipes de recherche. En effet, chaque équipe possède ses propres traitements pour fournir des grilles de température et de salinité et les climatologies associées. Les produits sont sous forme de grilles régulières globales sur plusieurs niveaux

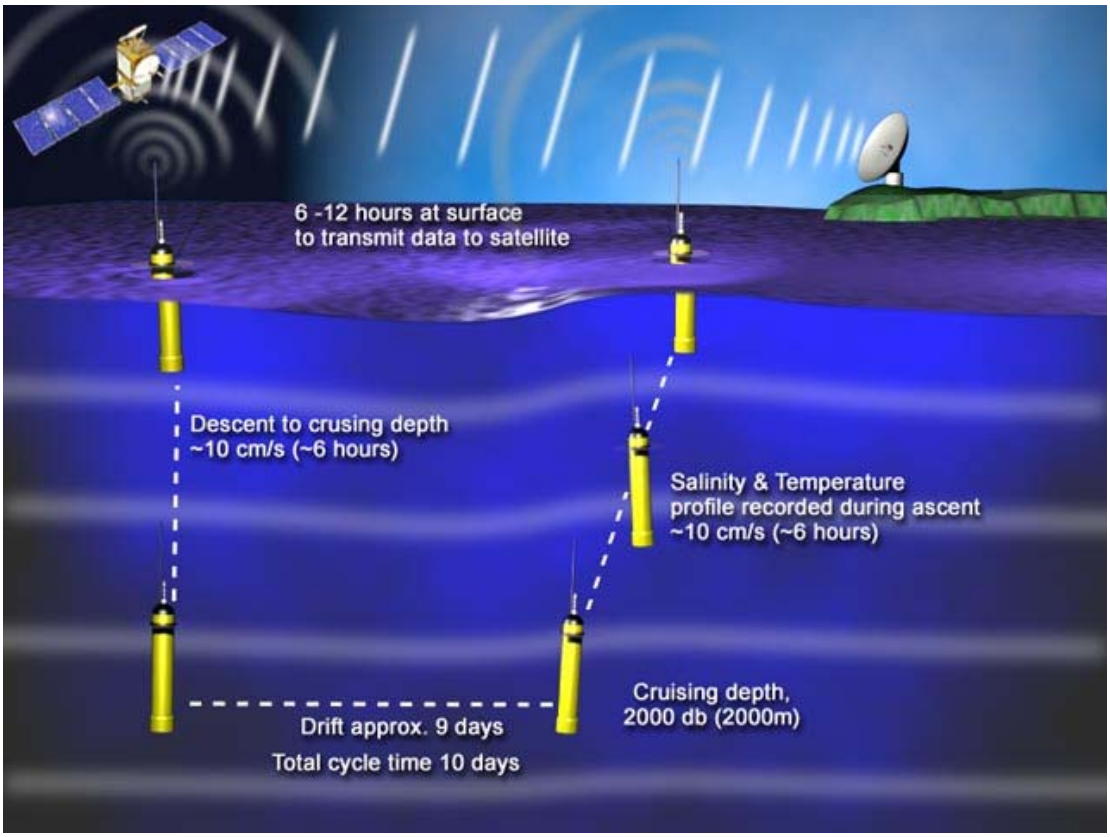

FIG. 4.2 – Schéma de fonctionnement d'une balise Argo.

de profondeur. Nous nous sommes intéressés principalement à quatre bases de données qui proposent des traitements différents. Ces bases de données sont produites par CLS (*Guinehut et al.* [2009]), SCRIPPS (*Roemmich and Gilson* [2009]), IPRC (http ://apdrc.soest.hawaii.edu/projects/argo/) et NOAA (*Levitus et al.* [2009]). Nous avons calculé pour chaque jeu de données, le niveau de la mer stérique jusqu'à 900 mètres pour CLS, SCRIPPS et IPRC et 700 mètres pour les données de la NOAA par soucis d'homogénéité pour les comparaisons futures. Ainsi la figure 4.3 nous renseigne sur les différentes estimations du niveau de la mer stérique entre 1993 et 2009.

La courbe verte représente l'évolution du niveau de la mer thermostérique (variation de la température uniquement) jusqu'à 700 mètres de profondeur à partir de 1993 jusqu'en 2009 basée sur les données de la NOAA (*Levitus et al.* [2009]). Cette contribution du niveau de la mer observé représente l'expansion thermique des océans en moyenne globale. Dans le rapport de l'IPCC-AR4 (2007), cette contribution thermostérique expliquait 50% de la hausse du niveau de la mer observé entre 1993 et 2003, ce qui est confirmé par la courbe verte. D'après cette estimation du niveau de la mer thermostérique,

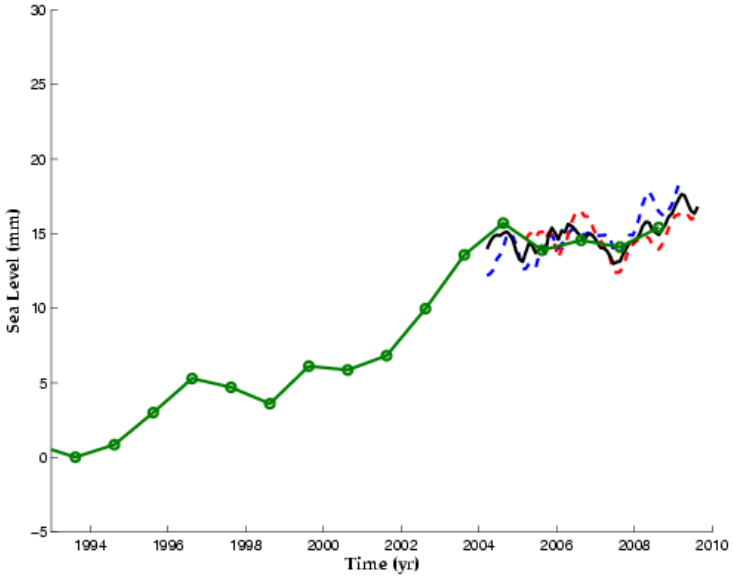

FIG. 4.3 – Evolution de la contribution stérique en moyenne globale basée sur les données de température et de salinité de différents groupes de recherche (courbe verte : NOAA ; courbe bleue : CLS ; courbe noire : SCRIPPS et courbe rouge : IPRC

depuis 2003, nous observons une pause dans le réchauffement des océans tandis que le niveau de la mer continu à croître avec cependant une vitesse plus faible entre 2002-2008. Ce constat est confirmé avec les variations du niveau de la mer stérique (on considère maintenant non seulement les variations de température mais aussi de salinité) basées sur différents produits fournis par les équipes de recherche du SCRIPPS (courbe noire, *Roemmich and Gilson* [2009]), de CLS (courbe bleue, *Guinehut et al.* [2009]) et de l'IPRC (courbe rouge) sur la période commune entre 2004 et 2009. La pause observée dans le niveau de la mer thermostérique (courbe verte) est confirmée par les estimations du niveau de la mer stérique basées sur les produits de CLS, du SCRIPPS et de l'IPRC qui prennent seulement en compte les données des flotteurs profilant Argo. Toutefois, une reprise à la hausse de cette contribution à partir de 2008 est visible, ainsi cette pause semble n'être que temporaire.

4.2 La contribution du signal massique de l'océan : études des données de GRACE

Grâce à la mission spatiale gravimétrique GRACE lancée en 2002, il est dorénavant possible d'estimer les variations de masse d'eau des divers

réservoirs terrestres tels que les océans, les calottes polaires mais aussi les plus grands bassins hydrologiques de la planète. Ainsi, il est possible d'en déduire les contributions respectives de chaque composante à la hausse totale observée du niveau de la mer en moyenne globale entre 2002 et 2009.

4.2.1 La mission spatiale GRACE

L'objectif de la mission GRACE est d'étudier les variations spatio-temporelles du champ de gravité terrestre. Cette mission, développée par la NASA (USA) et le DLR (Allemagne), est constituée de deux satellites jumeaux, lancés le 17 mars 2002, ayant la même orbite polaire (d'altitude 485 km et d'inclinaison 89 degrés) séparés d'environ 220km. Le principe de cette mission est le suivant : le changement local de gravité modifie la distance entre les deux satellites qui est mesurée par un système émetteur/récepteur radioélectrique dans la bande K (précision à 10 μm). Leurs orbites sont calculées avec une précision centimétrique à l'aide d'un récepteur GPS. Les variations de la gravité terrestre sont ainsi mesurées avec une résolution temporelle de l'ordre du mois. La résolution spatiale au sol est de l'ordre de 400km. A ces échelles, les faibles variations spatio-temporelles du champ de gravité résultent principalement des redistributions de masses dans les enveloppes fluides superficielles de la Terre (atmosphère, océans, réservoirs d'eaux continentales et calottes polaires). Ainsi, GRACE voit non seulement les variations à long terme de l'hydrologie continentale mais aussi la signature du rebond post-glaciaire c'est-à-dire, la réponse visco-élastique dûe à la fonte des grandes calottes polaires du dernier maximum glaciaire il y a environ 18 000 ans. L'étude de ces variations de gravité permet d'estimer celles de masse des océans, des grandes calottes polaires -Groenland et Antarctique-, ainsi que les variations du stock d'eaux continentales. Notons toutefois que les données de GRACE sont des valeurs de masse intégrées selon la verticale et donc, il est important d'utiliser d'autres sources de données afin de séparer les différentes sources susceptibles d'engendrer des changements de gravité.

Les solutions du champ de gravité sont calculées par plusieurs groupes scientifiques liés à la mission spatiale gravimétrique GRACE tels que le « Center for Space Research » (CSR) de l'Université du Texas à Austin, le « Geoforschungszentrum » (GFZ) à Postdam et le « Jet Propulsion Laboratory » (JPL) de la NASA à Pasadena, en Californie. D'autres groupes non affiliés au départ à la mission calculent des solutions. C'est le cas du « Goddard Space Flight Center » (NASA, *Rowlands* [2005]), le « Delft Institute of Earth Observation and

Space Systems » (DEOS ; *Kusche* [2007]), le « Groupe de Recherche de Géodésie Spatiale » (GRGS, *Bruinsma et al.* [2010]), l'« Institute de Theoretical Geodesy » (ITG) à l'Université de Bonn (*Kurtenbach et al.* [2009]). La plupart des groupes fournissent des solutions mensuelles, certain de ces groupes calculent des solutions sur des périodes plus fines de 10 jours. Généralement, les solutions GRACE sont exprimées sous forme de coefficients en harmonique sphérique (typiquement entre 60 et 100 ce qui correspond à des longueurs d'onde de 400 à 700 km). Ces solutions sont corrigées des effets de charge de l'atmosphère, de la redistribution barotrope des masses d'eau océanique et de la marée lors du traitement des données à l'aide de modèles numériques de circulation (*Bettadpur* [2007]). Chaque groupe possède son propre traitement de données qui génère des différences à chaque solution. A chaque nouvel algorithme de traitement, les solutions sont recalculées systématiquement du début de la mission ce qui a mis en évidence des améliorations de leur qualité. De plus, les données de GRACE sont exprimées en termes de hauteurs d'eau équivalente. L'hypothèse sousjacente est la redistribution de masse d'eau qui s'effectue dans les couches superficielles des enveloppes fluides de la planète (*Swenson and Wahr* [2002]). Lors de nos études, nous avons traité les solutions fournies par les groupes du CSR, GFZ, JPL (*Chambers* [2006]) et du GRGS (*Bruinsma et al.* [2010]).

Le plus grand défi lors du traitement des données GRACE est l'estimation précise des erreurs des solutions. Deux catégories d'erreur existent (*Schmidt et al.* [2008]) :

- les erreurs dûes aux algorithmes utilisés lors du traitement des données (avec notamment les erreurs de mesures de GRACE et les erreurs liées au modèles numériques prises en compte dans le traitement pour retirer les signaux géophysiques). Les erreurs liées aux phénomènes physiques non modélisés ou encore la contamination par d'autres signaux géophysiques vont rentrer dans cette catégorie d'erreur.

- les erreurs post traitement liées aux lissages des données pour réduire le bruit haute fréquence et les erreurs de « leakage » dûes à la contamination d'une région en dehors de la celle étudiée.

Lors du calcul des harmoniques sphériques, certains coefficients vont entrer en résonance du fait de la résolution spatio-temporelle limitée du système et induire du bruit haute fréquence représenté par des bandes nord-sud visibles dans les cartes des géoïdes (*Swenson and Wahr* [2002]; *Han et al.* [2005]; *Ramillien et al.* [2005]; *Chen et al.* [2006c]).

4.2.2 Le signal massique des océans

La figure 4.4 montre les variations du signal massique des océans en moyenne globale entre +/- 89° de latitude pour les années récentes entre 2002 et 2009. Ces courbes sont basées sur les données GRACE fournies par différents groupes de recherche du GRGS (courbe bleue), du GFZ (courbe noire), du CSR (courbe rouge) et du JPL (courbe rose) sur les périodes juillet 2002 - avril 2009, octobre 2002 - février 2009, août 2002 - mars 2009 et août 2002 - mars 2009 respectivement. Les signaux saisonniers annuel et semi-annuel ont été retirés de ces courbes. Ces différentes estimations montrent une tendance faible et une forte variabilité interannuelle. Les tendances sont égales à 0.08 +/- 0.06 mm/an (GRGS), -0.23 +/- 0.15 (GFZ), -0.42 +/- 0.13 mm/an (CSR) et 0.25 +/- 0.15 mm/an (JPL) sur la période commune de ces quatre solutions entre octobre 2002 et février 2009. Notons une forte divergence entre ces différentes estimations pour le signal massique des océans. Il en est de même pour la variabilité interannuelle qui n'est pas la même pour les quatre courbes. En effet, on observe un minimum local fin 2004 et un maximum local début 2005 en phase pour les quatre courbes. Un autre minimum local est visible début 2007. Néanmoins, un déphasage de ce minimum pour les quatre solutions est visible. La variabilité interannuelle ne se compare pas facilement sur ces quatre estimations.

Comme nous l'avons évoqué précédemment, GRACE mesure les redistributions de masse des enveloppes fluides de la planète qui doivent être corrigées du rebond post-glaciaire.

4.2.3 Le rebond post-glaciaire

Le rebond post-glaciaire (également appelé ajustement isostatique ou glacio-isostasie) se définit comme le soulèvement des masses terrestres consécutif à la fonte des calottes glaciaires (*Peltier* [2009]) et aux variations de gravité dues à la redistribution des masses d'eau (entre la fonte des glaces et les apports d'eaux douces aux océans, *Mitrovica et al.* [2001]). Ces masses terrestres, alors comprimées sous les charges de glace, se sont relevées au cours de la période post-glaciaire du fait du phénomène d'isostasie. Ce phénomène affecte principalement les régions aux hautes latitudes telles que l'Amérique du Nord (grands lacs et la baie d'Hudson), la Sibérie, le Groenland, l'Ecosse, la Fennoscandie et le nord du Danemark. Dans ce travail, nous avons considéré deux

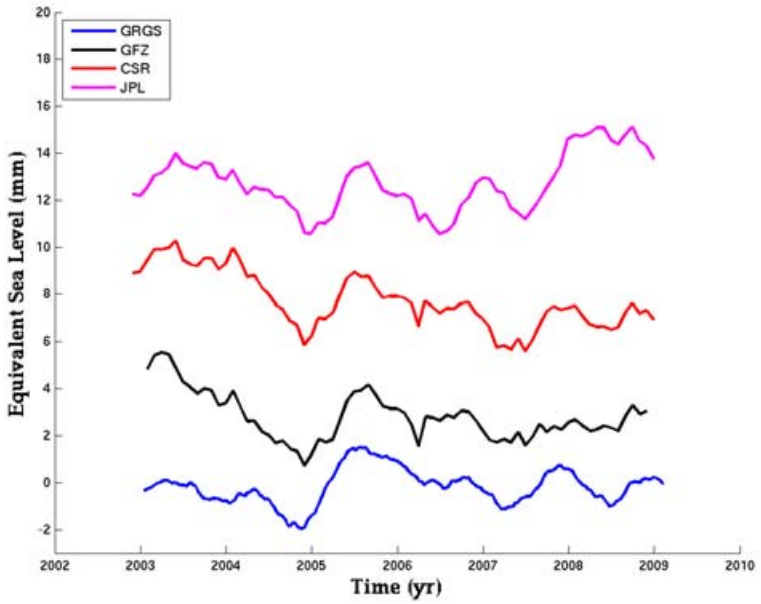

FIG. 4.4 – Moyennes globales du signal massique des océans basées sur les solutions GRACE fournis par les groupes de recherche du GRGS (courbe bleue), du GFZ (courbe noire), du CSR (courbe rouge) et du JPL (courbe rose). Les signaux saisonniers à 6 et 12 mois sont retirés.

estimations différentes pour corriger ce phénomène : les corrections de *Peltier* [2009] et celle de *Paulson et al.* [2007]. En effet, ces auteurs utilisent des modèles numériques pour estimer ces vitesses de rebond. Or, ces modèles sont entachés d'erreurs principalement dues aux profils de viscosité du manteau terrestre mais aussi à l'histoire de la déglaciation qui sont des facteurs assez mal connus de nos jours. Néanmoins, un effort considérable est réalisé pour prendre en compte des données de GPS et GRACE dans des régions où le signal du rebond post-glaciaire est prédominant dans le but d'améliorer les estimations de ces modèles numériques. Cependant, les estimations ne convergent pas et *Peltier* [2009] conseille de prendre une correction de 1.95 mm/an tandis que l'estimation proposée d'après *Paulson et al.* [2007] est plus faible, de l'ordre de 1 mm/an.

La figure 4.5 représente les estimations du signal massique de l'océan en corrigeant les courbes du rebond post-glaciaire (nous considérons ici la correction conseillée par *Peltier* [2009] qui vaut 1.95 mm/an). Les courbes sont calculées entre +/- 89° de latitude sur les années récentes entre 2002 et 2009 basées sur les données GRACE fournis par le GRGS (courbe bleue), le GFZ

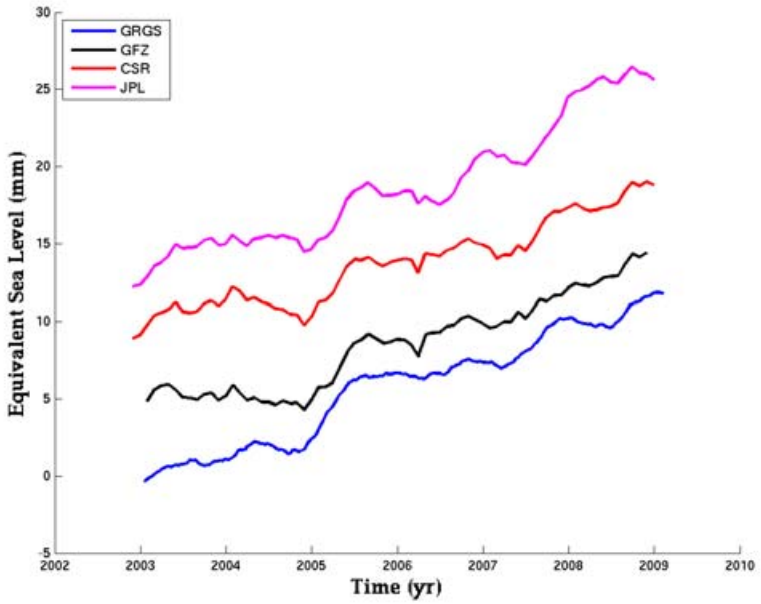

FIG. 4.5 – Moyennes globales du signal massique des océans basées sur les solutions GRACE fournies par les groupes de recherche du GRGS (courbe bleue), du GFZ (courbe noire), du CSR (courbe rouge) et du JPL (courbe rose) avec l'ajout du GIA de *Peltier* [2009] comptant pour 1.95 mm/an. Les signaux saisonniers à 6 et 12 mois sont retirés. Les courbes sont lissées sur 5 mois.

(courbe noire), le CSR (courbe rouge) et le JPL (courbe rose) sur les mêmes périodes que précédemment. Les tendances sont maintenant égales à 2.03 +/- 0.06 pour le GRGS, 1.71 +/- 0.15 pour le GFZ, 1.53 +/- 0.13 pour le CSR et 2.2 +/- 0.15 pour le JPL sur la période commune d'octobre 2002 à février 2009. Nous pouvons noter une divergence non négligeable dans les estimations de ces différentes tendances. La majorité du signal massique de l'océan est comprise dans la correction du rebond post-glaciaire. Ainsi, une bonne estimation de ce signal masse de l'océan passe par une bonne estimation du rebond post-glaciaire, qui à ce jour, présente beaucoup d'incertitudes.

Afin de palier au mieux à ce problème et d'obtenir l'estimation la plus précise possible du rebond post-glaciaire, nous allons dans les paragraphes suivant, considérer les diverses contributions qui affectent le signal massique des océans. Le but étant d'avoir la meilleure estimation pour les études de bilan qui seront exposées à la fin de ce chapitre.

4.2.4 Bilans de masse des calottes polaires

Pour les années récentes, beaucoup de travaux se sont appuyés sur les données de la mission spatiale gravimétrique GRACE et pour la première fois, un bilan global de masse a pu être réalisé pour les calottes polaires (*Ramillien et al.* [2006]; *Wouters et al.* [2008]; *Cazenave et al.* [2009]; *Peltier* [2009]; *Baur et al.* [2009]; *Velicogna* [2009]; *Chen et al.* [2009]).

La figure 4.6 montre la perte de masse pour les calottes polaires du Groenland et de l'Antarctique que nous avons calculée à partir des données GRACE du GRGS (*Bruinsma et al.* [2010]). Cette perte est estimée respectivement à -151 Gt/an et -134 Gt/an. Toutefois, nous avons corrigé ces données de GRACE du rebond post-glaciaire. Ce phénomène est *quasi* négligeable pour le Groenland et sa valeur est de l'ordre de 9 Gt/an (*Peltier* [2004]). Par contre pour l'Antarctique, cette correction est de l'ordre de 101 +/- 40 Gt/an (*Ivins and James* [2005]). En transposant ces valeurs en équivalent niveau de la mer, nous obtenons 0.42 mm/an et 0.37 mm/an sur la période 2002-2009 respectivement pour le Groenland et l'Antarctique. Ces nouvelles estimations sont plus importantes que celles obtenues lors du dernier rapport de l'IPCC (2007). En effet, ce rapport indiquait que ces deux calottes polaires contribuaient à une hausse du niveau marin de l'ordre de 0.2 mm/an chacune sur la période 1993-2003 (*Lemke et al.* [2007]; *Allison et al.* [2009]). Ces nouvelles estimations démontrent une accélération dans la perte de masse des calottes polaires et donc, d'un apport plus important à la hausse observée du niveau de la mer.

La figure 4.7 montre la série temporelle, basée sur les données du GRGS (*Bruinsma et al.* [2010]), du gain de masse aux océans dû à la fonte des deux grandes calottes polaires du Groenland et de l'Antarctique. Les signaux saisonniers à 6 et 12 mois ont été retirés. Cette courbe est exprimée en équivalent niveau de la mer. Nous notons une forte variabilité interannuelle autour d'une tendance de l'ordre de 0.8 +/- 0.05 mm/an. Cette estimation concorde avec les récentes publications qui estiment la perte de masse des calottes polaires à 1 mm/an en niveau de la mer équivalent (*Velicogna* [2009]; *Chen et al.* [2009]).

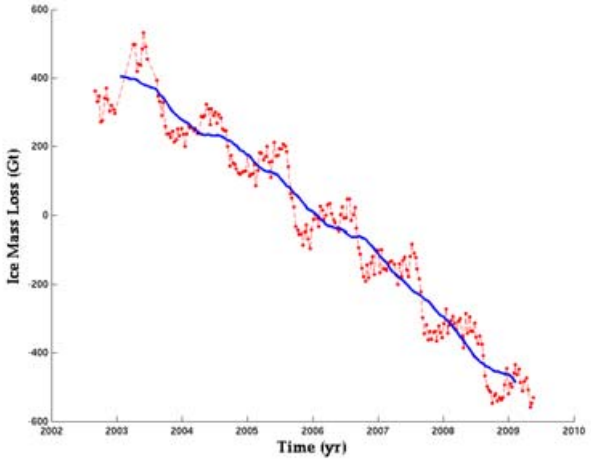

(a) Perte de masse de la calotte du Groenland

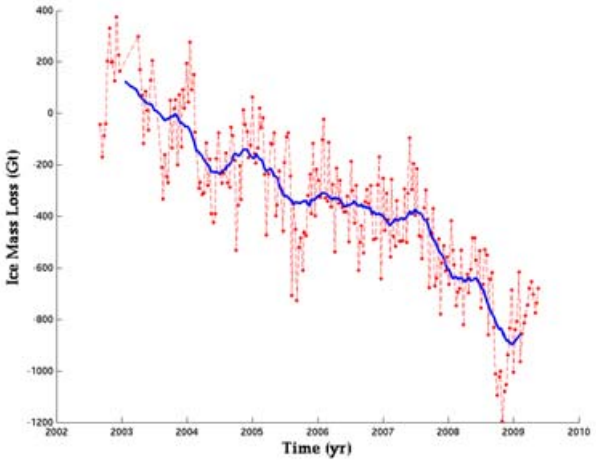

(b) Perte de masse de la calotte de l'Antarctique

FIG. 4.6 – Séries temporelles de la perte de masse des calottes polaires du Groenland et de l'Antarctique déduites des données GRACE du GRGS (courbe rouge : signal total, courbe bleue : signal résiduel après retrait des signaux saisonniers). Les courbes sont lissées sur 5 mois (*Bruinsma et al.* [2010])

4.2.5 Variabilité interannuelle et régionale du niveau de la mer sur la période 2002-2009 à partir des données d'altimétrie spatiale, des flotteurs Argo et de la gravimétrie spatiale GRACE : résumé de l'article publié dans le journal « Ocean Dynamics »

Introduction et résumé de l'article

Lors de cette étude, nous estimons les différentes contributions de l'élévation du niveau de la mer en moyenne globale mais aussi en variabilité

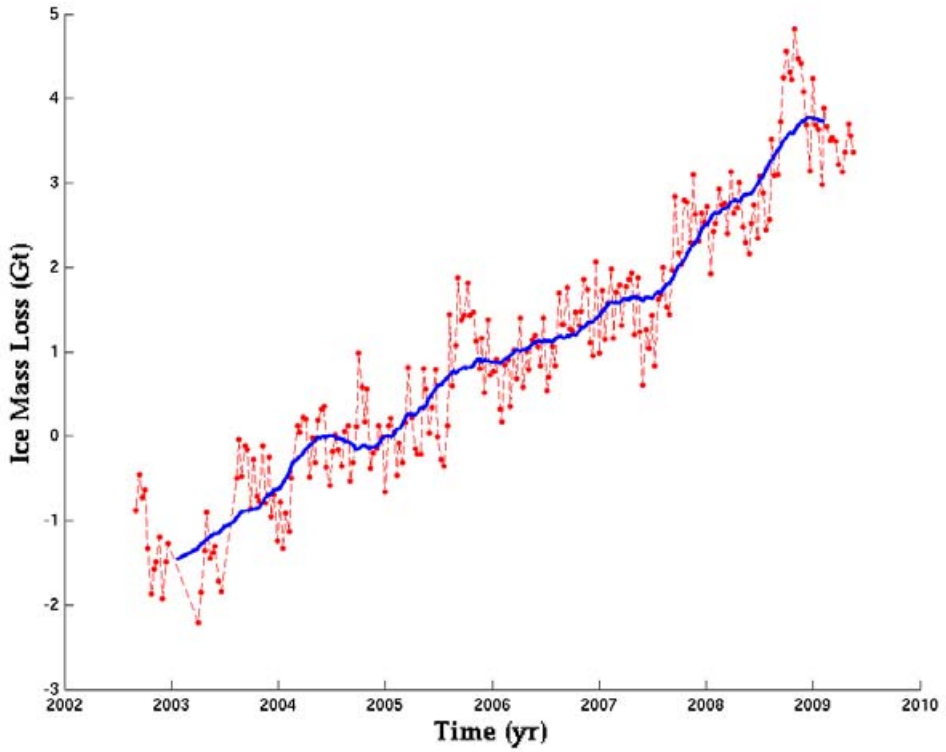

FIG. 4.7 – Série temporelle du gain de masse aux océans dû à la fonte des calottes polaires à partir des données GRACE du GRGS. La courbe rouge représente le signal total et la courbe bleue est filtrée des signaux saisonniers et lissée sur 5 mois (*Bruinsma et al.* [2010])

régionale sur la période 2002-2009. Pour cela, nous analysons le niveau de la mer observé par altimétrie spatiale, le niveau de la mer stérique à l'aide de plusieurs produits basés sur les données Argo (NOAA, CLS, SCRIPPS et IPRC) et enfin, le signal massique des océans déduit des données de la mission spatiale gravimétrique GRACE.

Après la description des données utilisées dans cette étude, nous regardons la variabilité régionale du niveau de la mer observé et stérique puis, du signal massique des océans. Nous nous focalisons tout particulièrement sur l'étude des cartographies régionales des tendances. Un très bon accord entre le niveau de la mer observé et la composante stérique est observé. Par la suite les modes de variabilité du niveau de la mer observé et stérique sont examinés à l'aide d'une analyse en composante principale (EOFs). Dans les deux cas, nous trouvons que le signal El Niño Southern Oscillation (ENSO) explique en

grande partie la variabilité observée, avec notamment un El Nino assez faible en 2006 et un fort épisode La Nina en 2007-2008. Cette variabilité climatique explique en grande partie la variabilité régionale du niveau de la mer observé, par altimétrie spatiale, mais aussi du niveau de la mer stérique déduit des données Argo. Une forte signature des trois événements successifs du dipôle de l'océan Indien (IOD : Indian Ocean Dipole) pour les années 2006, 2007 et 2008 est mise en évidence. L'IOD est un mode de variabilité de l'océan Indien. Les mécanismes de ce phénomène sont les suivant : au cours des mois d'été les alizés, portant normalement vers l'est, ralentissent et se renversent (*Saji et al.* [1999]; *Schott et al.* [2009]) en longeant les côtes d'Indonésie. Ces vents favorisent la remonté de la thermocline et donc d'un « Upwelling » qui va apporter de l'eau froide en subsurface. Les vents vont pousser les eaux de surface qui vont se réchauffer pour s'accumuler dans la partie ouest de l'Océan Indien. Par des phénomènes complexes d'interaction ocean-atmosphère, la circulation atmosphérique en est affectée et va entrainer des inondations en Afrique de l'Est et des sècheresses en Indonésie. Nous utilisons dans cette étude un indice climatique caractérisant ce phénomène : le « Dipole Mode Index » (DMI) défini comme la différence de SST (En anglais, « Sea Surface Temperature ») entre les bassins Tropicaux Ouest (50° E-70° E, 10° S-10° N) et Est (90° E-110° E, 108 S-Equateur) de l'océan Indien. Dans cette partie, la cartographie des tendances du signal massique des océans déduit des données de GRACE est comparée au niveau de la mer observé corrigé de l'effet stérique. Un désaccord entre ces deux estimations est mis en évidence, nous pensons que le rapport signal sur bruit des données GRACE n'est pas assez satifaisant sur les océans pour faire ce genre de comparaison.

Ensuite, le niveau de la mer observé, le niveau de la mer stérique et le signal massique des océans en moyenne globale en terme de tendance et de variabilité interannuelle sont examinés. Puis, nous discutons de la valeur de GIA à appliquer afin de fermer le bilan de la hausse observée du niveau de la mer pour les années récentes.

Ocean Dynamics
DOI 10.1007/s10236-010-0324-0

Regional and interannual variability in sea level over 2002–2009 based on satellite altimetry, Argo float data and GRACE ocean mass

William Llovel · Stéphanie Guinehut · Anny Cazenave

Received: 5 February 2010 / Accepted: 23 July 2010

Abstract In this study, we have estimated the different sea level components (observed sea level from satellite altimetry, steric sea level from in situ hydrography—including Argo profiling floats, and ocean mass from Gravity Recovery and Climate Experiment; GRACE), in terms of regional and interannual variability, over 2002–2009. We compute the steric sea level using different temperature (and salinity) data sets processed by different groups (SCRIPPS, CLS, IPRC, and NOAA) and first focus on the regional variability in steric and altimetry-based sea level. In addition to El Nino–La Nina signatures, the observed and steric sea level data show clear impact of three successive Indian Ocean Dipoles in 2006, 2007, and 2008 in the Indian Ocean. We next study the spatial trend patterns in ocean mass signal by comparing GRACE observations over the oceans with observed minus steric sea level. While in some regions, reasonably good agreement is observed, discrepancy is noticed in some others due to still large regional trend errors in Argo and GRACE data, as well as to a possible (unknown) deep ocean contribution. In terms of global mean, interannual variability in altimetry-based minus steric sea level and GRACE-based ocean mass appear significantly correlated. However, large differences are reported when short-term trends are estimated (using both GRACE and Argo data). This prevents us to draw any clear conclusion on the sea level budget over the recent years from the comparison between altimetry-based, steric sea level, and GRACE-based ocean mass trends, nor does it not allow us to constrain the Glacial Isostatic Adjustment correction to apply to GRACE-based ocean mass term using this observational approach.

Keywords Sea level rise · Satellite altimetry · GRACE · Argo · Steric sea level · Ocean mass

Responsible Editor: Birgit Andrea Klein

W. Llovel (✉) · A. Cazenave
LEGOS/OMP,
14, avenue E. Belin,
31400 Toulouse, France
e-mail: william.llovel@legos.obs-mip.fr

S. Guinehut
CLS,
Ramonville St Agne,
France

1 Introduction

Sea level change is one of the most important consequences of ongoing global warming. Many studies attempted to understand the mechanisms involved in the global and regional sea level variations. According to the Intergovernmental Panel on Climate Change (IPCC) 4th Assessment Report, the observed rate of global mean sea level rise over the 1993–2003 decade is estimated to be 3.1±0.7 mm/year (2-sigma uncertainty), with ~50% (i.e., 1.6±0.5 mm/year—2-sigma uncertainty) attributed to ocean thermal expansion, and ~40% associated with land ice melt (Bindoff et al. 2007). Recent studies have investigated the sea level budget for the past few years (Willis et al. 2008; Cazenave et al. 2009; Leuliette and Miller 2009; Peltier 2009). For the period 2003–2009, the rate of observed sea level rise, estimated by satellite altimetry, amounts to 2.6±0.4 mm/year (Ablain et al. 2009 updated). Over this time span, the steric sea level contribution, essentially estimated from Argo-based ocean temperature and salinity data (Roemmich and Gilson 2009), varies from −0.5±0.5 mm/year from mid-2003 to mid-2007 (Willis et al. 2008) to +0.8±0.8 mm/year over January 2004–December 2007 (Leuliette and Miller 2009), suggesting a pause in ocean thermal expansion (hence, ocean warming) compared to the 1993–2003 decade. This has led to the suggestion that increased land ice melt

Published online: 26 August 2010

would explain the difference between satellite-based and Argo-based steric sea level change (e.g., Cazenave et al. 2009; Peltier 2009; Cazenave and Llovel 2010). Except for a brief discussion in Willis et al. (2008), the above studies essentially looked at global mean changes and did not address the regional variability. Regional variability in sea level was studied for earlier time spans, for example the 1993–2003 period (e.g., Lombard et al. 2005; Bindoff et al. 2007). These studies showed the dominant role of non-uniform thermal expansion change for explaining the spatial patterns in sea level trends, with some contribution from salinity change (e.g., Wunsch et al. 2007; Lombard et al. 2009). At regional scale, circulation change and self-gravitation associated with water mass redistribution at the earth's surface may also produce a regional signature in sea level (e.g., Stammer 2008; Milne et al. 2009). Here, we investigate the regional and interannual variability in sea level over the Argo and Gravity Recovery and Climate Experiment (GRACE) periods (i.e., since 2002/2004). Using Argo-based ocean temperature and salinity data processed by different teams as well as different GRACE-based ocean mass products, we try to separate the steric and mass contributions of altimetry-based regional variability in sea level over the past few years. In a second part of the paper, we look at interannual fluctuations and short-term trends in the global mean sea level using altimetry, Argo, and GRACE observations.

2 Data sets used in this study

2.1 Satellite altimetry-based sea level

Here, we use the Ssalto/duacs products provided by Collecte Localisation Satellite (CLS; http://www.aviso.oceanobs.com/fr/accueil/index.html). This sea level data set is available as $0.25° \times 0.25°$ grids at weekly interval. From January 2002 to December 2008, the whole time span considered in this study, sea level data are principally based on Jason-1 (but also ENVISAT and GFO satellites with lower weight). Geophysical and environmental corrections have been applied, including the inverted barometer correction (see Ablain et al. 2009 for more details).

2.2 Argo-based steric sea level data

Several gridded temperature T and salinity S fields are available from different research teams: SCRIPPS Institution of Oceanography, International Pacific Research Center (IPRC), and National Oceanic and Atmospheric Administration (NOAA). These data sets can be downloaded either from http://www.argo.ucsd.edu/Gridded_Fields.html website for SCRIPPS and IPRC data sets (Roemmich and Gilson 2009; http://apdrc.soest.hawaii.edu/projects/DOT/), or www.nodc.noaa.gov for the NOAA fields. The latter are based on gridded temperature fields from Argo plus other in situ measurements (e.g., XBT, CTD, moorings data, etc.; Levitus et al. 2009) while SCRIPPS and IPRC fields use T and S Argo data only. We also use T and S Argo data processed at CLS (Guinehut et al. 2009).

These temperature and salinity data have passed through several quality control processes (see the Argo quality control manual for more details, Wong et al. 2008). Each team has its own data editing and processing approach, leading to some differences in the final products. For example, Guinehut et al. (2009) compare dynamic height anomalies estimated from Argo and satellite altimetry at collocated points and further delete Argo profiles when discrepancies are noticed between the two types of data. Figure 1a–d shows the coverage of Argo profiles for the month of January of years 2002, 2003, 2004, and 2005, as used to construct the CLS data set. We note large data gaps, especially in the southern hemisphere, for years 2002 and 2003. As of early 2004, the coverage improves significantly and remains quite suitable beyond. SCRIPPS, NOAA, and CLS use an optimal interpolation technique in order to provide T, S gridded fields whereas IPRC applies a variational analysis approach. More details on data, data editing and computational techniques can be found at http://www.argo.ucsd.edu/Gridded_Fields.html and in Guinehut et al. (2009) and Levitus et al. (2009).

We have downloaded the SCRIPPS, IPRC, and CLS data from the Coriolis Global Data Acquisition Center (http://www.coriolis.eu.org), and have computed steric sea level grids using the T/S Argo-based gridded fields, except for the NOAA dataset that provides T data only. To compute the steric sea level, we considered the 0–900 m depth range for SCRIPPS, IPRC, and CLS data (the depth range common to the three datasets; note that Argo profiles exist below 900 m but these are not used in the CLS processing), and the 0–700 m depth range for NOAA data.

The four data sets cover different time spans:

- SCRIPPS: January 2004 to October 2009; data at monthly interval
- IPRC: January 2005 to September 2009; data at monthly interval
- CLS: January 2002 to April 2009; data at monthly interval
- NOAA: January 2002 to September 2009; data at 3-month interval

In the following, we will consider the January 2004–December 2008 time span to compute spatial trend maps (five full years common to the NOAA, SCRIPPS, and CLS data sets) and the January 2004–April 2009 time span for computing an average steric sea level time series (using NOAA, SCRIPPS, and CLS data).

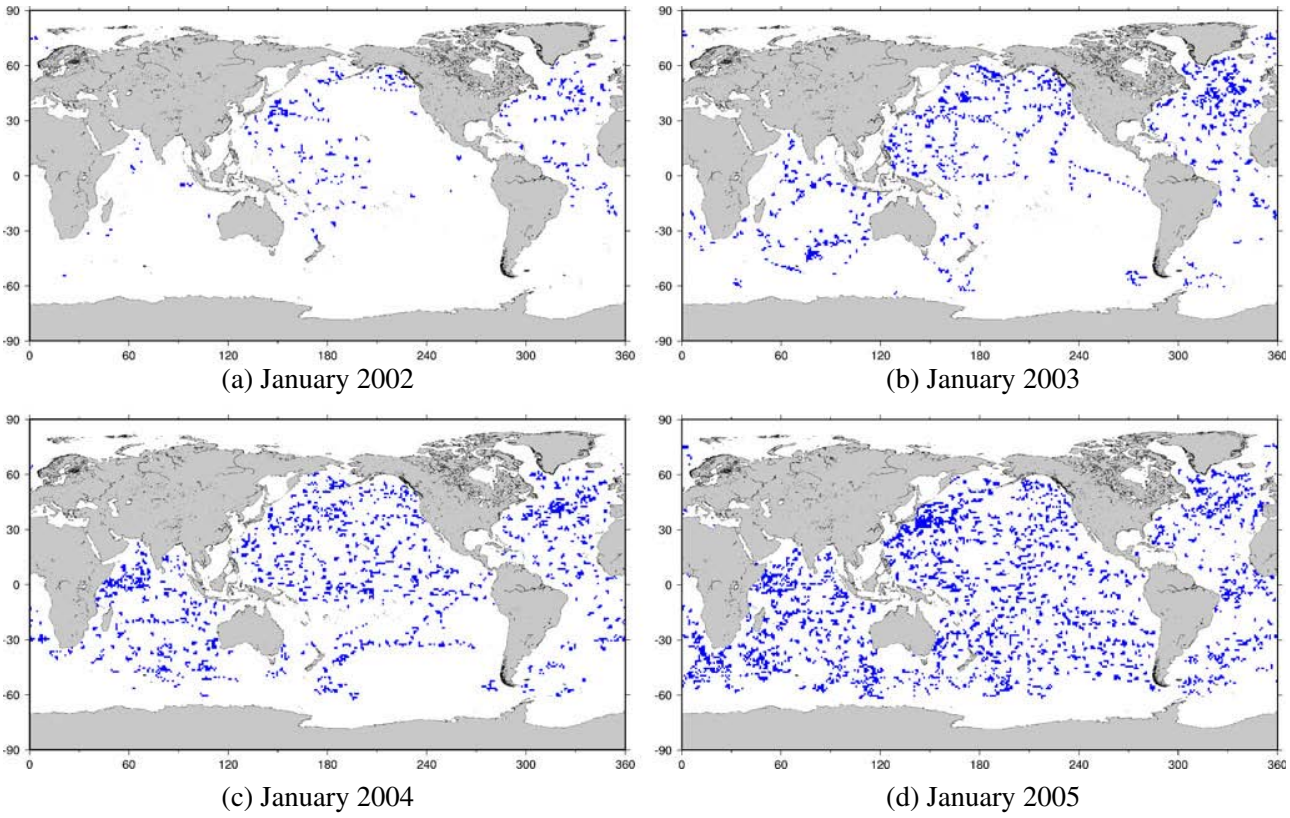

Fig. 1 Argo data distribution as used by Guinehut et al. (2009) for the month of January and years 2002–2005

2.3 GRACE-based ocean mass data

About 7 years of gravity data from the GRACE mission are now available. This satellite mission was launched in March 2002 to measure temporal change of the earth gravity field at monthly interval. On land, GRACE mainly measures change in land water storage while over the oceans GRACE provides variations of the mass of the oceans (Wahr et al. 2004). At regional scale, ocean mass change results from redistribution of sea water by the ocean circulation plus local exchange of water with the atmosphere (through precipitation and evaporation). In terms of global mean, ocean mass change mainly results from water mass exchange with continental reservoirs (including the ice sheets). Several GRACE products have been released from teams involved in the GRACE project (CRS, JPL and GFZ), each time with substantial improvement (Chambers 2006). Other teams (e.g., GRGS, NASA/GSFC) also provide GRACE solutions based on different processing approaches. Here, we use the latest releases (RL04) from two groups: CSR and GFZ solutions (1°×1° ocean grids at monthly interval). This new data set (available at http://grace.jpl.nasa.gov/data/mass/) includes an implementation of the carefully calibrated combination of destripping and smoothing, with different half-width Gaussian filters (the solutions need to be smoothed because errors increase with wavelength; Swenson and Wahr 2002). Compared to earlier products (contaminated by north–south strips due to aliasing by the GRACE coverage of high-frequency signals of atmospheric and oceanic origin), the latest release is less noisy, mostly because of the destripping procedure applied to the data. The gridded ocean GRACE products are corrected for post-glacial rebound (the solid earth response to last deglaciation, also sensed by GRACE) using Paulson et al. (2007) model, and for the leakage due to land hydrology (Chambers 2006). The gridded time series we use in this study are based on the 500-km Gaussian smoothing and cover the following time spans: CRS—August 2002 to February 2009, GFZ—October 2002 to February 2009. GRACE solutions are expressed in terms of equivalent water height. In the following, we consider the average of the GFZ and CSR GRACE products.

3 Regional variability of altimetry-based, steric and altimetry-based minus steric sea level, and GRACE-based ocean mass

In this section, we compare the regional variability of observed sea level (from satellite altimetry), steric sea level, altimetry-based minus steric sea level, and ocean mass from GRACE.

3.1 Altimetry-based spatial patterns

Figure 2 shows the observed sea level trend map over January 2004–December 2008 (this is the time span common to the steric sea level data sets; see Section 2.2). Annual and semiannual signals have been removed at each grid mesh through a least-square adjustment to the data of sinusoids of 12- and 6-month periods. As we focus here on the regional variability, a global mean (uniform) trend of ~2.5 mm/year—the value that best fits the altimetry-based global mean sea level over 2004–2008—has been removed at each grid mesh. The spatial trend patterns in altimetry-based sea level displayed in Fig. 2 are dominated by the strong V-shaped ENSO (El Nino–Southern Oscillation)-related signal in the tropical western Pacific, and a highly negative anomaly along the central equatorial Pacific, probably due to the strong La Nina event in 2007–2008. While of smaller amplitude, a positive sea level trend anomaly affects the Indian Ocean, likely the effect of the three successive positive phases of the Indian Ocean Dipole (IOD) that occurred in 2006, 2007, and 2008 (Saji et al. 1999).

3.2 Steric sea level spatial patterns

Figure 3a–d compares over 2004–2008, spatial trend patterns in steric/thermosteric sea level for the SCRIPPS, IPRC, CLS, and NOAA data (a uniform mean trend is removed in each case using values adjusted over 2004-2008). The four maps roughly display the same spatial patterns in the three main oceans, e.g., the V-shape pattern characteristic of ENSO in the tropical Pacific. However, when looking in detail, important differences are noticed; in particular, when considering the regional trend amplitudes. To illustrate this, Fig. 3e shows the trend difference map

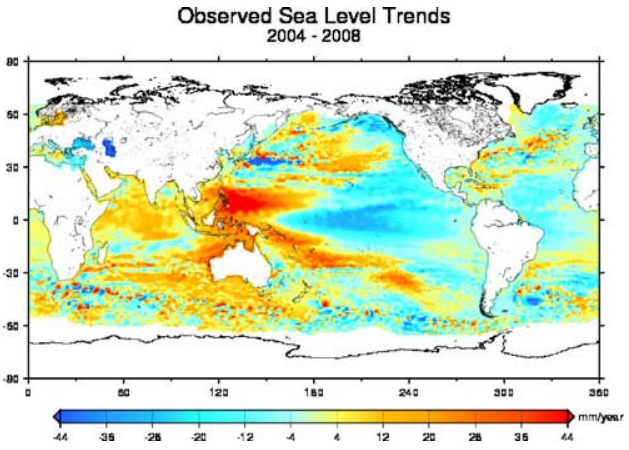

Fig. 2 Spatial trend patterns of observed (altimetry based) sea level (uniform trend removed) over Jan 2004–Dec 2008

between CLS and SCRIPPS. This residual map displays large (>10 mm/year) positive/negative trend differences in many regions (note in particular trend differences associated with the main features of the general circulation), as a result of larger trend values in the CLS map compared to SCRIPPS. It is hard at this stage to favor one data set versus the other. On the other hand, some regional differences noticed in the NOAA trend map compared to the others may result from salinity effects, not included in the latter.

In a recent study, Lyman et al. (2010) investigated the main causes of the large dispersion of the global mean upper ocean heat content (OHC; or equivalently of the thermosteric sea level) time series computed by different teams over the altimetry time span. Comparing eight different OHC time series, they found positive trends for all time series over 1993–2006 (hence, average ocean warming), but with very large dispersion (up to a factor 2–3). All curves flatten out after around 2003 (the beginning of our analysis), but again significant differences are noticed in the year-to-year variability from one curve to another (see Fig. 1 of Lyman et al. 2010). While some curves are rather flat, some others show slight positive trend since 2003. Lyman et al. further explore the causes of the OHC curves scatter. These include differences in data quality control procedure, adopted baseline climatology, corrections for XbT warm bias and other instrumental bias (e.g., Argo), mapping techniques and methods to fill data gaps, removal of the seasonal cycle, etc. This investigation shows that the largest sources of discrepancies arise from XbT bias corrections, with a maximum in years 2000–2002. Since about 2003, the dispersion (hence, uncertainty) decreases but is still significant (between 1×10^{22} and 1.5×10^{22}J, in OHC units) due mainly to differences in sampling procedures. Translated in thermosteric sea level, this gives an uncertainty of ~0.5–0.75 mm.

The regional comparison shown in Fig. 3a–d indicates that differences between data sets are not limited to the global mean interannual variability as reported by Lyman et al. (2010) but also affects the regional patterns, in particular their amplitude. No doubt that the causes (combination of data editing, sampling, mapping, instrumental corrections) are similar.

We averaged the two data sets (SCRIPPS and CLS) over January 2004 to December 2008 to compute a mean trend map (Fig. 4a; a uniform global mean steric trend has been removed). We do not include the NOAA data because salinity is not accounted for, which, at regional scale, could lead to some inconsistency. Comparison with the observed (altimetry based) trend map over the same time span (Fig. 2) shows overall good agreement in the three main oceans. But locally, some discrepancies are noticed. This is illustrated in Fig. 4b which shows the spatial trend difference map (difference

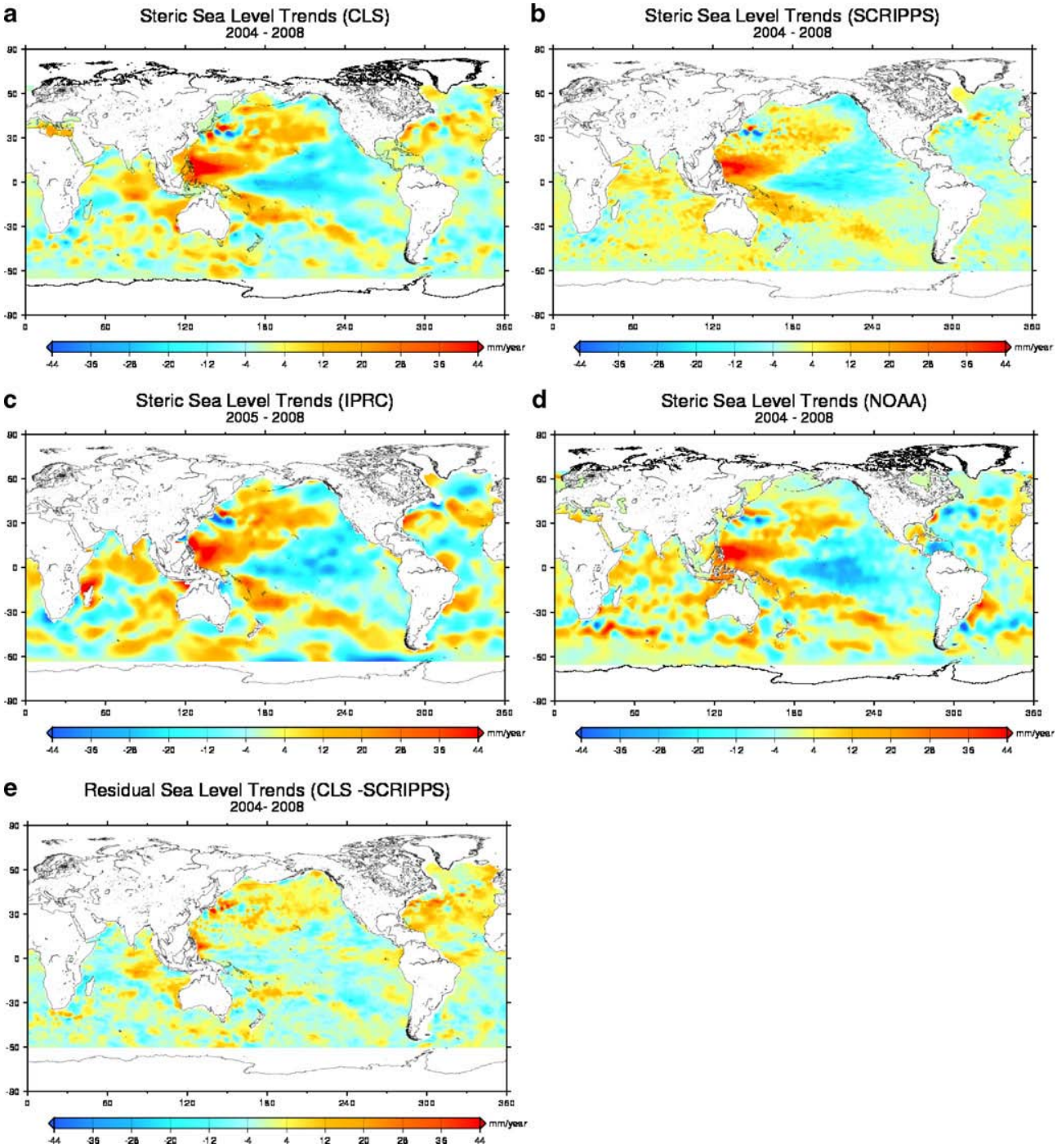

Fig. 3 Spatial trend patterns of steric/thermosteric sea level grids over January 2004–December 2008 for the CLS (**a**), SCRIPPS (**b**), IPRC (**c**), and NOAA (**d**); A uniform mean trend has been removed from each map. Difference trend map between CLS and SCRIPPS (**e**)

between altimetry-based and steric trends). Large positive and negative differences are noticed almost everywhere. These may result from uncertainties in Argo data processing but they could also reveal real signal due to regional ocean mass variations and deep ocean contribution (below 900 m)—see Section 3.4.

3.3 EOF analysis of observed (altimetry based) and steric sea level

We have investigated in more detail the regional variability in altimetry-based and steric sea level by using Empirical Orthogonal Functions (EOFs) analysis (Preisendorfer 1988;

Toumazou and Cretaux 2001). This method extracts the dominant modes of spatial variability of gridded sea level time series and separates the temporal and spatial components of the entire signal. The EOF analysis has been performed over a longer time span (2002–2009) than the shorter common period to all data sets. For that purpose, we use the CLS data set. Figure 5 shows the spatial patterns of EOF modes 1 of observed, altimetry-based (upper panel) and steric (middle panel) sea level (uniform mean trend removed). Similarly, in Fig. 6 are shown EOF modes 2 spatial patterns of observed, altimetry-based (upper panel) and steric (middle panel) sea level. On each figure, the temporal curves are shown in the lower panel (the black and blue curves correspond to observed and steric sea level, respectively). These first EOF modes explain ~8% and ~11% of the total observed and steric sea level variance, respectively, while EOF modes 2 account for ~6% and ~8% of the observed and steric total variance. From Figs. 5 and 6, we note good correlations between EOF modes 1 and 2 of the two signals, both in term of spatial patterns and temporal evolution (correlations of 0.95 and 0.8, respectively). The principal components (temporal curves) of modes 1 display positive peaks in early 2006 and early 2008 and a strongly negative peak in early 2007. On the other hand, principal components of modes 2 display positive peaks in late 2006 and mid-2008, and negative peaks in early 2006 and mid-2007. These features are likely the combined signatures of the 2006 El Nino, the 2007–2008 La Nina in the tropical Pacific (http://www.cpc.noaa.gov/products/analysis_monitoring/ensostuff/ensoyears.shtml) and the successive IOD events in the Indian Ocean. The IOD is an atmosphere–ocean interaction of the coupled climate of the tropical Indian Ocean which typically occurs during September–November (Behera et al. 2008; Schott et al. 2009). A positive IOD event translates into a sea surface temperature east–west dipole with warm/cold anomalies in the western/eastern Indian Ocean (e.g., Saji et al. 1999; Behera et al. 2006). As described in Schott et al. (2009), easterly trade winds create an upwelling off the Indonesian coast. This upwelling brings cold water which fills the eastern part of Indian Ocean, and then triggers a positive IOD event. Usually, a negative IOD follows a positive IOD, producing a quasi biennal oscillation in the IOD variability. In the recent years, anomalous positive IOD events have been reported (e.g., Vinayachandran et al. 2007; Horii et al. 2008; Luo et al. 2008; Behera et al. 2008; Cai et al. 2009): the positive IOD event of 2006 was followed by another positive IOD in 2007. Moreover, the 2007 positive IOD co-occurred during a La Nina event (the cold phase of ENSO), a rather unique situation, as usually, positive IOD are associated with the warm phase of ENSO (El Nino) (Behera et al. 2008). Another positive IOD developed in 2008 (Cai et al. 2009).

EOF modes 2 also show the signature of the IODs in the Indian Ocean, in addition to an El Nino signature in the eastern tropical Pacific, likely a result of the 2005–2007 El Nino events.

To see more clearly the IOD effects on sea level, we performed an EOF analysis over the Indian Ocean only. In Fig. 7 are presented EOF modes 1 of observed and steric sea level in the Indian Ocean. The west–east dipole is well visible on both observed and steric spatial maps. The temporal evolution is dominated by the 2006 IOD and to a lesser extent the 2008 IOD, as indicated by the good correlation of 0.6 between observed sea level mode 1 and the Dipole Mode Index—defined as the sea surface temperature difference between the western equatorial Indian Ocean (50°E–70°E and 10°S–10°N) and the south eastern equatorial Indian Ocean (90°E–110°E and 10°S–

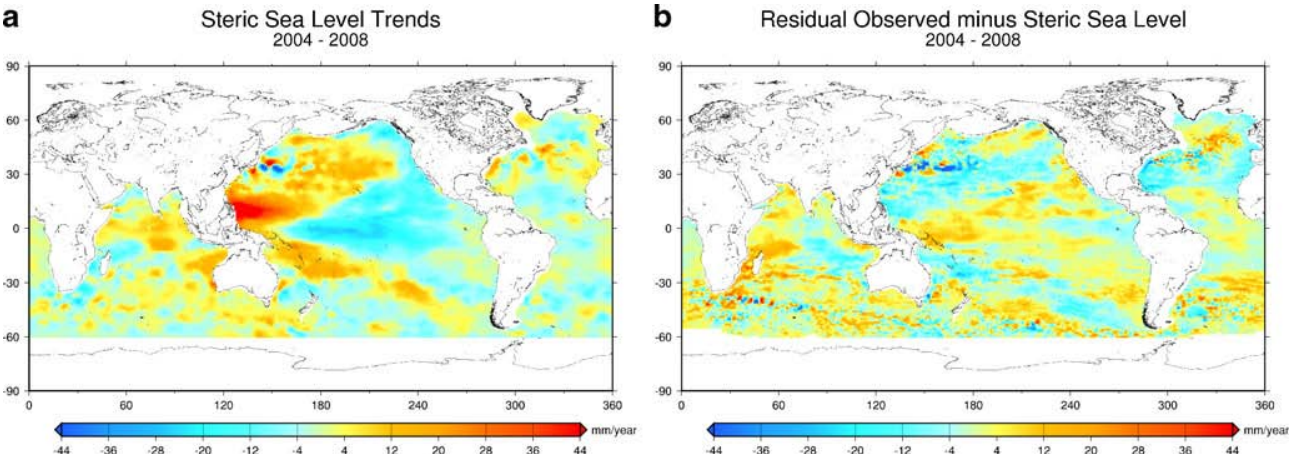

Fig. 4 **a** Spatial trend patterns in steric sea level based on the mean of the SCRIPPS and CLS data (uniform trend removed) over Jan 2002–Dec 2008. **b** Residual spatial trend map computed from the difference between altimetry-based and steric (mean of SCRIPPS and CLS) trend map

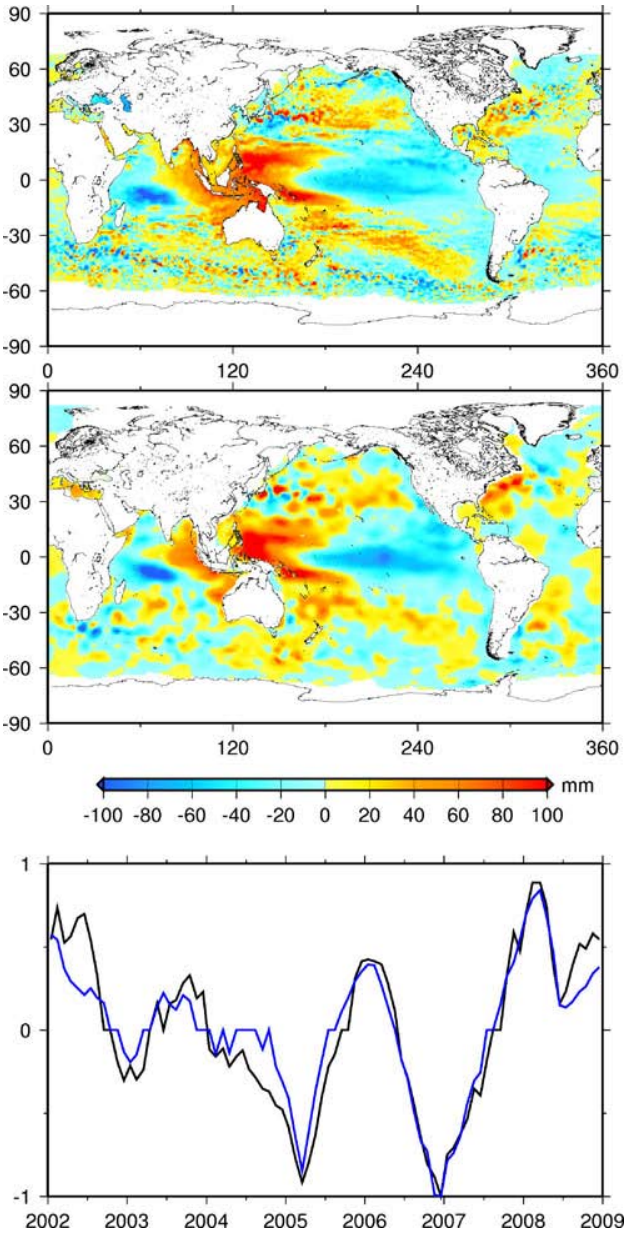

Fig. 5 EOF mode 1 spatial patterns of observed (*upper panel*) and steric–CLS data (*middle panel*) sea level. EOF mode 1 temporal curves (*lower panel*) of observed (*black curve*) and steric sea level (*blue curve*). Explained variances are 8% and 11% for observed and steric mode 1

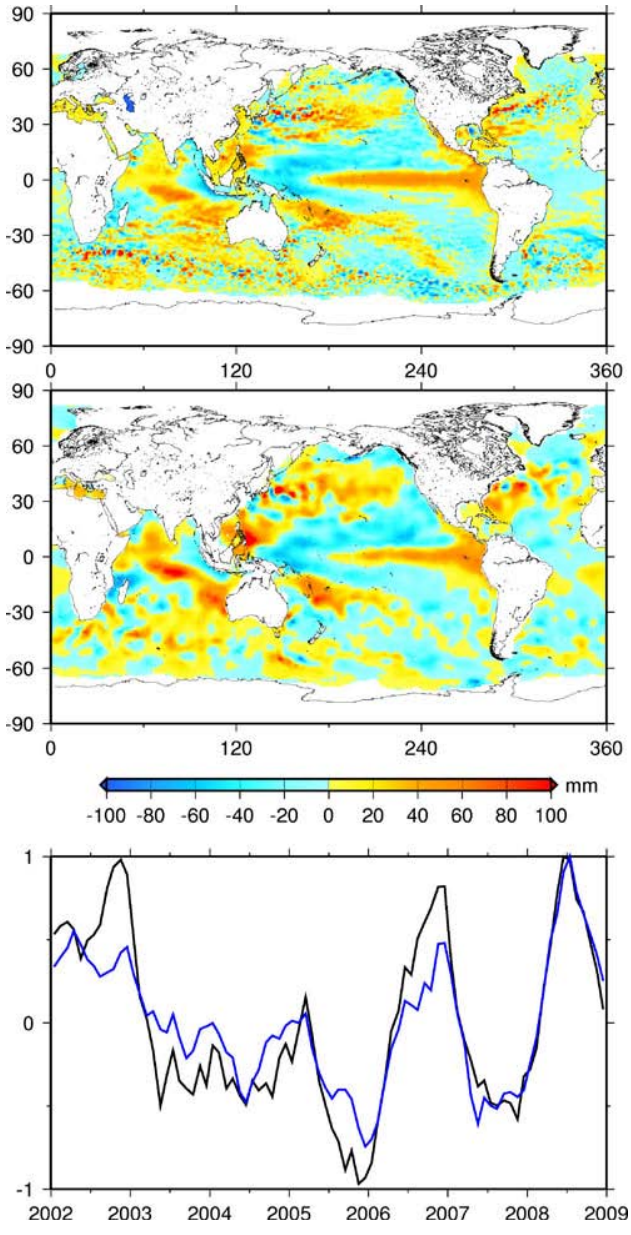

Fig. 6 EOF mode 2 spatial patterns of observed (*upper panel*) and steric–CLS data (*middle panel*) sea level. EOF mode 2 temporal curves (*lower panel*) of observed (*black curve*) and steric sea level (*blue curve*). Explained variances are 6% and 8% for observed and steric mode 2

0°N; Saji et al. 1999). In fact, the 2006 IOD event has larger amplitude than the 2008 one. The 2007 IOD produces a weaker signature in sea level. It is possible that the 2007 IOD produced more superficial temperature changes than the 2006 and 2008 events, hence its fingerprint is less visible in the steric (and observed) sea level which integrates also deeper changes along the water column.

3.4 Regional variability in ocean mass: comparison between altimetry-based minus steric sea level and GRACE-based ocean mass

At interannual time scale, global mean sea level variations can be explained by this equation:

$$\Delta H_{\text{sea level}} = \Delta H_{\text{steric}} + \Delta H_{\text{ocean mass}} \quad (1)$$

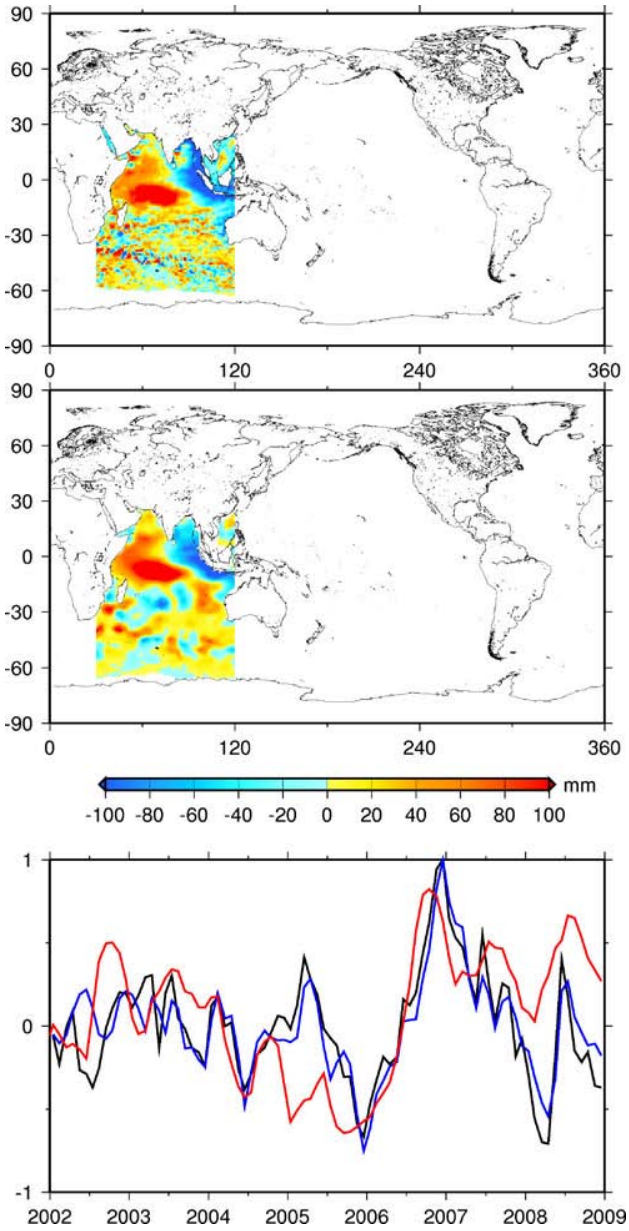

Fig. 7 EOF mode 1 spatial patterns of observed (*upper panel*) and steric–CLS data (*middle panel*) sea level in the Indian Ocean. EOF mode 1 temporal curves (*lower panel*) of observed (*black curve*) and steric sea level (*blue curve*); Dipole Mode Index superimposed (*red curve*). Explained variances are 9% and 16% for observed and steric mode 1

Where $\Delta H_{\text{sea level}}$ is total observed sea level, ΔH_{steric} is the steric component (i.e., the sea level variations due to temperature and salinity variations) and $\Delta H_{\text{ocean mass}}$ is sea level due to inputs and outputs of fresh water. Many studies have attempted to close the global mean sea level budget by comparing altimetry-based sea level trend with the sum of steric sea level and GRACE-based ocean mass trends (Willis et al. 2008; Leuliette and Miller 2009; Cazenave et al. 2009; Peltier 2009). Here, we also compare trends of the three quantities but at regional scale. Spatial trend patterns of GRACE-based ocean mass have been computed over January 2004 to December 2008 from an average the CSR and GFZ solutions. These have been compared to spatial trends in ocean mass deduced—over the same time span—from the difference between altimetry-based and steric sea level (Fig. 8a, b). While we could use here the map shown in Fig. 4b, we prefer to consider a residual trend grid based on differences between altimetry and CSL steric sea level computed at the location of the Argo data. Both grids have been filtered with the same 500-km Gaussian filter and a mean uniform trend has been removed to each grid. Comparing Fig. 8a and b is somewhat disappointing. Whereas in some regions, the two maps correlate well (North and South Atlantic, Northeast Pacific, western Indian Ocean), there is clear discrepancy in the eastern Indian Ocean. But note that in the eastern Indian Ocean, the strong signal seen in the GRACE trend map results from of the Earth crust readjustment after the 2004 Sumatra–Andaman earthquake; Han et al. 2006. The largest discrepancies are seen in the Northwest Pacific Ocean, where GRACE shows a large positive mass anomaly not seen the altimetry-based minus steric sea level. Chambers and Willis (2008) compared ocean bottom pressure inferred from both satellite altimetry minus Argo-based data and GRACE data, and found a good agreement in altimetry minus Argo and GRACE after regionally averaging the data over the North Pacific. However, direct comparison between maps (Fig. 8a and b) is less satisfactory, possibly a result of the low signal to noise ratio in the GRACE ocean data (Chambers 2006). A recent study by Quinn and Ponte (2010) discusses the uncertainty in ocean mass trends from GRACE comparing four different GRACE products (from CSR, GFZ, JPL, and GRGS). The authors investigate both global mean trend and spatial trend pattern differences over 2003–2008. They noticed that global mean ocean mass trends differ by up to 1 mm/year depending on the GRACE products. They investigated the different sources of differences (e.g., data processing and geoid calculation, post-processing corrections such as smoothing, destripping and hydrological leakage, etc.). They found substantial trend differences, larger than associated standard errors. In particular, the trend of the JPL solution departs quite significantly from the others. At regional scale, some common features are seen in the CSR, GFZ, and GRGS solutions, unlike in the JPL solution. Regional trend differences (>10 mm/year) are also reported. Among the causes of the reported discrepancies, differences between computed geoid solutions dominates but post-processing corrections can also lead to

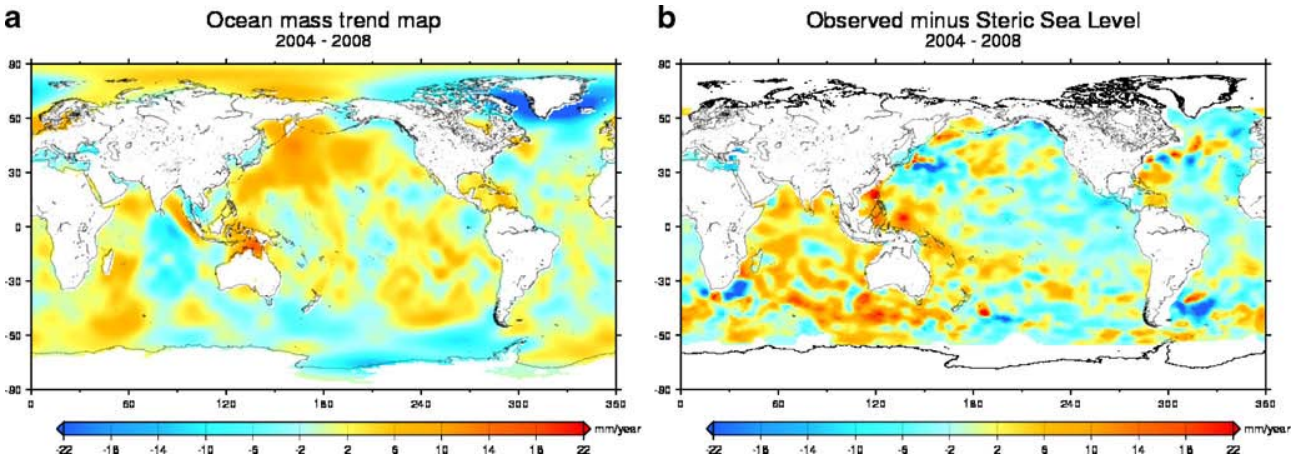

Fig. 8 Ocean mass trend map from GRACE (**a**) and altimetry-based minus steric sea level (**b**) over January 2004 December 2008. This map is based on the differences between observed and steric data at the location of Argo data (uniform mean trend removed from each map)

large trend differences. Globally and regionally, the CSR, GFZ, and GRGS solutions are the closest.

From our results and the study by Quinn and Ponte (2010), we conclude that it is not possible yet to obtain reliable regional trends in ocean mass, neither from GRACE nor from the differences between satellite altimetry and Argo-based sea level. The regional ocean mass signal is significantly lower than the total (observed) - steric regional signal. The important differences noted previously at regional scale between the different Argo data sets (Fig. 3e) certainly mask part of actual ocean mass signal. We cannot exclude, however, that deep ocean steric contribution contaminates the altimetry-based minus steric trend map. But the poor agreement noticed between Figs. 4b and 8b argues rather for still that large errors affecting Argo-based steric regional sea level. As discussed by Quinn and Ponte (2010), regional variability in GRACE ocean mass is also quite noisy, hence ocean mass spatial trend patterns from GRACE and altimetry-based minus steric sea level poorly agree. Hopefully, with the lengthening of the Argo and GRACE time series, the situation should improve in the near future.

4 Global mean observed and steric sea level, and ocean mass: short-term trends and interannual variability

4.1 Global mean steric sea level and ocean mass trends; inference on the short-term sea level budget and the Glacial Isostatic Adjustment correction

We have compared global mean steric/thermosteric sea level time series for the SCRIPPS, IPRC, CLS, and NOAA data. For that purpose, we averaged the gridded data sets over the 65°N and 65°S oceanic domain (with equi-area weighting). The SCRIPPS, IPRC, and CLS time series display a large annual signal of several millimeter amplitude. Because of its 3-month resolution, the NOAA time series has a smaller, smoother annual cycle. Table 1 summarizes amplitude and phase values of the steric annual cycle for the SCRIPPS, IPRC and CLS data. The annual amplitude ranges from 3.5 to 4.7 mm (in good agreement with previous studies; Willis et al. 2008; Leuliette and Miller 2009). Phases are also in good agreement with each other (Table 1). Figure 9a shows the four steric/thermosteric sea level time series (from January 2004 to April 2009) after removing the seasonal signal (12-month and a 6-month period sinusoids have been adjusted to each time series and removed). While the SCRIPPS and IPRC show similar year-to-year oscillations, on the whole, the curves do not really agree well on interannual time scale, as reported by Lyman et al. (2010). From these residual time series (seasonal signal removed), we also computed a mean trend over January 2004–April 2009 for the SCRIPPS, CLS, and NOAA data while for IPRC, the time span considered is January 2005–April 2009.

Table 1 Seasonal cycle amplitude, phase, and trend of steric sea level from different Argo-based and NOAA data computed from least squares fit to the data over their time spans

	Amplitude (mm) 2004–2008	Phase (degree) 2004–2008	Trend (mm/year)
SCRIPPS	4.5±0.3	100.±2.	0.35±0.2 Jan 2004–Apr 2009
IPRC	4.7±0.4	98.±3.	0.19±0.13 Jan. 2005–Apr 2009
CLS	3.5±0.34	95.±2.	0.9±0.1 Jan 2004–Apr 2009
NOAA	NA	NA	−0.1±0.2 Jan 2004–Apr 2009

Error bars 95% confidence interval

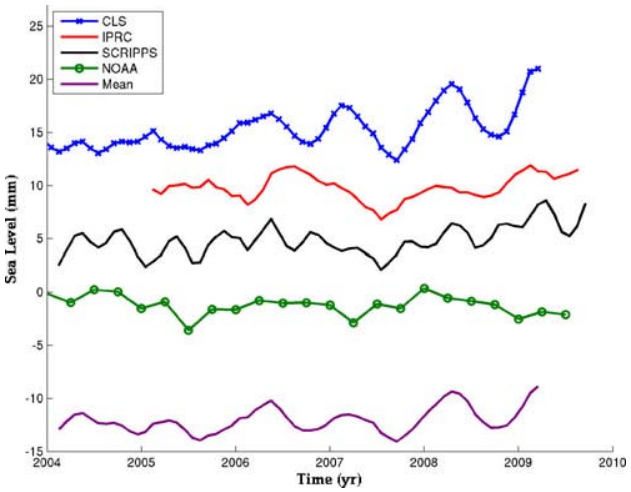

Fig. 9 Global mean steric sea level curves (seasonal signal removed) from CLS (*blue curve*), SCRIPPS (*black curve*) and IPRC (*red curve*) and NOAA (*green curve*) (*left panel*), and mean of SCRIPPS, CLS, and NOAA data (*violet*)

Values are given in Table 1. The CLS trend amounts to 0.9± 0.1 mm/year. The SCRIPPS and IPRC trends are smaller, of only 0.35±0.2 mm/year and 0.19±0.13 mm/year respectively (but note that the IPRC data only begin in 2005). Thermosteric trend based on the NOAA data set is slightly negative and equal to −0.1±0.2 mm/year. Trend differences appear much larger than their quoted standard deviations. For the NOAA data, salinity (not accounted for) can hardly explain the trend difference with the other data, since in terms of global mean, salinity effect on sea level is expected to be small (Wunsch et al. 2007). The main difference with other data comes from the considered depth range (0–700 m instead of 0–900 m) and the inclusion of XbT, CTD, and moorings data. It is worth noticing that the trend difference between NOAA and SCRIPPS is smaller than between CLS and SCRIPPS that only use Argo data. Thus, we conclude from this comparison that global mean steric trends estimated over the 5-year period (January 2004–April 2009) are still uncertain by several tenth of millimeter/year. We have averaged the NOAA, SCRIPPS and CLS time series over their overlapping period (January 2004 to April 2009; Fig. 9b; IPRC data not included). The mean trend of this curve amounts to 0.4±0.5 mm/year. The 0.5 mm/year uncertainty is computed from the deviation of individual trends to the mean. In view of the large uncertainty of the mean trend and according to Lyman et al. (2010) study, the large dispersion seen between the different Argo data sets at interannual time scale suggests that the steric sea level trend based on averaged NOAA, SCRIPPS and CLS data, as reported above, is probably not statistically significant.

We now examine the sea level budget in terms of 'short term trend' over the last few years. For that purpose, we compare altimetry-based sea level rise, steric sea level, and ocean mass trends. When doing this, we have to account for the post-glacial rebound effect, also called Glacial Isostatic Adjustment (GIA). GIA is the response of the Earth to the last deglaciation event of the Late Quaternary ice-age (Paulson et al. 2007; Peltier 2009; Milne et al. 2009). It affects estimates of the global mean sea level by satellite altimetry and ocean mass by GRACE, producing secular effects that need to be corrected for if one is interested in computing trends (Peltier 2009). On the altimetry-based rate of sea level rise, the GIA correction amounts to −0.3 mm/year (Peltier 2009). On globally averaged GRACE-based ocean mass trend, the correction is larger, in the range ∼−1 to −2 mm/year depending on which GIA model is adopted, which oceanic domain is considered for averaging (i.e., ±90° or ±65° latitude) and which smoothing is applied. For example, over the ±65° latitude domain and with a 500-km Gaussian smoothing, the GIA correction to GRACE ocean mass trend equals −1.2 mm/year and −1.9 mm/year for the Paulson et al. (2007) and Peltier (2009) models, respectively. Note that the Paulson et al. correction quoted here is that modified by Chambers et al. (2010) to account for the rotational feedback.

Instead of choosing one particular GIA model correction, we get around the problem and compare trends of altimetry-based sea level, steric sea level and GRACE-based ocean mass (without the GIA correction), then derive a range for the GIA correction to apply to GRACE ocean mass term. For the period January 2004–April 2009, the altimetry-based and steric sea level trends amount to 2.5±0.4 mm/year (the −0.3 mm/year GIA correction is accounted for) and 0.4±0.5 mm/year, respectively. The difference between observed sea level and upper ocean steric trends (2.1± 0.65 mm/year) consists of total ocean mass term (GIA correction included) and deep ocean contribution (plus errors of each estimate). In effect, the computed steric trend does not account for a possible contribution from the deep ocean as it concerns the upper 900 m of the ocean only. If one assumes, as in Antonov et al. (2005), that the deep ocean contribution is about 30% of the upper ocean steric effect, the total steric effect may be on the order of 0.5 mm/year, leading to a total ocean mass term of about 2.0± 0.65 mm/year. We can now compare this value with the direct mass trend estimate from GRACE. The GRACE data over the ocean available from the GRACE website are already corrected for the Paulson et al. GIA correction. Thus, we first remove it when computing the GRACE-based ocean mass trend, using the GIA data available from the GRACE website (note that another option would have been to estimate a deviation to the Paulson et al.'s GIA correction). The mean GRACE-based ocean mass trend (data averaged between ±65° latitude, no GIA correction applied) amounts to −0.3±0.2 mm/year between January

2004 and April 2009. Comparing this value with observed minus total steric sea level trend (~2 mm/year) leads to a GIA correction on the order of 2.3 mm/year. However, the uncertainty associated with this value is quite large. The GRACE ocean mass trend error (0.2 mm/year) is likely underestimated. According to Quinn and Ponte (2010), a more reasonable value is 0.5 mm/year. A quadratic combination of the GRACE and altimetry minus steric trend uncertainties leads to a more realistic error of 0.8 mm/year for the estimated ocean mass GIA correction. In view of the uncertainty on the deep ocean contribution to the steric trend, a more likely uncertainty for this GIA correction is around 1 mm/year. It is thus clear that the method described above is not still able to constrain the GIA ocean mass term. The largest source of errors comes from Argo-based steric trend estimates and unknown deep ocean contribution. A recent study by von Schuckmann et al. (2009) estimates to 1.01±0.13 mm/year the steric trend (over 2003–2008) for the upper 2000 m of the ocean for this correction. This is twice the value we have used here. A larger steric contribution would reduce the derived ocean mass GIA correction (to around 1.8 mm/year for the von Schuckmann et al.' steric estimate).

4.2 Interannual variability in global mean ocean mass

In this section, we examine the interannual variability of the GRACE-based global averaged ocean mass between January 2004 and February 2009 and compare it with observed sea level minus steric effects.

In Fig. 10, the mean GRACE-based ocean mass curve is superimposed to the difference between observed global mean sea level and steric effects (mean of SCRIPPS, CLS, and NOAA data as computed previously). The two curves have been detrended over the considered time span and the seasonal signal has been removed. As we can see, ocean mass inferred from the difference between altimetry-based global mean sea level and steric effects do not perfectly agree but at least phasing is good except in 2008 where the two curves are in phase opposition. The correlation between GRACE-based ocean mass and observed minus steric sea level is equal to 0.51.

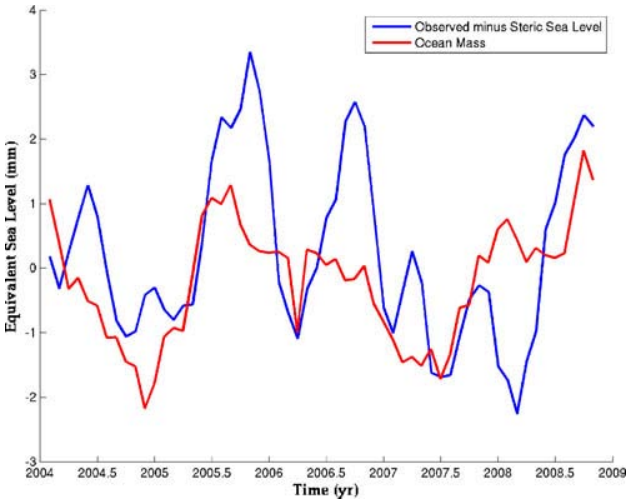

Fig. 10 Global mean ocean mass based on: GRACE (*red curve*); observed (altimetry-based) minus steric sea level—mean of SCRIPPS, CLS, and NOAA data (*blue curve*). Both curves are detrended

5 Conclusion

In this study, we have estimated the different components of the sea level variations both in term of regional variability and global mean over the recent years: ocean mass change and steric/thermosteric sea level by combining remote sensing (satellite altimetry and space gravimetry) and in situ data (four different Argo data sets). The different steric estimates provided by SCRIPPS, CLS, and IPRC groups agree well at the seasonal time scale both in amplitude and phase. Nevertheless, we note important discrepancy in trend estimates. On the other hand, the regional patterns generally agree even if amplitudes are smaller in SCRIPPS data. This suggests that additional efforts are needed in processing Argo data to provide consensus results.

We also noticed poor agreement in the regional variability in ocean mass estimated by GRACE data (direct estimation) and by the difference between observed and steric sea level (indirect estimation). While the cause of this discrepancy remains unclear, it may result from combined effects of sparse Argo coverage in some regions, uncertainties arising from the Argo data processing, (unknown) deep ocean contribution, and low GRACE signal-to-noise ratio over the oceans. However, when averaging the data over the oceanic domain, significant (>0.5) correlation is found at the interannual time scale between GRACE ocean mass and observed minus steric sea level. Another conclusion of this study concerns the GIA correction that needs to be applied to the GRACE-based ocean mass trend. To close the sea level budget by comparing altimetry-based rate of sea level rise with steric and GRACE-based ocean mass trends, a GIA correction close to −2 mm/year is inferred for the GRACE ocean mass term. However, associated uncertainty is estimated to 1 mm/year. Thus, the method developed here is not yet able to constrain this correction. This prevents us to prefer one model versus the other. Still important differences in Argo-based steric sea level and GRACE-based ocean mass trends computed with data processed by different groups are reported, in agreement with two recently published studies by Lyman et al. (2010) and Quinn and Ponte (2010). As time series lengthen, the approach developed in this study may become

more reliable and more decisive conclusions will follow, either to explain the regional variability or to close the sea level budget.

Acknowledgments We thank 2 anonymous reviewers for very useful comments. William Llovel PhD grant is supported by CNRS and Region Midi- Pyrenees. GRACE data were processed by D. P. Chambers, supported by the NASA Earth Science REASoN GRACE Project, and are available at http://grace.jpl.nasa.gov. The Argo data were collected and made freely available by the international Argo project (http://www.argo.ucsd.edu). The altimeter products were produced by SSALTO/DUACS and distributed by AVISO with support from CNES.

References

Ablain M, Cazenave A, Valladeau G, Guinehut S (2009) A new assessment of the error budget of global mean sea level rate estimated by satellite altimetry over 1993–2008. Ocean Sci 5:193–201

Antonov JI, Levitus S, Boyer TP (2005) Thermosteric sea level rise, 1955–2003. Geophys Res Lett 32:L12602. doi:10.1029/2005GL023112

Behera SK, Luo JJ, Masson S, Rao SA, Sakum H, Yamagata T (2006) A CGCM study on the interaction between IOD and ENSO. J Climate 19(9):1688–1705

Behera SK, Luo J-J, Yamagata T (2008) Unusual IOD event of 2007. Geophys Res Lett 35:L14S11. doi:10.1029/2008GL034122

Bindoff N, Willebrand J, Artale V, Cazenave A, Gregory J, Gulev S, Hanawa K, Le Quéré C, Levitus S, Nojiri Y, Shum CK, Talley L, Unnikrishnan A (2007) Observations: oceanic climate and sea level. In: Solomon S, Qin D, Manning M, Chen Z, Marquis M, Averyt KB, Tignor M, Miller HL (eds) Climate change 2007: the physical science basis. Contribution of Working Group I to the Fourth Assessment report of the Intergovernmental Panel on Climate Change. Cambridge University Press, Cambridge

Cai W, Pan A, Roemmich D, Cowan T, Guo X (2009) Argo profiles a rare occurrence of three consecutive positive Indian Ocean Dipole events, 2006–2008. Geophys Res Lett 36:L08701. doi:10.1029/2008GL037038

Cazenave A, Llovel W (2010) Contemporary sea level rise. Annu Rev Mar Sci 2:145–173. doi:10.1146/annurev-marine-120308-081105

Cazenave A, Dominh K, Guinehut S, Berthier E, Llovel W, Ramillien G, Ablain M, Larnicol G (2009) Sea level budget over 2003–2008: a reevaluation from GRACE space gravimetry, satellite altimetry and Argo. Glob Planet Change 65:83–88

Chambers DP (2006) Evaluation of new GRACE time–variable gravity data over the ocean. Geophys Res Lett 33(17):LI7603. doi:10.1029/2006GL027296

Chambers DP, Willis JK (2008) Analysis of large-scale ocean bottom pressure variability in the North Pacific. J Geophys Res 113: C11003. doi:10.1029/2008JC004930

Chambers DP, Whar J, Tamisiea ME, Nerem RS (2010) Ocean mass from GRACE and glacial isostatic adjustment (in press)

Guinehut S, Coatanoan C, Dhomps AL, Le Traon PY, Larnicol G (2009) On the use of satellite altimeter data in argo quality control. Journal of Atmospheric and Oceanic Technology 26 (2):395–402. doi:10.1175/2008JTECHO648.1

Han SC, Shum CK, Bevis M, Ji C, Kuo CY (2006) Crustal dilatation observed by GRACE after the 2004 Sumatra–Andaman earthquake. Science 313(5787):658–662

Horii T, Hase H, Ueki I, Masumoto Y (2008) Oceanic precondition and evolution of the 2006 Indian Ocean Dipole. Geophys Res Lett 35(3):L03607. doi:10.1029/2007GL032464

Leuliette EW, Miller L (2009) Closing the sea level rise budget with altimetry, Argo, and GRACE. Geophys Res Lett 36:L04608. doi:10.1029/2008GL036010

Levitus S, Antonov JI, Boyer TP, Locarnini RA, Garcia HE, Mishonov AV (2009) Global ocean heat content 1955–2008 in light of recently revealed instrumentation problems. Geophys Res Lett 36:L07608. doi:10.1029/2008GL037155

Lombard A, Cazenave A, Le Traon PY, Ishii M (2005) Contribution of thermal expansion to present-day sea-level change revisited. Glob Planet Change 47(1):1–16. doi:10.1016/j.gloplacha.2004.11.016

Lombard A, Garric G, Penduff T (2009) Regional patterns of observed sea level change: insights from a 1/4A degrees global ocean/sea-ice hindcast. Ocean Dyn 59(3):433–449

Luo JJ, Behera S, Masumoto Y, Sakuma H (2008) Successful prediction of the consecutive IOD in 2006 and 2007. Geophys Res Lett 35(4):L14S02. doi:10.1029/2007GL032793

Lyman JM, Godd SA, Gouretski VV, Ishii M, Johnson GC, Palmer MD, Smith DM, Willis JK (2010) Robust warming of the global upper ocean. Nature 465:334–337. doi:10.1038/nature09043

Milne GA, Gehrels WR, Hughes CW, Tamisiea ME (2009) Identifying the causes of sea-level change. Nat Geosci 2(7):471–478. doi:10.1038/ngeo544

Paulson A, Zhong S, Wahr J (2007) Inference of mantle viscosity from GRACE and relative sea level data. Geophys J Int 171(2):497–508

Quinn KJ, Ponte RM (2010) Uncertainty in ocean mass trends from GRACE. Geophys J Int 181:762–768. doi:10.1111/j.1365-246X.2010.04508x

Peltier WR (2009) Closure of the budget of global sea level rise over the GRACE era: the importance and magnitudes of the required corrections for global glacial isostatic adjustment. Quatern Sci Rev 28:17–18

Preisendorfer RW (1988) Principal component analysis in meteorology and oceanography. Developments in Atmospheric Science, vol. 17. Elsevier. pp 425

Roemmich D, Gilson J (2009) The 2004–2008 mean and annual cycle of temperature, salinity and steric height in the global ocean from the Argo program. Prog Oceanogr 82:81–100

Saji NH, Goswami BN, Inayachandran BN, Yamagata T (1999) A dipole mode in the tropical Indian Ocean. Nature 401:360–363

Schott FA, Shang-Ping X, McCreary P (2009) Indian ocean circulation and climate variability. Rev Geophys 47:RG1002

Stammer D (2008) Response of the global ocean to Greenland and Antarctic ice melting. J Geophys Res 113(06):C06022

Swenson S, Wahr J (2002) Methods for inferring regional surface mass anomalies from Gravity Recovery and Climate Experiment (GRACE) measurements of time–variable gravity. J Geophys Res 107(B9):2193. doi:10.1029/2001JB000576

Toumazou V, Cretaux JF (2001) Using a Lanczos eigensolver in the computation of empirical orthogonal functions. Mon Weather Rev 129:1243–1250

Vinayachandran PN, Kurian J, Neema CP (2007) Indian Ocean response to anomalous conditions in 2006. Geophys Res Lett 34 (5):L15602

von Schuckmann K, Gaillard F, Le Traon PY (2009) Global hydrographic variability patterns during 2003–2008. J Geophys Res. doi:10.1029/2008JC005237

Wahr J, Swenson S, Zlotnicki V, Velicogna I (2004) Time–variable gravity from GRACE: first results. Geophys Res Lett 31:L11501. doi:10.1029/2004GL019779

Wong APS, et al. (2008) Argo quality control manual, version 2.31. Ar-um-04-01, pp 33

Willis JK, Chambers DP, Nerem RS (2008) Assessing the globally averaged sea level budget on seasonal to interannual timescales. J Geophys Res 113:C06015. doi:10.1029/2007JC004517

Wunsch C, Ponte RM, Heimbach P (2007) Decadal trends in sea level patterns: 1993–2004. J Clim. doi:10.1175/2007JCLI1840.1

4.3 La contribution des eaux continentales

4.3.1 Généralités

L'autre grand phénomène induisant des variations actuelles du niveau moyen de la mer concerne les échanges d'eau entre les océans et les réservoirs continentaux. Sur Terre, l'eau s'échange selon un cycle complexe entre les océans, l'atmosphère et les continents (cf. figure 4.8). Le cycle terrestre de l'eau peut être défini par l'équation suivante (d'après *Chen et al.* [1998]; *Minster et al.* [1999]) :

$$\Delta M_{Oceans} + \Delta M_{Atmosphere} + \Delta M_{Continents} = 0 \tag{4.1}$$

L'équation 4.1 traduit la conservation de la masse d'eau du système Terre. La durée de séjour de l'eau dans l'atmosphère est d'environ une à deux semaines. Aux échelles de temps qui nous intéressent, allant du mois à l'année, cette contribution peut être négligée. L'équation 4.1 devient donc :

$$\Delta M_{Oceans} = -\Delta M_{Continents} \tag{4.2}$$

Ce cycle joue un rôle dominant dans les processus physiques qui influent sur le climat terrestre et ses changements dans le temps. Les redistributions de masses d'eau s'effectuent via des échanges de masse et d'énergie (par précipitation, évapotranspiration et transfert dans les réseaux hydrographiques) ou par gravité (ruissellement). Ces redistributions de masse d'eau affectent les circulations globales de l'atmosphère et des océans. De plus, l'intensité de ces redistributions est fortement corrélée aux événements climatiques tels qu'El Nino et La Nina, les sécheresses extrêmes et les inondations, événements orageux saisonniers (IPCC, 2007).

A l'échelle d'un bassin versant, le changement du stock d'eau terrestre (Terrestrial Water Storage, TWS), étant une composante majeure du cycle de l'eau, se définit comme la variation de l'eau contenue dans le sol, les réservoirs de surface, le manteau neigeux, la végétation, les aquifères et les nappes phréatiques. La figure 4.9 schématise ces différents réservoirs.

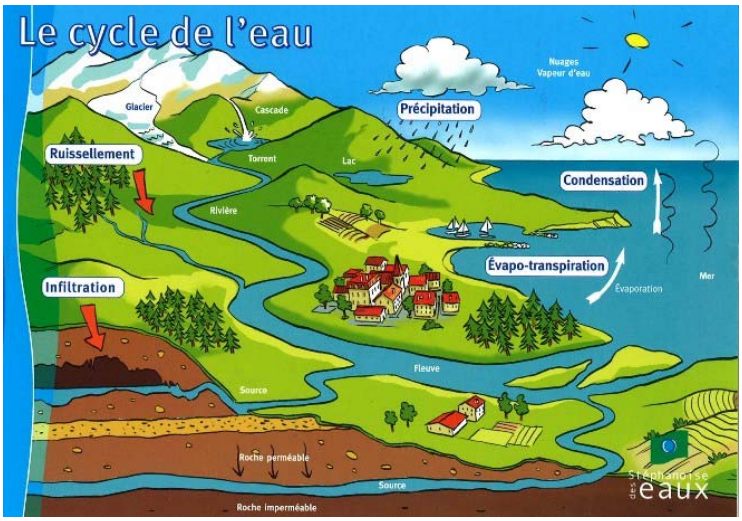

FIG. 4.8 – Cycle global de l'eau

Cette quantité est liée au bilan entre les précipitations (P), l'évapotranspiration (ET) et le ruissellement (R) sur une zone ou un bassin donnés via l'équation du bilan du stock d'eau :

$$\frac{\mathrm{d}(TWS)}{\mathrm{d}t} = P - ET - R \tag{4.3}$$

Les variations des stocks d'eau sur les continents, dûes à la variabilité climatique ou bien aux activités humaines, contribuent de façon directe aux variations du niveau marin. Hélas, jusqu'à présent, cette contribution était extrêmement difficile à estimer globalement à cause du manque de mesures *in situ*. Ainsi, les seules estimations possibles jusqu'ici étaient basées sur des modèles numériques d'hydrologie continentale développés initialement pour les études de climat, calculant les échanges de masse et d'énergie entre la surface et la basse atmosphère en réponse au forçage par les précipitations. Ces modèles estiment aussi les changements du stock d'eau dans les différents réservoirs.

De récentes études montrent que les variations du stock d'eau du sol dûes à la variabilité climatique naturelle ne présentent pas de tendance à long terme pour les dernières décennies. Néanmoins, ces études montrent des fluctuations

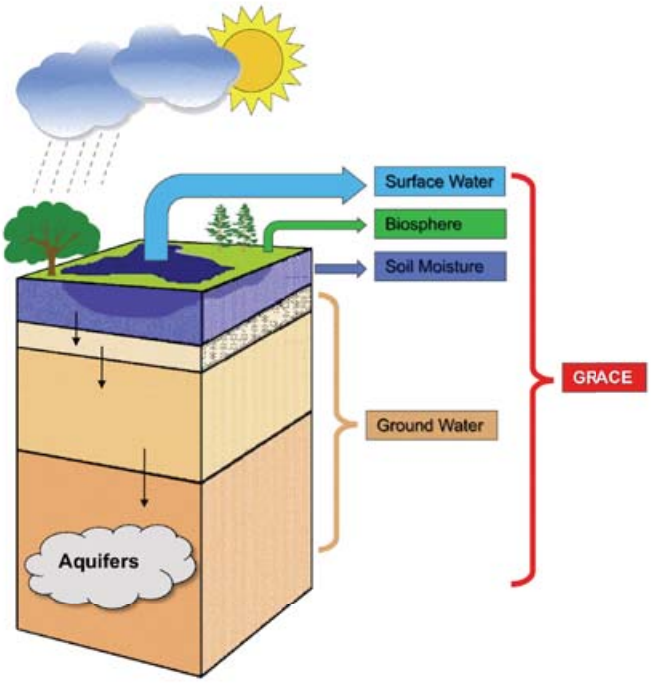

FIG. 4.9 – Réservoirs continentaux du stock d'eau terrestre (source LEGOS).

interannuelles à décennales significatives de l'ordre de quelques millimètres en équivalent niveau de la mer (*Milly et al.* [2003]; *Ngo-Duc et al.* [2005]).

Les activités humaines ont un impact direct sur les variations du stock d'eaux continentales et affectent directement le niveau de la mer. Les contributions les plus importantes proviennent du pompage des eaux souterraines, pour l'agriculture, l'industrie ou bien les usages domestiques (*Huntington* [2008]). Cet effet est incertain mais estimé à +0.3 mm/an (*Church et al.* [2010]).

Un autre effet est celui lié à la construction de barrages sur les fleuves et la rétention de l'eau dans ces réservoirs. Une étude récente estime à -0.55 mm/an la baisse associée au niveau moyen global des mers dûe à l'eau stockée dans plus de 30 000 barrages (*Chao et al.* [2008]).

Depuis 2002, avec l'apport de la mission spatiale GRACE, les variations des stocks d'eau peuvent être maintenant mesurées à grande échelle et en global. Nous allons maintenant analyser le signal des eaux continentales sur les 33

plus grands bassins hydrologiques de la planète et la contribution de ce signal au niveau moyen global de la mer.

4.3.2 Les années récentes : La contribution des eaux continentales en moyenne globale à la hausse du niveau de la mer sur la période 2002-2009 : article publié dans le journal « Comptes rendus de l'Académie des Sciences »

Introduction et résumé de l'article

Au cours de cette étude, la variation des stocks d'eau dans les principaux réservoirs continentaux sur le niveau de la mer est estimée grâce aux données de la mission spatiale gravimétrique GRACE sur la période d'août 2002 à juillet 2009. On considère ici les 31 plus grands bassins hydrologiques du monde et les bassins des mers d'Aral et de la Caspienne (d'après la cartographie mondiale réalisée par *Oki and Sud* [1998]). Sur cette période d'étude, nous trouvons que le bassin de l'Amazone tend à stocker de l'eau dans son bassin hydrologique et, ce stock d'eau est très proche du signal total du stock d'eaux continentales. Ceci est principalement dû à deux épisodes très humides en 2006 et 2008. Ces épisodes ont suivi une forte sècheresse en 2005 d'où un très fort contraste sur la période considérée. D'autres bassins hydrologiques ont une tendance positive sur la période d'étude. C'est le cas par exemple des bassins de la Lena, du Yenisey ou bien de l'Ob. A l'inverse, d'autres bassins ont tendance à perdre de l'eau en particulier le Mississippi et le Gange-Brahmapoutre (voir figure 5 de l'article). Néanmoins, la tendance globale de ces 33 bassins hydrologiques est positive et ce stock d'eaux continentales compte pour 80 +/- 27 km^3/an. Exprimée en équivalent niveau de la mer, celà correspond à une tendance négative de l'ordre de -0.22 +/- 0.05 mm/an. Cette contribution est faible cependant, elle confirme les estimations faites à partir de modèles numériques (*Milly et al.* [2003]; *Ngo-Duc et al.* [2005]; *Church et al.* [2010]). Pour la plupart des bassins, sauf pour les bassins de la Lena et du Yenissei, le signal est dominé par de la variabilité interannuelle.

Dernièrement, nous avons réalisé le même travail avec les produits fournis par le GRGS (*Bruinsma et al.* [2010]). L'histogramme suivant résume les tendances pour les 33 bassins hydrologiques considérés à partir des données du GRGS et avec la moyenne des trois solutions calculées par *Chambers* [2006]. Les données du GRGS ont été corrigées du rebond post-glaciaire (correction de

Paulson et al. [2007]) comme c'est le cas avec les données du CSR, GFZ et du JPL (*Chambers* [2006]). Les deux estimations sont assez cohérentes. En effet, ces résultats montrent que le bassin de l'Amazone domine le signal total du stock d'eaux continentales. De plus, le comportement général des bassins est *quasi* identique en terme de stockage ou de diminution du stock d'eau. Cependant, les estimations des tendances sont assez différentes dans certains cas. En général, les estimations réalisées à partir des données du GRGS sont plus importantes en valeurs absolues. Ce constat est probablement dû au filtrage utilisé lors du traitement des données réalisé par *Chambers* [2006].

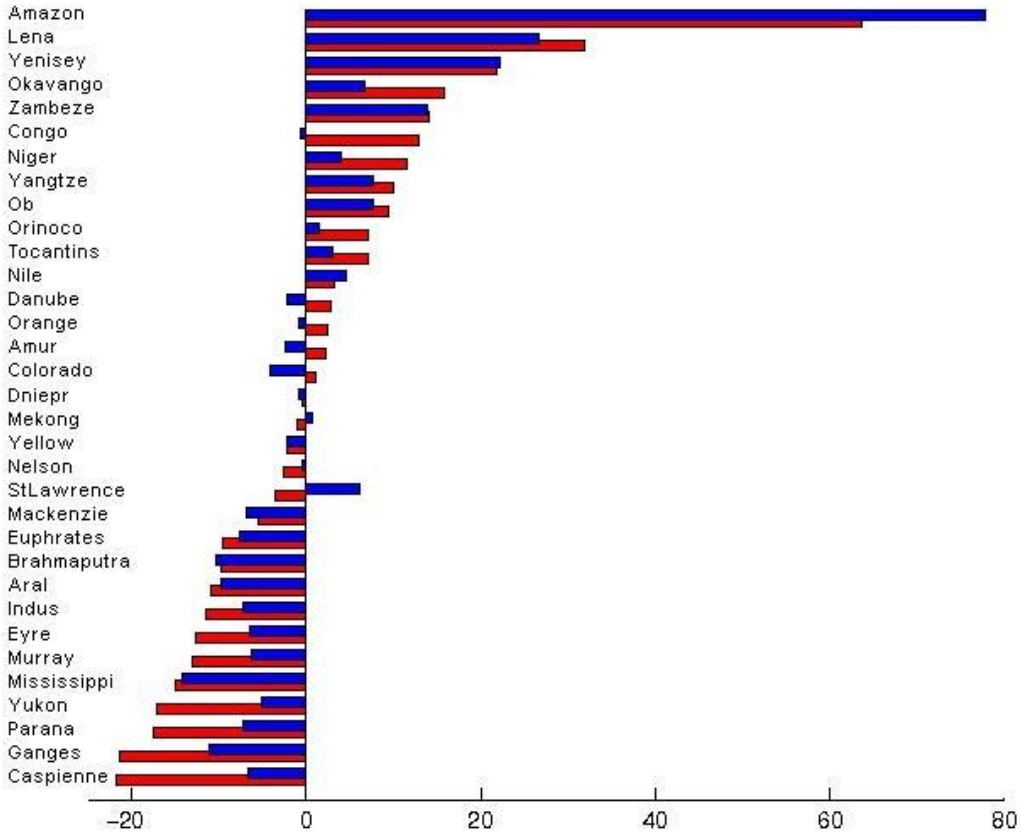

Fig. 4.10 – Histogrammes des tendances des 33 bassins hydrologiques réalisés à partir des données du GRGS (histogramme rouge, *Bruinsma et al.* [2010]) et de la moyenne des données du GFZ, CSR et JPL (histogramme bleu, *Chambers* [2006]).

En sommant les contributions de chaque bassin, nous trouvons que les bassins hydrologiques ont tendance à stocker de l'eau entre 2002 et 2009 à partir des données du GRGS. Ce résultat est similaire à notre précédente étude (*Llovel et al.* [2010a]). En effet, lors de cette étude, nous estimons une tendance à

stocker de l'eau à hauteur de + 80.6 +/- 15.7 km^3/an. Avec les produits fournis par le GRGS, nous trouvons une contribution du même ordre de grandeur et de l'ordre de 42.9 +/- 9.4 km^3/an. En équivalent niveau de la mer, les estimations comptent pour -0.12 +/- 0.05 mm/an et -0.22 +/- 0.05 mm/an respectivement pour les données du GRGS et la moyenne du CSR, GFZ et JPL. Malgré les différences de traitement des données GRACE, nous notons un bon accord entre ces deux estimations du stock d'eau à l'élévation observée du niveau de la mer des années récentes.

C. R. Geoscience 342 (2010) 179–188

Contents lists available at ScienceDirect

Comptes Rendus Geoscience

www.sciencedirect.com

External geophysics, climate and environment

Global land water storage change from GRACE over 2002–2009; Inference on sea level

Variation des stocks d'eau sur les continents à partir de GRACE sur la période 2002–2009 ; influence sur le niveau de la mer

William Llovel [a,*], Mélanie Becker [a], Anny Cazenave [a], Jean-François Crétaux [a], Guillaume Ramillien [b]

[a] *LEGOS-CNES, OMP, 18, avenue E.- Belin, 31400 Toulouse, France*
[b] *DTP, OMP, 31400 Toulouse, France*

ARTICLE INFO

Article history:
Received 16 June 2009
Accepted after revision 14 December 2009
Available online 12 March 2010

Presented by Ghislain de Marsily

Keywords:
GRACE
Land water storage
Space gravimetry data

ABSTRACT

Global change in land water storage and its effect on sea level is estimated over a 7-year time span (August 2002 to July 2009) using space gravimetry data from GRACE. The 33 World largest river basins are considered. We focus on the year-to-year variability and construct a total land water storage time series that we further express in equivalent sea level time series. The short-term trend in total water storage adjusted over this 7-year time span is positive and amounts to 80.6 ± 15.7 km^3/yr (net water storage excess). Most of the positive contribution arises from the Amazon and Siberian basins (Lena and Yenisei), followed by the Zambezi, Orinoco and Ob basins. The largest negative contributions (water deficit) come from the Mississippi, Ganges, Brahmaputra, Aral, Euphrates, Indus and Parana. Expressed in terms of equivalent sea level, total water volume change over 2002–2009 leads to a small negative contribution to sea level of -0.22 ± 0.05 mm/yr. The time series for each basin clearly show that year-to-year variability dominates so that the value estimated in this study cannot be considered as representative of a long-term trend. We also compare the interannual variability of total land water storage (removing the mean trend over the studied time span) with interannual variability in sea level (corrected for thermal expansion). A correlation of ~0.6 is found. Phasing, in particular, is correct. Thus, at least part of the interannual variability of the global mean sea level can be attributed to land water storage fluctuations.

Mots clés :
GRACE
Stock d'eau
Données de gravimetrie spatiale

RÉSUMÉ

L'effet de la variation des stocks d'eau dans les réservoirs continentaux sur le niveau de la mer est estimé à partir des données de gravimétrie spatiale GRACE (qui fournissent les variations du stock d'eau intégré verticalement) sur une période de sept ans (août 2002 à juillet 2009). On considère les 33 plus grands bassins hydrographiques du monde. L'étude se concentre sur la variabilité interannuelle et on calcule une série temporelle du stock d'eau total, ainsi que la tendance de chaque bassin et la tendance totale sur la période. Plusieurs bassins présentent une tendance positive de stock d'eau sur 2002–2009 (Amazone, Lena, Yenisei, Zambèze, Orénoque et Ob). D'autres bassins montrent un déficit d'eau sur la période: Mississipi, Gange, Brahmapoutre, Aral, Euphrates, Indus et Parana. La

* Corresponding author.
E-mail address: william.llovel@legos.obs-mip.fr (W. Llovel).

1631-0713/$ – see front matter
doi:10.1016/j.crte.2009.12.004

variation du stock total d'eau est positive et estimée à 80,6 ± 15,7 km^3 par an, ce qui correspond à une contribution totale négative au niveau de la mer, de –0,22 ± 0,05 mm par an. Un autre aspect de cette étude concerne les fluctuations interannuelles du stock d'eau total que l'on compare aux variations interannuelles du niveau de la mer (après correction de l'expansion thermique des océans). Une corrélation de ∼0,6 est observée, avec en particulier un bon phasage entre les oscillations des deux séries. Ce résultat suggère que la variabilité interannuelle du niveau moyen de la mer est en partie due aux oscillations du stock d'eau sur les continents.

1. Introduction

For the recent decades, sea level variations depend mainly on global climate change induced by anthropogenic greenhouse gases emissions as well as on natural climate variability. The two main factors causing sea level change (globally and regionally) are thermal expansion of sea waters and fresh water mass exchange between oceans and land (Bindoff et al, 2007; Lombard et al., 2006; Nerem et al., 2006). For example, as ocean warms in response to global warming, sea water expands, and thus sea level rises. As mountain glaciers melt in response to increasing air temperature, sea level rises because of fresh water mass input to the oceans. Similarly, ice mass loss from the ice sheets causes sea level rise. Modification of the land hydrological cycle due to climate variability and direct anthropogenic forcing may also affect sea level: on interannual to decadal time scales, more water on land means less water in the oceans, and inversely (Milly et al., 2010). While thermal expansion and land ice melt have been recently the object of numerous investigations, e.g., (Bindoff et al, 2007), the terrestrial water contribution to sea level remains poorly known, mainly because global in situ observations on land water storage are lacking. Estimates have been provided on the basis of global hydrological modelling for the past decades (Milly et al., 2003; Ngo-Duc et al., 2005). Their results are discussed below. The only study based on observations (Ramillien et al., 2008b) estimated the land water storage change on sea level using space gravimetry data from the GRACE space mission (launched in 2002). Based on only 3 years of GRACE data (February 2003 to February 2006), it concluded to a slight positive contribution to sea level changes over that time span, of ∼0.2 mm/yr. Here, we provide an update of this study that considers 7 years of GRACE data (from August 2002 to July 2009) instead of 3 years and uses improved GRACE products (see below). We consider the 33 largest river basins worldwide to estimate land water storage change (short-term trend and interannual variability). Summing up all contributions, we deduce the total land water storage trend over the 7-year time span and its contribution to sea level. We also compare the interannual variability in total land water storage with detrended global mean sea level corrected for thermal expansion.

2. Effect of land water storage change on sea level

Excluding ice sheets and glaciers, fresh water on land is stored in various reservoirs: snow pack, rivers, lakes, man-made reservoirs, wetlands and inundated areas, root zone (upper few meters of the soil) and aquifers (ground water reservoirs). Terrestrial waters are continuously exchanged with atmosphere and oceans through vertical and horizontal mass fluxes (evaporation, transpiration of the vegetation, surface runoff and underground flow). They are an integral part of the global climate system, with important links and feedbacks generated through its influence on surface energy and moisture fluxes between continental water, atmosphere and oceans. Thus, climate change and variability modify land water storage. Some human activities also directly affect water storage: for example, removal of ground water from aquifers by pumping (particularly in arid regions), building of artificial water reservoirs by construction of dams on rivers and wetland drainage. Other anthropogenic effects on land waters result from change of physical characteristics of the land surface by urbanization and land use associated with agriculture and deforestation. All these effects that modify the water budget in river basins, have consequently an impact on sea level.

To estimate the contribution of land water storage change on sea level, we can simply consider the conservation of water mass in the Earth's system (as done in previous studies, e.g., Chen et al., 1998; Milly et al., 2003). On time scales of years to decades, solid Earth stores can be neglected, so that only changes in terrestrial reservoirs, ocean and atmosphere can be considered, with the mass conservation as follows:

$$\Delta M_{\mathrm{cont}} + \Delta M_{\mathrm{ocean}} + \Delta M_{\mathrm{atm}} = 0 \quad (1)$$

where ΔM represents changes in water mass for the three reservoirs (continents, ocean and atmosphere).

Previous studies have shown that water vapour change in the atmosphere cannot be neglected at the annual time scale. On interannual time scale (as considered here), we assume that the atmospheric storage is negligible (because of global warming, an increase of atmospheric water vapour is expected but no reliable estimates are available). Besides, because of the water holding capacity of the atmosphere, even with higher temperature, this contribution is expected to be small – as far as sea level change is concerned – (Milly et al., 2010). Thus Eq. (1) becomes:

$$\Delta M_{\mathrm{ocean}} = -\Delta M_{\mathrm{cont}} \quad (2)$$

$\Delta M_{\mathrm{ocean}}$ represents the change in mass of the ocean due to total fresh water input from continents (i.e., land waters plus ice melt). It can be further expressed in terms of sea level change by simply dividing the total continental water

volume change by the mean surface of the oceans (assumed equal to $360 \times 10^6\,km^2$) and changing its sign. In the following, we only consider the land water contribution (the purpose of this study). The associated ΔM_{cont} component may then be quantified in estimating the change in water storage W in World river basins. At a river basin scale, temporal change in water storage W is related to precipitation P, evapotranspiration E and river runoff R through the water balance equation:

$$dW/dt = P - E - R \quad (3)$$

If P, E and R, or W were known globally, it would be possible to use these hydrological parameters to estimate the effect of land water storage change on sea level.

3. Previous studies

For the past decades, variations in land water storage caused by climate change and variability cannot be directly estimated from observations because these are almost inexistent at global continental scale (except for precipitation, but according to Eq. (3), either W or P-E-R need to be known). However, global hydrological models (or land surface models) developed for atmospheric and climatic studies can be used for estimating W. The models compute the water and energy balance at the earth surface, as well as water storage change in response to prescribed variations of near-surface atmospheric data (precipitation, temperature, humidity and wind) and radiation. Using atmospheric re-analyses over 1950–2000 and the Orchidee land surface model outputs, Ngo-Duc et al., 2005 estimated W globally and its contribution to sea level. They found no climatic long-term trend in W but large interannual/decadal fluctuations, of several millimetres amplitude when translated in sea level equivalent. A similar result was also found by Milly et al., 2003 using the Land Dynamics model over 1980–2000.

Direct human intervention on land water storage and induced sea level changes have been estimated in several studies (e.g., Chao, 1995; Chao et al, 2008; Gornitz, 2001; Sahagian, 2000). These results have been recently reviewed by Hungtington, 2008 and Milly et al., 2010. The largest contributions come from ground water pumping (either for agriculture, industrial and domestic use) and reservoir filling. Surface water depletion has a non-negligible contribution. Although detailed information is lacking, and estimates vary significantly between authors, ground water depletion may have contributed to past decades sea level rise by 0.55–0.64 mm/yr (Hungtington, 2008). During the past 50 years, several tens of thousands dams have been constructed over world rivers, leading to water impoundment into artificial reservoirs, hence negative contribution to sea level. Several attempts have been made to estimate the total volume of water stored in artificial reservoirs over the past half century (e.g., Chao, 1995; Gornitz, 2001; Vörösmarty et al., 1997). The recent study by Chao et al. (Chao et al, 2008) which reconstructs water impoundment history of nearly 30 000 reservoirs built during the 20th century, estimates to –0.55 mm/yr the contribution to sea level of dams and artificial reservoirs during the past half century. Hence, for the last few decades, effects on sea level from ground water depletion and water impoundment behind dams roughly cancel each other.

For the recent years, total land water storage W can be estimated from observations of the GRACE space gravimetry mission. The GRACE mission, launched in 2002, was developed by NASA (USA) and DLR (Germany) to measure spatio-temporal change of the Earth gravity field at a monthly interval. On time scales ranging from months to decades, temporal gravity variations mainly result from surface redistribution of water inside and among the outer fluid envelopes of the Earth (Ramillien et al., 2008a; Tapley et al., 2004; Wahr et al, 2004). On land, GRACE thus provides measurements of total water storage change W in river basins.

A recent study by Ramillien et al., 2008b estimated the water volume trend in the 27 largest river basins worldwide using space gravimetry data from GRACE over a 3-year time span (February 2003 to February 2006) and found either positive or negative water volume change over that period depending on the location of the river basins. The net water volume change was slightly negative (i.e., water loss), corresponding to <0.2 mm/yr sea level rise. We will see below that the length of the time series is critical when estimating trends in land water storage as total water storage in river basins is dominantly seasonal and interannual. As noted above, the global hydrological models runs for the past few decades did not report any long-term trend in global water storage but large interannual fluctuations. Thus, results from the present study are expected to be different from that of Ramillien et al., 2008b because of the more than twice longer time span of analysis.

4. GRACE data analysis

4.1. Data

Raw GRACE data are processed by different groups belonging to the GRACE project (Center for Space Research -CSR – and Jet Propulsion Laboratory-JPL – in the USA, and Geo-ForschungsZentrum-GFZ – in Germany). GRACE data are also processed by other groups (GSFC/NASA in the USA; GRGS in France and DUT in The Netherlands). The GRACE products delivered over land by all groups are time series of equivalent water height, expressed either in terms of spherical harmonic expansion or as gridded data. Several GRACE product releases have been available from the GRACE project, each time with substantial improvement. Here, we use the latest release (RL04) of three solutions: the CSR, JPL and GFZ solutions ($1^\circ \times 1^\circ$ global grids at monthly interval). This new data set (available at http://grace.jpl.nasa.gov/data/mass/) includes an implementation of the carefully calibrated combination of destripping and smoothing, with a 300 km half-width Gaussian filter (Chambers, 2006). Compared to earlier products (contaminated by north-south strips due to aliasing by the GRACE coverage of high-frequency signals of atmospheric and oceanic origins), the latest release is less noisy because of the destripping procedure applied to the data. Thus, it

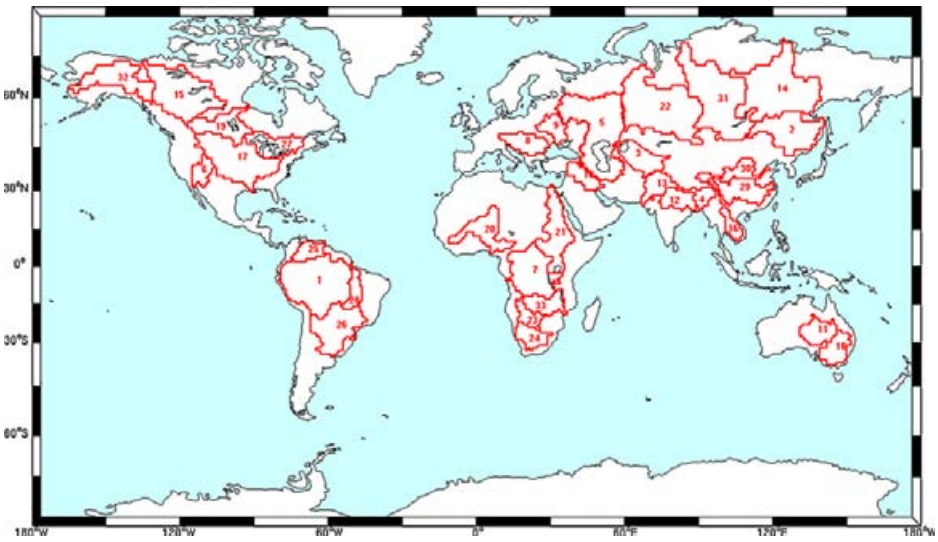

Fig. 1. Map showing the contours of the 33 river basins.

Fig. 1. Carte des contours des 33 bassins versants.

needs less spatial smoothing than earlier solutions. As a result the signal amplitude attenuation is less critical than in previous analyses. The gridded GRACE products are corrected for post-glacial rebound (the solid Earth response to last deglaciation, also sensed by GRACE) using Paulson et al., 2007 model. Thus, the post-glacial rebound contamination to high-latitude river basins storage is expected to be small (but of course model dependent). The gridded time series cover the August 2002 through July 2009 time span. In this analysis, we average the three GRACE data sets (CSR, JPL and GFZ) in order to increase the signal to noise ratio. If one month of data is missing in one data set, we consider the other two when averaging.

We consider the 33 largest World river basins. Their location is shown in Fig. 1 and their number and characteristics are summarized in Table 1. The river basin contours are based on masks of 0.5° resolution from Oki and Sud, 1998. To estimate the water storage contribution of individual river basins, we simply spatially average, for each month, GRACE equivalent water height over the area included inside the basin contours (after adjustment of the grids resolution), then multiply by the basin area to estimate water storage (in km^3). We repeat the analysis for the three GRACE products and then compute the mean of the three time series for each river basin. For each month, the uncertainty of the water storage estimate is computed from the standard deviation of each solution with respect to the mean.

4.2. Data errors

There are two main sources of error affecting the computation of GRACE-based water storage: to reduce spatial noise affecting GRACE data at short-wavelength, smoothing is necessary, which reduces the amplitude of the storage signal. Another problem is related to the signal contamination from neighboring regions (often called

Table 1
List of the 33 river basins considered in this study: Names and associated number, area, trend over 2002–2009 in water storage from GRACE and associated uncertainty.

Tableau 1
Liste des 33 bassins hydrologiques considérés dans cette étude: Noms et numéro associés, aire, tendance sur la période 2002–2009 en termes de stock d'eau déduit de GRACE avec les erreurs associées.

Basin Number/name	Area (10^6 km^2)	Water storage trend (km^3/yr)	Trend error (km^3/yr)
1 Amazon	6.20	77.8	9.3
2 Amur	1.6	−2.4	2.3
3 Aral	1.2	−9.7	1.9
4 Brahmaputra	0.68	−10.3	0.9
5 Volga/Caspienne	3.7	−6.7	4.8
6 Colorado	0.65	−4.0	0.7
7 Congo	3.83	−0.7	6.1
8 Danube	0.82	−2.2	1.5
9 Dniepr	0.52	−0.9	0.7
10 Euphrates	0.75	−7.5	1.2
11 Eyre	1.2	−6.4	0.8
12 Ganges	0.94	−11.0	1.1
13 Indus	0.98	−7.1	1.2
14 Lena	2.47	26.6	2.3
15 Mackenzie	1.74	−6.8	1.2
16 Mekong	0.81	0.8	1.2
17 Mississippi	3.3	−14.2	3.6
18 Murray	1.1	−6.3	1.0
19 Nelson	1.07	−0.5	1.2
20 Niger	2.15	4.0	1.2
21 Nile	3.13	4.7	2.5
22 Ob	2.91	7.8	3.0
23 Okavango	0.79	6.7	1.1
24 Orange	1.0	−0.8	0.8
25 Orinoco	0.9	1.5	1.5
26 Parana	2.93	−7.1	3.7
27 St Lawrence	1.11	6.2	1.3
28 Tocantins	0.89	3.1	2.1
29 Yangtze	1.81	7.8	1.3
30 Yellow	0.76	−2.1	0.9
31 Yenisey	2.54	22.3	1.8
32 Yukon	0.85	−5.1	0.9
33 Zambeze	1.35	14.0	3.1

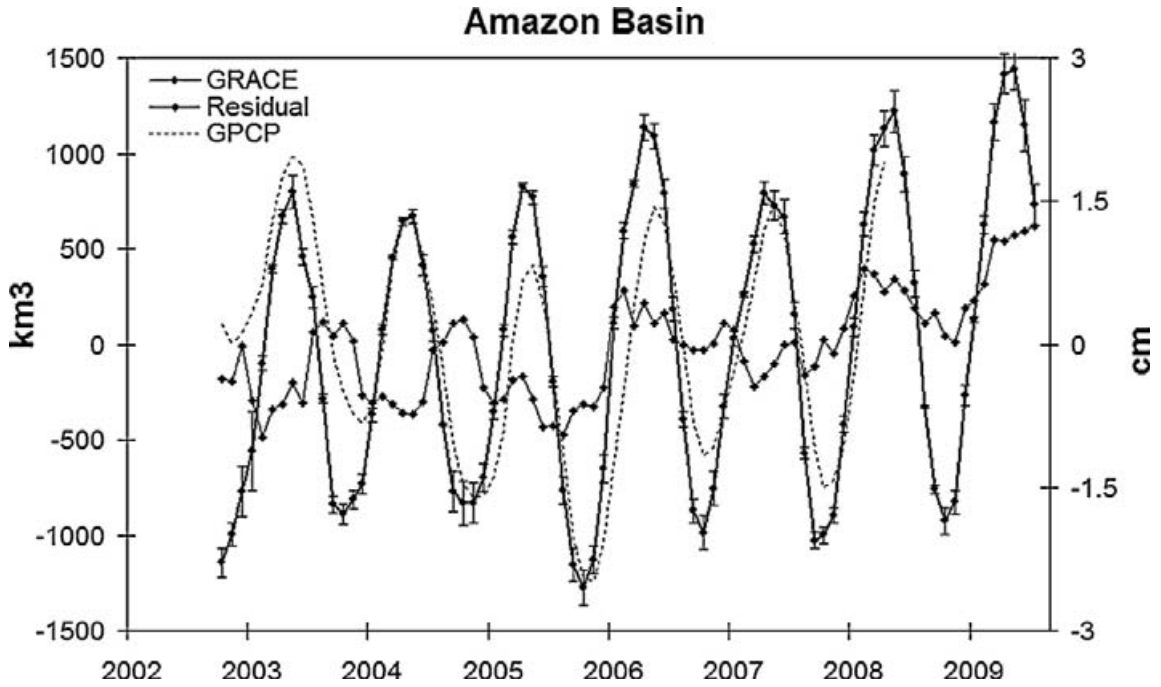

Fig. 2. Water storage change (in km^3) from GRACE over the Amazon basin. Solid curve: total signal; Solid dotted curve: residual signal (seasonal cycle removed). The dashed curve represents time-integrated precipitation over the basin (in cm).

Fig. 2. Variations du stock d'eau (en km^3) calculé à partir de GRACE sur le bassin de l'Amazone. Trait plein: signal total ; trait plein avec carrés: signal résiduel (cycles saisonniers retirés). La courbe en pointillé représente les précipitations intégrées temporellement sur le bassin (en cm).

leakage). The basins considered here have a size equal or larger than $\sim 10^6$ km^2, nearly five times the GRACE resolution (of the order of 2×10^5 km^2). However, for the smallest basins, water storage from surrounding ones may leak into the considered region, thus pollute the estimated water storage. These errors are discussed in several papers (e.g., Ramillien et al., 2008a; Schmidt et al., 2008; Seo et al., 2006; Swenson and Wahr, 2002; Syed et al., 2008).

In this study, we analyze the effects of smoothing and leakage using synthetic hydrology data. For that purpose, we use monthly $0.5^\circ \times 0.5^\circ$ grids of total water storage from the Water Gap Hydrological Model – WGHM – (Doll et al., 2003). To quantify the amplitude attenuation due to smoothing, we apply the same Gaussian filter (300 km half-width) to the WGHM data when averaging over each river basin (as done for the GRACE data) and compare the corresponding storage with and without smoothing. For the basins considered in this study, attenuation due to smoothing is small (<10%). To quantify the leakage, we apply the same procedure as in Ramillien et al., 2008b. For each month and each basin, the global WGHM model grid is modified by setting zero values over the considered river basins, keeping the model values outside the basin. This modified data set is then expanded in spherical harmonics up to degree 60 (equivalent to the GRACE resolution). The leakage signal is then estimated by convoluting this spherical harmonic expansion with that of the geographical mask representing the river basin (see Ramillien et al., 2008b), for more details). As noted previously, the leakage signal is mainly seasonal and on the order of 5% to 15% of the 'model' annual signal, depending on the basin. In terms of trend, the error is negligible, but we cannot exclude that hydrological models like WGHM do not perfectly reproduce the interannual and trend signal.

5. GRACE-based water storage change: Results

We now examine water volume time series over the 33 largest World river basins. We present separately the case of the Amazon basin (Fig. 2). Because of its huge dimension, its corresponding water volume variations dominate all other basins. A large annual cycle is observed. The residual curve also shows large fluctuations of ± 300 km^3 amplitude. What is particularly noticeable is an abrupt positive excursion occurring at the end of 2005, right after a temporary minimum in water storage in mid-2005 (Chen et al., 2005). The end of year 2008 also shows an abrupt increase in water storage. Link between GRACE-based water storage change and precipitation patterns over the Amazon basin have been shown in several previous publications. For example, two recent studies (Chen et al., 2005; Xavier et al., 2010[1]) which focus on the interannual time scale report a high correlation between year-to-year fluctuations of average precipitation and GRACE-based water storage. Several hydrological events have affected the Amazon basin over the

[1] L. Xavier, A. Cazenave, O.C. Rotunno Filho and M. Becker, Interannual variability in water storage over 2003–2007 in the Amazon Basin from GRACE space gravimetry, in situ river level and precipitation data, Remot. Sens. Env. (2010) in revision.

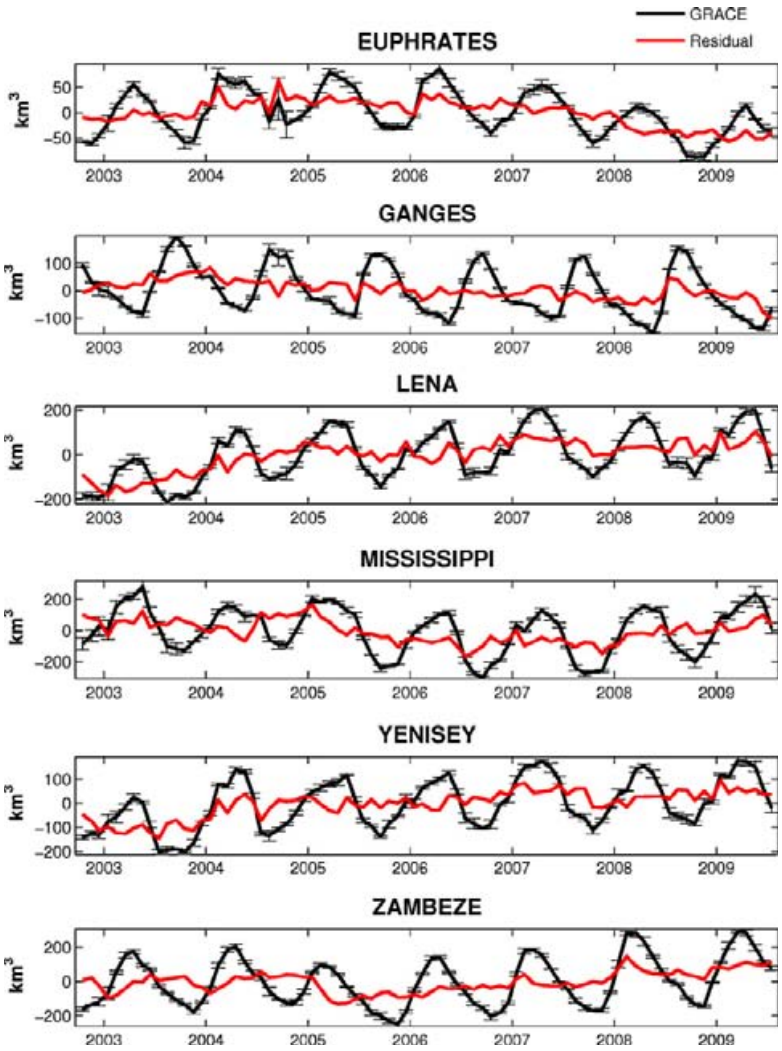

Fig. 3. Water storage change (in km^3) from GRACE over a selection of 6 basins (Euphrates, Ganges, Lena, Mississippi, Yenisei and Zambezi). Solid black curve: land water signal with uncertainty; red (lighter) curve: residual signal (seasonal cycle removed).

Fig. 3. Variations du stock d'eau (en km^3) calculé à partir de GRACE sur 6 bassins versants (Euphrate, Gange, Lena, Mississippi, Yenisei et Zambézi). Courbe noire : signal total ; courbe rouge (plus claire) : signal résiduel (cycles saisonniers retirés).

recent years: a severe drought in the second part of 2005, followed by a wet episode in early 2006. Other wet periods are also observed in early 2008 and 2009. The studies show that the 2005 dry conditions (rain deficit) affect essentially the western part of the Amazon basin while the 2006 and 2008 wet episodes affect the eastern part. To illustrate the relationship between rainfall and water storage, we have superimposed in Fig. 2, time-integrated precipitation averaged over the Amazon basin and GRACE-based water storage (from the water balance equation, GRACE-based water storage W should be compared to time-integrated precipitation). Precipitation data are obtained from the Global Precipitation Climatology Project (http://lwf.ncdc.noaa.gov/oa/wmo/wdcamet-ncdc/). We can clearly see the high level of correlation between time integrated precipitation and water storage inferred from GRACE.

In Fig. 3 are presented for a few basins (Euphrates, Ganges, Lena, Mississipi, Yenisey and Zambezi, selected among the largest contributors to sea level changes), the water volume time series (whole signal) and the residuals after removing the seasonal signal (annual and semi-annual cycles). For each basin, we have compared the interannual water storage from GRACE (i.e., the residual time series) with model data from the GLDAS (Global Land Data Assimilation System)/Noah (Rodell et al., 2004). A few examples are presented in Fig. 4 (Colorado, Danube, Nelson, Parana, Okavongo and Yantgze; this selection allows to show another set of residual time series, covering different regions of the world). We note for all basins a very good agreement between GRACE and GLDAS, not only for the seasonal cycle (for which the signal is generally dominant), but also at the interannual time scale. As shown in several previous studies, this gives confidence in the GRACE results, even at interannual time scale.

For each residual curve, we have computed a linear trend over the 7-year time span (further called 'short-term trend'). We are well aware that the time span is still short but this allows to provide an order of magnitude of the land

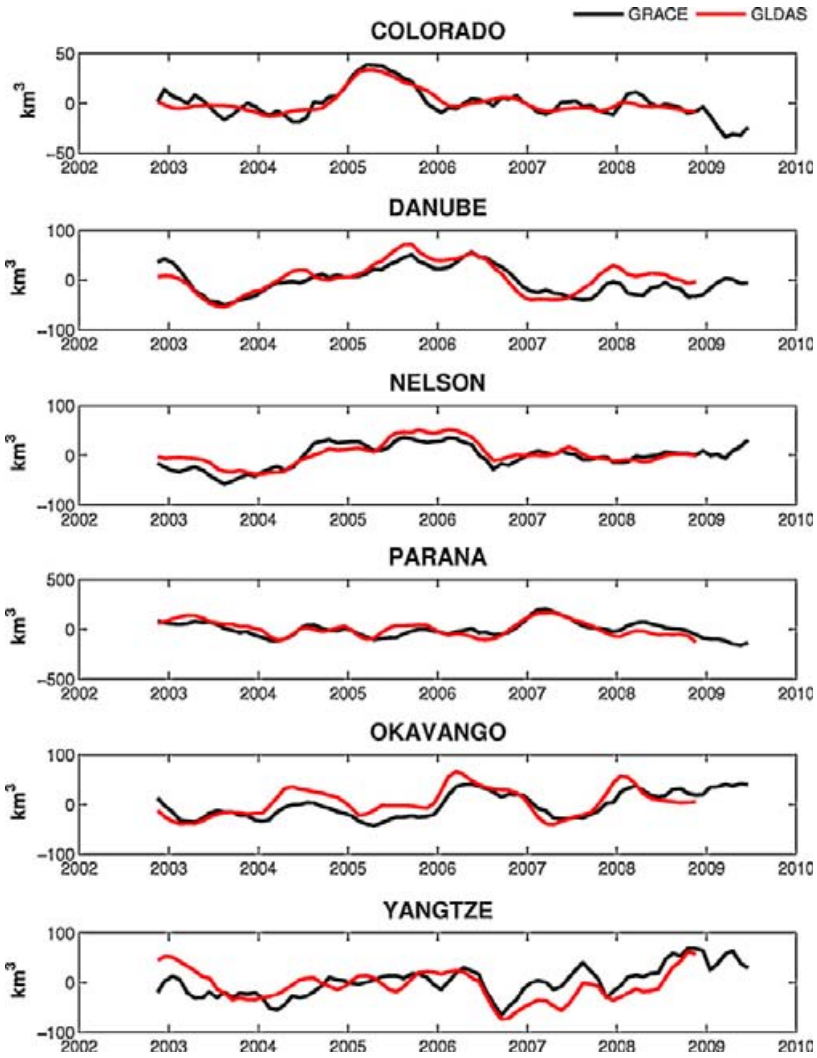

Fig. 4. Interannual water storage variability (in km^3) over a selection of 6 basins (Colorado, Danube, Nelson, Parana, Okavango and Yangtze). Solid black curve: land water signal from GRACE; red (lighter) curve: GLDAS model result.

Fig. 4. Variations interannuelles du stock d'eau (en km^3) calculé à partir de GRACE sur 6 bassins versants (Colorado, Danube, Nelson, Parana, Okavango et Yangtze). Courbe noire : signal GRACE ; courbe rouge (plus claire) : signal GLDAS.

water contribution to sea level rise. GRACE-based water storage trends over 2002–2009 are gathered in Table 1 and shown in Fig. 5. The largest water storage short-term trend is due to the Amazon basin ($+77.8 \pm 9.3$ km^3/yr). As shown in Fig. 2, this positive trend results from a change in water storage regime as of early 2006, from dry to wet conditions. In Ramillien et al., 2008b, we found a trend of –18 km^3/yr for the 3-year period (February 2003 to February 2006). Of course, the present study finds the same trend value over this smaller time span. The fact that the trend value becomes positive when increasing the length of the time series is due to the strong increase in water storage in early 2006. Water storage remains high beyond that date. Thus, the computed trend value becomes positive (in fact what we see here in a succession of positive steps in the time series in 2006, 2008 and 2009, with dry conditions during years 2003 through 2005 and wet conditions beyond).

The next largest positive contributions come from the Lena and Yenisey basins located in Siberia (trends of 26.6 ± 2.3 km^3/yr and 22.3 ± 1.8 km^3/yr respectively). Analysis of rainfall data (from the Global Precipitation Climatology Project; http://lwf.ncdc.noaa.gov/oa/wmo/wdcamet-ncdc/) indicates positive trends in precipitation over the Siberian river basins over 2002–2009 (not shown). The largest negative trends are observed for the Mississipi (-14.2 ± 3.6 km^3/yr), the Ganges and Brahmaputra (-11.0 ± 1.1 km^3/yr and $-10.3. \pm 0.9$ km^3/yr). Loss of water in the Ganges region has been confirmed by two recent publications (Rodell et al., 2009; Tiwari et al., 2009) and attributed to intensive ground water pumping for crop irrigation. We do not wish to reiterate the comment made above for the Amazon basin about the comparison between Ramillien et al. (Ramillien et al., 2008b) but it is clear that estimated short-term trends greatly depend on the length of the time series. This is so because year-to-year fluctuations dominate the water storage signal.

We have summed up the 33 water volume time series (with and without the seasonal cycles). Corresponding

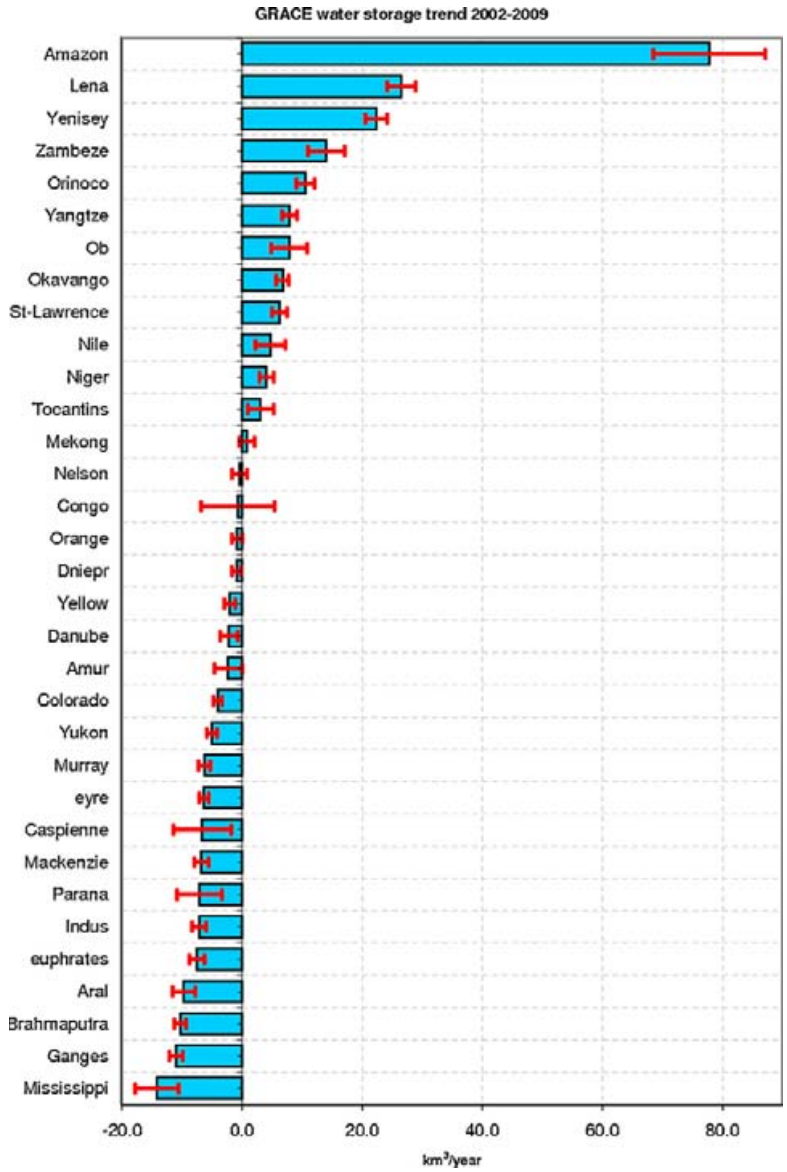

Fig. 5. Histogram of the largest positive and negative basin storage trends estimated from GRACE over the 7-year time span.

Fig. 5. Histogramme des tendances les plus significatives des stocks d'eau estimées à partir de GRACE, comme décrit dans le Tableau 1.

curves are shown in Fig. 6. Both curves are dominated by the Amazon contribution. The residual curve (annual cycle removed) exhibits significant year-to-year variability on the order of 500 km^3. The mean trend of the residual water volume change is $+80.6 \pm 15.7$ km^3/yr.

6. Land waters and sea level

Converting the positive short-term trend in land water storage ($+80.6 \pm 15.7$ km^3/yr) estimated from GRACE between August 2002 and July 2009 into sea level equivalent leads to a negative sea level trend of $\sim -0.22 \pm 0.05$ mm/yr over this time span.

Satellite altimetry observations available since 1993 indicate that sea level has been rising by 3.4 ± 0.4 mm/yr between 1993 and 2009 (Ablain et al., 2009). Knowledge of the contribution of thermal expansion, glaciers melting and mass change of the ice sheets has considerably improved in recent years (Bindoff et al, 2007). Although none of these climate factors change linearly with time, on average over the 1993–2008 time span, ocean warming, glaciers melting and ice sheet mass loss have each contributed by ~30% to global mean sea level rise (Cazenave and Llovel, 2010). The negative short-term trend contribution for terrestrial water storage determined in this study over the past 7 years is small and within the uncertainty of observed sea level trend and estimated climate contributions. It is of similar magnitude as land surface model results (Milly et al., 2003; Ngo-Duc et al., 2005) and previous GRACE-based estimate (Ramillien et al., 2008b), but of opposite sign with the latter study based on only 3 years of data. The fact that the land water component oscillates from positive to negative values depending on the

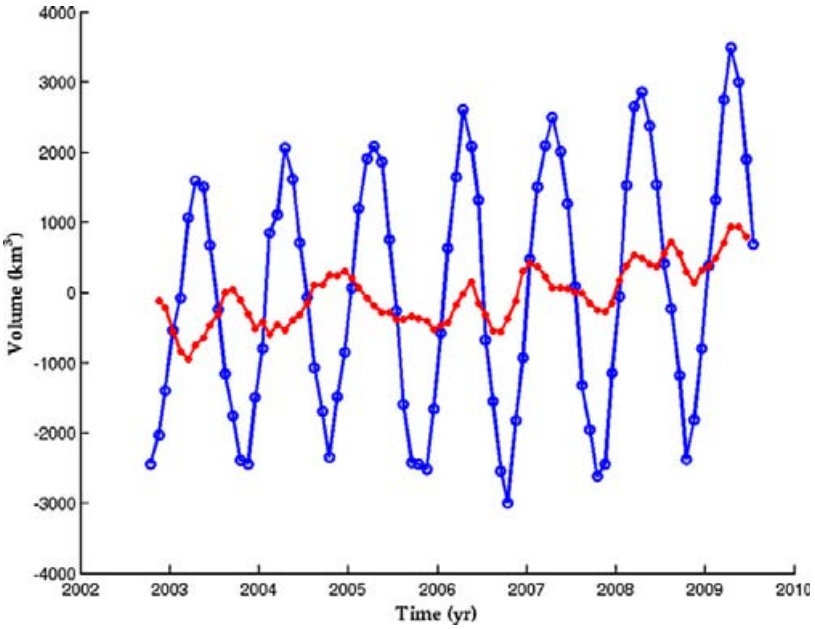

Fig. 6. Total land water storage change from GRACE (sum of the 33 basins contributions). Solid blue (darker) curve: total signal; Red (lighter) curve: residual signal (seasonal cycle removed). Unit in km^3.

Fig. 6. Variation du stock d'eau continental total d'après GRACE (somme des contributions des 33 bassins). Courbe bleue (plus foncée) : signal total; courbe rouge (plus claire) : signal résiduel (cycles saisonniers retirés). Unité en km^3.

time span strongly suggests the dominance of interannual variability for this component (as shown by model results).

To further investigate the contribution of year-to-year variability in land water storage to sea level, we now compare the GRACE-based total water storage computed above (expressed in terms of equivalent sea level) with observed, detrended sea level (corrected for thermal expansion).

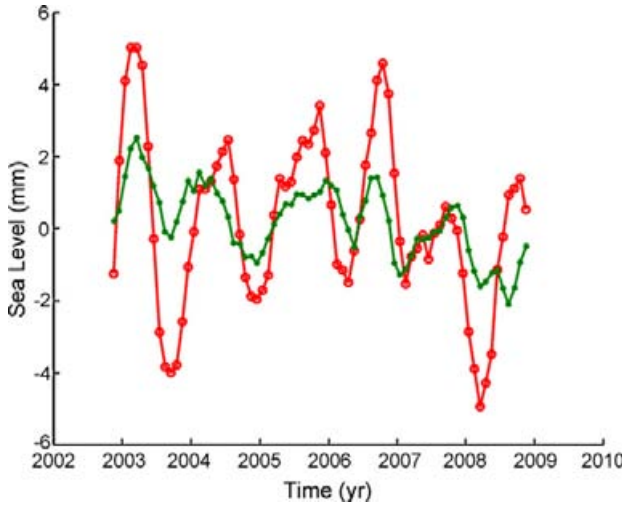

Fig. 7. Year-to-year fluctuations of the (detrended) global mean sea level corrected for thermal expansion (red [lighter] curve) and of total land water storage from GRACE – expressed in equivalent sea level – (green [darker] curve). Units in mm.

Fig. 7. Variabilité interannuelle du niveau moyen de la mer (tendance retirée et corrigée de l'expansion thermique, courbe rouge [plus claire]) et variabilité interannuelle du stock d'eau continental total d'après GRACE – exprimé en equivalent niveau de la mer (courbe verte [plus foncée]). Unités en mm.

The thermal expansion contribution, based on (Guinehut et al., 2009), has been subtracted to the global mean sea level curve (based on Topex/Poseidon and Jason-1 altimetry). The difference time series has been detrended since we focus now on the interannual variability. Results are shown in Fig. 7 which compares interannual variability in global mean sea level (corrected for thermal expansion) and land water storage oscillations. A 3-month smoothing has been applied to both time series. We note a clear correlation between the two curves, amounting to ~0.6. The phasing is particularly good. This is an interesting result since, so far, the origin of interannual fluctuations of the global mean sea level remained unexplained. The result obtained in this study suggests that year-to-year fluctuations of total water storage on land – mainly related to climate variability – is responsible, at least partly, for the interannual variability of the global mean sea level.

7. Conclusion

In this study, we have estimated the contribution of total land water storage variations to sea level changes using GRACE data over a 7-year period (August 2002 to July 2009). The 33 largest World basins of the world are considered. We find that over this time span, the Amazon basin dominates the total land water signal. This is due to particularly wet conditions as of early 2006 which lasted until 2009. These wet conditions contrast with a previous drought episode in 2005. The Siberian basins (Lena, Yenisey and Ob) also show water storage increase. On the other hand, some basins have lost water during the

time span, in particular the Mississippi and the Ganges-Brahmaputra basins. In the latter basins, water loss is possibly of anthropogenic origin (groundwater withdrawal for irrigation). The net water storage trend is positive over the 7-year time span. When translated into equivalent sea level, this gives a small negative contribution of -0.22 ± 0.05 mm/yr. This is a small contribution which confirms earlier modelling results. On the other hand, the water storage time series clearly show that -except for the two Siberian basins (Lena and Yenissei)-, the signal is dominated by interannual variability. We have compared the year-to-year variability of total land water storage with interannual fluctuations of the global mean sea level (corrected for thermal expansion). The two signals are positively correlated (correlation coefficient of $\sim$0.6). This suggests that interannual variability of the global mean sea level is at least partly caused by year-to-year variability of land water storage. Such a result is new.

Acknowledgements

We thank Katia Laval and three anonymous reviewers for their comments. W. Llovel and M. Becker are supported by grants from CNRS and the Region Midi-Pyrénées, and the RTRA-STAE respectively. GRACE data were processed by D. P. Chambers, supported by the NASA Earth Science REASoN GRACE Project, and are available at http://grace.jpl.nasa.gov.

References

Ablain, M., Cazenave, A., Guinehut, S., Valladeau, G., 2009. A new assessment of global mean sea level from altimeters highlights a reduction of global slope from 2005 to 2008 in agreement with in-situ measurements. Ocean Sci. 5 (2), 193–201.

Bindoff, N., Willebrand, J., Artale, V., Cazenave, A., Gregory, J., Gulev, S., Hanawa, H., Le Quéré, C., Levitus, S., Nojiri, Y., Shum, C.K., Talley, L., Unnikrishnan, A., 2007. Observations: oceanic climate and sea level. In: Solomon, S., Qin, D., Manning, M., Chen, Z., Marquis, M., Averyt, K.B., Tignor, M., Miller, H.L. (Eds.), Climate Change 2007: The Physical Science Basis. Contribution of Working Group I to the Fourth Assessment Report of the Intergovernmental Panel on Climate Change. Cambridge University Press, UK, and New York, USA.

Cazenave, A., Llovel, W., 2010. Contemporary sea level rise, Annual Review OF Marine Science, 2, 145–173.

Chambers:, D.P., 2006. Evaluation of new GRACE time-variable gravity data over the ocean. Geophys. Res. Lett. 33 (17), Ll7603.

Chao, B.F., 1995. Anthropogenic impact on global geodynamics due to reservoir water impoundment. Geophys. Res. Lett. 22, 3529–3532.

Chao, B.F., Wu, Y.H., Li, Y.S., 2008. Impact of artificial reservoir water impoundment on global sea level, Science, doi:10.1126/science.1154580.

Chen, J.L., et al., 1998. Seasonal global water mass budget and mean sea level variations. Geophys. Res. Lett. 25, 3555–3558.

Chen, J.L., Wilson,C.R., Tapley, B.D., Yang, Z.L., Niu, G.Y., 2005. 2005 drought event in the Amazon River basin as measured by GRACE and estimated by climate models. J. Geophys. Res.-Solid Earth, doi:10.1029/2008JB006056.

Doll, P., Kaspar, F., Lehner, B., 2003. A global hydrological model for deriving water availability indicators: model tuning and validation. J. Hydrol. 270, 105–134.

Gornitz, V., 2001. In: Douglas, B.C., Kearney, M.S., Leatherman, S.P. (Eds.), Impoundment, Groundwater Mining, and Other Hydrologic Transformations: Impacts on Global Sea Level Rise, Sea Level Rise. History and Consequences. Academic Press, San Diego, California, pp. 97–119.

Guinehut,S., Coatanoan, C., Dhomps, A.L., Le Traon, P.Y., Larnicol, G., 2009. On the use os satellite altimeter data in Argo quality control, J. Atm. Ocean. Tech., AMS, doi:10.1175/2008JTECHO648.1.

Hungtington, T.G., 2008. Can we dismiss the effect of changes in land water storage on sea level rise. Hydrol. Process. 22, 717–723.

Lombard, A., Cazenave, A., Le Traon, P.Y., Guinehut, S., Cabanes, C., 2006. Perspectives on present-day sea level change. Ocean Dyn. 56, 445–451 , doi:10.10007/s10236-005-0046-x.

Milly, P.C.D., Cazenave, A., Gennero, M.C., 2003. Contribution of climate-driven change in continental water storage to recent sea-level rise, Proc. Natl. Acad. Sci., 100, 13158–13161, doi:10.1073/pnas.2134014100.

Milly, P.C.D., Cazenave, A., Famiglietti, J., Gornitz, V., Laval, K., Lettenmaier, D., Sahagian, D., Wahr, J., Wilson, C., 2010. Terrestrial water storage contributions to sea level rise and variability. In: Church, J., Woodworth, P., Aarup, T., Wilson, S. (Eds.), Proceedings of the WCRP workshop 'Understanding sea level rise and variability', Blackwell Publishing, Inc.

Nerem, S., Leuliette, E., Cazenave, A., 2006. Present-day sea level change. C.R. Geoscience 338 (14-15), 1077–1083.

Ngo-Duc, T., Laval, K., Polcher, J., Lombard, A., Cazenave, A., 2005. Effects of land water storage on global mean sea level over the past 50 years, Geophys. Res. Lett., 32, L09704, doi:10.1029/2005GL022719.

Oki, T., Sud, Y.C., 1998. Design of Total Runoff Integrating Pathways (TRIP)–A Global River Channel Network. Earth Int., vol. 2., Paper 1.

Paulson, A., Zhong, S., Wahr, J., 2007. Inference of mantle viscosity from GRACE and relative sea level data. Geophys. J. Int. 171, 497–508.

Ramillien, G., Famiglietti, J., Wahr, J., 2008a. Detection of continental hydrology and glaciology signals from GRACE: a review. Survey Geophys. 29, 361–374.

Ramillien, G., Bouhours, S., Lombard, A., Cazenave, A., Flechtner, F., Schmidt, R., 2008b. Land water contributions from GRACE to sea level rise over 2002-2006. Glob. Planet. Change 60, 381–392.

Rodell, M., et al., 2004. The Global Land Data Assimilation System. Bull. Am. Meteorol. Soc. 85 (3), 381–394.

Rodell, M., Velicogna, I., Famiglietti, J.S., 2009. Satellite-based estimates of groundwater depletion in India. Nature 460 (7258), 999–1080.

Sahagian, D., 2000. Global physical effects of anthropogenic hydrological alterations: sea level and water redistribution. Glob. Planet. Change 25, 39–48.

Schmidt, R., Flechtner, F., Meyer, U., Neumayer, K.H., Dahle, C., König, R., Kusche, J., 2008. Hydrological signals observed by the GRACE satellites. Survey Geophys. 29, 319–334.

Seo, K.W., Wilson, C.R., Famiglietti, J.S., Chen, J.L., Rodell, M., 2006. Terrestrial water mass load changes from Gravity Recovery and Climate Experiment (GRACE). Water Resour. Res. 42, W05417.

Swenson, S., Wahr, J., 2002. Methods of inferring regional surface mass anomalies from Gravity Recovery and Climate Experiment (GRACE) measurements of time variable gravity. J. Geophys. Res. 107 (B9), 2193.

Syed, T.H., Famiglietti, J.S., Rodell, M., Chen, J.L., Wilson, C.E., 2008. Analysis of terrestrial water storage changes from GRACE and GLDAS. Water Resour. Res. 44, W02433.

Tapley, B.D., Bettadpur, S., Ries, J.C., Thompson, P.F., Watkins, M.M., 2004. GRACE measurements of mass variability in the Earth system. Science 305, 503–505.

Tiwari, V.M., Wahr J., Swenson S., 2009. Dwindling groundwater resources in northern India, from satellite gravity observations, Geophys. Res. Lett., 36, doi:10.1029/2009GL039401.

Vörösmarty, C.J., Sharma, K.P., Fekete, B.M., Copeland, A.H., Holden, J., Marble, J., Lough, J.A., 1997. The storage and aging of continental runoff in large reservoir systems of the world. Ambio 26, 210–219.

Wahr, J., Swenson, S., Zlotnicki, V., Velicogna, I., 2004. Time-variable gravity from GRACE: First results, Geophys. Res. Lett., 31, L11501, doi:10.1029/2004GL019779.

4.3.3 Variabilité interannuelle des eaux continentales : études sur les périodes : 2002-2009, 1993-2003 et 1950-1995. Article publié dans le journal « Global and Planetary Change ».

Introduction et résumé de l'article

Dans l'article précédent, nous avons mis en évidence les tendances du stock d'eaux continentales sur la période récente entre 2002 et 2009 à l'aide de données spatiales de GRACE. Nous allons maintenant regarder plus en détail la variabilité interannuelle du niveau de la mer en moyenne globale. Nous avons comparé la variabilité interannuelle des eaux continentales (exprimée en équivalent niveau de la mer) aux variations interannuelles du niveau de la mer en moyenne globale. Pour cela, nous avons corrigé l'effet stérique du niveau de la mer observé par altimétrie spatiale. Cette comparaison est encourageante car la corrélation est de l'ordre de 0.6 . La variabilité interannuelle du niveau de la mer observé est en partie expliquée par les variations du stock d'eaux continentales. La question sousjacente est de savoir si l'utilisation d'un modèle d'hydrologie continentale confirme ce résultat basé sur des mesures spatiales et *in situ*. Et, ensuite, si ce résultat est similaire sur des périodes plus longues.

Le modèle hydrologique ISBA

Le modèle d'hydrologie continentale ISBA a été développé au CNRM (Centre National de la Recherche Météorologique) par *Noilhan and Planton* [1989]. Ce modèle numérique global repose sur une physique simple dépendant seulement de quelques paramètres liés au type de sol et de végétation. Ce modèle dispose de deux couches hydrologiques - une couche superficielle de surface incluse dans la couche totale de sol décrivant la zone racinaire - et de la représentation de la végétation. Les bilans d'énergie d'eau en surface et dans le sol sont modélisés de façon à reproduire la réalité des processus physiques observés (*Decharme* [2005], thèse de doctorat). Le modèle de routage des fleuves TRIP (*Oki and Sud* [1998]) a été couplé à ISBA afin de modéliser le ruissellement de l'eau des continents vers les océans. La composante neige est calculée dans le modèle numérique ISBA (*Douville et al.* [1995]) mais aussi la représentation du gel dans le sol (*Boone et al.* [2000]). Ce modèle est forcé par les flux météorologiques fournis par l'Université de Princeton avec un échantillonnage toutes les 3 heures. Cette base de données découle directement des réanalyses NCEP-NCAR (National Center of Environmental Prediction-National Center for Atmospheric Research). Les différents paramètres sortant de ce modèle hydro-

logique nous intéressent tout particulièrement car l'eau qui peut être stockée sur les continents peut influer sur les variations du niveau marin global.

Les années récentes : 2002-2009

Dans un premier temps, nous avons comparé la variabilité interannuelle des eaux continentales aux variations interannuelles du niveau moyen global de la mer observé en le corrigeant de l'effet stérique. Nous avons, dans un second temps, comparé ces deux estimations aux sorties du modèle numérique d'hydrologie continentale ISBA. La figure 4.11 représente ces diverses comparaisons.

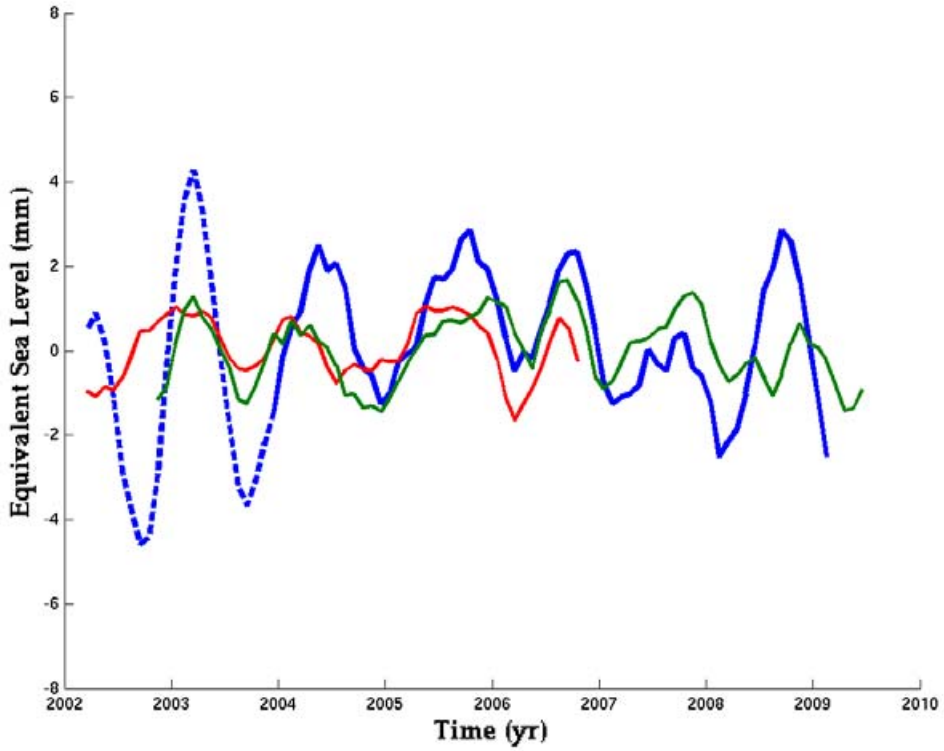

FIG. 4.11 – Variabilité interannuelle du niveau de la mer observé et corrigé de l'expansion stérique (courbe bleue), des stocks d'eaux continentales observés par GRACE (courbe verte) et déduits du modèle numérique ISBA (courbe rouge) (Pour chaque courbe une tendance moyenne est retirée)

La figure 4.11 illustre le rôle du stock des eaux continentales dans les variations interannuelles du niveau de la mer observé et corrigé du niveau de la mer stérique (estimation basée sur les données de CLS, *Guinehut et al.*

[2009]). Nous avons retiré une tendance aux différentes courbes. La courbe bleue représente le niveau de la mer corrigé du niveau de la mer stérique. Cette courbe est en pointillée avant 2004 du fait de la couverture incomplète des données Argo et donc de la mauvaise estimation de la contribution stérique. La courbe verte représente le stock total d'eaux continentales exprimé en terme de niveau de la mer équivalent déduit des données de GRACE (moyenne des trois solutions CSR, GFZ et JPL calculées par *Chambers* [2006]). La courbe rouge est la même quantité estimée à partir du modèle hydrologique ISBA-TRIP développé au CNRM (*Decharme et al.* [2006]; *Alkama et al.* [2010]; *Decharme et al.* [2010]).

La correspondance entre ces différentes courbes de la figure 4.11 est intéressante. La corrélation entre le niveau de la mer corrigé de l'effet stérique et les variations du stock d'eaux continentales (exprimées en niveau de la mer équivalent) est de l'ordre de 0.6 (pour les données GRACE et le modèle ISBA). Ces résultats suggèrent que la variabilité interannuelle du niveau de la mer est partiellement expliquée par les fluctuations du stock d'eaux continentales. Un autre constat très intéressant est l'homogénéité des résultats entre : les données altimétriques corrigées du niveau de la mer stérique (données des flotteurs Argo), de la mission spatiale gravimétrique GRACE et du modèle numérique hydrologique ISBA, sachant que ces données sont totalement indépendantes.

La période altimétrique : 1993-2003

Après l'étude des années récentes, nous nous sommes penchés sur la période altimétrique entre 1993-2003. Pour cela, nous avons comparé les données altimétriques fournis par le Goddard Space Flight Center (GSFC) de la NASA (*Beckley et al.* [2010]) et celle de CLS (*Ablain et al.* [2009]) aux estimations des eaux continentales du modèle numérique ISBA (*Alkama et al.* [2010]; *Decharme et al.* [2010]).

La figure 4.12 représente la variabilité interannuelle du niveau de la mer observé par altimétrie spatiale (Topex/Poseidon et Jason-1) et la variabilité interannuelle des stocks d'eaux continentales exprimés en niveau de la mer équivalent (courbe bleue, basée sur les données du GSFC, *Beckley et al.* [2010] et la courbe noire basée sur les données de CLS, *Ablain et al.* [2009]). Nous observons une bonne corrélation entre le niveau de la mer observé et l'estimation du stock d'eaux continentales exprimé en niveau de la mer équivalent sur la période de 1993 à 2003. Néanmoins, d'après ces courbes, le niveau de la mer observé basé sur les données du GSFC (*Beckley et al.* [2010]) montre une meilleure cohérence avec les variations des eaux continentales (corrélation de

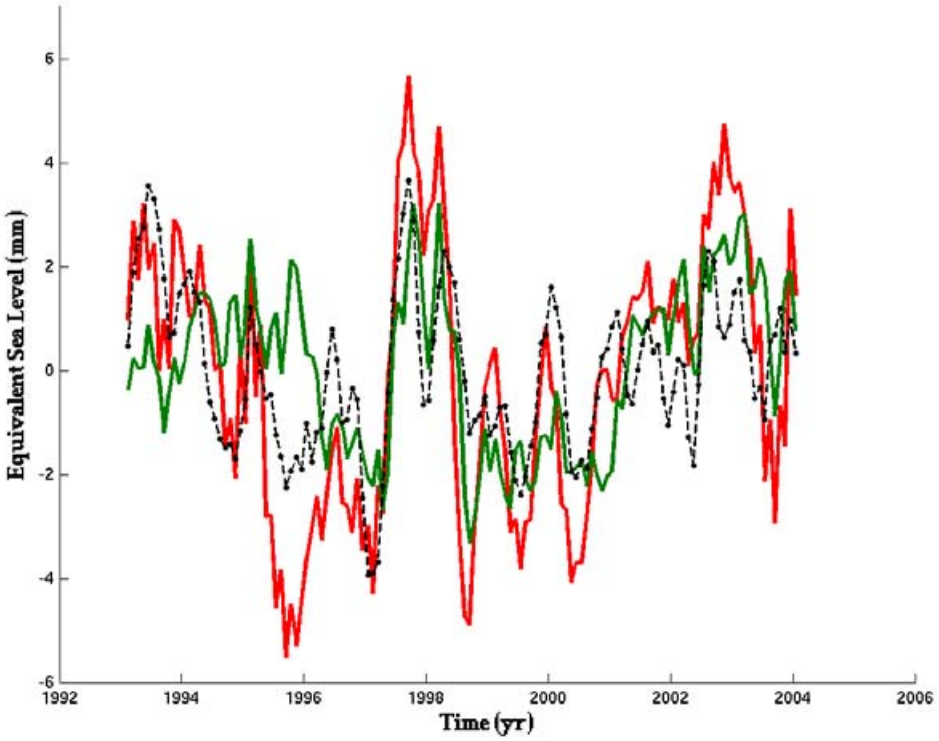

FIG. 4.12 – Séries temporelles du niveau de la mer observé (courbe rouge, à partir des données d'altimétrie spatiale fournis par le GSFC, *Beckley et al.* [2010] et courbe noire à partir des données d'altimétrie spatiale fournis par CLS, *Ablain et al.* [2009]). La courbe verte représente la contribution du stock d'eaux continentales exprimé en niveau de la mer équivalent du modèle numérique d'hydrologie ISBA. Les signaux saisonniers sont retirés pour chaque courbe et la tendance moyenne respective a aussi été retranchée. La courbe du niveau de la mer observée par marégraphie est lissée à l'aide d'une moyenne glissante sur 3 mois.

0.5 contre 0.34 avec les données de CLS). En effet, l'accord en ces deux courbes est bien meilleur durant l'événement El Niño de 1997-1998. La courbe du niveau de la mer basée sur les données de CLS décroche pendant cet événement. Toutefois, nous notons un accord moins bon avant 1996 et après 2003. Ce constat est probablement dû au fait que nous ne corrigeons pas du niveau de la mer stérique. En effet, les estimations du niveau de la mer stérique en terme de variabilité interannuelle (en moyenne globale) n'apporte pas de résultat concluant. Ceci est probablement dû au manque de données hydrographiques dans le but d'estimer correctement cette partie du signal du niveau de la mer.

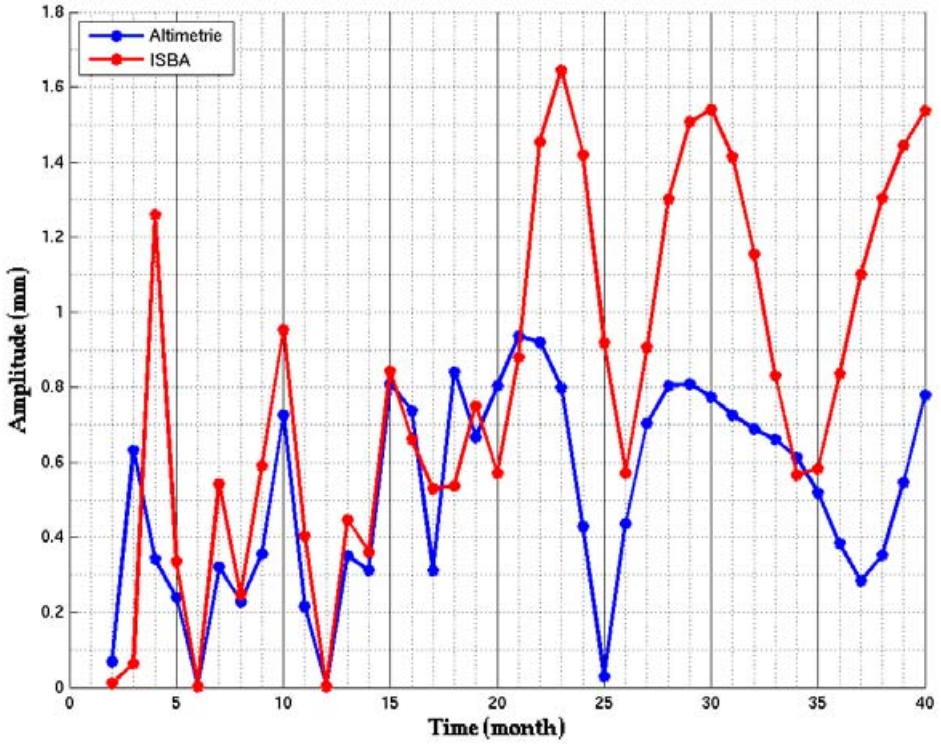

FIG. 4.13 – Spectres des séries temporelles du niveau de la mer observé par altimétrie spatiale (courbe bleue : spectre du niveau de la mer observé basé sur les données du GSFC, *Beckley et al.* [2010]) et de la contribution des eaux continentales en niveau de la mer équivalent (courbe rouge, *Alkama et al.* [2010]; *Decharme et al.* [2010]) du modèle numérique d'hydrologie continentale ISBA. Dans chaqu'un des cas les signaux saisonniers ont été retirés avant l'analyse harmonique sur la période commune entre 1993 et 2003.

La figure 4.13 représente les spectres des données d'altimétrie spatiale du GSFC (*Beckley et al.* [2010]) et du signal des eaux continentales du modèle ISBA exprimé en niveau de la mer équivalent (*Alkama et al.* [2010]; *Decharme et al.* [2010]). Ces deux spectres montrent de fortes corrélations entre les signaux impliquées dans ces séries temporelles. Pour les courtes périodes, nous notons que l'altimétrie a un fort signal à 3 mois tandis que le modèle hydrologique présente un pic à 4 mois. Les deux amplitudes présentent un facteur 2 entre elles. Sinon, pour les périodes de 7, 10, 13, 15 mois, les deux spectres montrent un très bon accord. Les eaux continentales expliquent donc une par-

tie de la variabilité interannuelle (périodes supérieures à 12 mois) du niveau de la mer pour les périodes considérées et une partie de la variabilité intra-annuelle (périodes inférieures à 12 mois). Après, un décalage entre les *maxima* aussi bien en terme d'amplitude qu'en terme de phase est visible. Néanmoins, nous trouvons du signal sur les bandes 20-23 mois et 27-32 mois pour le signal du niveau de la mer observé, tandis que le signal des eaux continentales existe plutôt autour des bandes de périodes 22-24 et 28-32. Toutefois, nous observons un déphasage de quelques mois pour les signaux de période supérieure à 20 mois.

Nous avons montré que les eaux continentales expliquent une partie de la variabilité interannuelle du niveau de la mer observé par altimétrie spatiale. Par contre, nous ne sommes pas encore en mesure d'expliquer entièrement toute la variabilité interannuelle observée.

La période Marégraphique : 1950-1995

Nous comparons ici la variabilité du niveau de la mer observée par les données des marégraphes (*Jevrejeva et al.* [2006, 2008]) en moyenne globale avec les variations du stock d'eaux continentales calculé à l'aide du modèle numérique d'hydrologie ISBA sur la période 1950-1995. La figure 4.14 représente cette comparaison. Ces deux courbes ont été normalisées. En effet, les données marégraphiques ne nous renseignent que sur la partie côtière des océans et non sur la partie hauturière. Or, une étude récente de *Prandi et al.* [2009] montre que la variabilité interannuelle en moyenne globale est plus importante pour le niveau de la mer côtier observé par les marégraphes par rapport aux données d'altimétrie spatiale. Ces auteurs montrent que les marégraphes voient une élévation du niveau de la mer du même ordre de grandeur que l'altimétrie spatiale avec, toutefois une plus forte variabilité interannuelle due à la distribution non homogène des marégraphes. C'est pour ces raisons que nous avons normalisé les deux courbes. De ce fait, nous focalisons cette étude sur les amplitudes relatives et les phases des différents signaux.

La figure 4.14 montre la bonne corrélation (0.5) entre ces deux signaux dans les hautes fréquences. Cependant, les basses fréquences ne sont toujours pas expliquées par les variations d'eau terrestre. Néanmoins, n'oublions pas que les calottes polaires ne sont pas prises en compte dans cette comparaison, du fait de la non existence de données tant *in situ* que des modélisations. Afin de discriminer les signaux responsables de cette variabilité, nous allons analyser les spectres de ces deux courbes.

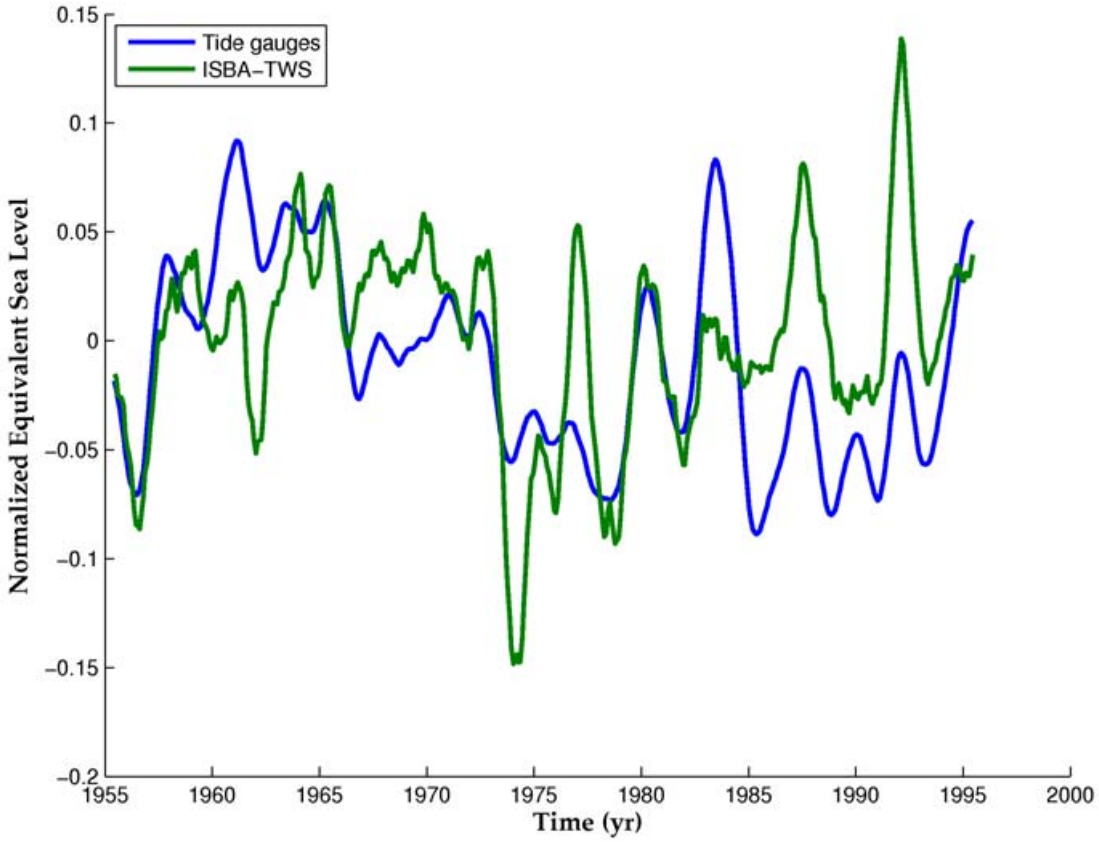

FIG. 4.14 – Séries temporelles du niveau de la mer observé (courbe bleue) à partir des données des marégraphes utilisés dans les études de *Jevrejeva et al.* [2006, 2008]. La courbe verte représente la contribution du stock d'eaux continentales exprimé en niveau de la mer équivalent et déduit du modèle d'hydrologie ISBA (*Alkama et al.* [2010]; *Decharme et al.* [2010]. Les signaux saisonniers sont retirés pour chaque courbe et la tendance moyenne respective a aussi été retranchée. La courbe du niveau de la mer observée par les marégraphes est lissée grâce à une moyenne glissante sur 11 mois. Les courbes sont normalisées.

La figure 4.15 représente les spectres du niveau de la mer observé par les marégraphes (courbe bleue, *Jevrejeva et al.* [2006, 2008]), de la contribution des eaux continentales exprimée en niveau de la mer équivalent (courbe rouge). Ces spectres mettent en évidence des signaux majeurs entre 3-4 ans et 6-7

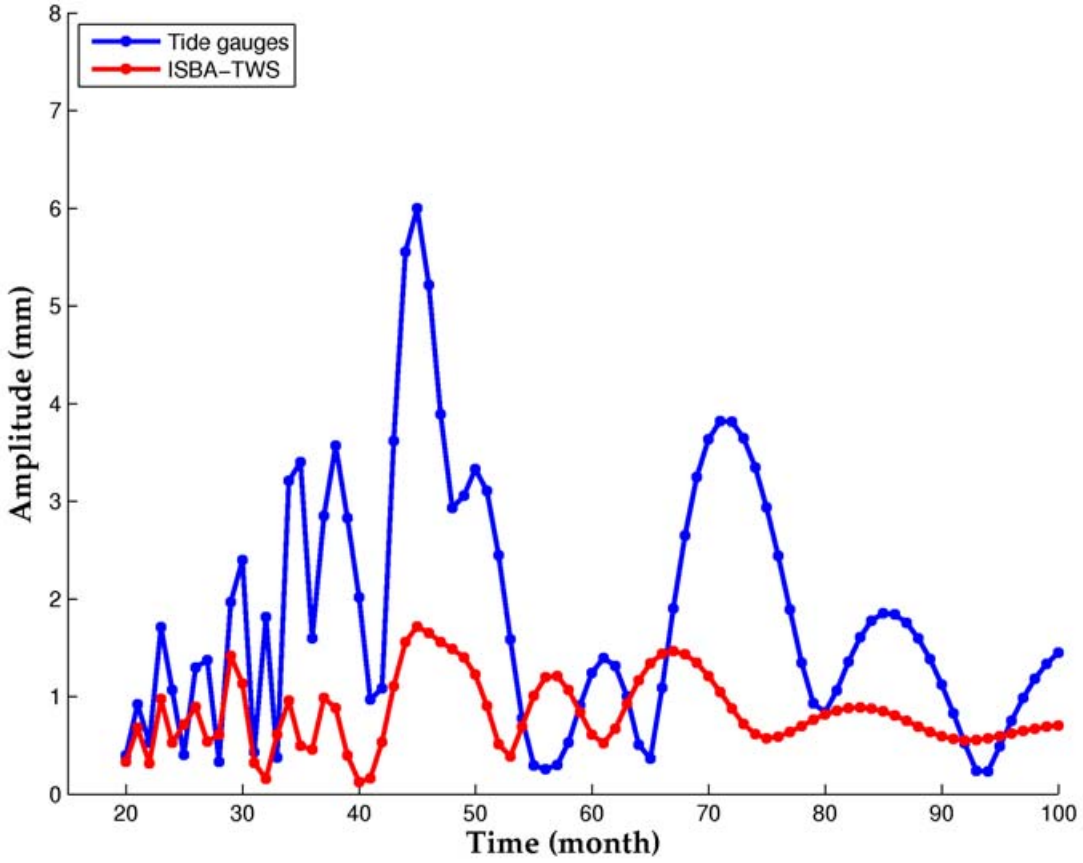

FIG. 4.15 – Spectres des séries temporelles du niveau de la mer observé par les marégraphes (courbe bleue, *Jevrejeva et al.* [2006, 2008]), de la contribution des eaux continentales en niveau de la mer équivalent (courbe rouge) et du SOI (Southern Oscillation Index) un *proxi* d'ENSO. Dans chaqu'un des cas les signaux saisonniers ont été retirés avant l'analyse harmonique sur la période commune entre 1955 et 1995.

ans présent dans les séries temporelles des variations du niveau de la mer en moyenne globale et la variation du stock des eaux continentales.

L'utilisation du modèle d'hydrologie continentale confirme les résultats suggérés par GRACE. Ainsi, la variation en moyenne globale du stock des eaux continentales explique une partie de la variabilité interannuelle du niveau de la mer observé pour les années récentes mais aussi pour les dernières décennies.

Global and Planetary Change 75 (2011) 76–82

Contents lists available at ScienceDirect

Global and Planetary Change

journal homepage: www.elsevier.com/locate/gloplacha

Terrestrial waters and sea level variations on interannual time scale

W. Llovel [a,*], M. Becker [a], A. Cazenave [a], S. Jevrejeva [b], R. Alkama [c], B. Decharme [c], H. Douville [c], M. Ablain [d], B. Beckley [e]

[a] LEGOS/OMP, 14 avenue Edouard Belin, Toulouse, France
[b] Proudman Oceanographic Laboratory, Liverpool, UK
[c] CNRM, 42 avenue Gaspard Coriolis, Toulouse, France
[d] CLS, Ramonville Saint Agne, France
[e] NASA/Goddard Space Flight Center, Greenbelt, USA

ARTICLE INFO

Article history:
Received 25 May 2010
Accepted 18 October 2010
Available online 26 October 2010

Keywords:
land water storage
sea level variations
tide gauges
satellite altimetry

ABSTRACT

On decadal to multidecadal time scales, thermal expansion of sea waters and land ice loss are the main contributors to sea level variations. However, modification of the terrestrial water cycle due to climate variability and direct anthropogenic forcing may also affect sea level. For the past decades, variations in land water storage and corresponding effects on sea level cannot be directly estimated from observations because these are almost unexistent at global continental scale. However, global hydrological models developed for atmospheric and climatic studies can be used for estimating total water storage. For the recent years (since mid-2002), terrestrial water storage change can be directly estimated from observations of the GRACE space gravimetry mission. In this study, we analyse the interannual variability of total land water storage, and investigate its contribution to mean sea level variability at interannual time scale. We consider three different periods that, each, depend on data availability: (1) GRACE era (2003–2009), (2) 1993–2003 and (3) 1955–1995. For the GRACE era (period 1), change in land water storage is estimated using different GRACE products over the 33 largest river basins worldwide. For periods 2 and 3, we use outputs from the ISBA-TRIP (Interactions between Soil, Biosphere, and Atmosphere—Total Runoff Integrating Pathways) global hydrological model. For each time span, we compare change in land water storage (expressed in sea level equivalent) to observed mean sea level, either from satellite altimetry (periods 1 and 2) or tide gauge records (period 3). For each data set and each time span, a trend has been removed as we focus on the interannual variability. We show that whatever the period considered, interannual variability of the mean sea level is essentially explained by interannual fluctuations in land water storage, with the largest contributions arising from tropical river basins.

1. Introduction

On decadal to multidecadal time scales, thermal expansion of sea waters and land ice loss are the main contributors to sea level variations (Bindoff et al., 2007). However, modification of the terrestrial water cycle due to climate variability and direct anthropogenic forcing may also affect sea level (Milly et al., 2010). While in recent years, thermal expansion and land ice melt were the object of numerous investigations (Bindoff et al., 2007; see also Cazenave and Llovel, 2010 for a review), the terrestrial water contribution to sea level has been less studied (Milly et al., 2010). For the past decades, variations in land water storage caused by climate change and variability cannot be directly estimated from observations because these are almost unexistent at global continental scale. However, global hydrological models (or land surface models) developed for atmospheric and climatic studies can be used for estimating total water storage (Milly et al., 2010). The models compute the mass and energy balance at the Earth surface, as well as water storage change in soil in response to prescribed variations of near-surface atmospheric data (precipitation, temperature, humidity and wind) and radiation. Using atmospheric re-analyses and the Orchidee land surface model outputs, Ngo-Duc et al. (2005a) estimated the terrestrial water storage contribution to sea level over 1950–2000. They found no climatic long-term trend but large interannual/decadal fluctuations, of several millimetre amplitudes when translated into sea level equivalent. A similar result was also found by Milly et al. (2003) using the Land Dynamics model over 1980–2000. Direct human intervention on land water storage and induced sea level changes have been estimated in several studies (e.g., Chao, 1995; Sahagian, 2000; Gornitz, 2001; Chao et al., 2008). The largest contributions come from groundwater pumping (either for agriculture, industrial and domestic use) and reservoir filling. Surface water depletion has a non

* Corresponding author.
E-mail address: william.llovel@legos.obs-mip.fr (W. Llovel).

0921-8181/$ – see front matter © 2010 Elsevier B.V. All rights reserved.
doi:10.1016/j.gloplacha.2010.10.008

negligible contribution. Although detailed information is lacking, and estimates vary significantly between authors, ground water depletion may have contributed to past decades sea level rise by 0.55–0.64 mm/yr (e.g., Gornitz, 2001). A recent update by Wada et al. (2010) suggests an even larger contribution of groundwater depletion, of 0.8 ± 0.1 mm/yr sea level rise over 1960–2000. During the past 50 years, several tens of thousands of dams have been constructed over world rivers, leading to water impoundment into artificial reservoirs, hence negative contribution to sea level. Several attempts have been made to estimate the total volume of water stored in artificial reservoirs over the past half century (e.g., Chao, 1995; Vörösmarty et al., 1997; Sahagian, 2000; Gornitz, 2001). Chao et al. (2008) reconstructed water impoundment history of nearly 30,000 reservoirs constructed during the 20th century and estimated a −0.55 mm/yr contribution to sea level due to dams and artificial reservoirs during the past half century. Hence, for the last few decades, effects on sea level from groundwater depletion and water impoundment behind dams are of the same order of magnitude and opposite sign. However, a slight positive residual contribution to sea level, of ~0.25 mm/yr, may be expected if the groundwater depletion component dominates.

For the recent years, terrestrial water storage (TWS) change can also be estimated from observations of the GRACE space gravimetry mission. The GRACE mission, launched in 2002, was developed by US National Aeronautics and Space Administration (NASA) and the German Aerospace Centre (DLR), to measure spatio-temporal change of the Earth gravity field at a monthly interval (Tapley et al., 2004). On time scales ranging from months to decades, these temporal gravity variations mainly result from surface redistribution of water inside and among the outer fluid envelopes of the Earth (Wahr et al., 2004). Thus, on land, GRACE provides measurements of TWS change in river basins. Two recent studies (Ramillien et al., 2008; Llovel et al., 2010a) have estimated the water volume trend in the ~30 largest river basins worldwide using GRACE, and found small net water volume change globally since 2003, with a ±0.2 mm/yr sea level rise contribution.

In the present study, we focus on the interannual variability of TWS rather than on the trend, and investigate its contribution to mean sea level variability. We consider three different periods which each depends on data availability: (1) 2003–2009 (GRACE era), (2) 1993–2003 and (3) 1955–1995. For the GRACE era (period 1), accordingly, we use GRACE data to estimate TWS. For periods 2 and 3, we estimate TWS variations from outputs of the ISBA-TRIP (Interactions between Soil, Biosphere, and Atmosphere—Total Runoff Integrating Pathways) global hydrological model (Alkama et al., 2010). For sea level, we used tide gauge-based values for period 3 and satellite altimetry for periods 1 and 2 (see Section 3).

2. Effect of land water storage change on sea level

Excluding ice sheets and glaciers, fresh water on land is stored in various reservoirs: snow pack, rivers, lakes, man-made reservoirs, wetlands and inundated areas, root zone (upper few meters of the soil) and aquifers (groundwater reservoirs). Terrestrial waters are continuously exchanged with atmosphere and oceans through vertical and horizontal mass fluxes (precipitation, evaporation, transpiration of the vegetation, surface runoff and underground flow). This exchange is an integral part of the global climate system, with important links and feedbacks generated through its influence on surface energy and moisture fluxes between continental water, atmosphere and oceans. Thus climate change and variability modify TWS. As briefly discussed earlier, human activities also directly affect TWS.

To estimate the contribution of TWS variations on sea level, we can simply consider the conservation of water mass in the Earth's system as in previous studies (e.g., Chen et al., 1998). On time scales of years to decades, solid Earth stores can be neglected, so that only changes in terrestrial reservoirs, ocean and atmosphere can be considered, with the mass conservation as follows:

$$\Delta M_{cont} + \Delta M_{ocean} + \Delta M_{atm} = 0 \quad (1)$$

where ΔM represents changes in water mass for the three reservoirs: continents, ocean and atmosphere.

Previous studies have shown that water vapour change in the atmosphere cannot be neglected at the annual time scale (Chen et al., 1998; Minster et al., 1999). On multidecadal time scale, it is generally considered that change in atmospheric water storage is negligible (Trenberth and Smith, 2005), even if because of global warming, an increase of atmospheric water vapour is expected. However, because of the water holding capacity of the atmosphere, even with higher temperature, this contribution is expected to be small as far as sea level change is concerned. Trenberth and Smith (2005) showed that, on interannual time scale, water vapour fluctuations are mostly associated with ENSO (El Nino-Southern Oscillation) events and lead to up to ~0.5×10^{15} kg variations of the mass of the atmosphere. When translated into sea level equivalent, this corresponds to sea level fluctuations at the mm level. This is not negligible considering the range of interannual fluctuations of the global mean sea level during ENSO events (of about 8 mm; see later). However in the present study, we choose to ignore the water vapour contribution.

Thus Eq. (1) becomes:

$$\Delta M_{ocean} \approx -\Delta M_{cont}. \quad (2)$$

ΔM_{ocean} represents the change with time in mass of the ocean due to total fresh water input from continents (i.e., land waters plus land ice melt). It can be further expressed in terms of equivalent sea level change by simply dividing the total continental water volume change by the mean surface of the oceans (assumed equal to 360×10^6 km^2) and changing its sign. In the following, we only consider the land water contribution because it is the purpose of the present study (keeping in mind that global land ice fluctuations may eventually slightly contribute to the sea level interannual signal). The associated ΔM_{cont} component may then be quantified in estimating the change in water storage on land (with $\Delta M_{cont} = \Delta TWS$).

At a river basin scale, temporal change in water storage TWS is related to precipitation P, evapotranspiration E and river runoff R through the water balance equation:

$$dTWS/dt = P - E - R \quad (3)$$

If P, E and R, or TWS were known globally, it would be possible to use these hydrological parameters to estimate the effect of land water storage on sea level. GRACE space gravimetry provides direct measurements of TWS while hydrological models solve Eq. (3) to estimate TWS.

3. Data used in this study

3.1. Sea level data

For periods 1 (2003–2009) and 2 (1993–2003) GMSL is derived from satellite altimetry (Topex/Poseidon, Jason-1 and Jason-2). Data from two different groups are considered (CLS — Collecte Localisation Satellites, update from Ablain et al., 2009 and NASA/GSFC — Goddard Space Flight Center, Beckley et al., 2010). While altimetry-based GMSL trends agree well whatever the data processing group, slight differences are noticed on interannual time scale, as we will see later.

The altimetry data are corrected for the standard geophysical and environmental corrections, including instrumental drifts and bias (see Ablain et al., 2009; Beckley et al., 2010 for details).

For period 3 (1955–1995), we considered global mean sea level (GMSL) time series computed by Jevrejeva et al. (2006) from tide gauge records. These authors used 1023 RLR (Revised Local Reference) tide gauge records (monthly data) from the Permanent Service for Mean Sea Level (PSMSL) (Woodworth and Player, 2003). However, they excluded data from Japan due to lack of information about vertical land motion during earthquake events, as well as data from the Baltic Sea because they may not be representative of the global ocean. This led to a total of about 800 stations usable for the global mean sea level reconstruction. The maximum number of tide gauges in a given year is 585. No inverted barometer correction was applied. Tide gauge records were corrected for glacial isostatic adjustment (GIA) of the solid Earth (Peltier, 2001). To overcome geographical bias (sampling issue of station locations) a "virtual station" method has been used. In this method, stations close to each other are weighted much less than isolated ones and uncertainties depend on how considered stations are locally representative of the estimated sea level. Global mean sea level (GMSL) data and their errors (Jevrejeva et al., 2006) are available from http://www.psmsl.org/products/reconstructions/jevrejevaetal2006.php.

3.2. Terrestrial water storage

3.2.1. The ISBA-TRIP global hydrological model

ISBA is a relatively simple land surface model (LSM) that uses the force-restore method to calculate the time variation of the surface energy and water budgets (Noilhan and Planton, 1989) including snow pack evolution based on a simple one-layer scheme (Douville et al., 1995). The soil hydrology is represented by three layers: a thin surface layer (1 cm) included in the rooting layer and a third layer to distinguish between the rooting depth and the total soil depth (Boone et al., 1999). An exponential profile of the saturated hydraulic conductivity with soil depth is also assumed for the soil column. This type of profile attempts to represent the fact that roots and organic matter favor the development of macropores and enhance water movement near the soil surface, and that soil compaction is an obstacle for vertical water transport in the deep soil (Decharme et al., 2006). The soil water content varies with surface infiltration, soil evaporation, plant transpiration and deep drainage. The infiltration rate is computed as the difference between the through-fall rate and the surface runoff. The through-fall rate is the sum of rainfall not intercepted by the canopy, dripping from the interception reservoir and snowmelt from the snow pack. ISBA also uses a comprehensive parameterization of sub-grid hydrology to account for the heterogeneity of precipitation, topography and vegetation within each grid cell (Decharme and Douville, 2006).

The total runoff integrating pathways (TRIP) was developed at Tokyo University by Oki and Sud (1998). It is a simple river routing model (RRM) used to convert the daily runoff simulated by ISBA into river discharge on a global river channel network here defined at 1° by 1° resolution. The runoff part of the simulated TWS can be validated using direct comparison between simulated and observed discharge. TRIP is a simple linear model based on a single prognostic equation for the water mass within each grid cell of the hydrologic network. In other words, TRIP only simulates a surface stream reservoir and the stream flow velocity is assumed constant and uniform at 0.5 m s^{-1}.

The outputs of the ISBA-TRIP model cover the period January 1950 to December 2006, with values given at monthly interval on a $1°\times1°$ grid. They are based on a run in forced mode. The global meteorological forcing was provided by the Princeton University (available online at http://hydrology.princeton.edu) on a 3-hourly time step and at a 1° resolution (see Alkama et al., 2010 for more details).

3.2.2. GRACE data

Raw GRACE data are processed by different groups belonging to the GRACE project (Center for Space Research —CSR, Jet Propulsion Laboratory —JPL— in the USA and Geo-ForschungsZentrum —GFZ— in Germany). GRACE data are also processed by other groups (GSFC/NASA in the USA; GRGS — Groupe de Recherche en Géodésie Spatiale — in France and DUT — Delft University of Technology— in The Netherlands). The GRACE products delivered over land by all groups are time series of equivalent water height, expressed either in terms of spherical harmonic expansion or as gridded data. Several GRACE product releases have been available from the GRACE project, each time with substantial improvement. Here we use different GRACE data sets: (1) the latest release (RL04) from the TELLUS website (http://grace.jpl.nasa.gov/data/mass/) for three solutions: the CSR, GFZ and JPL solutions ($1°\times1°$ global grids at monthly interval). The RL04 release includes an implementation of the carefully calibrated combination of destripping and smoothing, with a 300 km half-width Gaussian filter (Chambers, 2006). These GRACE products are also corrected for post-glacial rebound (the solid Earth response to last deglaciation, also sensed by GRACE) using the Paulson et al. (2007) model (but note that, as we focus here on interannual variability, we do not need to take care of this purely secular effect). These time series cover the period from August 2002 through July 2009. We also analysed GRGS solutions (updated from Biancale et al., 2007; data available at http://bgi.cnes.fr:8110/geoid-variations/). Processing of the GRGS GRACE data is described in detail in Bruinsma et al. (2010). The data consist of 10-day $1°\times1°$ gridded solutions expressed in equivalent water height (their actual spatial resolution is about 400 km; Bruinsma et al., 2010). They cover the period from July 2002 to April 2009.

As in Llovel et al. (2010a), we computed water storage change over the 33 largest world river basins (see Fig. 1 for location). The river basin contours are based on masks of 1° resolution from Oki and Sud (1998). To estimate the water storage (i.e., water volume) contribution of individual river basins at each time step, the spatial average of GRACE equivalent water height has been computed over the area included inside the basin contour, then multiplied by the basin area. This analysis was repeated for each of the three CSR, GFZ and JPL GRACE products, from which an average TWS time series was deduced. Similar calculations were performed with the GRGS solutions.

4. Results

Each sea level and TWS time series has been detrended and the seasonal cycles (annual plus semi-annual) have been removed (12-month and a 6-month period sinusoids have been adjusted to each time series and removed). Each residual time series had its mean value set to zero over the time span of interest. TWS from both GRACE and ISBA-TRIP outputs was further expressed in terms of equivalent sea level (ESL) as explained in Section 2. In the following, this quantity is called TWS-ESL.

4.1. Period 1 (2003–2009)

For period 1 (2003–2009) GMSL is based on satellite altimetry data (updated from Ablain et al., 2009). For this time span, we have removed steric effects from the GMSL (i.e., the effects of ocean temperature and salinity) before comparing sea level variations with GRACE-based TWS-ESL. In effect, sea level variations result from both steric and mass effects. As we focus here on a mass component (the land water storage contribution), it is appropriate to remove the steric effects to observed global mean sea level. This is done using Argo profiling floats data processed by Guinehut et al. (2009). The steric sea level computation is described in another paper (Llovel et al., 2010b). Fig. 2 compares interannual variability in GMSL (corrected for steric effects) and TWS-ESL from GRACE (sum of the 33 river basin contributions). The two GRACE time series are shown (i.e., the mean CSR/GFZ/JPL solution and the GRGS solution). Fig. 2

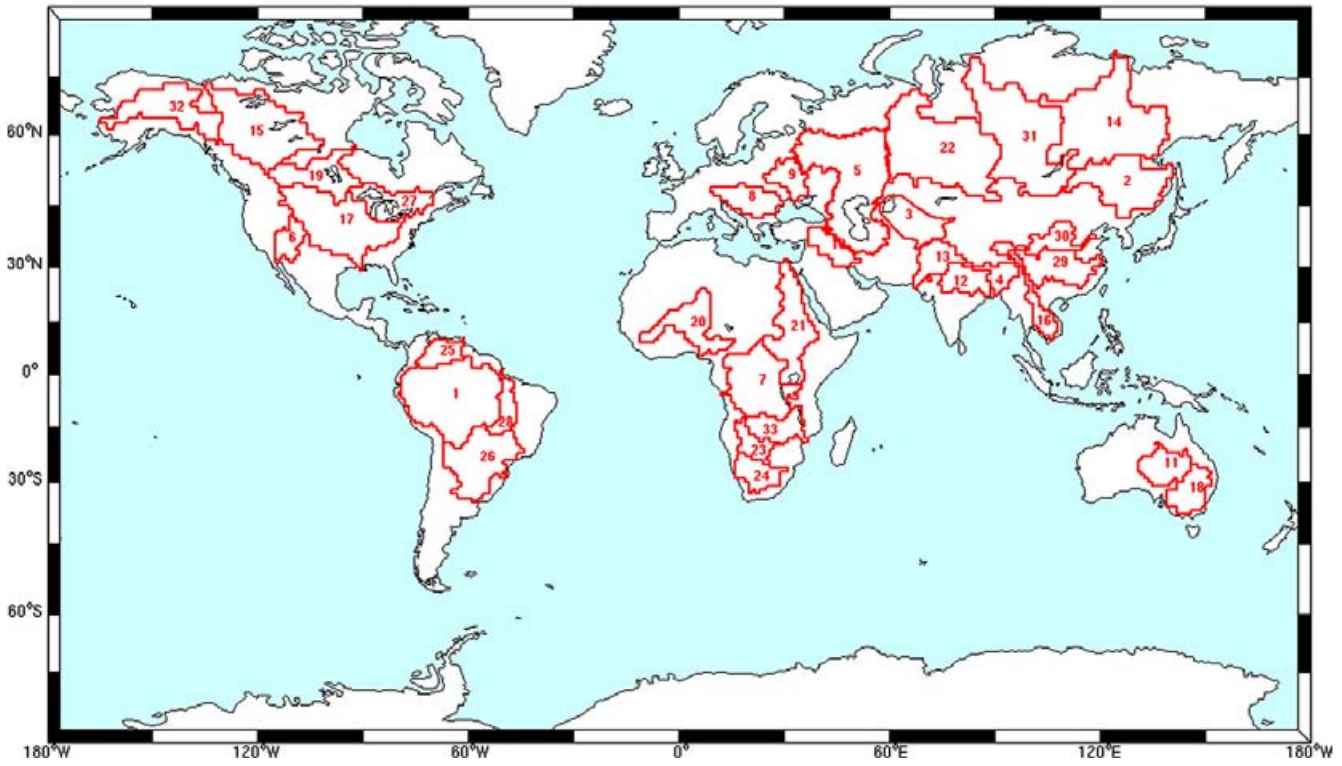

Fig. 1. Location of the 33 river basins used for computing TWS from GRACE and ISBA-TRIP data. List of the 33 river basins considered and associated number: 1: Amazon, 2: Amur, 3: Aral, 4: Brahmaputra, 5: Caspienne/Volga, 6: Colorado, 7: Congo, 8: Danube, 9: Dniepr, 10: Euphrates, 11: Eyre, 12: Ganges, 13: Indus, 14: Lena, 15: Mackenzie, 16: Mekong, 17: Mississippi, 18: Murray, 19: Nelson, 20: Niger, 21: Nile, 22: Ob, 23: Okavango, 24: Orange, 25: Orinoco, 26: Parana, 27: St-Lawrence, 28: Tocantins, 29: Yangtze, 30: Yellow, 31: Yenisey, 32: Yukon, and 33: Zambeze.

also shows TWS-ESL from the ISBA-TRIP model (same 33 river basins). As mentioned previously, all time series are detrended and seasonal signal has been removed. A 3-month running mean smoothing was applied to the data.

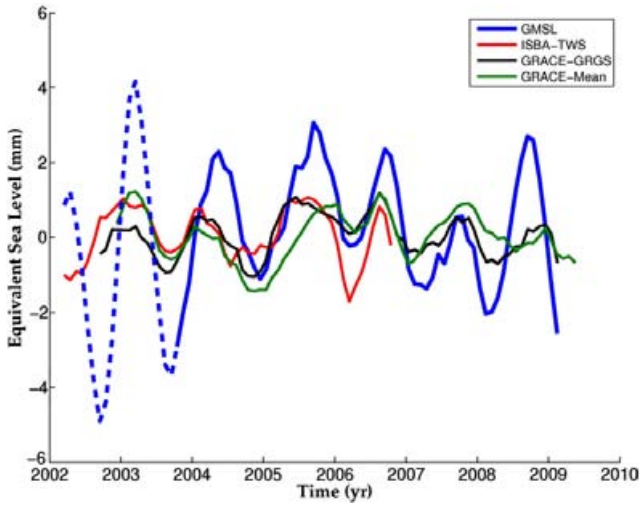

Fig. 2. Interannual variability of the altimetry-based global mean sea level (GMSL) corrected for thermal expansion over 2003–2009 (blue curve —data from Llovel et al., 2010b) and terrestrial water storage (expressed in equivalent sea level) —TWS-ESL from the ISBA-TRIP model (red curve) and GRACE (green curve: data from the mean CSR/GFZ/JPL; black curve: data from GRGS updated from Llovel et al., 2010a). The time series are detrended, and the seasonal cycle is removed. The time series are smoothed with a 3-month window.

Looking at Fig. 2, we first note that the two GRACE solutions agree reasonably well (correlation coefficient of 0.61 at the 95% confidence level). They also agree well with ISBA-TRIP TWS-ESL over their overlapping time span. Interannual fluctuations in GMSL (corrected for steric effects) are positively correlated with TWS-ESL (correlation coefficient of 0.5 and 0.7 with the mean CSR/GFZ/JPL and GRGS solutions respectively at the 95% confidence level). We note that the agreement between sea level and TWS improves beyond 2004. As discussed in Llovel et al. (2010b), the poor Argo coverage in 2002–2003 underestimates the steric sea level correction. For that reason, the corrected sea level for 2002–2003 is shown by a dashed curve. However, the overall agreement over the 2003–2009 time span is good. This result suggests that for the recent years, interannual variability of GMSL is, at least partly, caused by year-to-year variability of land water storage. Fig. 2 is suggestive of nearly annual fluctuations. However, as already mentioned, the annual cycle has been removed. A spectral analysis –not shown– of the three TWS-ESL time series (i.e., the two GRACE solutions and the ISBA-TRIP outputs, with data at monthly interval) displays peaks in the 14–16 month and 24–25 month wavebands. The origin of these signals is unclear and needs further investigation.

Following the conclusions of Ngo-Duc et al. (2005b), we investigated whether the tropical river basins mostly contribute to the TWS interannual variability. For that purpose, we constructed the GRACE-based TWS time series (data from GRGS only), considering only the following basins: Amazon, Orinoco, Niger, Congo, Okavango, Indus, Ganges and Mekong. The corresponding curve, expressed in water volume is shown in Fig. 3. For comparison the curve for the 33 basins is superimposed. Fig. 3 clearly shows the dominant contribution of the tropical river basins. On Fig. 3 we also show the Amazon contribution. Interestingly, the Amazon basin alone is a major contribution to the total signal. Thus we conclude that interannual variability in sea level is highly associated with water fluctuations of the Amazon basin.

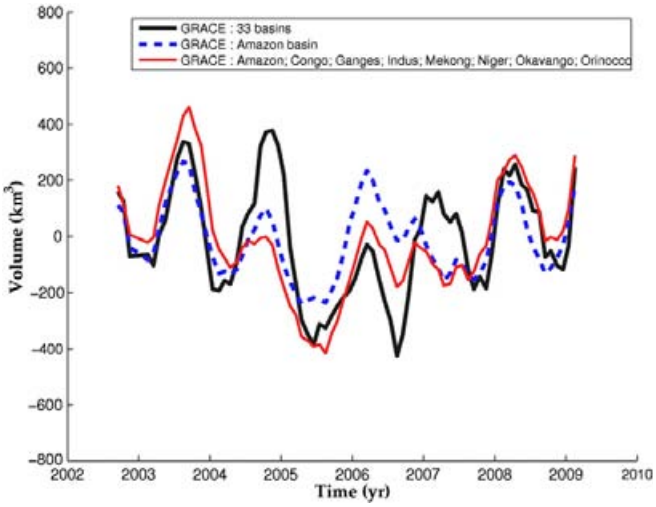

Fig. 3. TWS variability (data from GRGS) over 2003–2009: total (33 river basins; black curve); contribution from 8 tropical river basins (red curve: 1: Amazon, 7: Congo, 12: Ganges, 13: Indus, 16: Mekong, 20: Niger, 23: Okavango, and 25: Orinoco) and contribution from the Amazon only (blue curve). The time series are detrended, and the seasonal cycle is removed. The time series are smoothed with a 3-month window.

4.2. Period 2 (1993–2003)

For this time span (1993–2003), we compared TWS-ESL from ISBA-TRIP with the altimetry-based global mean sea level. Here we show two altimetry-based GMSL curves (from Ablain et al., 2009 —called CLS, and from Beckley et al., 2010 —called GSFC). A 3-month running mean smoothing was applied to the data. The CLS (Fig. 4a) and GSFC (Fig. 4b) sea level curves, superimposed to ISBA-TRIP TWS-ESL, are presented separately for clarity. As for period 1, the two quantities can be directly compared. However, unlike for period 1, we did not correct for steric effects here. For the pre-Argo period, steric effects are mostly based on XbT temperature data, subjects to significant uncertainties. A recent study by Lyman et al. (2010) compares different global ocean heat content curves computed by different teams for the period 1993–2008 and shows large difference in interannual variability, especially for the pre-Argo years (before 2002), revealing large uncertainties introduced by the XbT measurements (in particular the XbT depth bias correction). As global heat content and thermal expansion follow similar time evolution, we choose to not correct sea level for steric effects, in order not to introduce spurious noise on interannual time scale.

Fig. 4a,b shows significant correlation (~0.5 and ~0.7 with CLS and GSFC products respectively at the 95% confidence level) between altimetry-based sea level and TWS-ESL (from ISBA-TRIP), especially during the 1997–1998 ENSO event, and also between 2002 and 2004 (another ENSO period). During such events, positive sea level anomalies seem to essentially result from land water storage change (more specifically, from water deficit on land). The study by Ngo-Duc et al. (2005b) analysed the cause for a higher/smaller than normal annual cycle in GMSL (based on Topex/Poseidon altimetry) in 1997–1998, during the large 1997–1998 ENSO event. Using the Orchidee LSM, run in a coupled mode with the Atmospheric General Circulation Model of the Laboratoire de Meteorologie Dynamique, they showed that higher/smaller annual amplitude in sea level (corrected for thermal expansion) in 1997/1998 could be explained by higher/smaller TWS-ESL, as a result of particularly dry conditions on land due to important precipitation deficit over tropical land (inside the 20°N–20°S domain) during this ENSO event. Year-to-year fluctuations in TWS annual amplitude translate into interannual variability. This is exactly what Fig. 4a,b shows during the 1997–1998 ENSO. Previous results based on the Orchidee LSM are indeed confirmed when using

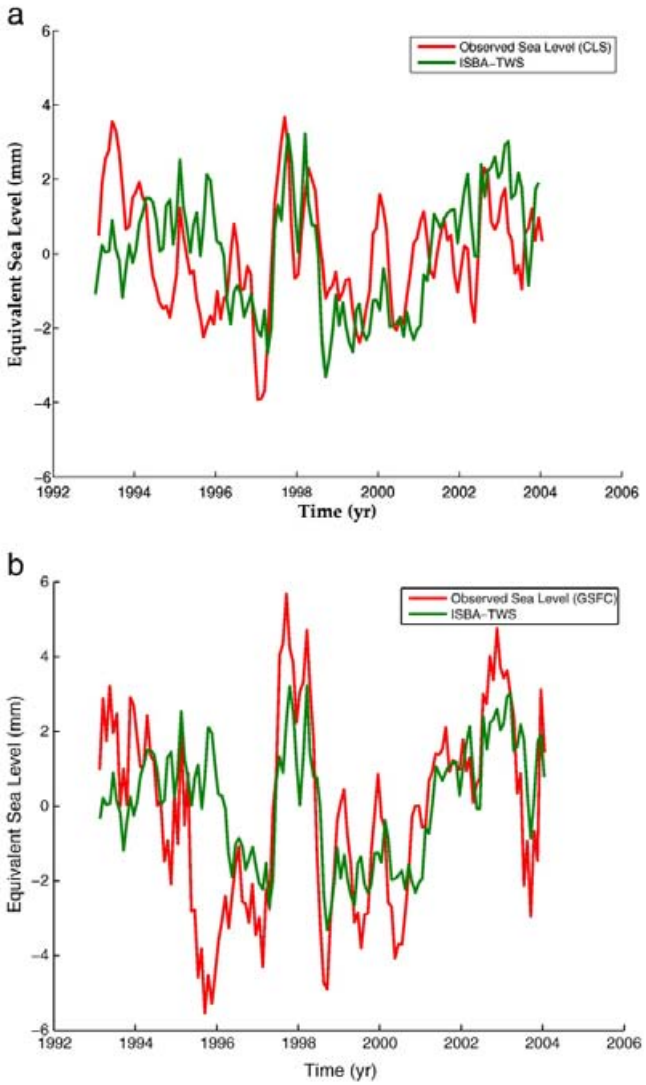

Fig. 4. Interannual variability of the altimetry-based global mean sea level (solid curve) and terrestrial water storage (expressed in equivalent sea level) —TWS-ESL from the ISBA-TRIP model (dashed curve) over 1993–2003. (a) Global mean sea level from Ablain et al. (2009) — CLS; (b) global mean sea level from Beckley et al. (2010) —GSFC. The time series are detrended, and the seasonal cycle is removed. The time series are smoothed with a 3-month window.

the ISBA-TRIP model. Thus, we can quantitatively explain GMSL anomaly in 1997–1998 by a net water deficit on land during this ENSO event. The good correspondence seen between GMSL and TWS-ESL around 2002–2004 (another ENSO period) suggests that the same hydrological conditions produce similar effects.

In Fig. 4a,b, we note some discrepancy between sea level and TWS-ESL in 1995. We cannot exclude a steric origin (as steric effects are not corrected for). However, the two sea level curves do not perfectly coincide at this epoch, suggesting that some efforts should be made to better estimate interannual variability in global mean sea level. Besides, these disagreements could be due to some other phenomena not considered or modelled in the ISBA-TRIP model.

4.3. Period 3 (1955–1995)

Fig. 5 shows the interannual to decadal variability in sea level (based on tide gauge data from Jevrejeva et al., 2006) and TWS-ESL (from ISBA-TRIP) between 1955 and 1995. Here the two curves have

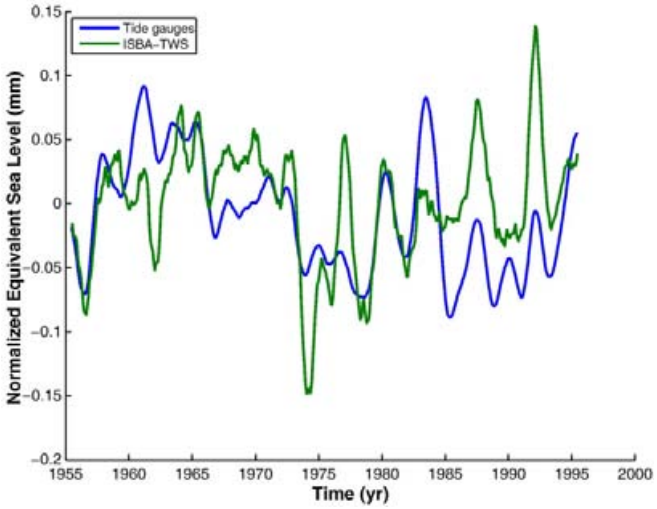

Fig. 5. Interannual variability of the global mean sea level (solid curve; data from Jevrejeva et al., 2006) and terrestrial water storage (expressed in equivalent sea level) —TWS-ESL from the ISBA-TRIP model (dashed curve)— between 1955 and 1995. The time series are detrended, and the seasonal cycle is removed. The time series are smoothed with an 11-month window.

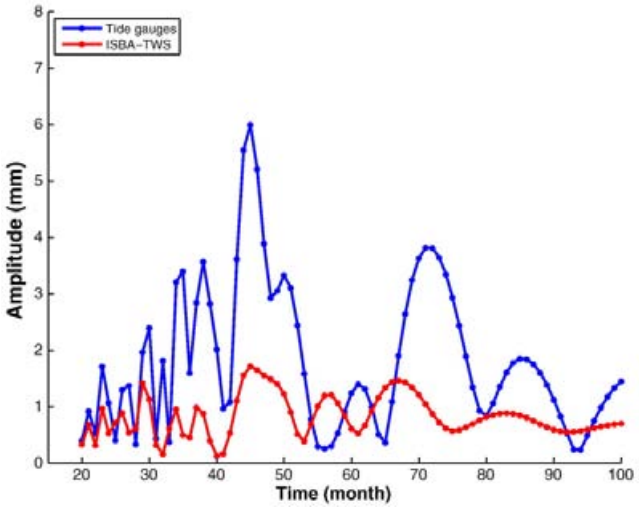

Fig. 6. Amplitude spectra of the data shown in Fig. 5 (sea level data: solid curve; TWS-ESL: dashed curve).

been normalized (norm defined by the largest singular value of the time series). In effect, as shown in Prandi et al. (2009), coastal mean sea level displays higher interannual variability than GMSL based on global data coverage (e.g. from satellite altimetry). This is a sampling effect due to sparse tide gauge records when compared to the 'true' global mean computed with quasi global altimetry data. For comparing with TWS-ESL (which represents a global signal), we thus decided to normalize both time series to not artificially enhance the observed coastal sea level variability. As for period 2, steric effects have not been corrected for. An 11-month running mean smoothing has been applied to the data. From Fig. 5, we note that the two curves are positively correlated (correlation of ~0.5 at the 95% confidence level). The fluctuations are suggestive of ENSO (El Nino-Southern Oscillation)-type variability (as observed in 1997–1998 during period 2). For example, we note positive sea level and TWS-ESL anomalies in 1982–1983 and 1986–1987, periods of strong ENSO events. We performed a spectral analysis (based on data at monthly interval) of mean sea level and TWS-ESL (note that in this case mean sea level and TWS-ESL are not normalized). Amplitude spectra are shown in Fig. 6. Dominant peaks in sea level and TWS-ESL are seen around 3–4 years 6–7 years, as expected for a dominant ENSO forcing. Previous studies (e.g., Merrifield et al., 2009; Nerem et al., 2010) have reported high correlation between detrended global mean sea level (over the altimetry period) and ENSO proxies, in particular the Multivariate ENSO Index —MEI (MEI is computed with the six main observed variables over the tropical Pacific which are sea level pressure, zonal and meridional components of the surface wind, sea surface temperature, surface air temperature, and total cloudiness fraction of the sky, for more information see Wolter, 1987). Nerem et al. (2010) suggest that the observed correlation could result from either a change in ocean heat content associated with ENSO or a change in land/ocean precipitation patterns during ENSO. Our analysis of TWS suggests that it is rather the second process that leads to the observed correlation, more specifically the change in land water storage during ENSO events.

5. Discussion

The results presented earlier for three different time frames (2003–2009, 1993–2003 and 1955–1995) reveal the important contribution of global terrestrial water storage variations to the interannual variability of the global mean sea level. For periods 2 (1993–2003) and 3 (1955–1995) the results are based on the ISBA-TRIP model. Furthermore, for period 1 (2003–2009) we used GRACE space gravimetry data. This study reports a dominant ENSO signature in interannual GMSL and TWS fluctuations. Quantitative comparison with global terrestrial water storage variations shows that the process involved is water exchange between land river basins and oceans, with drier than normal land during ENSO events. As suggested by Ngo-Duc et al. (2005b), tropical basins are probably the regions mostly involved in this exchange. The Amazon basin in particular shows a dominant contribution (at least for period 1) in the exchange of water between land and oceans on interannual time scale. This study points towards a significant influence of the terrestrial water cycle on sea level. It provides an explanation of processes involved in the correlation reported by Nerem et al. (2010) between GMSL and ENSO proxies. It also provides a quantitative explanation of the origin of the interannual variability in sea level. This interannual variability in sea level has been noticed in many previous studies, but so far had remained unexplained. Besides, another potential contribution remains to be investigated: the atmospheric water vapour reservoir. Variability of water vapour may eventually explain part of the difference between global mean sea level and land water storage at interannual time scale.

Acknowledgements

W. Llovel is supported by a PhD Grant from CNRS and the Region Midi-Pyrenees. M. Becker and R. Alkama are supported by Post Doctoral fellowships from the ANR project 'CECILE' and the RTRA-STAE project 'CYMENT'. We thank R.S. Nerem and two anonymous reviewers for very useful comments. GRACE data of the TELLUS website were processed by D. P. Chambers, supported by the NASA Earth Science REASoN GRACE Project, and are available at http://grace.jpl.nasa.gov.

References

Ablain, M., Cazenave, A., Guinehut, S., Valladeau, G., 2009. A new assessment of global mean sea level from altimeters highlights a reduction of global slope from 2005 to 2008 in agreement with in-situ measurements. Ocean Sci. 5 (2), 193–201.

Alkama, R., Decharme, B., Douville, H., Voldoire, A., Tyteca, S., Le Moigne, P., Becker, M., Cazenave, A., Sheffield, J., 2010. Global evaluation of the ISBA-TRIP continental hydrological system. Part 1: comparison to GRACE terrestrial water storage estimates and in-situ river discharges. J. Hydromet. 583–600. doi:10.1175/2010JHM1211.1.

Beckley, B.D., Zelensky, N.P., Holmes, S.A., Lemoine, F.G., Ray, R.D., Mitchum, G.T., Desai, S., Brown, S.T., 2010. Assessment of the Jason-2 extension to the TOPEX/Poseidon, Jason-1 sea surface height time series for global mean sea level monitoring. Mar. Geodesy 33 (1), 447–471.

Biancale, R., Lemoine, J.-M., Balmino, G., Loyer, S., Bruisma, S., Perosanz, F., Marty, J.-C., Gégout, P., 2007. 3 Years of Geoid Variations from GRACE and LAGEOS Data at 10-day Intervals from July 2002 to March 2005, CNES/GRGS Product. data available on CD-ROM, also on BGI web page: http://bgi.cnes.fr/.

Bindoff, N., Willebrand, J., Artale, V., Cazenave, A., Gregory, J., Gulev, S., Hanawa, K., Le Quéré, C., Levitus, S., Nojiri, Y., Shum, C.K., Talley, L., Unnikrishnan, A., 2007. Observations: oceanic climate and sea level. In: Solomon, S., Qin, D., Manning, M., Chen, Z., Marquis, M., Averyt, K.B., Tignor, M., Miller, H.L. (Eds.), Climate Change 2007: The Physical Science Basis. Contribution of Working Group I to the Fourth Assessment Report of the Intergouvernmental Panel on Climate Change. Cambridge University Press, Cambridge, UK, and New York, USA.

Boone, A., Calvet, J.-C., Noilhan, J., 1999. Inclusion of a third soil layer in a land-surface scheme using the force-restore method. J. Appl. Meteorol. 38, 1611–1630.

Bruinsma, S., Lemoine, J.M., Biancale, R., Vales, N., 2010. CNES/GRGS 10-day gravity field models (release 2) and their evaluation. Adv. Space Res. 45 (4), 587–601. doi:10.1016/j.asr.2009.10.012.

Cazenave, A., Llovel, W., 2010. Contemporary sea level rise. Annu. Rev. Mar. Sci. 2, 145–173.

Chambers, D.P., 2006. Evaluation of new GRACE time-variable gravity data over the ocean. Geophys. Res. Lett. 33 (17), LI7603.

Chao, B.F., 1995. Anthropogenic impact on global geodynamics due to reservoir water impoundment. Geophys. Res. Lett. 22, 3529–3532.

Chao, B.F., Wu, Y.H., Li, Y.S., 2008. Impact of artificial reservoir water impoundment on global sea level. Science 320 (5873), 212–214.

Chen, J.L., et al., 1998. Seasonal global water mass budget and mean sea level variations. Geophys. Res. Lett. 25, 3555–3558.

Decharme, B., Douville, H., 2006. Introduction of a sub-grid hydrology in the ISBA land surface model. Climate Dyn. 26, 65–78.

Decharme, B., Douville, H., Boone, A., Habets, F., Noilhan, J., 2006. Impact of an exponential profile of saturated hydraulic conductivity within the ISBA LSM: simulations over the Rhône Basin. J. Hydromet. 7, 61–80.

Douville, H., Royer, J.-F., Mahfouf, J.-F., 1995. A new snow parameterization for the Météo-France climate model. Part 1: validation in stand-alone experiments. Climate Dyn. 12, 21–35.

Gornitz, V., 2001. Impoundment, groundwater mining, and other hydrologic transformations: impacts on global sea level rise. In: Douglas, B.C., Kearney, M.S., Leatherman, S.P. (Eds.), Sea Level Rise, History and Consequences. Academic Press, San Diego, California, pp. 97–119.

Guinehut, S., Coatanoan, C., Dhomps, A.L., Le Traon, P.Y., Larnicol, G., 2009. On the use of satellite altimeter data in Argo quality control. J. Atmos. Oceanic Technol. 26, 395–402.

Jevrejeva, S., Grinsted, A., Moore, J.C., Holgate, S., 2006. Nonlinear trends and multiyear cycles in sea level records. J. Geophys. Res. 111, C09012. doi:10.1029/2005JC003229.

Llovel, W., Becker, M., Cazenave, A., Crétaux, J.F., 2010a. Contribution of land water storage change to global mean sea level from GRACE and satellite altimetry. C.R. Geosci. 342, 179–188.

Llovel, W., Guinehut, S., Cazenave, A., 2010b. Regional and interannual variability in sea level over 2002–2009 based on satellite altimetry, Argo float data and GRACE ocean mass. Ocean Dyn. 60, 1193–1204. doi:10.1007/s10236-010-0324.

Lyman, J., Good, S.A., Gouretski, V.V., Ishii, M., Johnson, G.C., Palmer, M.D., Smith, D.M., Willis, J.K., 2010. Robust warming of the global upper ocean. Nature 465, 334–337.

Merrifield, M., Nerem, R.S., Mitchum, G.T., Miller, L., Leuliette, E., Gill, S., Woodworth, P.L., 2009. Sea level variations, 2008 annual assessment [in "State of the Climate in 2008"]. Bull. Am. Meteorol. Soc. 90 (8), S62–S196.

Milly, P.C.D., Cazenave, A., Gennero, M.C., 2003. Contribution of climate-driven change in continental water storage to recent sea-level rise. Proc. Natl Acad. Sci. 100, 13158–13161. doi:10.1073/pnas.2134014100.

Milly, P.C.D., Cazenave, A., Famiglietti, J., Gornitz, V., Laval, K., Lettenmaier, D., Sahagian, D., Wahr, J., Wilson, C., 2010. Terrestrial water storage contributions to sea level rise and variability. In: Church, J., Woodworth, P., Aarup, T., Wilson, S., et al. (Eds.), Proceedings of the WCRP Workshop 'Understanding sea level rise and variability'. Blackwell Publishing, Inc.

Minster, J.F., Cazenave, A., Serafini, Y.V., Mercier, F., Gennero, M.C., Rogel, P., 1999. Annual cycle in mean sea level from Topex-Poseidon and ERS-1: inferences on the global hydrological cycle. Glob. Planet. Change 20, 57–66.

Nerem, R.S., Chambers, D.P., Choe, C., Mitchum, G.T., 2010. Estimating mean sea level change from the TOPEX and Jason altimeter missions. Mar. Geodesy 33 (1), 435–446.

Ngo-Duc, T., Laval, K., Polcher, J., Lombard, A., Cazenave, A., 2005a. Effects of land water storage on global mean sea level ofer the past 50 years. Geophys. Res. Lett. 32, L09704. doi:10.1029/2005GL022719.

Ngo-Duc, T., Laval, K., Polcher, Y., Cazenave, A., 2005b. Analyses of the contribution of continental water to sea level variations during the 1997–1998 ENSO event; comparison between the AMIP simulations and the Topex/Poseidon satellite data. J. Geophys. Res. 110, DO9103. doi:10.1029/2004JD004940.

Noilhan, J., Planton, S., 1989. A simple parameterization of land surface processes for meteorological models. Mon. Weather Rev. 117, 536–549.

Oki, T., Sud, Y.C., 1998. Design of Total Runoff Integrating Pathways (TRIP)— a global river channel network. Earth Interact. 2 (1), 1–37.

Paulson, A., Zhong, S., Wahr, J., 2007. Inference of mantle viscosity from GRACE and relative sea level data. Geophys. J. Int. 171, 497–508.

Peltier, W.R., 2001. Global glacial isostatic adjustment and modern instrumental records of relative sea level history. In: Douglas, B.C., Kearney, M.S., Leatherman, S.P. (Eds.), Sea Level Rise. Elsevier, New York.

Prandi, P., Cazenave, A., Becker, M., 2009. Is coastal mean sea level rising faster than the global mean? A comparison between tide gauges and satellite altimetry over 1993–2007. Geophys. Res. Lett. 36. doi:10.1029/2008GL036564, 2009.

Ramillien, R., Bouhours, S., Lombard, A., Cazenave, A., Flechtner, F., Schmidt, R., 2008. Land water contributions from GRACE to sea level rise over 2002–2006. Glob. Planet. Change 60, 381–392.

Sahagian, D., 2000. Global physical effects of anthropogenic hydrological alterations: sea level and water redistribution. Glob. Planet. Change 25, 39–48.

Tapley, B.D., Bettadpur, S., Ries, J.C., Thompson, P.F., Watkins, M.M., 2004. GRACE measurements of mass variability in the Earth system. Science 305, 503–505.

Trenberth, K.E., Smith, L., 2005. The mass of the atmosphere: a constraint on global analyses. J. Climate 18, 864–875.

Vörösmarty, C.J., Sharma, K.P., Fekete, B.M., Copeland, A.H., Holden, J., Marble, J., Lough, J.A., 1997. The storage and aging of continental runoff in large reservoir systems of the world. Ambio 26, 210–219.

Wada, Y., van Beek, L.P.H., van Kempen, C.M., Reckman, J.W.T.M., Vasak, S., Bierkens, M.F.P., 2010. Global depletion of groundwater resources. Geophys. Res. Lett. 37, L20402. doi:10.1029/2010GL044571.

Wahr, J., Swenson, S., Zlotnicki, V., Velicogna, I., 2004. Time-variable gravity from GRACE: first results. Geophys. Res. Lett. 31, L11501. doi:10.1029/2004GL019779.

Wolter, K., 1987. The Southern Oscillation in surface circulation and climate over the tropical Atlantic, Eastern Pacific, and Indian Oceans as captured by cluster analysis. J. Climate Appl. Meteorol. 26, 540–558.

Woodworth, P.L., Player, R., 2003. The permanent service for mean sea level: an update to the 21st century. J. Coast. Res. 19, 287–295.

4.4 Bilans du niveau de la mer en moyenne globale

Dans les paragraphes précédents, nous avons passé en revue les différentes contributions qui affectent les variations du niveau moyen global des océans sur les périodes 1993-2003 (dernier rapport de l'IPCC) et 2002-2009. Nous allons dans cette dernière partie nous intéresser à la période totale 1993-2009 et établir un bilan de l'évolution du niveau marin en moyenne globale.

4.4.1 Synthèse des différentes contributions aux variations du niveau de la mer sur les périodes 1993-2009 et 2003-2009

Synthèse et bilan du niveau de la mer

La figure 4.16 montre l'évolution depuis 1993 du niveau moyen global des mers entre 65°S et 65°N (courbe bleue, *Ablain et al.* [2009]). Sur la période 1993-2009, la hausse en moyenne globale du niveau de la mer est évaluée à 3.4 +/- 0.4 mm/an (après l'application des corrections géophysiques et des effets du rebond post-glaiciaire ; *Ablain et al.* [2009]). Sur cette même figure, nous avons superposé la composante thermostérique du niveau de la mer basée à partir des données de la NOAA (courbe verte, *Levitus et al.* [2009]). Sur cette même courbe et à la fin de la période, trois courbes sont superposées à cette composante thermostérique qui représentent le niveau de la mer stérique déduits des produits de CLS, SCRIPPS et de l'IPRC (voir discussion sur le niveau de la mer stérique). La courbe noire représente le signal massique des océans. Avant 2003 cette courbe est seulement basée sur les estimations de la fonte des calottes polaires et des glaciers de montagne (IPCC, 2007). A partir de 2003, cette courbe est basée sur les données de la mission spatiale GRACE (moyenne des trois solutions disponibles : CSR, GFZ et JPL, voir discussion sur le signal massique des océans). Enfin, la courbe rouge représente la somme du niveau de la mer stérique (moyenne des quatre différentes estimations) et du signal massique des océans basé sur les données GRACE (moyenne des quatre différentes estimations). Cette courbe représente la somme des contributions climatiques à la hausse observée du niveau de la mer sur la période altimétrique totale de 1993 à 2009. Ces deux courbes se comportent de façon similaire en terme de tendance avant 2003. En revanche, à partir de 2003, la variabilité interannuelle des deux courbes n'est pas similaire et présente des différences. Néanmoins, le

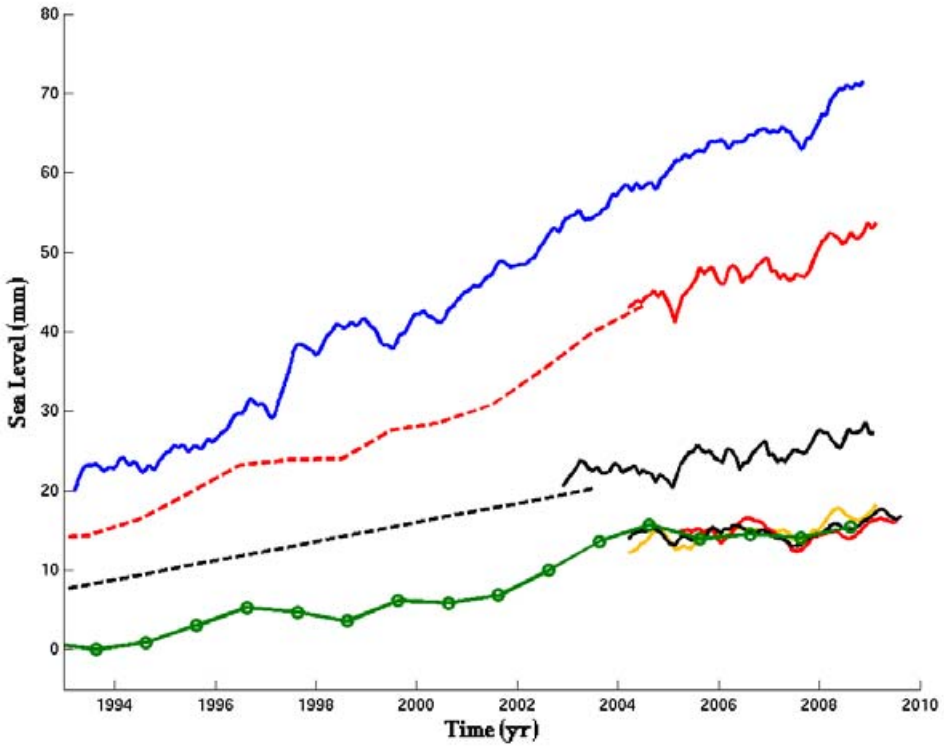

FIG. 4.16 – Evolution du niveau moyen global de la mer observé par altimétrie spatiale -Topex/Poseidon, Jason-1 et Jason-2 - (courbe bleue, *Ablain et al.* [2009]). Somme des effets stériques - données de CLS - et de masse de l'océan - données GRACE - (courbe rouge). Evolution du signal masse de l'océan (courbe noire) basée sur les estimations de l'IPCC jusqu'en 2003 puis estimer directement avec les données de la mission spatiale GRACE (moyenne des trois produits CSR, GFZ et JPL ; *Chambers* [2006]). Evolution de la contribution stérique basée sur les données de température et de salinité de différents groupes de recherche (courbe verte : NOAA (*Levitus et al.* [2009] ; courbe jaune : CLS (*Guinehut et al.* [2009] ; courbe noire : SCRIPPS (*Roemmich and Gilson* [2009]) et courbe rouge : IPRC (http ://apdrc.soest.hawaii.edu/projects/argo/)

minimum local de 2007 est observé dans les deux estimations du niveau moyen global de la mer.

Nous pouvons maintenant établir un bilan des différentes contributions qui influent sur les variations globales du niveau de la mer et faire une étude de bilan pour les périodes 1993-2009 et 2003-2009.

	1993-2009	2003-2009
(1) Expansion stérique	1.1 +/- 0.1 (*Levitus et al.* [2009]	0.62 +/- 0.4 (*Llovel et al.* [2010b])
(2) Masse des océans	—	1.8 +/- 0.34 (*Llovel et al.* [2010b])
(3) Glaciers de montagne	1.1 +/- 0.25 (*Cazenave and Llovel* [2010])	1.15 +/- 0.37 (*Meier et al.* [2007], *Cogley* [2009])
(4) Antarctique Groenland	0.3 +/- 0.15 0.4 +/- 0.15 (Estimations fig 3.5)	0.5 +/- 0.05 0.6 +/- 0.05 (Estimations fig 3.5)
(5) Eaux continentales	—	-0.22 +/- 0.05 (*Llovel et al.* [2010a])
Somme (1)+(3)+(4)+(5)	2.9 +/- 0.35	2.65 +/- 0.55
(6) Niveau de la mer Observé	3.3 +/- 0.4	2.7 +/- 0.4
Différence	0.4 +/- 0.4	0.05 +/- 0.68

TAB. 4.1 – Bilan de la hausse du niveau marin entre 1993-2009 et 2002-2009 en mm/an

Le tableau 4.1 établit les bilans du niveau de la mer sur les périodes de 1993-2009 et 2003-2009.

La période altimétrique totale : 1993-2009

Sur la période de 1993 à 2009, la hausse du niveau de la mer en moyenne globale est évaluée à 3.3 +/- 0.4 mm/an. L'expansion thermique, sur la même période d'étude, compte pour 1.1 +/- 0.1 mm/an (*Levitus et al.* [2009]). Cette valeur est inférieure à celle donnée dans le dernier rapport de l'IPCC-AR4 (2007) sur la période 1993-2003. En retirant au niveau de la mer global la composante thermostérique, nous avons directement accès à l'augmentation du signal massique des océans qui compte pour 2.2 +/- 0.4 mm/an. L'apport d'eau douce aux océans provenant des glaciers de montagne est estimé à 1.1 +/- 0.25 mm/an. De plus, nous déduisons à partir de la compilation de plusieurs publications récentes une contribution de 0.7 mm/an, à la hausse observée du niveau de la mer, dûe à la fonte des calottes polaires (0.4 mm/an et 0.3 mm/an pour les contributions respectives du Groenland et de l'Antarctique). Ces estimations conduisent à un apport d'eau douce aux océans égal à 1.8 mm/an. Cette estimation est plus faible que la contribution du signal massique des océans déduite de la soustraction de la composante thermostérique au niveau de la mer observé. Le bilan du niveau de la mer est fermé avec les barres d'erreurs

associées. De plus, sur cette période le signal massique de l'océan domine le niveau de la mer thermostérique.

Les années récentes : 2003-2009

Comme nous l'avons vu précédemment, l'estimation du niveau de la mer stérique, basé sur les données du projet international Argo, montre une tendance à la pause dans le réchauffement des océans. Néanmoins, le niveau moyen global de la mer continue à augmenter avec, cependant un taux plus faible égal à 2.7 +/- 0.4 mm/an (*Ablain et al.* [2009]; *Cazenave and Llovel* [2010]). Avec l'aide de la mission GRACE, nous pouvons à présent mesurer le signal massique des océans pour la première fois (*Chambers* [2006]). De ce fait, les estimations divergent et les valeurs s'échelonnent de 1.1 mm/an d'après *Leuliette and Miller* [2009] à 2.1 mm/an d'après *Cazenave et al.* [2009] sur la période 2003-2007. Ces estimations diffèrent selon le modèle numérique de GIA considéré et donc des paramètres et des hypothèses pris en compte lors du calcul de ces valeurs de rebond.

Les études sur le bilan de masse des glaciers de montagne révèlent une accélération de perte de masse et une contribution au niveau de la mer comptant pour 1.4 +/- 0.25 mm/an (exprimée en niveau de la mer équivalent) pour les années récentes (*Meier et al.* [2007]; *Cogley* [2009]). Les calottes polaires montrent aussi une accélération de perte de masse pour les années récentes basée sur plusieurs techniques spatiales. Par exemple, *Rignot et al.* [2008] estime que la fonte de l'Antarctique contribue à élever le niveau de la mer de 0.56 mm/an. Cette estimation est en accord avec les études réalisées à l'aide des données de GRACE qui estiment une contribution de l'ordre de 0.55 +/- 0.06 mm/an (*Cazenave et al.* [2009]). La fonte de la calotte polaire du Groenland contribue elle aussi à élever le niveau de la mer de 0.4 +/- 0.05 mm/an. Cette valeur est aussi en relation avec les différentes études basées sur les données de GRACE. En utilisant les techniques d'altimétrie laser, *Slobbe et al.* [2009] estiment que la perte de masse du Groenland contribue à élever le niveau de la mer en moyenne globale de 0.39 +/- 0.2 mm/an.

Ces diverses contributions climatiques expliquent 2.65 +/- 0.55 mm/an du niveau de la mer observé qui compte pour 2.7 +/- 0.4 mm/an. Sur cette période, nous arrivons à fermer le bilan du niveau de la mer en moyenne globale de façon plus satisfaisante, avec cependant une incertitude assez forte. Notons aussi que sur cette période, la contribution dominante est l'apport d'eau douce aux océans par la fonte des glaciers de montagne et des calottes polaires.

En effet, ces deux réservoirs expliquent près de 80% de la hausse observée du niveau des océans.

4.4.2 Résumé d'un article de revue sur les contributions et les bilans du niveau de la mer : « Contemporary Sea Level Rise », article publié dans le journal « Annual Review of Marine Science »

Introduction et résumé de l'article

Dans cet article, nous avons passé en revue les différentes techniques pour mesurer et étudier le niveau de la mer sur le siècle entier. Nous avons ensuite réalisé des bilans en terme de tendance du niveau de la mer sur différentes périodes. En effet, dans le bilan du niveau de la mer sur la période altimétrique totale 1993-2007, nous traitons séparément les périodes 1993-2003 et 2003-2007. Le découpage de ces deux périodes est assez naturel du fait de l'apport des données de température et de salinité avec une couverture spatio-temporelle *quasi* globale du projet international Argo (début de déploiement vers l'an 2000) et le lancement du satellite gravimétrique GRACE (en 2002) qui nous renseigne sur le signal massique de l'océan. De ce fait, les études de bilan sur les variations du niveau marin mais surtout les différentes contributions climatiques peuvent maintenant être mieux quantifiées.

Lors de ce travail, nous mettons en évidence la signature de la variabilité régionale sur les vitesses du niveau de la mer. Cette variabilité régionale est expliquée par le niveau de la mer stérique. En effet, le réchauffement des océans n'est pas uniforme et par endroit, l'océan tend à se refroidir. Ce constat a été mis en évidence dans un premier temps par les données hydrographiques *in situ* mais aussi, plus récemment, à l'aide de modèles numériques de circulation océanique.

Nous discutons aussi des projections futures du niveau moyen global de la mer et des incertitudes des modèles climatiques couplés de l'IPCC. Malheureusement, nous soupçonnons que les projections pour le siècle futur sont sous estimées du fait de la mauvaise connaissance de la dynamique des calottes polaires et donc des incertitudes liées à la modélisation de celles-ci. Des études récentes réalisées par *Rahmstorf* [2007]; *Vermeer and Rahmstorf* [2009] estiment en moyenne globale la hausse du niveau de la mer à l'aide d'une relation liant les variations temporelles du niveau de la mer en moyenne globale

avec la température moyenne du globe. Ces projections de hausses du niveau marin pour 2100 sont de l'ordre de 50 et 130 cm. La compilation des différentes estimations réalisées à l'aide de ces méthodes semi-empiriques montrent une hausse de 90 cm en moyenne globale. Cette valeur est trois fois supérieure à l'estimation faite dans le dernier rapport de l'IPCC-AR4 (2007).

Enfin, nous évoquons les conséquences de la hausse observée du niveau de la mer en moyenne globale. Les impacts côtiers de cette hausse sont aujourd'hui assez bien connus. Ces impacts incluent les inondations associées aux tempêtes, l'érosion du trait de côte, l'intrusion d'eau salée dans les eaux souterraines, les nappes phréatiques et les aquifères (*Nicholls* [2002, 2007]). Dans plusieurs parties du globe, la hausse du niveau de la mer peut être combinée avec d'autres phénomènes physiques d'origine climatique et/ou anthropique. Par exemple dans les grands deltas, l'accumulation de sédiments crée une subsidence du plancher océanique et donc un mouvement qui peut venir polluer les enregistrements marégraphiques. Ou encore, la subsidence des grandes villes qui ont vu leur niveau de référence baisser lors du XX^{e} siècle (Tokyo avec 5 mètres, Shangai ou Bangkok avec 3 mètres, *Nicholls* [2007]).

Contemporary Sea Level Rise

Anny Cazenave and William Llovel

Laboratoire d'études en géophysique et océanographie spatiales LEGOS-CNES, Observatoire Midi-Pyrénées; email: anny.cazenave@cnes.fr, william.llovel@legos.obs-mip.fr

Annu. Rev. Mar. Sci. 2010. 2:145–73

First published online as a Review in Advance on September 28, 2009

The *Annual Review of Marine Science* is online at marine.annualreviews.org

This article's doi:
10.1146/annurev-marine-120308-081105

1941-1405/10/0115-0145$20.00

Key Words

sea level rise, climate change, land ice melt, ocean warming

Abstract

Measuring sea level change and understanding its causes has considerably improved in the recent years, essentially because new in situ and remote sensing observations have become available. Here we report on most recent results on contemporary sea level rise. We first present sea level observations from tide gauges over the twentieth century and from satellite altimetry since the early 1990s. We next discuss the most recent progress made in quantifying the processes causing sea level change on timescales ranging from years to decades, i.e., thermal expansion of the oceans, land ice mass loss, and land water–storage change. We show that for the 1993–2007 time span, the sum of climate-related contributions (2.85 ± 0.35 mm year^{-1}) is only slightly less than altimetry-based sea level rise (3.3 ± 0.4 mm year^{-1}): ~30% of the observed rate of rise is due to ocean thermal expansion and ~55% results from land ice melt. Recent acceleration in glacier melting and ice mass loss from the ice sheets increases the latter contribution up to 80% for the past five years. We also review the main causes of regional variability in sea level trends: The dominant contribution results from nonuniform changes in ocean thermal expansion.

1. INTRODUCTION

Sea level is a very sensitive index of climate change and variability and, in fact, responds to change in several components of the climate system. For example, as oceans respond to global warming, sea waters warm and expand, and thus sea level rises. Coupled atmosphere-ocean perturbations, like El Nino–Southern Oscillation, affect sea level in a rather complex manner. As mountain glaciers melt because of increasing air temperature, sea level rises because of freshwater mass input to the oceans. Modification of the land hydrological cycle due to climate variability and anthropogenic forcing leads accordingly to increased or decreased runoff, and ultimately to sea level change. Change in the mass balance of the ice sheets also has a direct effect on sea level. Even the solid Earth affects sea level through ongoing processes of glacial isostatic adjustment (GIA) due to the deglaciation event of the last Quaternary ice age.

While sea level has remained almost stable during the last two to three millennia (i.e., since the end of the last deglaciation; Lambeck et al. 2004), changes have been measured shortly after the beginning of the industrial era. In fact, tide gauge measurements available since the late nineteenth century show significant sea level rise during the twentieth century (e.g., Douglas 2001). For more than 15 years now, the global mean sea level has been routinely measured at 10-day intervals over the whole oceanic domain with high-precision satellite altimetry, and such observations show clear evidence of global mean sea level rise. However, important regional variability has also been reported.

Quasi-global in situ ocean temperature data made available in recent years have allowed quantification of the contribution of ocean warming to sea level rise. In addition, mountain glacier surveys and satellite measurements of the mass balance of the ice sheets available since the early 1990s have provided new information on the land ice contribution. Finally, space-based gravity data from the recently launched GRACE mission now allow determination of the land water–storage component, while also providing important constraints on the mass balance of the ice sheets. The fourth Assessment Report (AR4) of the Intergovernmental Panel on Climate Change (IPCC), published in 2007, summarized current observations on sea level and on contributing climate factors (Bindoff et al. 2007). In this review, we present the most recent findings on these topics, including new results published since the IPCC AR4 and the previous review by Cazenave & Nerem (2004). Most of the discussion concerns the last 50 years, with a focus on the satellite altimetry era (since 1993).

2. SEA LEVEL OBSERVATIONS

In this section, we present observations of global mean sea level changes available from tide gauges and satellite altimetry over the last century and, in particular, over the past two decades. We also discuss the regional variability in sea level trends evidenced by satellite altimetry and past sea level reconstructions.

2.1. Past Century Sea Level Rise

Our knowledge of past century sea level change comes from tide gauge measurements taken along continental coastlines and islands. The largest tide gauge database of monthly and annual mean sea level records is the Permanent Service for Mean Sea Level (PSMSL, available at **http://www.pol.ac.uk/psmsl**) (Woodworth & Player 2003), which contains data for the twentieth century from ~2000 sites maintained by ~200 nations. Unfortunately, the records are somewhat inhomogeneous in terms of data length and quality. The number and distribution of tide gauges in the past cannot compare to today's dense network, thus older data is incomplete. For long-term sea level studies, for instance, only ~10% of the data set is useable. Moreover, some tide gauges

have not functioned continuously over time, therefore large data gaps are observed for a significant number of them. Others have functioned only for a limited time span.

Another well-known difficulty arises from the fact that tide gauges measure sea level relative to the ground, hence they also monitor crustal motions. In active tectonic and volcanic regions, or in areas subject to strong ground subsidence due to other natural causes (e.g., sediment loading in river deltas) or human activities (e.g., ground water pumping and oil/gas extraction), tide gauge data are directly affected by the corresponding ground motions. Post glacial rebound (also called glacial isostatic adjustment, or GIA) is another process that gives rise to vertical land movement. Thus correction is needed to interpret tide gauge measurements in terms of absolute sea level change. In recent years, precise positioning systems, i.e., the global positioning system (GPS), have been installed at a few tide gauge sites to monitor land motions. But the equipped sites remain few and the GPS records minimal (Woppelmann et al. 2007). Geodynamic models of GIA have been developed (e.g., Peltier 2004, Paulson et al. 2007) so that tide gauge records can be corrected for this effect.

Several studies have concentrated on estimating past century sea level rise from historical tide gauges. Some authors conducted careful selection of the tide gauges, considering only those located in stable continental regions and displaying nearly continuous measurements over several decades, leading them to keep only a small number of good quality records of limited spatial coverage (e.g., Douglas 2001, Holgate & Woodworth 2004, Holgate 2007). Other studies considered larger sets of tide gauges, up to several hundreds, and developed either regional grouping or reconstruction methods (see section 2.4) to provide an historical sea level curve (e.g., Jevrejeva et al. 2006, Church et al. 2004, Church & White 2006).

Figure 1 compares two estimates of the global mean sea level since 1900 (i.e., yearly averages from Church et al. 2004 and Jevrejeva et al. 2006). We note that between 1900 and 1930 the rate of rise was modest. Since then the rate increased and amounted to 1.8 ± 0.3 mm year^{-1} over the

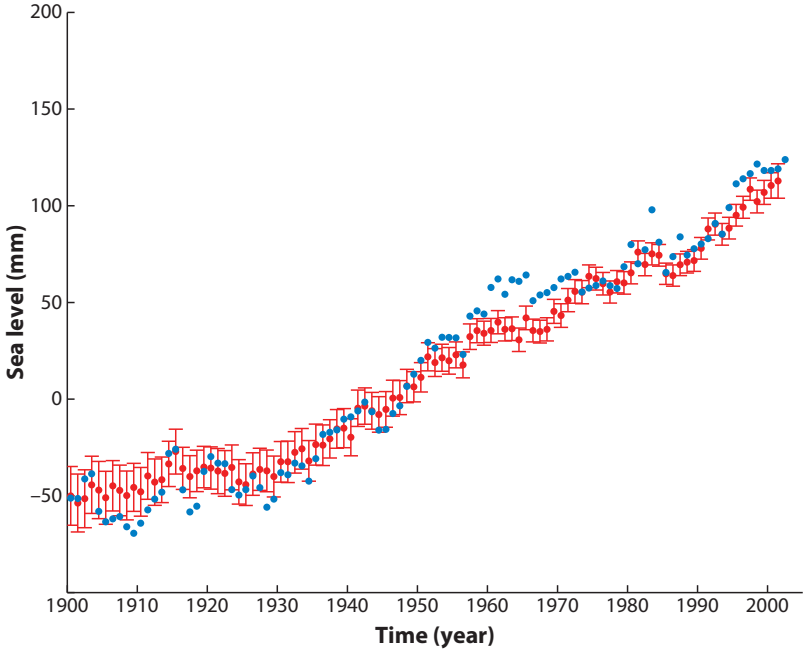

Figure 1

Observed global mean sea level (from tide gauges) between 1900 and 2001. Red dots are from Church et al. (2004). Blue dots are from Jevrejeva et al. (2006).

past 50 years. Also clearly apparent in **Figure 1** are large decadal fluctuations superimposed to the linear trend. Spectral analysis of global mean sea level rates displays high energy in the 4–8 year waveband, likely linked to El Nino-Southern Oscillation (ENSO) frequency (e.g., Chambers et al. 2002, Hebrard et al. 2008). Lower-frequency oscillations (>20 years) in global mean sea level rate have been reported (e.g., Church & White 2006, Holgate 2007, Jevrejeva et al. 2006). Church et al. (2005) and Grinsted et al. (2007) showed that major volcanic eruptions induce temporary cooling of the oceans, thus producing a small negative signature in the global mean sea level curve.

Analyzing tide gauge records from 1870 through 2004, Church & White (2006) detected an acceleration in the rate of sea level rise of 0.013 ± 0.006 mm year^{-2}. Another global mean sea level reconstruction from 1700 to the present (Jevrejeva et al. 2008) reported a sea level acceleration of $\sim$0.01 mm year^{-2}. In a recent compilation of regional and global sea level studies for the twentieth century, Woodworth et al. (2008) conclude that significant accelerations (either positive or negative) occurred at particular epochs, but often these accelerations have a regional signature consistent with regional-scale, natural climate variability (see below).

2.2. Altimetry Era (Last Two Decades)

Since the early 1990s, satellite altimetry has become the main tool for precisely and continuously measuring sea level with quasi-global coverage and short revisit time. The concept of the satellite altimetry measurement is simple: The onboard radar altimeter transmits microwave radiation toward the sea surface that partly reflects back to the satellite. Measurement of the round-trip travel time provides the height of the satellite above the instantaneous sea surface (i.e., the range). The quantity of interest in oceanography is the sea-surface height above a reference fixed surface (typically a conventional reference ellipsoid); it is obtained by the difference between the altitude of the satellite above the reference (deduced from precise orbitography) and the range measurement. The estimated sea-surface height requires correction for various factors due to atmospheric delay and biases between the mean electromagnetic scattering surface and the sea at the air-sea interface. Other corrections due to geophysical effects, e.g., solid Earth, polar, and ocean tidal effects, are also applied. Since the mid-1970s, several altimetry missions have been launched. However, it is only two decades later, with the launch of the Topex/Poseidon mission in 1992, that errors affecting altimetry-derived sea-surface height dropped below the 10-cm level, allowing precise detection of ocean dynamics for the first time.

It is worth mentioning that global monitoring of sea level change was not initially included in the Topex/Poseidon mission goals. In effect, to measure global mean sea level rise with a <5% uncertainty, a precision of $\sim$0.1 mm year^{-1} in the rate of rise is necessary, implying a precision of 1–2 cm on individual sea-surface height measurements. This requirement implies thorough control of all possible errors affecting the altimetry system (in particular, instrumental drifts) and data processing. It has pushed altimetric systems toward their ultimate performance limit (e.g., Nerem 1995). While early Topex/Poseidon precision was >5 cm for a single sea-surface height measurement (Chelton et al. 2001), further progress in the various data processing steps has decreased this error level to $\sim$1–2 cm (e.g., Leuliette et al. 2004, Nerem et al. 2006), a performance also valid for the successors of Topex/Poseidon—Jason-1 and Jason-2 launched in 2001 and 2008, respectively.

Figure 2 shows the temporal evolution of the global mean sea level from satellite altimetry between January 1993 and December 2008. This curve is based on Topex/Poseidon until 2001, on combined Topex/Poseidon and Jason-1 data between 2002 and 2005, and on Jason-1 data since then. In **Figure 2** the annual cycle has been removed and a 90-day smoothing applied. The global mean sea level increases almost linearly over this 16-year time span. The positive anomaly seen

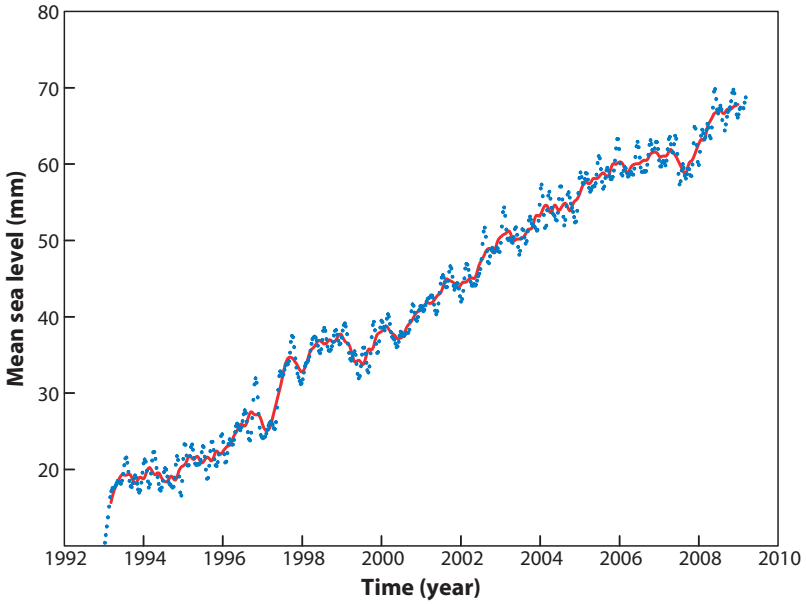

Figure 2

Global mean sea level from satellite altimetry between January 1993 and December 2008. Annual cycle has been removed. Blue dots are raw 10-day data. Red line corresponds to a 90-day smoothing of the raw data. The −0.3 mm year^{-1} GIA correction has been removed.

between 1997 and 1999 is related to the 1997–1998 ENSO event (see section 3.3). Similarly, the negative anomaly occurring by the end of 2007 is possibly related to the recent La Nina (the cold phase of ENSO). The rate of rise estimated over 1993–2008 amounts to 3.1 mm year^{-1} (with a formal uncertainty of 0.1 mm year^{-1}). Precision/accuracy of altimetry-derived rate of sea level rise has been assessed through error budget analyses and comparisons with high-quality tide gauge data (e.g., Mitchum 2000; Nerem & Mitchum 2001a,b; Leuliette et al. 2004; Ablain et al. 2009), leading to a more likely uncertainty of ∼0.4 mm year^{-1}. We modify it further. Accounting for the small correction of −0.3 mm year^{-1} due to global deformation of ocean basins in response to GIA (Peltier 2009), we thus get a rate of global mean sea level rise of 3.4 ± 0.4 mm year^{-1} over 1993–2008. Differences in estimates of altimetry-derived rate of sea level rise for the past 15 to 16 years by different investigators fall within the 0.4 mm year^{-1} range (e.g., Nerem et al. 2006; Beckley et al. 2007; Ablain et al. 2009; C.K. Shum, pers. commun.), suggesting that the 0.4 mm year^{-1} uncertainty is realistic.

2.3. Regional Sea Level Variability

Tide gauge records had previously suggested that sea level rise is not spatially uniform (e.g., last century's rate is twice as large at New York than at Buenos Aires). However, until the advent of satellite altimetry and its almost global coverage of the oceanic domain, mapping the regional variability was not possible. Satellite altimetry has revealed considerable regional variability in the rates of sea level change (**Figure 3*a***). To highlight this regional variability in the rates of sea level rise, a uniform (global mean) trend of 3.4 mm year^{-1} has been removed from **Figure 3*a***. **Figure 3*b*** shows the spatial trend patterns with respect to the global mean. In some regions, such as the western Pacific, North Atlantic around Greenland, southeast Indian, and Austral oceans, sea level rates are up to three times faster than the global mean (e.g., sea level is higher in these regions by ∼15 cm compared to 16 years ago), while the eastern Pacific and west Indian oceans

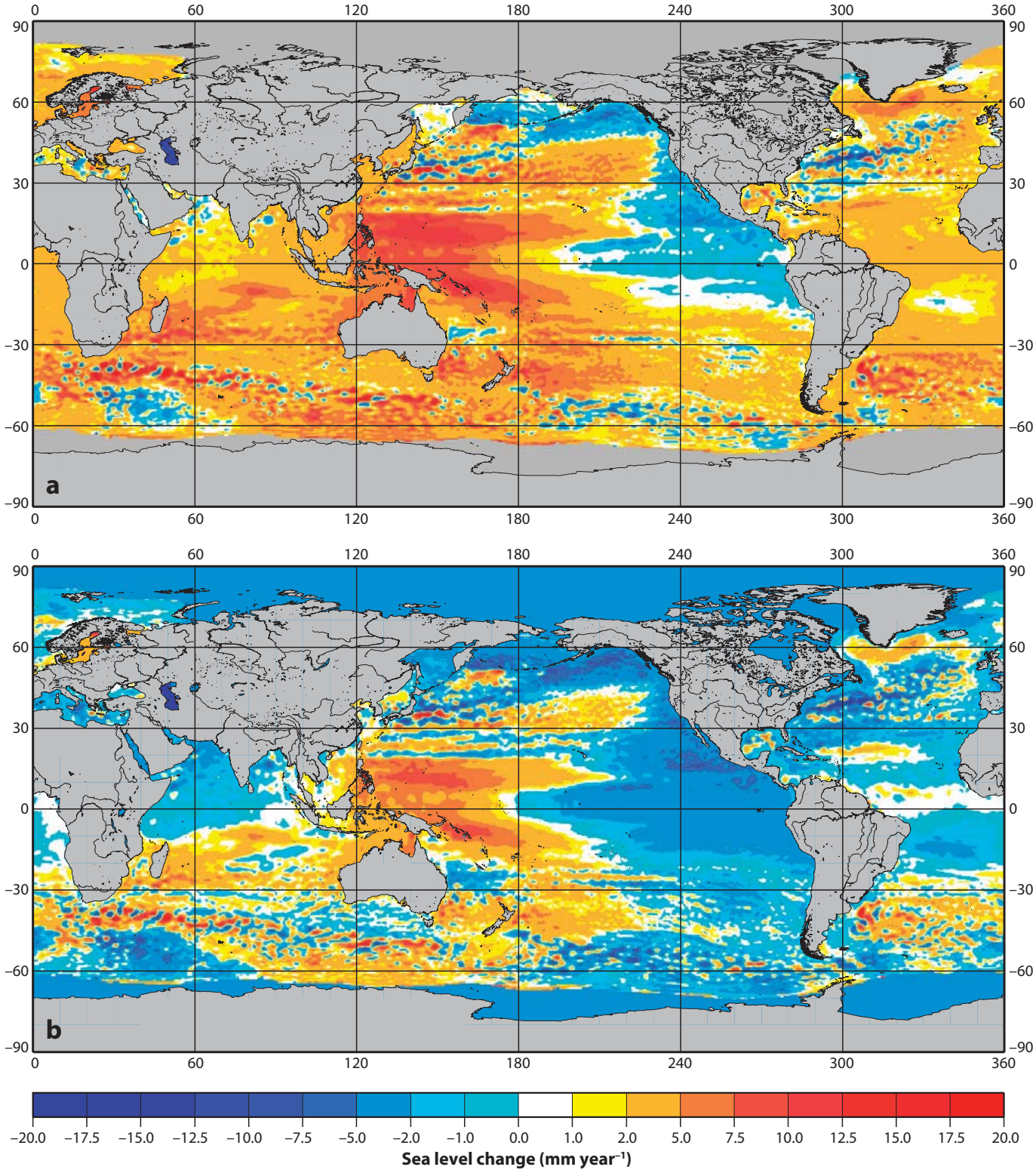

Figure 3

(*a*) Map of spatial trend patterns of observed sea level between January 1993 and December 2008. (*b*) Same as (*a*) but a uniform global mean trend of 3.4 mm year^{-1} has been removed.

exhibit a lower rate. In section 5, we discuss causes of nonuniform sea level change and see that ocean thermal expansion is the dominant factor at the origin of the observed spatial trend patterns (Cabanes et al. 2001, Lombard et al. 2005).

2.4. Two-Dimensional Past Sea Level Reconstructions

Trend patterns in thermal expansion were not stationary during the last few decades but fluctuated both in space and time in response to ENSO, NAO (North Atlantic Oscillation), and PDO (Pacific Decadal Oscillation) (e.g., Levitus et al. 2005, Lombard et al. 2005). This suggests that present-day sea level trend patterns, as seen in **Figure 3*a,b***, are not steady features and are not necessarily representative of the distant past (e.g., last century). Yet, it is important to be aware of past regional sea level variability, in particular, to validate climate models used to predict future sea level change at regional and global scales (in fact, significant uncertainties affect sea level projections for a wide range of spatio-temporal scales, e.g., Meehl et al. 2007). Unfortunately, for the last century, information on regional sea level variability is lacking. For that reason, a number of studies have attempted to reconstruct sea level for past decades in two dimensions (2D), combining sparse but long tide gauge records with global gridded (i.e., 2D) sea level (or sea level proxy) time-series of limited temporal coverage (either from satellite altimetry or ocean general circulation model, or OGCM, reanalyses) (Chambers et al. 2002, Church et al. 2004, Berge-Nguyen et al. 2008, Llovel et al. 2009).

In this approach, the dominant modes of regional variability are extracted from the statistical information contained in altimetry data or OGCM reanalyses. **Figure 4** shows spatial trend patterns (with respect to a uniform global mean trend) for the 1950–2003 time span, based on

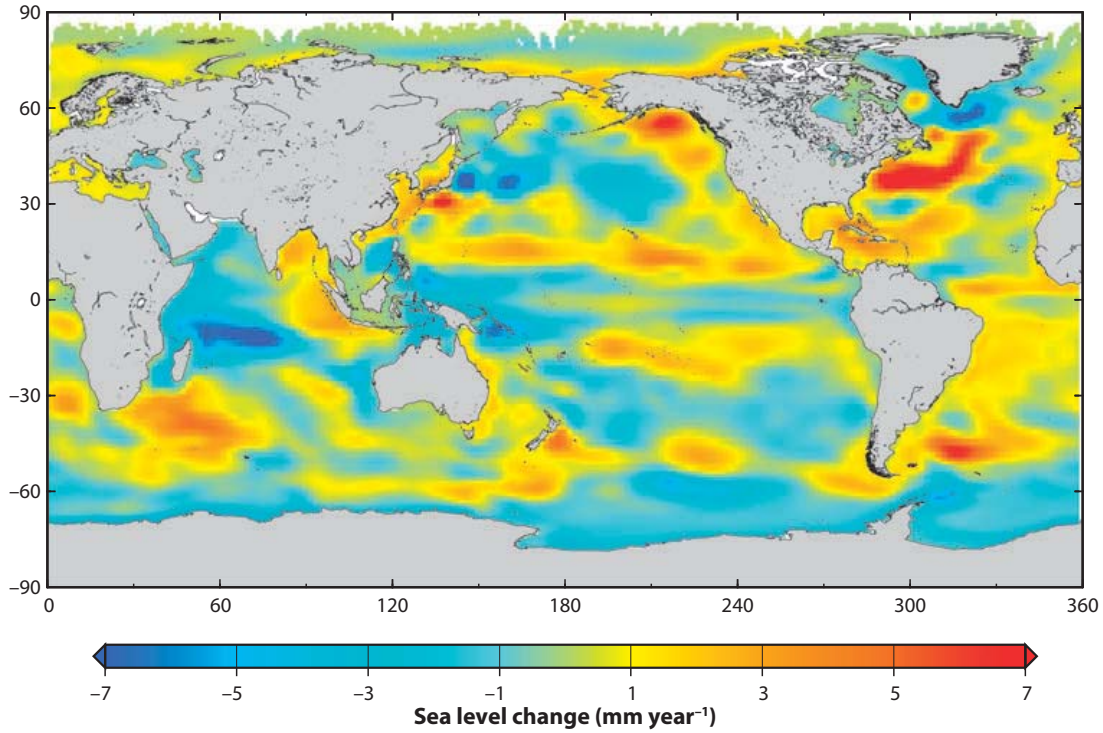

Figure 4

Map of spatial trend patterns of reconstructed sea level between 1950 and 2003 (adapated from Llovel et al. 2009).

the above-referenced paper by Llovel et al. We clearly see significant differences with the 1993–2008 patterns (**Figure 3*b***), confirming that regional variability observed for the recent years is not steady. The above studies have shown that the dominant mode of temporal variability of the spatial trend patterns is related to the decadal modulation of ENSO (Chambers et al. 2002, Church et al. 2004) but lower frequency oscillations are also present (Llovel et al. 2009).

3. CAUSES OF GLOBAL MEAN SEA LEVEL CHANGE

The two main causes of global mean sea level change are the addition of freshwater to ocean basins as a result of land ice loss and water exchange with terrestrial reservoirs (soil and underground reservoirs, lakes, snowpack, etc.), and thermal expansion of the sea waters in response to ocean warming. We examine each of these contributions below.

3.1. Ice Sheets

The mass balance of the ice sheets is a topic of considerable interest in the context of global warming and sea level rise. If totally melted, Greenland and West Antarctica would raise sea level by approximately 7 and 3–5 m, respectively. Thus, even a small amount of ice mass loss from the ice sheets would produce substantial sea level rise, with adverse societal and economic impacts on vulnerable low-lying coastal regions. Observations over the past two decades show rapid acceleration of outlet glaciers in Greenland and Antarctica (Howat et al. 2007, Witze 2008). For example, marine-terminating Jakobshavn Isbrae glacier on the west coast of Greenland has experienced rapid thinning and accelerated flow velocity since the early 1990s, reaching ~13 km year^{-1} in 2003 (Holland et al. 2008, Joughin et al. 2008). Glaciers draining into the Amundsen Sea, West Antarctica, have also rapidly retreated (e.g., Shepherd & Wingham 2007, Rignot et al. 2008a). These observations have been attributed to a dynamical response of the ice sheets to recent warming, with most of the ice sheet mass loss resulting from coastal glacier flow (Alley et al. 2007, 2008) (although for Greenland, surface melting also plays some role; Rignot et al. 2008b). Two main processes have been invoked to explain these observations: (*a*) lubrification of the ice-bedrock interface resulting from summer meltwater drainage through crevasses, and (*b*) weakening and breakup of the floating ice tongue, or ice shelf, that buttressed the ice stream. While the first mechanism may play some role in Greenland where substantial surface melting occurs in summer, glaciologists now favor the second mechanism as the main explanation for recent dynamical changes affecting the ice sheets (e.g., Alley et al. 2008, Holland et al. 2008). Because the ice shelf is in contact with the sea, sea water warming (e.g., Gille 2008, Holland et al. 2008) and ocean circulation changes may trigger basal melting and further breakup, accelerating ice flow (Alley et al. 2008).

Since the early 1990s, different remote-sensing techniques have offered new insight on contemporary mass change of the ice sheets (e.g., Wingham et al. 2006). Radar altimetry (e.g., ERS-1/2 and Envisat satellites) as well as airborne and satellite laser altimetry (ICESat satellite since 2003) allow monitoring ice sheet elevation change, a quantity further expressed in terms of ice volume change. The synthetic aperture radar interferometry (InSAR) technique provides measurements of glacier surface flow and, hence, ice discharge into the oceans if glacier thickness is known. When combined with other parameters of surface mass balance (mainly snow accumulation), the net ice sheet mass balance can then be derived. Space gravimetry from the GRACE space mission (since 2002) is another tool for measuring the mass balance of the ice sheets, with nearly complete coverage of the high-latitude regions up to 89°N/S. The basic quantity measured by GRACE is spatio-temporal change of the Earth's gravity field, which can be converted, over the ice sheets, into ice mass change.

Comparing results from different techniques is not easy, because each technique has its own bias and limitations, e.g., differences in spatial and temporal sampling, measurement errors, contamination from unrelated signals, and lack of direct information on ice mass (except for GRACE). For example, radar altimetry misses narrow coastal glaciers because of the large radar footprint, and measured elevations are much less reliable over steep undulated surfaces than over flat high-elevation surfaces. Ice elevation change requires correction for ice compaction; uncertainty in surface density (snow or ice) when converting elevation change into mass change is an important source of error. To be helpful for mass balance estimates, InSAR needs information on ice thickness, a quantity difficult to estimate. GRACE space gravimetry is sensitive to solid Earth mass change, in particular, that associated with GIA. Over Antarctica, where the GIA effect is of the same order of magnitude as the ice mass change, the poorly known GIA correction is a source of significant uncertainty. In spite of these problems, satellite-based sensors clearly show accelerated ice mass loss from the ice sheets over the recent years.

Greenland mass balance (last two decades). Comparison of elevation changes from successive airborne laser altimetry surveys indicated significant ice mass loss in near coastal regions of Greenland (Krabill et al. 2004). In contrast, satellite radar altimetry suggested elevation increase in Greenland's interior for the 1992–2003 period (Johannessen et al. 2005, Zwally et al. 2005). Using InSAR observations, Rignot & Kanagaratnam (2006) detected widespread glacier ice flow acceleration since 1996. Recent results from GRACE (Velicogna & Wahr 2006a, Ramillien et al. 2006, Chen et al. 2006a, Lutchke et al. 2006, Cazenave et al. 2009, Wouters et al. 2008, Peltier 2009) and ICESat (Slobbe et al. 2009) confirm other remote-sensing results (e.g., Rignot et al. 2008b), i.e., ice mass loss from coastal regions of southern Greenland, although quite large dispersion between the different investigations is noticed. GRACE results indicate accelerated ice mass loss from coastal regions of the Greenland ice sheet since 2002/2003. Many more references about the Greenland mass balance can be found in IPCC AR4 (Lemke et al. 2007).

Antarctica mass balance (last two decades). Laser airborne, laser and radar satellite altimetry, as well as InSAR surveys over West Antarctica reported accelerated ice mass loss in the Amundsen Sea sector during the past decade (Rignot & Thomas 2002, Thomas et al. 2004). Davis et al. (2005) analyzed satellite radar altimetry measurements over 1992–2003 and found significant elevation decrease, especially in the Admunsen Sea sector.

GRACE observations over West Antarctica also show important mass loss over the past few years (Velicogna & Wahr 2006b, Ramillien et al. 2006, Chen et al. 2006b, Cazenave et al. 2009, Peltier 2009). However, because of GIA contamination, GRACE results over Antarctica are more uncertain than over Greenland. Over Antarctica, the GIA effect is of the same order of magnitude as present-day ice mass change (Ivins & James 2005, Peltier 2009). However, the GIA correction depends on still poorly known parameters, e.g., Earth's mantle viscosity structure and deglaciation history. It is available from modeling only, with significant differences between models.

A recent analysis over 85% of Antarctica's coastline by Rignot et al. (2008a), combining InSAR data with regional climate modeling over 1992–2006, confirms earlier results, i.e., widespread ice mass loss in West Antarctica (Amundsen and Bellingshausen seas and Antarctica Peninsula), with loss concentrated in narrow outlet glaciers. In comparison, East Antarctica was found in near balance.

Remote sensing–based estimates of the mass balance of the two ice sheets are summarized in **Figure 5*a,b*** (updated from Cazenave 2006). Since approximately 2003, we note a clear acceleration of ice mass loss from the Greenland ice sheet. For 1993–2003, IPCC AR4 (Lemke et al. 2007) estimated the Greenland contribution to sea level at 0.21 ± 0.035 mm year^{-1}. For 2003–2007,

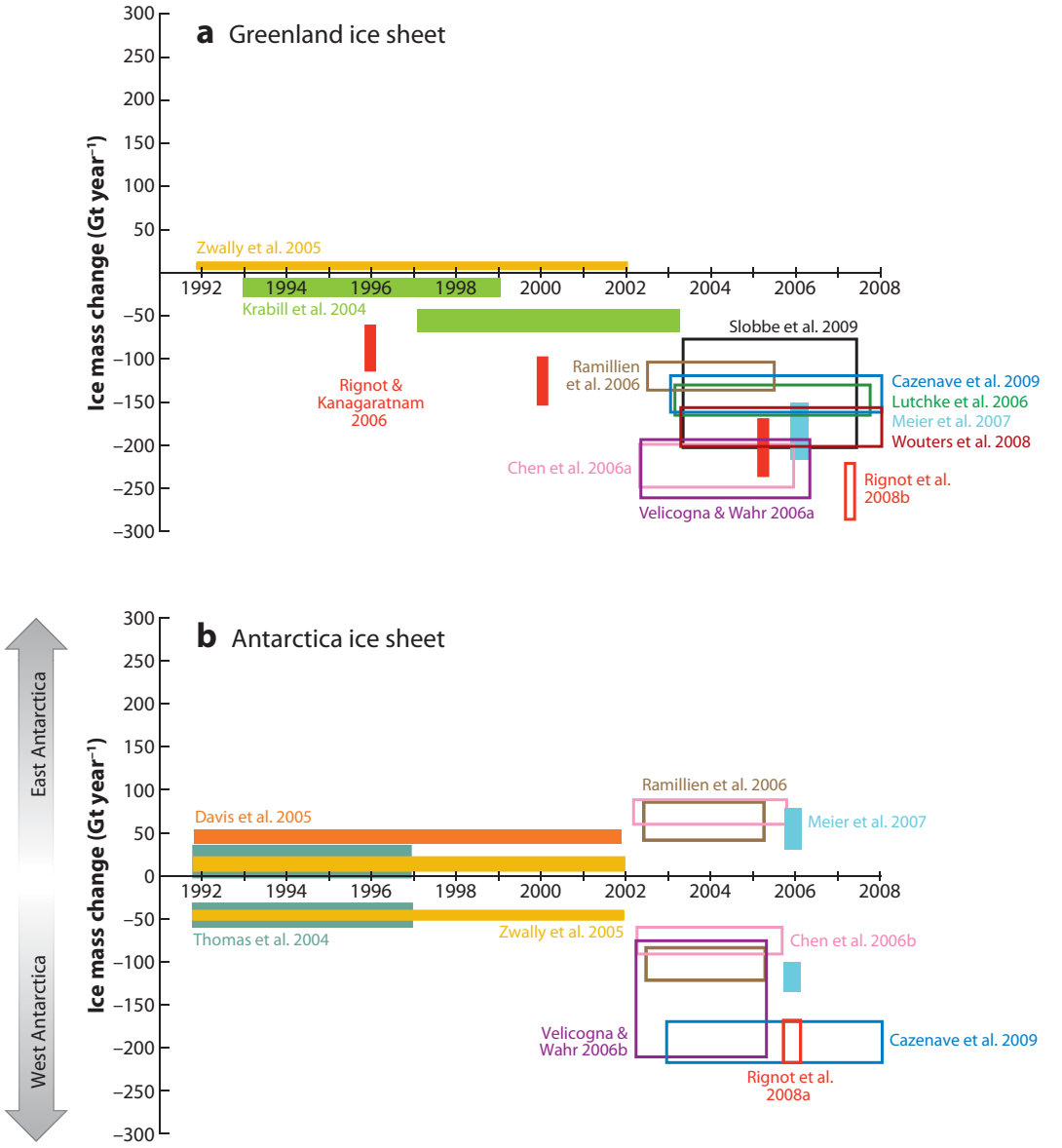

Figure 5

(*a*) Compilation of Greenland ice sheet mass loss based on remote-sensing observations between 1992 and 2008. (*b*) Same as (*a*) but for the Antarctica ice sheet (redrawn from Cazenave 2006).

the mean contribution of Greenland to sea level increased to ~0.5 mm year^{-1} (average of values shown in **Figure 5*a***). In West Antarctica, acceleration is also visible but less than for Greenland. Total Antarctica contribution to sea level was estimated by IPCC AR4 at 0.21 ± 0.17 mm year^{-1} for 1993–2003.

3.2. Glaciers

Glaciers are very sensitive to global warming. Observations indicate that since the 1970s most of the world's glaciers are retreating and thinning, with noticeable acceleration since the early 1990s. Glaciers represent an ~35 cm sea level equivalent, potentially another significant source of freshwater mass to be added to the world's oceans, thereby raising sea level.

Mass balance estimates of glaciers are based either on in situ measurements (monitoring of the annual mean snow accumulation and ice loss from melt) or geodetic techniques (measurements of surface elevation and area change from airborne altimetry or digital elevation models). The data (available at **http://www.geo.unizh.ch/wgms/**) are collected by the World Glacier Monitoring Service (WGMS) on approximately 300 glaciers worldwide tracked over the past decades, and since 1980 include information for approximately 30 reference glaciers in nine mountain ranges since 1980.

On the basis of published results, the IPCC AR4 estimated the glaciers' contribution to sea level rise at 0.77 ± 0.22 mm year^{-1} over 1993–2003 (Lemke et al. 2007). Since the IPCC AR4 publication (IPCC 2007), a few updated estimates of GIC loss have been proposed from traditional mass balance measurements (Kaser et al. 2006, Meier et al. 2007, Cogley 2009). A number of space-based (from GRACE and satellite imagery) indicators of glacier mass changes have also been published for particular ice fields and confirm enhanced glacier mass loss (e.g., Patagonia: Chen et al. 2007; Alaska: Chen et al. 2006c, Lutchke et al. 2008, Peltier 2009; Himalaya: Berthier et al. 2007). Kaser et al. (2006) reported a contribution to sea level rise of 0.98 ± 0.19 mm year^{-1} for 2001–2004, a value slightly larger than during the previous decade. Using the same data as Kaser et al. (2006) and assuming that ice losses by glaciers increased linearly with time since the year 2000, Meier et al. (2007) found the glacier contribution to be 1.1 ± 0.24 mm year^{-1} for 2006. Recently, Cogley (2009) provided an updated compilation of global average glacier mass balance up to 2005. Cogley's results indicate a contribution to sea level of 1.4 ± 0.2 mm year^{-1} for 2001–2005, a value larger than earlier estimates due to better representation of tidewater glaciers.

3.3. Land Waters

Excluding ice sheets and glaciers, freshwater is stored in various reservoirs: snow pack, rivers, lakes, man-made reservoirs, wetlands and inundated areas, root zone (upper few meters of the soil), and aquifers (ground water reservoirs). Land waters are continuously exchanged with atmosphere and oceans through vertical and horizontal mass fluxes (evaporation, transpiration of the vegetation, surface and underground runoff) and are an integral part of the global climate system, with important links and feedbacks generated through influences on surface energy and moisture fluxes between land water, atmosphere, and oceans. Thus climate change and variability modify land water storage. Some human activities also directly affect water storage, e.g., pumping ground water out of aquifers (particularly in arid regions), damming rivers to create artificial water reservoirs, and draining wetlands. Other anthropogenic effects on land waters result from changing the physical characteristics of the land through urbanization, agriculture, and deforestation. All these effects impact sea level by either increasing or decreasing runoff.

Climatic and anthropogenic contributions of land waters to sea level (past few decades). Variations in land water storage caused by climate change and variability over the past few decades cannot be directly estimated from observations because these are almost nonexistent at a global scale. However, global hydrological models (or land surface models) developed for atmospheric and climatic studies can be used for this purpose. The models compute the water and energy balance at the earth surface, providing water storage change in response to prescribed variations of near-surface atmospheric data (precipitation, temperature, humidity, and wind) and radiation. Using atmospheric reanalyses over 1950–2000 and the Orchidee land surface model, Ngo-Duc et al. (2005a) found no climatic long-term trend in sea level but large interannual/decadal fluctuations of several millimeters amplitude, a result also found by Milly et al. (2003) based on the Land

Dynamics model over 1980–2000. In another model-based study, Ngo-Duc et al. (2005b) showed that the positive anomaly visible in sea level in 1997–1998 (see **Figure 2**) was associated with a change in land water storage in the tropics in response to the 1997/1998 ENSO event.

Direct human intervention on land water storage and induced sea level changes have been estimated in several studies (e.g., Chao 1995, Sahagian 2000, Gornitz 2001). These results have been recently reviewed by Huntington (2008) and Milly et al. (2009). The largest contributions come from pumping ground water (for agriculture, industrial, and domestic use) and filling reservoirs. Although detailed information is lacking, and estimates vary significantly between authors, ground water depletion may have contributed to past decades' sea level rise by 0.55–0.64 mm year^{-1} (Huntington 2008).

Over the past half-century, tens of thousands of dams have been constructed over world rivers to create artificial reservoirs, and hence negative contribution to sea level. Several attempts have been made to estimate the total volume of water stored in artificial reservoirs over the last 50 years (e.g., Chao 1995, Gornitz 2001, Vorosmarty et al. 2003). The recent study by Chao et al. (2008), which reconstructs the history of water impoundment in the nearly 30,000 reservoirs built during the twentieth century, estimates the contribution to sea level of dams and artificial reservoirs at -0.55 mm year^{-1} during the past half-century and points out that without dam building, sea level rise would have been larger. However, opposite effects on sea level from ground water depletion may have somewhat canceled effects of water impoundment through dams.

Satellite altimetry and space gravimetry estimates of surface and total water storage contributions (recent years). While satellite altimetry has been developed and optimized for open oceans, numerous studies used this technique to monitor lake and river water levels. Water level time-series for >15 years based on Topex/Poseidon, Jason-1, and Envisat altimetry missions are now available for several hundreds of continental lakes. Using water level time-series over lakes from the HYDROWEB database (available at **http://www.legos.obs-mip.fr/soa/hydrologie/hydroweb/**), we can estimate the water volume change of the largest surface water bodies since the early 1990s. For the period 1993–2008, water storage of the Caspian and Aral seas, East African lakes, and North American lakes decreased on average. Considering the 15 largest lakes, we estimate lake water contribution to sea level rise for the period 1993–2008 at approximately $+0.1$ mm year^{-1} (the largest contributions coming from the Caspian and Aral seas, and Lake Huron in North America, the latter two having been strongly affected by nonclimatic, anthropogenic forcing). However, lake water storage is dominated by interannual variability, therefore the contribution estimated for the past ~15 years does not reflect any long-term trend.

GRACE measures temporal changes of the vertically integrated water column (surface waters, soil moisture, underground waters). Thus GRACE cannot separate the contribution of individual reservoirs. In addition, GRACE does not discriminate between climate and direct anthropogenic components. Ramillien et al. (2008) estimated the water volume trend in the 27 largest river basins worldwide using GRACE data from 2003–2006 and found either positive or negative water volume change over that period, depending on the location of the river basins. The net water volume change was slightly negative (i.e., water loss), corresponding to <0.2 mm year^{-1} sea level rise. An update of this study using a longer GRACE data set (2002–2008) over the world's 32 largest river basins gives a negative contribution to sea level of ~ -0.2 mm year^{-1} (W. Llovel, K. DoMinh, A. Cazenave, J.F. Cretaux, M. Becker, unpublished manuscript), suggesting that over a few years time span, the land water signal is dominated by interannual variability.

Figure 6 compares GRACE-based total land water storage variations (annual signal removed), expressed in equivalent sea level, with altimetry-based, detrended global mean sea level corrected for ocean thermal expansion (annual signal removed) for the years 2003–2007. A significant

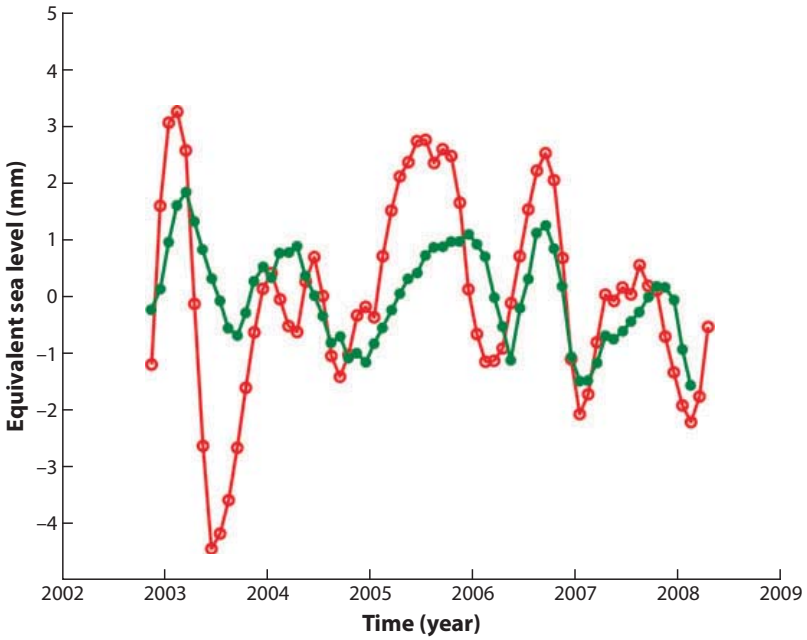

Figure 6

For the years 2003–2007, total land water storage variations from GRACE expressed in equivalent sea level (annual signal removed) are shown by the green line. Detrended global mean sea level observed by satellite altimetry, corrected for ocean thermal expansion (annual signal removed), is shown by the red line (from W. Llovel, K. DoMinh, A. Cazenave, J.F. Cretaux, and M. Becker, unpublished manuscript).

correlation is noticed betwwen the two curves shown, suggesting that year-to-year fluctuations of the global mean sea level (corrected for ocean thermal expansion) can be at least partly explained by the effects of total land water storage oscillations.

To conclude, climate-driven change in land water storage produces mainly interannual to decadal fluctuations but (so far) no long-term trend. This is in contrast to direct human-induced change in land hydrology, which clearly has led to secular—either positive or negative—change in sea level over the past half-century. However, the two major contributions—ground water depletion and reservoir filling—could have more or less canceled each other out. But this may no longer be true in the future: While dam building is clearly decelerating (e.g., Chao et al. 2008), ground water pumping will likely continue at a sustained rate, with a positive contribution to sea level.

3.4. Ocean Temperature and Salinity Changes

Anomalies in temperature and salinity in the ocean water column change density, which further gives rise to sea level variations (classically called steric variations, or thermosteric or halosteric if associated with only temperature or salinity variations, respectively). We first discuss the contribution of temperature variations.

In situ hydrographic measurements collected mainly by ships since the middle of the twentieth century have suggested that in terms of global mean, the oceans have warmed. Since the late 1960s, ocean temperature has been essentially measured with expandable bathythermographs (XBT) along ship tracks, complemented by mechanical bathythermographs (MBT) and Conductivity-Temperature-Depth (CTD) systems. Recently, an international program of profiling floats, Argo (available at **http://www.argo.ucsd.edu**) (Roemmich & Owens 2000), has been set up, providing

temperature and salinity measurements globally down to 2000 m with a revisit time of ~40 days. The Argo network was almost complete by the end of 2003. Historical as well as modern in situ hydrographic measurements are stored in the World Ocean Database (WOD) with regular updates (Boyer et al. 2006). Two major problems affect XBT historical measurements: (1) systematic bias due to uncertainty in assigning a correct depth value to each temperature measurement, and (2) previously sparse data coverage, both geographically and in the deep ocean. XBT instruments do not directly measure depth as they fall within the water column. Traditionally, depth is deduced from a fall-rate equation and time elapsed since the probe entered the sea surface. Even with calibrated fall-rate equations (Hanawa et al. 1995), systematic depth errors are assumed to remain (Gouretski & Koltermann 2007). The problem of sparse data coverage in the past can hardly be overcome, unless OGCMs with data assimilation are used (see section 5). Thus estimates of ocean heat content and thermal expansion for the past are biased by lack of data in certain regions, in particular, in the Southern Hemisphere (Levitus et al. 2005, Antonov et al. 2005). In spite of these limitations, several analyses of global ocean temperature have been conducted in recent years (Domingues et al. 2008; Guinehut et al. 2004; Ishii et al. 2006; Ishii & Kimoto 2009; Levitus et al. 2005, 2009; Willis et al. 2004). Most recent analyses take special care of systematic depth bias corrections affecting XBT and MBT measurements, and here we report only the latest results (Domingues et al. 2008, Ishii & Kimoto 2009, Levitus et al. 2009).

Compared to earlier analyses, new analyses show substantial reduction of spurious large interannual anomalies in ocean heat content, in particular, during the mid-1970s. **Figure 7** shows the evolution of the ocean thermal expansion since 1955 from Levitus et al. (2009) and Ishii & Kimoto (2009) (temperature data down to 700 m). Also shown is the residual sea level, i.e., observed sea level (data from Church et al. 2004) minus thermal expansion (for each data set). The mean thermal expansion trend over 1955–2001 is 0.4 ± 0.01 mm year^{-1} and 0.3 ± 0.01 mm year^{-1}

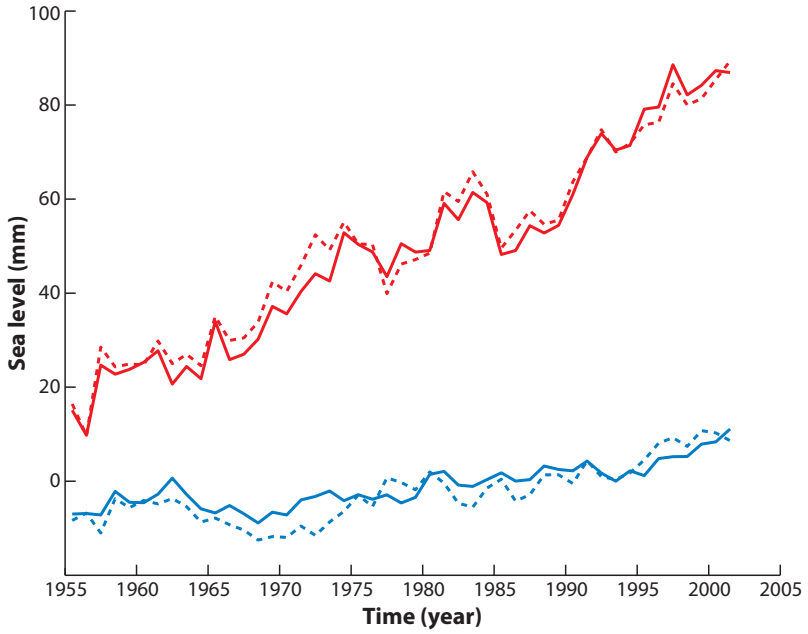

Figure 7

Blue lines: thermosteric sea level (or thermal expansion) between 1955 and 2001 from Ishii & Kimoto (2009) (solid line) and Levitus et al. (2009) (dashed line). Red lines: residual sea level, i.e., observed global mean sea level from Church et al. (2004) minus thermal expansion (solid and dashed lines refer to Ishii & Kimoto and Levitus et al. thermal expansion data, respectively).

for the Levitus et al. and Ishii & Kimoto data, respectively. Based on a reconstruction of ocean temperatures, Domingues et al. (2008) estimate the thermal expansion trend over 1961–2003 at 0.5 ± 0.08 mm year^{-1}. The mean trend in residual sea level over 1955–2001 is ~1.5 mm year^{-1}, which represents the ocean mass increase over that period (plus eventually, a deep ocean temperature contribution not accounted for in the thermal expansion curves; see, e.g., Johnson et al. 2007). This ocean mass trend is three times larger than the thermal expansion trend.

According to Levitus et al. (2001, 2009), heat stored in the oceans during the last four decades (~16×10^{22} J) is roughly 15 times greater than heat stored on continents, and roughly 20 times that stored inside the atmosphere, indicating that ~85% of excess heat from the climate system over that period has accumulated in the oceans. From climate modeling with different forcing agents (greenhouse gases, solar irradiance, aerosols, albedo, and land use), Hansen et al. (2005) show that the Earth is currently in a state of energy imbalance, amounting to 0.85 ± 15 W m^{-2} (i.e., excess energy absorbed from the sun versus reemitted to space). This value is in agreement with satellite-based observations at the top of the atmosphere for 2001–2004 (Trenberth et al. 2009). Levitus' value for ocean heat storage over the last 40 years corresponds to a contribution of ~0.3 W m^{-2} (after scaling by the ocean surface), i.e., ~1/3 of the Earth's total energy imbalance. However, if one considers ocean heat storage over the altimetry era (in the range of 0.6–0.7 W m^{-2}), the ocean contribution becomes dominant.

Figure 8 shows thermosteric sea level curves since 1993 based on Ishii & Kimoto (2009) and Levitus et al. (2009) temperature data (down to 700 m). On the altimetry time span (1993–2006/2007), thermal expansion trends amount to 1.1 ± 0.25 mm year^{-1} and 0.9 ± 0.2 mm year^{-1} for Ishii & Kimoto and for Levitus et al., respectively, with a mean of ~1 ± 0.3 mm year^{-1}. This trend is lower than that reported by IPCC AR4 over 1993–2003, 1.6 ± 0.3 mm year^{-1} (Bindoff et al. 2007), which is likely a result of the plateau in ocean heat

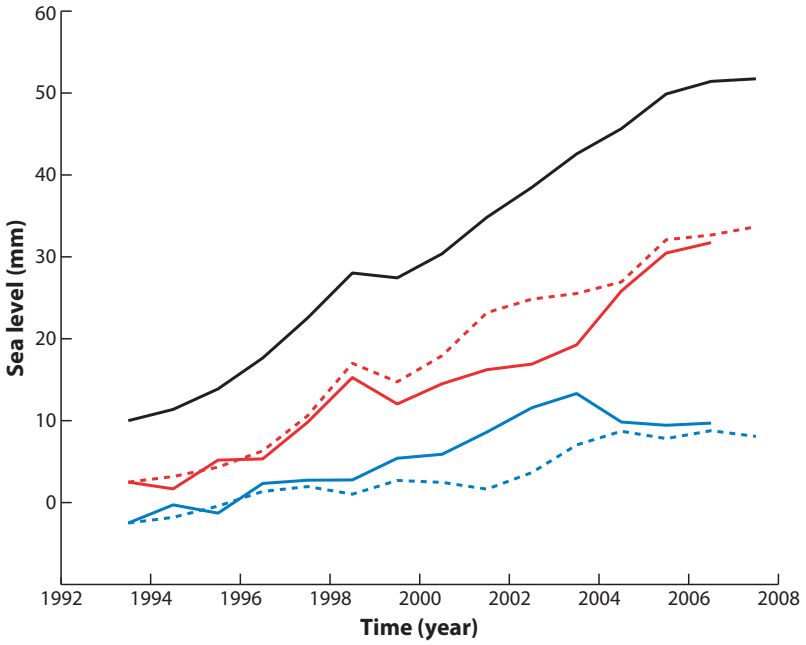

Figure 8

Blue lines: thermosteric sea level (or thermal expansion) since 1993 from Ishii & Kimoto (2009) (solid line, up to 2006) and Levitus et al. (2009) (dashed line, up to 2007). Black line: altimetry-based global mean sea level (annual averages). Red lines: residual sea level, i.e., observed global mean sea level minus thermal expansion (solid and dashed lines refer to Ishii & Kimoto and Levitus et al. thermal expansion data, respectively).

content seen beyond 2003 (see section 4). **Figure 8** also shows altimetry-based sea level (annual averages) and residual sea level curves (observed minus thermosteric sea level). The mean residual trend amounts to 2.3 mm year^{-1} and essentially represents the ocean mass increase.

Recent results based on Argo show that since approximately 2003, thermal expansion is following a plateau (after correcting for instrumental drifts of some Argo probes: Early estimates of Argo-based thermal expansion, Lyman et al. 2006 showed a negative trend as of 2003; however, instrumental problems were subsequently reported on some probes, leading to cold bias, hence artificial ocean cooling). For the recent years, thermal expansion rates range from -0.5 ± 0.5 mm year^{-1} over 2003–2007 (Willis et al. 2008) to $+0.4 \pm 0.1$ mm year^{-1} over 2004–2007 (Cazenave et al. 2009) and $+0.8 \pm 0.8$ mm year^{-1} over 2004–2007 (Leuliette & Miller 2009). The 2003 data coverage is very sparse and it is likely that the Willis et al. (2008) value is biased low for that reason. The recent flattening of the thermal expansion curve likely reflects natural short-term variability. Similar short-term plateaus are also well visible in the past (see **Figure 7**).

Assuming constant total salt content, density changes arising from redistribution of salinity by the ocean circulation (halosteric effect) has no effect on the global mean sea level (although it does at local/regional scales, Wunsch et al. 2007). On the other hand, freshwater addition to the oceans due to increased river runoff and precipitation, as well as ice melting, modifies ocean salinity. If global measurements of salinity were available, it would be possible to estimate the global mean change of salinity and deduce the amount of freshwater added to the oceans. Ultimately, this would provide an estimate of ocean mass change and its contribution to sea level. Unfortunately, the coverage of salinity measurements is very sparse for the past decades, preventing reliable estimates of global mean ocean mass change by this method (although, because of sufficient coverage of salinity profiles over the North Atlantic, Boyer et al. 2007 were able to determine regional changes in freshwater content over 1955–2006). However, with space gravimetry data from GRACE, it is now possible to directly estimate the change in global mean mass of the oceans (see section 4).

4. SEA LEVEL BUDGET

The IPCC AR4 summarized the sea level budget for two periods (1961–2003 and 1993–2003) (Bindoff et al. 2007). For 1961–2003, the contributions of thermal expansion, glaciers, and ice sheets were estimated at 0.4 ± 0.06 mm year^{-1}, 0.5 ± 0.1 mm year^{-1}, and 0.2 ± 0.2 mm year^{-1}, respectively (quoted error bars are one standard deviation from the mean). Their sum of 1.1 ± 0.25 mm year^{-1} was compared to the 1.8 mm year^{-1} rate of sea level rise observed over that period. The IPCC AR4 concluded that the sea level budget of the past four decades was not closed. For the 1993–2003 decade, the contribution of thermal expansion, glaciers, and ice sheets was estimated at 1.6 ± 0.25 mm year^{-1}, 0.8 ± 0.11 mm year^{-1}, and 0.4 ± 0.2 mm year^{-1}, respectively, with a sum of 2.8 ± 0.35 mm year^{-1}—in rather good agreement with the altimetry-based rate of rise, 3.1 ± 0.4 mm year^{-1}.

Since the IPCC AR4 publication (IPCC 2007), new results have appeared in the literature, in particular, for thermal expansion. Recently reprocessed ocean temperature data (Domingues et al. 2008, Levitus et al. 2009, Ishii & Kimoto 2009) do not lead to any important revision for the thermal expansion rate of the past four to five decades (see section 3.4), although the interannual variability has been greatly reduced. Because there are no new estimates for the land ice contribution for the past few decades, we concentrate instead on the altimetry period (since 1993), for which several new results are available. **Table 1** presents sea level budget since 1993. Two time spans are considered: 1993–2007 and 2003–2007.

Table 1 Sea level budget for two time spans (1993–2007, 2003–2007)*

Sea level rise (mm year^{-1})	1993–2007	2003–2007
Observed	3.3 ± 0.4	2.5 ± 0.4 (Ablain et al. 2009)
Thermal expansion	1.0 ± 0.3 (mean of Levitus et al. 2009 and Ishii & Kimoto 2009 values)	0.25 ± 0.8 (Argo) (mean of Willis et al. 2008, Cazenave et al. 2009, and Leuliette & Miller 2009 values)
Ocean mass	2.3 ± 0.5 (observed rate minus thermal expansion)	2.1 ± 0.1 (GRACE with a −2 mm year^{-1} GIA correction, Cazenave et al. 2009)
Glaciers	1.1 ± 0.25 (based on Kaser et al. 2006 and Meier et al. 2007)	1.4 ± 0.25 (Cogley 2009)
Total ice sheets (Greenland & Antarctic)	0.7 ± 0.2 0.4 ± 0.15 0.3 ± 0.15 (compilation of published results)	1.0 ± 0.2 0.5 ± 0.15 0.5 ± 0.15 (compilation of published results)
Land waters	—	−0.2 ± 0.1 (W. Llovel, K. DoMinh, A. Cazenave, J.F. Cretaux, M. Becker, unpublished manuscript)
Sum of (2 + 4 + 5 + 6)	2.85 ± 0.35	2.45 ± 0.85
Observed rate minus sum	0.45	−0.05

* Quoted errors are one standard deviation. The observed sea level rate is GIA corrected (−0.3 mm year^{-1} removed).

1993–2007. Over 1993–2007, the altimetry-based rate of sea level rise was 3.3 ± 0.4 mm year^{-1}. Mean thermal expansion rate (average of Levitus et al. 2009 and Ishii & Kimoto 2009 values over their common time span) is 1.0 ± 0.3 mm year^{-1}. The rate difference between observed sea level rise and mean thermal expansion is 2.3 mm year^{-1}. This represents the ocean mass increase (plus eventually a deep ocean thermal contribution). For the glaciers' contribution since 1993, we use Kaser et al. (2006) and Meier et al. (2007) updates, leading to a value of 1.1 ± 0.25 mm year^{-1}. Although ice sheet mass loss is clearly not linear (see **Figure 5*a*,*b***), we deduce from a compilation of published results a mean contribution to sea level of ∼0.7 mm year^{-1} for the two ice sheets (∼0.4 mm year^{-1} for Greenland and ∼0.3 for Antarctica). This leads to a total ice component of ∼1.8 mm year^{-1}, lower than the 2.3 mm year^{-1} residual rate. As in IPCC AR4 for 1993–2003, the sea level budget is not totally closed. But over 1993–2007, the mass component dominates the thermal component (unlike over 1993–2003).

Recent developments: 2003–2008. As indicated above, Argo-based data on ocean thermal expansion indicate a less rapid increase since 2003 than during the previous decade, although sea level has continued to rise, but at a reduced rate of 2.5 ± 0.4 mm year^{-1} (Ablain et al. 2009). GRACE data averaged over the oceans provide a measure of the ocean mass change (e.g., Chambers et al. 2004). However, GRACE is also sensitive to GIA and the latter effect averaged over the oceanic domain is still uncertain, ranging from −1 mm year^{-1} (Paulson et al. 2007) to −2 mm year^{-1} (Peltier 2009). Depending on the assumed GIA correction, estimated ocean mass change over 2003–2007 ranges from 1.1 mm year^{-1} (Leuliette & Miller 2009) to 2.1 mm year^{-1} (Cazenave et al. 2009).

Independent estimates of glaciers and ice sheet contributions to sea level over the same time span can help discriminate between the two values. Meier et al. (2007) as well as Cogley (2009)

report accelerated glacier melting since 2003, leading to 1.4 ± 0.25 mm year^{-1} equivalent sea level rise in year 2006.

The mass balance of the ice sheets has been recently reevaluated using GRACE and other remote-sensing techniques. For example, Rignot et al. (2008a) find an Antarctica contribution to sea level of 0.56 mm year^{-1} for year 2006, in good agreement with the GRACE-based Antarctica mass balance estimate of 0.55 ± 0.06 mm year^{-1} (Cazenave et al. 2009). GRACE data also suggest an increased contribution from Greenland of 0.4 ± 0.05 mm year^{-1} (Wouters et al. 2008). Using ICESat laser altimetry, Slobbe et al. (2009) estimated the Greenland contribution over 2003–2008 at 0.39 ± 0.2 mm year^{-1}.

Summing all land ice components leads to 2.4 ± 0.35 mm year^{-1} equivalent sea level rise over 2003–2007, only slightly larger than the GRACE-based ocean mass increase if the largest GIA correction is considered. These new observations report accelerated land ice loss, which may have contributed to ~80% of the sea level rise in recent years, as compared to a 50% contribution over 1993–2003 (IPCC 2007).

Chambers (2006) and Lombard et al. (2007) showed that combining satellite altimetry and GRACE data provides an estimate of the steric component. In effect, satellite altimetry represents the sum of thermal expansion and ocean mass change, while GRACE averaged over the oceans measures the ocean mass change component only. The altimetry-derived contribution minus mass factors (using values presented in **Table 1**) shows a slightly positive trend of 0.3 mm year^{-1} over 2003–2007, in agreement with the Argo-based reduced thermosteric rate over that same period.

5. REGIONAL VARIABILITY IN SEA LEVEL TRENDS

Satellite altimetry has revealed strong regional variability in sea level trends (**Figure 2*a,b***). Several studies have shown that nonuniform ocean warming, hence nonuniform thermal expansion, is most responsible for the observed spatial trend patterns in sea level (e.g., Lombard et al. 2005). Recent studies based on ocean general circulation models, either with data assimilation (e.g., Carton & Giese 2008, Kohl & Stammer 2008, Wunsch et al. 2007) or without (Lombard et al. 2009), confirm that regional sea level trend patterns reported by satellite altimetry are mainly due to regional variability in thermal expansion. However, salinity changes are not negligible at regional scale. For example, using the ECCO (Estimating the Circulation and Climate Experiment of the Ocean) ocean circulation model with atmospheric data forcing and assimilation of a good deal of ocean data (in situ temperature and salinity, altimetry-based sea level, sea surface temperature, satellite-based surface winds, etc.), Wunsch et al. (2007) reproduced local sea level trend patterns observed by satellite altimetry over 1993–2004. They showed that thermal expansion change in the upper ocean is the dominant contribution to observed spatial trend patterns but also that approximately 25% of the temperature contribution is locally compensated by salinity. Lombard et al. (2009) were also able to reproduce spatial trend patterns using the high-resolution (0.25°) NEMO (Nucleus for European Models of the Ocean) ocean circulation model without data assimilation over 1993–2001.

Figure 9 (from Lombard et al. 2009) compares sea level trend patterns over 1993–2001 observed by satellite altimetry and computed by the NEMO model. A striking agreement is noticed between observations and model results. In **Figure 10*a,b*** are shown the separate contributions from temperature and salinity computed by the model. In some regions (e.g., equatorial Pacific and North Atlantic), effects of temperature and salinity are opposite and cancel each other, but in most other regions thermosteric trend patterns closely resemble observed trend patterns, as noted earlier by Wunsch et al. (2007).

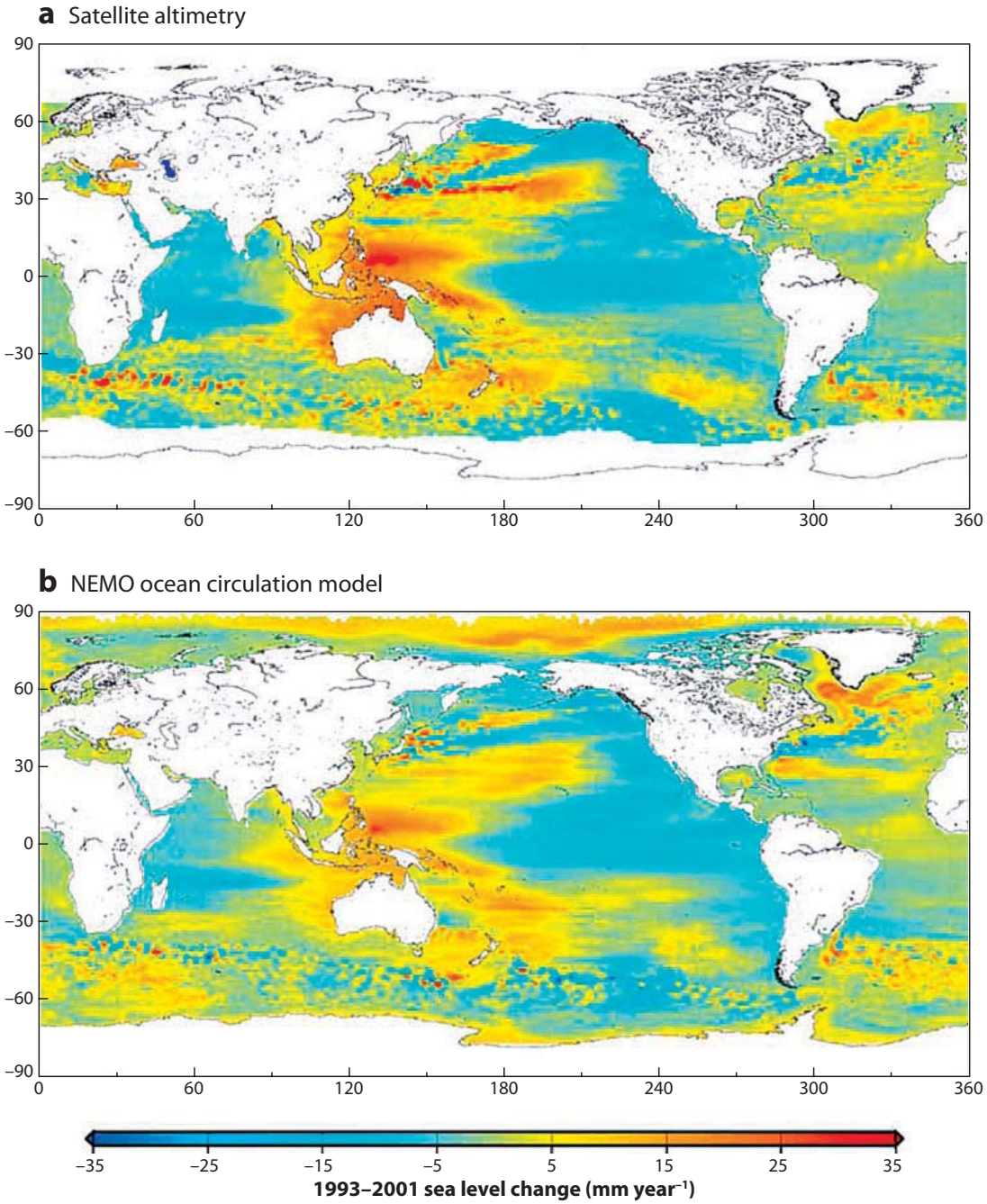

Figure 9

Spatial patterns in sea level trends over 1993–2001 observed by satellite altimetry (*a*) and computed by the NEMO ocean circulation model (*b*) (from Lombard et al. 2009).

Wunsch et al. (2007) discuss attribution of observed local/regional sea level trend patterns: (*a*) ocean warming and cooling, (*b*) freshwater exchange with the atmosphere and land via evaporation, precipitation, and runoff, and (*c*) redistribution of water mass via ocean advection. To these processes should also be added solid Earth processes due to gravity and ocean volume changes (discussed below). Concerning factors (*a*) through (*c*), Wunsch et al. (2007) showed that observed trend patterns result from a complex dynamical response of the ocean, involving forcing terms

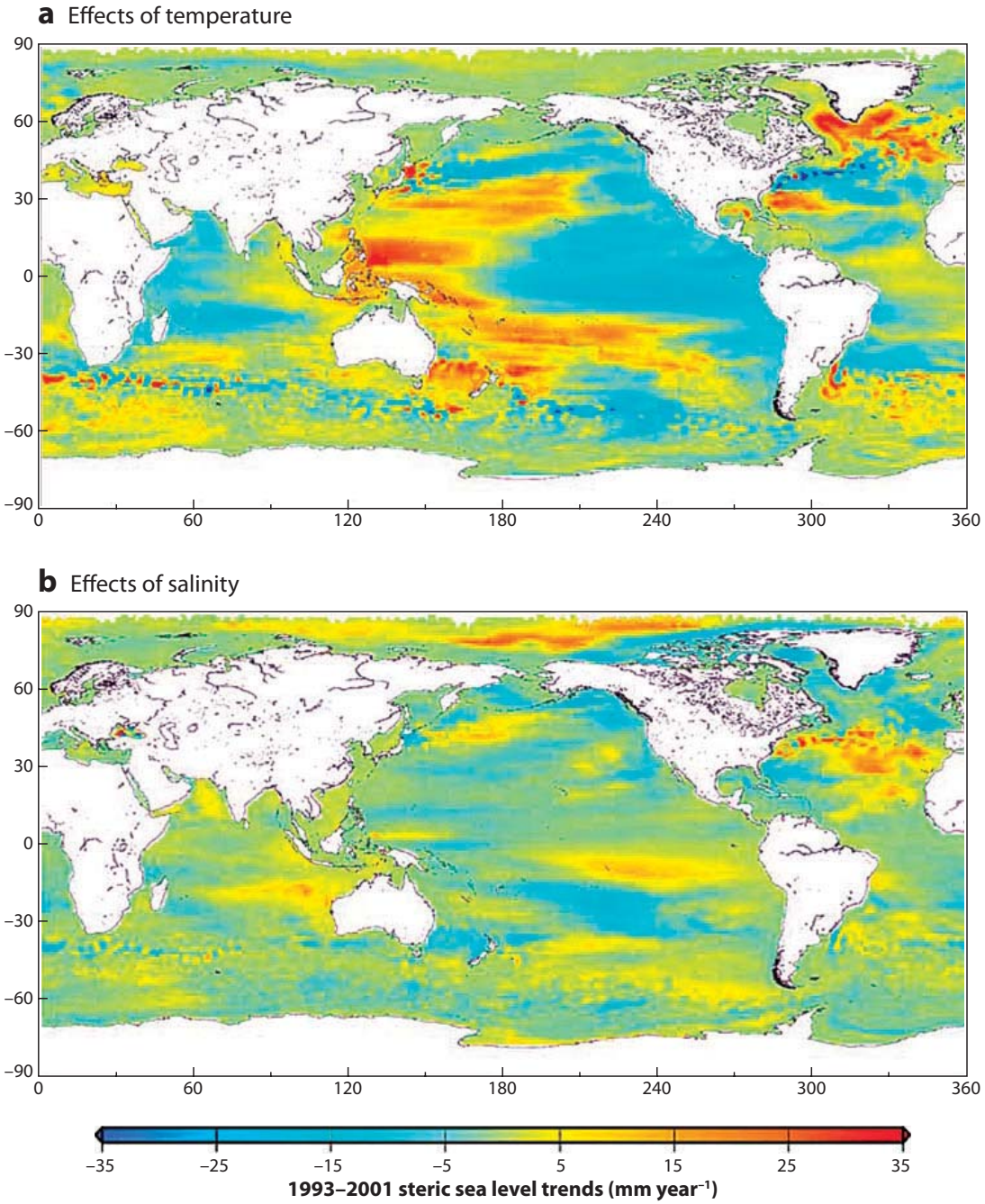

Figure 10

(*a*) Thermosteric (i.e., due to temperature only) sea level trend patterns over 1993–2001 computed by the NEMO ocean circulation model. (*b*) Same as (*a*) but for the effects of salinity only (from Lombard et al. 2009).

as well as water movements associated with wind stress. These authors also stressed that given the long memory time of the ocean, observed patterns reflect not only forcing patterns over the period considered but also forcing and internal changes that occurred in the past. This suggests that distribution of sea level trends observed by satellite altimetry over the last 16 years may not be steady but will eventually adjust, over much longer time spans, toward different geographical

patterns than those currently observed. Concerning the response of the ocean circulation to freshwater forcing associated with Greenland and Antarctic ice melting, using ECCO simulations, Stammer (2008) showed that significant sea level rise would be expected along the western coast of the North Atlantic in response to Greenland ice melting.

We have seen above that steric sea level change is the dominant contributor to the observed spatial trend patterns observed for sea level. However, other processes are expected to also give rise to regional sea level variations. This is the case for the response of the solid Earth to the last deglaciation (GIA) and to ongoing melting of land ice in response to global warming. These processes give rise to secular change of the geoid (an equipotential surface of the Earth's gravity field that coincides with the mean surface of the oceans at rest) and gravitational deformations of ocean basins and of the sea surface (Mitrovica et al. 2001, Plag 2006, Peltier 2009). Recently, Mitrovica et al. (2009) showed that rapid melting of the ice sheets and glaciers will lead to nonuniform sea level rise because of the changing mutual gravitational attraction between the ice sheet and the nearby ocean as well as the elastic deformation of the solid Earth to the load redistribution. Such regional sea level changes are broadscale but different for each melting source (Greenland, Antarctica, glaciers). To give an order of magnitude, they can reach up to 30% of the melt contribution to sea level rise.

Now that high-quality in situ temperature and salinity measurements with global coverage are available from the Argo observation system, it may become possible to detect the fingerprint of land ice melt (due to both gravitational and dynamical effects) using satellite altimetry data corrected for steric sea level (e.g., Milne et al. 2009).

6. SEA LEVEL PROJECTIONS

IPCC AR4 projections indicated that sea level should be higher than today's value by ~35 cm by the year 2100 (within a range of ± 15 cm due to model results dispersion and uncertainty over future greenhouse gas emissions) (Meehl et al. 2007). However, this value is likely a lower bound because physically realistic behavior of the ice sheets was not taken into account. As discussed in section 3.4, a large proportion of ice sheet mass loss results from coastal glacier flow into the ocean through dynamical instabilities. Such processes are only beginning to be understood and were not taken into account in the IPCC AR4 sea level projections. Recent studies by Rahmstorf (2007) and Horton et al. (2008) provided semi-empirical sea level projections based on a simple relationship established for the twentieth century between global mean sea level rate and global mean temperature. Using mean temperature projections from climate models, these studies extrapolated future global mean sea level. Projected range of sea level rise in 2100 by Rahmstorf (2007) (i.e., between ~50 and ~120 cm) directly reflects the temperature projections range. The middle value (~85 cm) is roughly twice the IPCC AR4 value. Whereas future sea level rates may not be as closely associated with global mean temperature as they are today (especially if ice sheet dynamics play a larger role in future), an approach such as Rahmstorf's offers independent insight on plausible ranges of future sea level rise and an interesting alternative to still uncertain coupled climate model projections.

Figure 11 shows the evolution of the global mean sea level between 1800 and 2100 based on observations for the nineteenth and twentieth centuries and model projections [from IPCC (2007) AR4 and the semi-empirical method by Rahmstorf 2007] for the twenty-first century.

We have seen that observed sea level rates present high regional variability around the global mean (**Figure 3*b***), and thus regional variablity is expected in the future. The mean regional sea level map for 2080–2099 (**Figure 12**) provided by IPCC AR4 (Meehl et al. 2007) from an ensemble mean over 16 coupled climate models shows higher than average sea level compared to 1980–1999 in the Arctic Ocean in response to increasing ocean temperature and decreasing salinity. On the

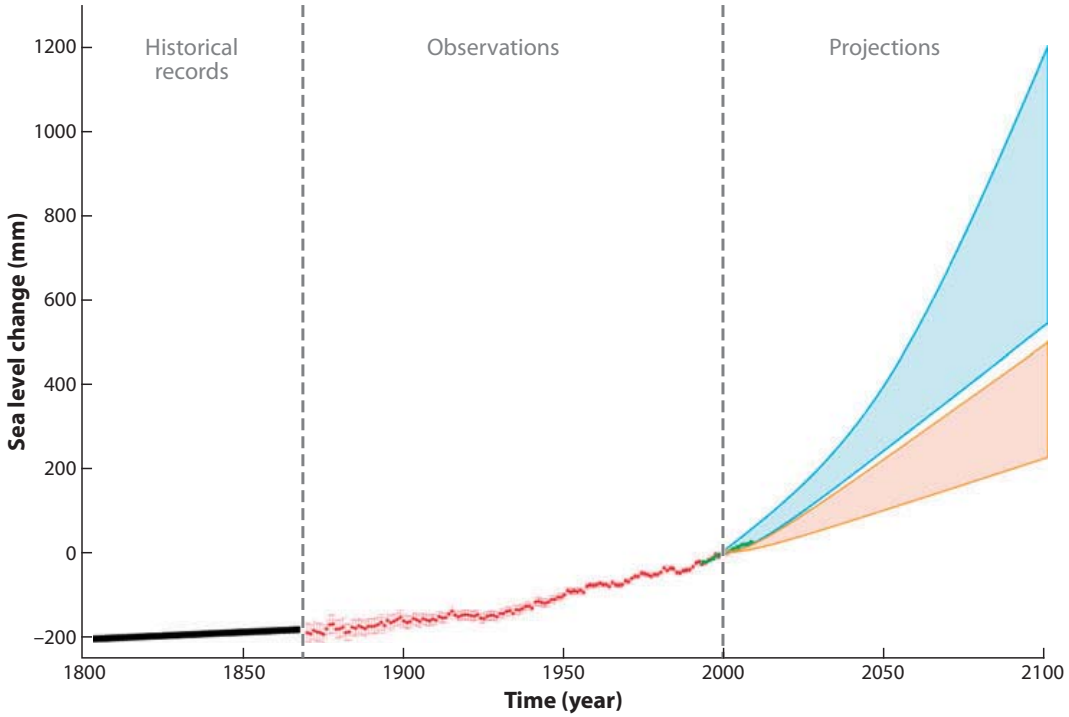

Figure 11

Evolution of the global mean sea level between 1800 and 2100 from observations (for the nineteenth and twentieth centuries) and model projections for the twenty-first century. The thick black line represents the long-term sea level based on various observations for the nineteenth century. The red line is based on tide gauge data (from Church et al. 2004). The green line is from satellite altimetry since 1993. The pink shaded region includes projections from coupled climate models [from IPCC (2007) AR4]. The light blue shaded region includes projections from Rahmstorf (2007).

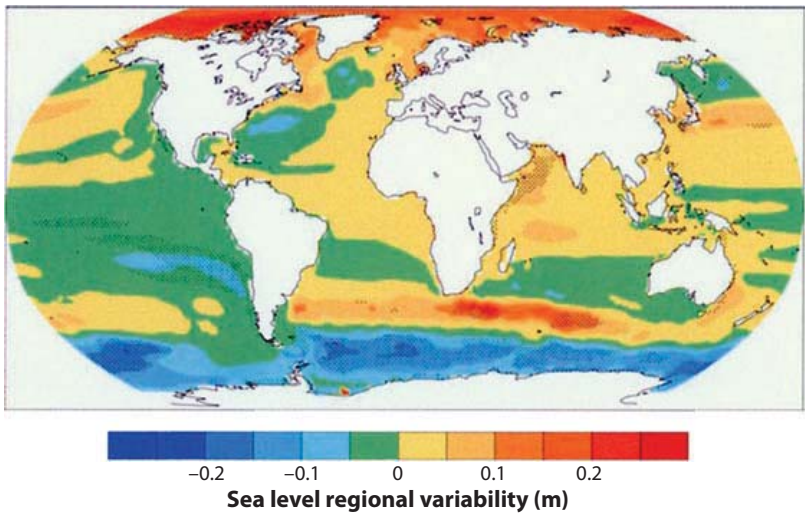

Figure 12

Regional sea level change (in metres) by the end of the twenty-first century due to ocean density and circulation changes, relative to the global average. This regional variability is calculated as the difference between averages for 2080–2099 and 1980–1999 under SRES scenario A1B, from an ensemble mean of 16 AOGCMs (Atmosphere-Ocean General Circulation Models). Reproduced from IPCC (2007) AR4.

other hand, a lower sea level is projected in the Austral Ocean. These model-based projections essentially reflect that part of the regional variability due to long-term climate signals but still poorly account for decadal/multidecadal natural variability. On a decadal timescale, spatial trend patterns may differ by a factor of 2 to 3 from the global mean sea level rise (see section 2.3). Regional sea level projections at 10- to 20-year intervals should be proposed by climate models. To evaluate future regional impacts, this information is of crucial importance.

7. COASTAL IMPACTS

Main physical impacts of sea level rise are rather well known (e.g., Nicholls 2002, 2007). These include (*a*) inundation and recurrent flooding in association with storm surges, (*b*) wetland loss, (*c*) shoreline erosion, (*d*) saltwater intrusion in surface water bodies and aquifers, and (*e*) rising water tables. In many coastal regions of the world, the effects of rising sea level act in combination with other natural and/or anthropogenic factors, such as decreased rate of fluvial sediment deposition in deltaic areas, ground subsidence due to tectonic activity, or ground water pumping and hydrocarbon extraction. Change in dominant wind, wave, and coastal current patterns in response to local or regional climate change and variability may also impact shoreline equilibrium.

Deltas are dynamical systems linking fluvial and coastal ocean processes (Ericson et al. 2006). Over the last 2000 years, agriculture has accelerated the growth of many world deltas (McManus 2002). But in recent decades, dam and reservoir construction and river diversion for irrigation considerably decreased sediment supply along numerous world rivers, destroying the natural equilibrium of many deltas.

Accelerated ground subsidence due to local groundwater withdrawal and hydrocarbon extraction is another problem that affects numerous coastal megacities. For example, during the twentieth century, Tokyo subsided by 5 m, Shangai by 3 m, and Bangkok by 2 m (Nicholls 2007). Hydrocarbon extraction in the Gulf of Mexico causes ground subsidence along the Gulf Coast in the range of 5–10 mm year^{-1} (Ericson et al. 2006). Whatever the causes, ground subsidence produces effective (relative) sea level rise that directly interacts with and amplifies climate-related sea level rise (i.e., long-term trend plus regional variability).

In terms of impacts, what is important is relative sea level rise, i.e., the combination of the climate-related sea level rise and ground subsidence. In many coastal regions of the world, these two factors are currently of the same order of magnitude, and hence produce higher relative sea level rise than the climate component alone. If sea level continues to rise at current rates, or more likely accelerates, then climate change impacts (sea level rise) may dominate. As mentioned in section 6, future sea level projections from coupled climate models are likely underestimated. In addition, climate models are not yet able to provide reliable data on regional variability (that superimposes positively or negatively on the global mean rise in sea level) for the next 20, 30, and 50 years. It is therefore very difficult to quantify future sea level rise in specific regions, and this should be among the priorities for the climate-modeling community. In parallel, multidisciplinary studies of sea level rise impacts that take an integrated approach involving all factors (climate change, anthropogenic forcing, solid earth processes, etc.) need to be developed.

8. CONCLUSION

Most recent developments indicate that sea level is currently rising, slightly faster since the early 1990s than during the previous decades. Owing to the recent progress in understanding the causes of present-day sea level rise, we can nearly close the sea level budget for the period 1993–2007. Approximately 30% of the rate of sea level rise is due to ocean thermal expansion in response to

ocean warming. Mass loss in mountain glaciers and ice sheets accounts for approximately another 55%. Since 2003 ocean thermal expansion rate has slightly reduced while sea level has continued to rise. Direct and indirect estimates of land ice contribution indicate that ocean mass increase explains roughly 80% of the past 5-year observed sea level rate. If, as most likely, recent thermal expansion pause is temporary, and if land ice shrinking continues to accelerate, the prevailing sea level may be the source of some surprise in the near future.

The recently launched Jason-2 satellite, the successor to Jason-1, will provide continuity in the monitoring of sea level variations from space, at least for the coming years. In addition to ocean temperature and salinity measurements from Argo, mass balance of the ice sheets from GRACE and other remote-sensing techniques, GRACE-based land water–storage change and in situ and remote observations of mountain glaciers are absolutely crucial for understanding sea level evolution with time and its response to climate change and variability. These observations also offer invaluable constraints to the climate models developed for future sea level projections.

Sea level is a climate parameter difficult to determine by climate models because it involves interactions of all components of the climate system (oceans, ice sheets and glaciers, atmosphere, land water reservoirs) on a wide range of spatial and temporal scales. Even the solid Earth through its elastic response to changing crust and mantle parameters, as well as water mass redistribution, affects sea level. Systematic monitoring of oceans, cryosphere, and land waters from in situ and space-observation systems are thus crucial to validate climate models, and hence improve future sea level projections. Considering the highly negative impact of future sea level rise for society, the multidisciplinary aspects of sea level rise (observations, modeling, coastal impact studies) should remain a major area of future climate research.

DISCLOSURE STATEMENT

The authors are not aware of any affiliations, memberships, funding, or financial holdings that might be perceived as affecting the objectivity of this review.

ACKNOWLEDGMENTS

We would like to thank a number of colleagues for useful information and helpful discussions on various aspects of the sea level topics. Special thanks to M. Ablain, R. Alley, D. Chambers, L.L. Fu, S. Guinehut, M. Ishii, S. Jevrejeva, G. Kaser, S. Levitus, A. Lombard, R. Nerem, R. Nicholls, R. Peltier, S. Rahmstorf, E. Rignot, C.K. Shum, K. Trenberth, J. Willis, and P. Woodworth.

LITERATURE CITED

Ablain M, Cazenave A, Valladeau G, Guinehut S. 2009. A new assessment of the error budget of global mean sea level rate estimated by satellite altimetry over 1993–2008. *Ocean Sci.* 5:193–201

Alley R, Fahnestock M, Joughin I. 2008. Understanding glacier flow in changing time. *Science* 322:1061–62

Alley R, Spencer M, Anandakrishnan S. 2007. Ice sheet mass balance, assessment, attribution and prognosis. *Ann. Glaciol.* 46:1–7

Antonov J, Levitus S, Boyer TP. 2005. Thermosteric sea level rise, 1955–2003. *Geophys. Res. Lett.* 32:L12602, doi:10.1029/2005GL023112

Beckley BD, Lemoine FG, Lutchke SB, Ray RD, Zelensky NP. 2007. A reassessment of global rise and regional mean sea level trends from TOPEX and Jason-1 altimetry based on revised reference frame and orbits. *Geophys. Res. Lett.* 34:L14608, doi:10.1029/2007GL030002

Berge-Nguyen M, Cazenave A, Lombard A, Llovel W, Cretaux JF. 2008. Reconstruction of past decades sea level using tide gauge, altimetry and in situ hydrographic data. *Glob. Planet. Change* 62:1–13

Berthier E, Arnaud Y, Kumar R, Ahmad S, Wagnon P, Chevallier P. 2007. Remote sensing estimates of glacier mass balances in the Himachal Pradesh (Western Himalaya, India). *Remote Sensing Environ.* 108(3):327–38, doi:10.1016/j.rse.2006.11.017

Bindoff N, Willebrand J, Artale V, Cazenave A, Gregory J, et al. 2007. Observations: Oceanic climate and sea level. In *Climate Change 2007: The Physical Science Basis. Contribution of Working Group I to the Fourth Assessment Report of the Intergovernmental Panel on Climate Change*, ed. S Solomon, et al. Cambridge, UK: Cambridge Univ. Press

Boyer TP, Antonov J, Baranova OK, Garcia H, Johnson DR, et al. 2006. Introduction, NOAA Atlas NESDIS 60. In *World Ocean Data Base 2005*, ed. S Levitus. U.S. Government Printing Office, Washington DC, 190 pp.

Boyer T, Levitus S, Antonov J, Locarnini R, Mishonov A. 2007. Changes in freshwater content in the North Atlantic Ocean, 1955–2006. *Geophys. Res. Lett.* 34:L16603, doi:10.1020/2007/GL030126

Cabanes C, Cazenave A, Le Provost C. 2001. Sea level rise during past 40 years determined from satellite and in situ observations. *Science* 294:840–42

Carton JA, Giese BS. 2008. A reanalysis of ocean climate using Simple Ocean Data Assimilation (SODA). *Month Weather Rev.* 136:2999–3017

Cazenave A, Nerem RS. 2004. Present-day sea level change: Observations and causes. *Rev. Geophys.* 42, doi:10.1029/2003RG000139

Cazenave A. 2006. How fast are the ice sheets melting? *Science* 314:1250–52

Cazenave A, Dominh K, Guinehut S, Berthier E, Llovel W, et al. 2009. Sea level budget over 2003–2008: A reevaluation from GRACE space gravimetry, satellite altimetry and Argo. *Glob. Planet. Change* 65:83–88, doi:10.1016/j/gloplacha.2008.10.004

Chambers DP, Mehlhaff CA, Urban TJ, Fujii D, Nerem RS. 2002. Low frequency variations in global mean sea level: 1950–2000. *J. Geophys. Res.* 107(C4):3026, doi:10.1029/2001JC001089

Chambers DP, Wahr J, Nerem RS. 2004. Preliminary observations of global ocean mass variations with GRACE. *Geophys. Res. Lett.* 31:L13310, doi:10.1029/2004GL020461

Chambers DP. 2006. Observing seasonal steric sea level variations with GRACE and satellite altimetry. *J. Geophys. Res.* 111(C3):C03010, doi:10.1029/2005JC002914

Chao BF. 1995. Anthropogenic impact on global geodynamics due to reservoir water impoundment. *Geophys. Res. Lett.* 22:3529–32

Chao BF, Wu YH, Li YS. 2008. Impact of artificial reservoir water impoundment on global sea level. *Science* 320:212–14, doi:10.1126/science.1154580

Chelton DB, Ries JC, Haines BJ, Fu L-L, Callahan PS. 2001. Satellite altimetry. In *Satellite Altimetry and Earth Sciences, A Handbook of Techniques and Applications*, ed. L-L Fu, A Cazenave, vol. 69, pp. 1–131. San Diego, CA: Academic Press

Chen JL, Wilson CR, Tapley BD. 2006a. Satellite gravity measurements confirm accelerated melting of the Greenland ice sheet. *Science* 313:1958

Chen JL, Wilson CR, Blankenship DD, Tapley BD. 2006b. Antarctic mass change rates from GRACE. *Geophys. Res. Lett.* 33:L11502, doi:10.1029/2006GL026369

Chen JL, Tapley BD, Wilson CR. 2006c. Alaskan mountain glacial melting observed by satellite gravimetry. *Earth Planet. Sci. Lett.* 248:368–78

Chen JL, Wilson CR, Tapley BD, Blankenship DD, Ivins ER. 2007. Patagonia icefield melting observed by Gravity Recovery and Climate Experiment (GRACE). *Geophys. Res. Lett.* 34:L22501, doi:10.1029/2007GL031871

Church JA, White NJ, Coleman R, Lambeck K, Mitrovica JX. 2004. Estimates of the regional distribution of sea-level rise over the 1950 to 2000 period. *J. Clim.* 17(13):2609–25

Church JA, White NJ, Arblaster JM. 2005. Significant decadal-scale impact of volcanic eruptions on sea level and ocean heat content. *Nature* 438:74–77

Church JA, White NJ. 2006. A 20th century acceleration in global sea-level rise. *Geophys. Res. Lett.* 33:L01602, doi:10.1029/2005GL024826

Cogley JC. 2009. Geodetic and direct mass balance measurements: Comparison and joint analysis. *Ann. Glaciol.* 50:96–100

Davis CH, Li Y, McConnell JR, Frey MF, Hanna E. 2005. Snowfall-driven growth in East Antarctica ice sheet mitigates recent sea level rise. *Science* 308:1898–907

Douglas BC. 2001. Sea level change in the era of the recording tide gauge. In *Sea Level Rise, History and Consequences*, ed. BC Douglas, MS Kearney, SP Leatherman, pp. 37–64. San Diego, CA: Academic Press

Domingues C, Church J, White N, Gleckler PJ, Wijffels SE, et al. 2008. Improved estimates of upper ocean warming and multidecadal sea level rise. *Nature* 453:1090–93, doi:10.1038/nature07080

Ericson JP, Vorosmarty CJ, Dingman SL, Ward LG, Meybeck L. 2006. Effective sea level rise and deltas: Causes of change and human dimension implications. *Glob. Planet. Change* 50:63–82

Gille ST. 2008. Decadal scale temperature trends in the southern hemisphere ocean. *J. Clim.* 21:4749–65

Gornitz V. 2001. Impoundment, groundwater mining, and other hydrologic transformations: Impacts on global sea level rise. In *Sea Level Rise, History and Consequences*, ed. BC Douglas, MS Kearney, SP Leatherman, pp. 97–119. San Diego, CA: Academic Press

Gouretski V, Koltermann KP. 2007. How much is the ocean really warming? *Geophys. Res. Lett.* 34:L011610, doi: 10.1029/GL027834

Grinsted A, Moore JC, Jevrejeva S. 2007. Observational evidence of volcanic impact on sea level and the global water cycle. *P.N.A.S.* 104(50):19730–34

Guinehut S, Le Traon P-Y, Larnicol G, Phillips S. 2004. Combining ARGO and remote-sensing data to estimate the ocean three-dimensional temperature fields. *J. Mar. Syst.* 46:85–98

Hanawa K, Rual P, Bailey R, Sy A, Szabados M. 1995. A new depth-time equation for Sippican or TSK T-7, T-6 and T-4 expandable bathythermographs (XBT). *Deep Sea Res. Part I* 42:1423–51

Hansen J, et al. 2005. Earth's energy imbalance: Confirmation and implications. *Science* 308:1431–35

Hebrard E, Llovel W, Cazenave A. 2008. Spectral analysis of 20th century mean sea level rates. Presented at Am. Geophys. Union, Fall Meeting, Dec. 2008, San Francisco

Holgate SJ, Woodworth PL. 2004. Evidence for enhanced coastal sea level rise during the 1990s. *Geophys. Res. Lett.* 31:L07305, doi:10.1029/2004GL019626

Holgate S. 2007. On the decadal rates of sea level change during the twentieth century. *Geophys. Res. Lett.* 34:L01602, doi:10.1029/2006GL028492

Holland D, Thomas RH, De Young B, Ribergaard MH, Lyberth B. 2008, Acceleration of Jakobshawn Isbrae triggered by warm subsurface ocean waters. *Nat. Geosci.* 1:659–64, doi:10.1038/ngeo316

Horton R, Herweijer C, Rosenzweig C, Liu J, Gornitz V, Ruane AC. 2008. Sea level rise projections from current generation CGCMs based on the semi-empirical method. *Geophys. Res. Lett.* 35:L02715, doi:10.1029/2007GL032486

Howat IM, Joughin IR, Scambos TA. 2007. Rapid changes in ice discharge from Greenland outlet glaciers. *Science* 315:1559–61, doi:10.1126/science.1138478

Huntington TG. 2008. Can we dismiss the effect of changes in land water storage on sea level rise? *Hydrol. Process.* 22:717–23

IPCC. 2007. *Fourth Assessment Report (AR4), Climate Change 2007: The Physical Science Basis*, Contribution of Working Group I to the Fourth Assessment Report of the Intergovernmental Panel on Climate Change, ed. S Solomon et al. Cambridge, UK: Cambridge Univ. Press

Ishii M, Kimoto M, Sakamoto K, Iwasaki SI. 2006. Steric sea level changes estimated from historical ocean subsurface temperature and salinity analyses. *J. Oceanogr.* 62(2):155–70

Ishii M, Kimoto M. 2009. Reevaluation of historical ocean heat content variations with varying XBT and MBT depth bias corrections. *J. Oceanogr.* 65:287–99

Ivins ER, James TS. 2005. Antarctic glacial isostatic adjustment: A new assessment. *Antarct. Sci.* 17(4):541–53

Jevrejeva S, Grinsted A, Moore JC, Holgate S. 2006. Nonlinear trends and multiyear cycles in sea level records. *J. Geophys. Res.* 111:C09012, doi:10.1029/2005/JC003229

Jevrejeva S, Moore JC, Grinsted A, Woodworth PL. 2008. Recent global sea level acceleration started over 200 years ago? *Geophys. Res. Lett.* 35:L08715, doi:10.1029/2008GL03361

Johannessen OM, Khvorostovsky K, Miles MW, Bobylev LP. 2005. Recent ice-sheet growth in the interior of Greenland. *Science* 310:1013–16

Johnson GC, Mecking S, Sloyan BM, Wijffels SE. 2007. Recent bottom water warming in the Pacific Ocean. *J. Clim.* 20:5365–75

Joughin I, Das SB, King M, Smith BE, Howat IM, Moon T. 2008. Seasonal speedup along the western flank of the Greenland ice sheet. *Science* 320:781–83

Kaser G, Cogley JG, Dyurgerov MB, Meier MF, Ohmura A. 2006. Mass balance of glaciers and ice caps: Consensus estimates for 1961–2004. *Geophys. Res. Lett.* 33:L19501, doi:10.1029/2006GL027511

Kohl A, Stammer D. 2008. Decadal sea level changes in the 50-year GECCO ocean synthesis. *J. Clim.* 21:1876–90

Krabill W, Hanna E, Huybrechts P, Abdalati W, Cappelen J, et al. 2004. Greenland Ice Sheet: Increased coastal thinning. *Geophys. Res. Lett.* 31:L24402, doi:10.1029/2004GL021533

Lambeck K, Anzidei M, Antonioli F, Benini A, Esposito A. 2004. Sea level in Roman time in the Central Mediterranean and implications for recent change. *Earth Planet. Sci. Lett.* 224:563–75

Lemke P, et al. 2007. Observations: Changes in snow, ice and frozen ground. In *Fourth Assessment Report* [*AR4*] *Climate Change 2007: The Physical Science Basis*, Contribution of Working Group I to the Fourth Assessment report of the Intergovernmental Panel on Climate Change, ed. S Solomon, et al. Cambridge, UK: Cambridge Univ. Press

Leuliette EW, Nerem RS, Mitchum GT. 2004. Results of TOPEX/Poseidon and Jason-1 Calibration to Construct a Continuous Record of Mean Sea Level. *Mar. Geodesy* 27:79–94

Leuliette E, Miller L. 2009. Closing the sea level rise budget with altimetry, Argo and GRACE. *Geophys. Res. Lett.* 36:L04608, doi: 10.1029/2008GL036010

Levitus S, Antonov JL, Wang J, Delworth TL, Dixon KW, Broccoli AJ. 2001. Anthropogenic warming of Earth's climate system. *Science* 292:267–70

Levitus S, Antonov JL, Boyer TP. 2005. Warming of the world ocean, 1955–2003. *Geophys. Res. Lett.* 32:L02604, doi:10.1029/2004GL021592

Levitus S, Antonov JL, Boyer TP, Locarnini RA, Garcia HE, Mishonov AV. 2009. Global Ocean heat content 1955–2008 in light of recently revealed instrumentation. *Geophys. Res. Lett.* 36:L07608, doi:10.1029/2008GL037155

Llovel W, Cazenave A, Rogel P, Berge-Nguyen M. 2009. 2-D reconstruction of past sea level (1950–2003) using tide gauge records and spatial patterns from a general ocean circulation model, in revision. *Clim. Past.* 5:1–11

Lombard A, Cazenave A, Le Traon PY, Ishii M. 2005. Contribution of thermal expansion to present-day sea level rise revisited. *Glob. Planet. Change* 47:1–16

Lombard A, Garcia DE, Cazenave A, Ramillin G, Fletcher, et al. 2007. Estimation of steric sea level variations from combined GRACE and satellite altimetry data. *Earth Planet. Sci. Lett.* 254:194–202

Lombard A, Garric G, Penduff T, Molines JM. 2009. Regional variability of sea level change using a global ocean model at 1/4 resolution. *Ocean Dyn*, doi: 10.1007/s10236-009-0161-6

Lutchke SB, Zwally HJ, Abdalati W, Rowlands DD, Ray RD, et al. 2006. Recent Greenland ice mass loss by drainage system from satellite gravimetry observations. *Sciencexpress* 314:1286–89, doi:10.1126/science.1130776

Lutchke SB, Arendt AA, Rowlands DD, McCarthy JJ, Larsen CF. 2008. Recent glacier mass changes in the Gulf of Alaska region from GRACE mascon solutions. *J. Glaciol.* 54(188):767–77

Lyman JM, Willis JK, Johnson GC. 2006. Recent cooling of the upper ocean. *Geophys. Res. Lett.* 33:L18604, doi:10.1029/2006GL027033

McManus J. 2002. Deltaic responses to changes in river regimes. *Mar. Chem.* 79:155–70

Meehl, et al. 2007. Global Climate Projections. In *Fourth Assessment Report* [*AR4*], *Climate Change 2007: The Physical Science Basis*, Contribution of Working Group I to the Fourth Assessment report of the Intergovernmental Panel on Climate Change, ed. S Solomon, et al. Cambridge, UK: Cambridge Univ. Press

Meier MF, Dyurgerov MB, Rick UK, O'Neel S, Pfeffer WT, et al. 2007. Glaciers dominate Eustatic sea-level rise in the 21st century. *Science* 317:1064–67

Milly PCD, Cazenave A, Gennero MC. 2003. Contribution of climate-driven change in continental water storage to recent sea-level rise. *Proc. Natl. Acad. Sci. USA* 100:13158–61

Milly PCD, Cazenave A, Famiglietti J, Gornitz V, Laval K, et al. 2009. Terrestrial water storage contributions to sea level rise and variability. In *Proceedings of the WCRP Workshop: Understanding Sea Level Rise and Variability*, ed. J Church, et al. Malden, MA: Blackwell

Milne G, Gehrels WR, Hughes C, Tamisiea M. 2009. Identyfying the causes of sea level changes. *Nat. Geosci.* 2:471–78
Mitchum GT. 2000. An Improved Calibration of Satellite Altimetric Heights Using Tide Gauge Sea Levels with Adjustment for Land Motion. *Mar. Geodesy* 23:145–66
Mitrovica JX, Tamisiea ME, Davis JL, Milne GA. 2001. Recent mass balance of polar ice sheets inferred from patterns of global sea-level change. *Nature* 409:1026–29
Mitrovica JX, Gomez N, Clark PU. 2009. The sea-level fingerprint of West Antarctic collapse. *Science* 323:753
Nicholls RJ. 2002. Rising sea level: potential impacts and responses. In *Issues in Environmental Science and Technology*, ed. RE Hester, RM Harrison. *Glob. Environ. Change* 17:83–107
Nicholls RJ. 2007. The impacts of sea level rise. *Ocean Challenge* 15(1):13–17
Nerem RS. 1995. Measuring global mean sea level variations using TOPEX/POSEIDON altimeter data. *J. Geophys. Res.* 100:25135–151
Nerem RS, Mitchum GT. 2001a. Observations of sea level change from satellite altimetry. In *Sea Level Rise: History and Consequences*, ed. BC Douglas, MS Kearney, SP Leatherman, pp. 121–63. San Diego, CA: Academic Press
Nerem RS, Mitchum GT. 2001b. Sea level change. In *Satellite Altimetry and Earth Sciences: A Handbook of Techniques and Applications*, ed. L Fu, A Cazenave, pp. 329–49. San Diego, CA: Academic Press
Nerem S, Leuliette E, Cazenave A. 2006. Present-day sea level change. *C.R. Geosci.* 338:1077–83
Ngo-Duc T, Laval K, Polcher Y, Lombard A, Cazenave A. 2005a. Effects of land water storage on the global mean sea level over the last half century. *Geophys. Res. Lett.* 32:L09704, doi:10.1029/2005GL022719
Ngo-Duc T, Laval K, Polcher Y, Cazenave A. 2005b. Analyses of the contribution of continental water to sea level variations during the 1997–1998 ENSO event: Comparison between the AMIP simulations and the Topex/Poseidon satellite data. *J. Geophys. Res.* 110:DO9103, doi: 10.1029/2004JD004940
Paulson A, Zhong S, Wahr J. 2007. Inference of mantle viscosity from GRACE and relative sea level data. *Geophys. J. Int.* 171:497–508
Peltier WR. 2004. Global glacial isostasy and the surface of the ice-age Earth: the ICE-5G (VM2) model and GRACE. *Annu. Rev. Earth Planet. Sci.* 32:111–49
Peltier WR. 2009. Closure of the budget of global sea level rise over the GRACE era: The importance and magnitudes of the required corrections for global isostatic adjustment. *Quart. Sci. Rev.* 28:1658–74
Plag HP. 2006. Recent relative sea level trends: An attempt to quantify forcing factors. *Philos. Trans. R. Soc. Lond. A* 364:1841–69
Ramillien G, Lombard A, Cazenave A, Ivins E, Llubes M, et al. 2006. Interannual variations of ice sheets mass balance from GRACE and sea level. *Glob. Planet. Change* 53:198–208
Ramillien G, Bouhours S, Lombard A, Cazenave A, Flechtner F, Schmidt R. 2008. Land water contributions from GRACE to sea level rise over 2002–2006. *Glob. Planet. Change* 60:381–92
Rahmstorf S. 2007. A semi-empirical approach to projecting future sea level rise. *Science* 315:368
Rignot E, Kanagaratnam P. 2006. Changes in the velocity structure of the Greenland ice sheet. *Science* 311:986–90
Rignot E, Thomas R. 2002. Mass balance of polar ice sheets. *Science* 297:1502–06
Rignot E, Bamber JL, Van Den Broecke MR, Davis C, Li Y, et al. 2008a. Recent Antarctic ice mass loss from radar interferometry and regional climate modelling. *Nat. Geosci.* 1:106–10
Rignot E, Box JE, Burgess E, Hanna E. 2008b. Mass balance of the Greenland ice sheet from 1958 to 2007. *Geophys. Res. Lett.* 35:L20502, doi:10.1029/2008GL035417
Roemmich D, Owens WB. 2000. The ARGO project: Global ocean observations for understanding and prediction of climate variability. *Oceanography* 13:45–50
Sahagian D. 2000. Global physical effects of anthropogenic hydrological alterations: Sea level and water redistribution. *Glob. Planet. Change* 25:39–48
Shepherd A, Wingham D. 2007. Recent sea level contributions of the Antarctic and Greenland ice sheets. *Science* 315:1529–32
Slobbe DC, Ditmar P, Linderbergh RC. 2009. Estimating the rates of mass change, ice volume change and snow volume change in Greenland from ICESat and GRACE data. *Geophys. J. Int.* 176:95–106
Stammer D. 2008. Response of the global ocean to Greenland and Antarctica melting. *J. Geophys. Res.* 113:C06022, doi:10.1029/2006JC001079

Thomas RH, Rignot E, Casassa G, Kanagaratnam P, Acuna C, et al. 2004. Accelerated sea level rise from west Antarctica. *Science* 306:255–58
Trenberth KE, Fasullo JT, Kiehl J. 2009. Earth's global energy budget. *Bull. Am. Meteorol. Soc.* 90:311–23
Velicogna I, Wahr J. 2006a. Revised Greenland mass balance from GRACE. *Nature* 443:329
Velicogna I, Wahr J. 2006b. Measurements of time-variable gravity show mass loss in Antarctica. *Sciencexpress* 311:1754–56, doi:10.1126/science.1123785
Vorosmarty CV, et al. 2003. Anthropogenic sediment retention: Major global impact from registered river impoundments. *Glob. Planet. Change* 39:169–90
Willis JK, Roemmich D, Cornuelle B. 2004. Interannual variability in upper ocean heat content, temperature, and thermosteric expansion on global scales. *J. Geophys. Res.* 109:C12036, doi:10.1029/2003JC002260
Willis JK, Chambers DT, Nerem RS. 2008. Assessing the globally averaged sea level budget on seasonal to interannual time scales. *J. Geophys. Res.* 113:C06015, doi:10.1029/2007JC004517
Wingham DJ, Shepherd A, Muir A, Marshall GJ. 2006. Mass balance of the Antarctic ice sheet. *Philos. Trans. R. Soc. A* 364:1627–35
Witze A. 2008. Loosing Greenland. *Science* 452:798–802
Woodworth PL, Player R. 2003. The permanent service for mean sea level: An update to the 21st century. *J. Coastal Res.* 19:287–95
Woodworth P, White NJ, Jevrejeva S, Holgate SJ, Chuch JA, Gehrels WR. 2008. Evidence for the accelerations of sea level on multi-decade and century time scales. *Int. J. Climatol.* 29:777–789, doi:10.1002/joc.1771
Woppelmann G, Martin Miguez B, Bouin MN, Altamimi Z. 2007. Geocentric sea level trend estimates from GPS analyses at relevant tide gauges worldwide. *Glob. Planet. Change* 57:396–406
Wouters B, Chambers D, Schrama EJO. 2008. GRACE observes small scale mass loss in Greenland. *Geophys. Res. Lett.* 35:L20501, doi: 10.1029/2008GL034816
Wunsch C, Ponte RM, Heimbach P. 2007. Decadal trends in sea level patterns: 1993–2004. *J. Clim.* 20:5889-911, doi:10.1175/2007JCLI1840.1
Zwally HJ, Giovinetto MB, Li J, Cornejo HG, Beckley MA, et al. 2005. Mass changes of the Greenland and Antarctica ice sheets and shelves and contributions to sea level rise: 1992–2002. *J. Glaciol.* 51:509–24

Chapitre 5

Les variations régionales du niveau de la mer

5.1 Période altimétrique : observations du niveau des mers entre 1993 et 2010

Avant le lancement du satellite altimétrique Topex/Poséïdon en 1992, il n'était pas possible de cartographier les variations régionales des vitesses du niveau de la mer. Toutefois, des différences de hausse du niveau marin enregistrées en divers sites marégraphiques suggèraient que cette hausse n'était pas uniforme (*Douglas* [2001]). Les données altimétriques ont confirmé en effet que les variations interannuelles du niveau de la mer présentaient des différences régionales. Dans certaines régions, les vitesses d'élévation du niveau de la mer peuvent atteindre jusqu'à 3 fois la valeur de la moyenne globale (par exemple la région du Pacifique ouest). En revanche, dans d'autres régions (bassin Pacifique est), le niveau de la mer descend. La figure 5.1 montre cette distribution régionale des vitesses du niveau de la mer. Ces taux sont calculés sur la période entre janvier 1993 et novembre 2009 soit presque 17 ans de données. Les études et la connaissance de cette répartition géographique des tendances du niveau de la mer sont d'une importance capitale pour l'évaluation des risques socio-économiques et sur les populations côtières.

La structure spatiale des tendances du niveau de la mer est fortement marquée par la signature de phénomènes climatiques tel que ENSO (El Niño Southern Oscillation) dans le Pacifique tropical (*Lombard et al.* [2005]). La figure 5.2 compare les distributions géographiques des tendances du niveau de la mer sur les périodes : (a)1993-1996, (b)1993-1999, (c)1993-2003 et (d)1993-2009. Ces comparaisons mettent en évidence une forte variabilité interannuelle

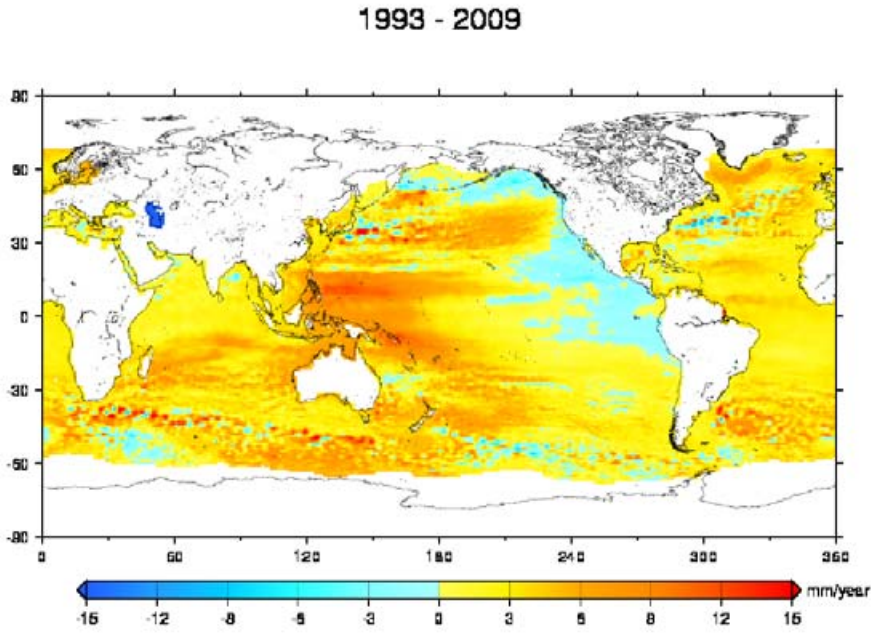

FIG. 5.1 – Distribution géographique des taux de variation du niveau de la mer entre janvier 1993 et novembre 2009 (source CLS-LEGOS).

mais aussi régionale, principalement due au phénomène ENSO montrant une structure dipolaire dans le bassin tropical de l'océan Pacifique. En effet, les 4 cartes de la figure 5.2 présentent les mêmes caractéristiques à savoir des anomalies positives à l'ouest et des anomalies plutôt négatives dans la partie est du bassin Pacifique tropical avec cependant des valeurs differentes selon la période considérée. Nous voyons bien que les structures régionales des tendances du niveau de la mer ne sont pas stationnaires au cours du temps. Effectivement, l'océan Indien, l'océan Atlantique sud ou encore la mer Méditerranée ne présentent pas les mêmes structures spatiales des tendances du niveau de la mer selon les périodes analysées.

5.2 Les causes de la variabilité régionale du niveau de la mer : la composante thermostérique

Pour la période 1993-2003, la distribution géographique des tendances du niveau de la mer thermostérique expliquait les structures régionales observées

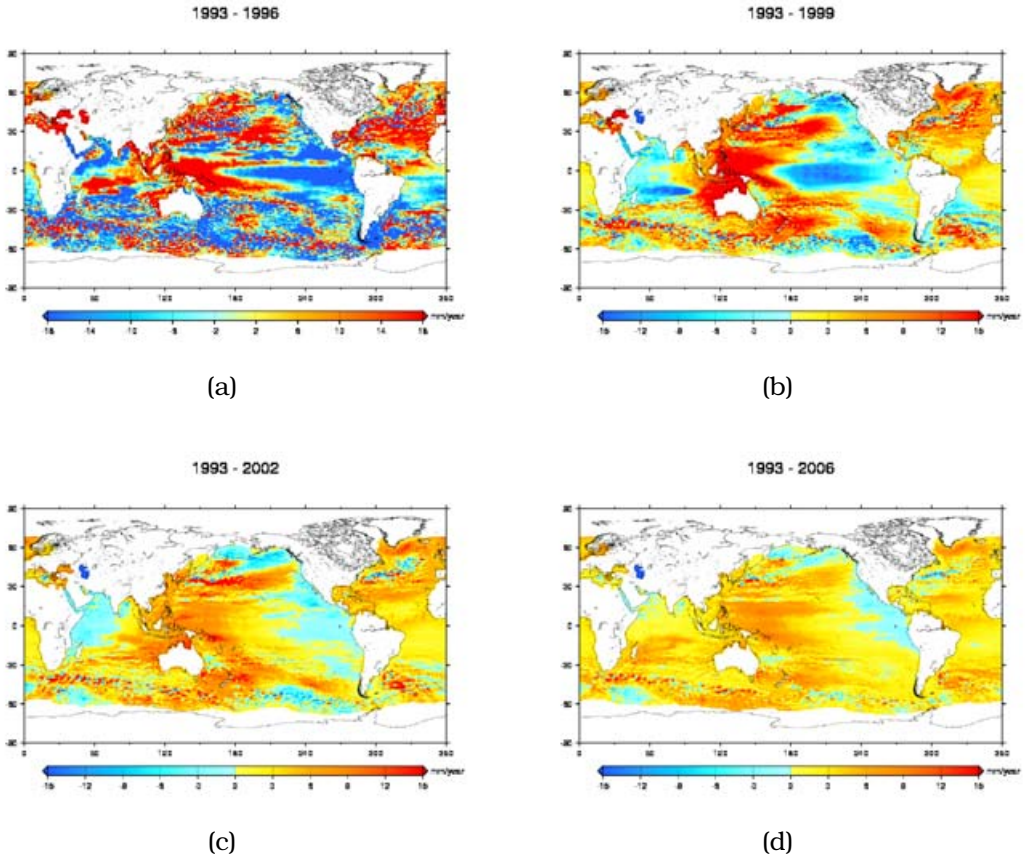

FIG. 5.2 – Cartographie des vitesses d'évolution du niveau de la mer sur les périodes (a) 1993-1996, (b) 1993-1999, (c) 1993-2003 et (d) 1993-2006.

par altimétrie spatiale sur cette même période. En effet, à partir de 4 bases de données différentes, *Lombard et al.* [2006] ont montré que les tendances du niveau de la mer thermostérique étaient fortement corrélées avec celles du niveau de la mer observé par le satellite altimétrique Topex/Poseidon (voir aussi *Bindoff et al.* [2007]).

La figure 5.3 présente la cartographie des tendances du niveau de la mer thermostérique à partir des données fournies par *Levitus et al.* [2009] sur la période 1993-2009. La conclusion de l'étude de *Lombard et al.* [2006] est confirmée par la comparaison des distributions géographiques des tendances du niveau de la mer thermostérique (5.3(a)) et du niveau de la mer observé par altimétrie spatiale (5.3(b)).

La figure 5.4 montre la distribution régionale des tendances du niveau de la mer thermostérique calculées à partir d'une autre base de données de

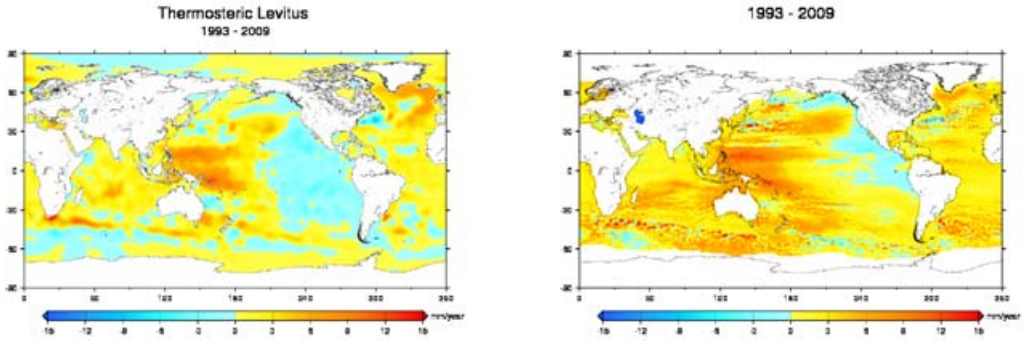

(a) Niveau de la mer thermostérique (b) Niveau de la mer observé

FIG. 5.3 – Cartographie régionale du niveau de la mer (a) thermostérique (jusqu'à 700m, *Levitus et al.* [2009]) et (b) observé par altimétrie spatiale entre 1993 et 2009

température (données de *Ishii and Kimoto* [2009]) sur la période 1993-2006 (période plus courte car les données après décembre 2006 ne sont pas disponibles). Sur cette nouvelle période d'étude, les structures principales des vitesses de l'expansion thermique se comparent bien aux structures régionales du niveau de la mer observé. Nous retrouvons bien la structure dipolaire du Pacifique tropical. Nous trouvons aussi de bons accords avec les structures des bassins du Pacifique nord et de l'Atlantique nord entre le niveau de la mer thermostérique et observé. Néanmoins, il existe quelques différences notamment dans les bassins de l'océan Indien et du Pacifique sud, où les tendances sont différentes.

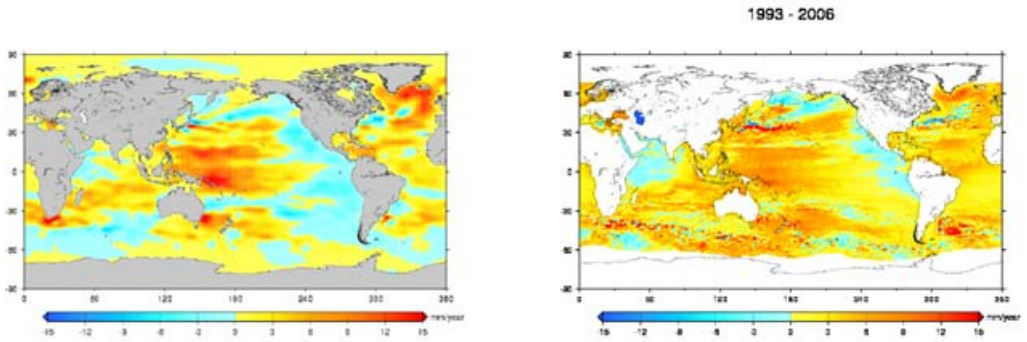

(a) Niveau de la mer thermostérique (b) Niveau de la mer observé

FIG. 5.4 – Cartographie régionale du niveau de la mer (a) thermostérique (jusqu'à 700m, *Ishii and Kimoto* [2009]) et (b) observé par altimétrie spatiale entre 1993 et 2006.

Ces comparaisons des cartographies des tendances du niveau de la mer thermostérique confirment que l'expansion thermique des océans contribue de manière significative à la répartition géographique des tendances du niveau de la mer observé sur la période altimétrique totale. Ces analyses confirment les résultats résumés dans le dernier rapport de l'IPCC-AR4 (*Bindoff et al.* [2007]).

5.3 Interprétation du signal résiduel entre les variations observées du niveau de la mer et l'expansion thermique des océans : les différences régionales

Le niveau de la mer thermostérique explique en grande partie les structures régionales des taux de variation du niveau de la mer observé par altimétrie spatiale. Cependant, des différences subsistent entre les cartographies des tendances du niveau de la mer observé et de la composante thermostérique. La carte de la figure 5.5 correspond à la distribution géographique des taux résiduels sur la période 1993-2009 entre le niveau de la mer observé et l'expansion thermique.

Plusieurs grandes structures correspondent à des résidus régionaux positifs. Ceci correspond à un signal du niveau de la mer observé plus important que la contribution thermostérique. Ces différences sont dûes à divers facteur : la salinité, la contribution des couches profondes, le rebond post-glaciaire et les effets de la circulation océanique.

- Le niveau de la mer halostérique

Nous savons que le niveau de la mer halostérique (variation de la salinité uniquement) ne contribue *quasiment* pas en moyenne globale au signal du niveau de la mer. Mais, cette composante présente une signature régionale non négligeable (*Wunsch et al.* [2007]; *Lombard et al.* [2009]). Dans certaines régions, une augmentation de la salinité induit des variations du niveau de la mer qui compensent l'expansion thermique. Une augmentation locale de la

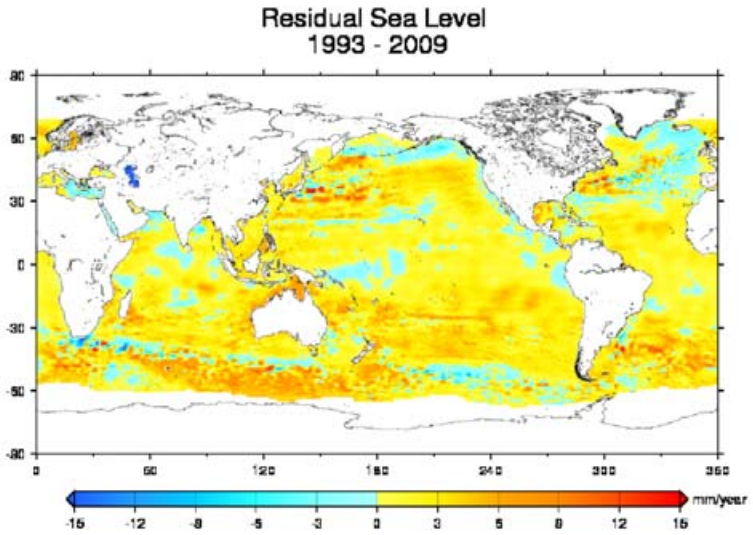

FIG. 5.5 – Cartographie régionale des résidus des vitesses entre le niveau de la mer observé (par altimétrie spatiale) et la composante thermostérique (calculée à partir des données de *Levitus et al.* [2009]) sur la période 1993-2009.

salinité de la colonne fluide implique une baisse du niveau de la mer stérique (*Wunsch et al.* [2007]).

- La contribution des couches profondes

Un autre facteur pouvant expliquer les différences de la figure 5.5 est la contribution des couches profondes non prises en compte (au-delà de 700m) lors de l'estimation des vitesses de variation du niveau de la mer thermostérique (figures 5.3(a) et 5.4(a)). *Antonov et al.* [2005] estiment que les couches profondes peuvent contribuer jusqu'à 30% du signal thermostérique total. Or la couverture des données hydrographiques au-dessous de 700m est trop faible sur la période altimétrique totale pour estimer avec précision la contribution des couches profondes aux variations régionales du niveau de la mer. Ce problème est en partie résolu avec les flotteurs profilant Argo. Nous

avons maintenant accès aux données de température et de salinité jusqu'à 2000m pour les années récentes seulement.

- Les variations de masse d'eau douce entre les océans et les continents

Les apports et les retraits de masse d'eau douce aux océans modifient localement le bilan hydrologique Evaporation-Précipitations-Ruissellement. Ces variations du bilan hydrologique peuvent entraîner des variations locales du niveau de la mer. Ces variations des paramètres hydrologiques, qui ont une influence directe sur la salinité locale des eaux de surface des océans, sont liées aux variations du bilan Précipitations-Evaporation sur les océans, à la fonte des glaciers de montagne, des calottes polaires ainsi qu'aux échanges d'eau douce avec les continents.

- Le signal du rebond post-glaciaire : effet de la dernière déglaciation

La Terre solide et les océans enregistrent la réponse de la fonte des grandes calottes polaires du dernier maximum glaciaire, il y a -20 000 ans. La réponse élastique et viscoélastique de la Terre solide engendre des modifications non uniformes dans les taux de variation du niveau de la mer (*Peltier* [2004]; *Plag* [2006]). La fonte des calottes de glace se traduit par les variations locales de self-gravité ainsi que des déformations de la Terre sous la charge variable engendrée par ces masses d'eau. Ce phénomène produit une élévation de la croûte terrestre aux emplacements des anciennes calottes glaciaires et, des baisses locales aux alentours de celles-ci. De plus, ce phénomène se caractérise par des variations régionales du niveau de la mer résultant des effets de self-gravitation, de déformation de la croûte mais aussi de la rotation terrestre en raison de la redistribution de masse.

- Effets de la fonte actuelle des glaciers de montagne et des calottes polaires

La fonte actuelle des glaciers de montagne, du Groenland et de l'Antarctique, engendre des variations régionales des vitesses du niveau de la mer. *Mitrovica et al.* [2001, 2009] et *Tamisiea et al.* [2001] ont utilisé un modèle de Terre viscoélastique de Maxwell afin de caractériser la distribution régionale des changements des vitesses du niveau de la mer au moment de la fonte partielle de chacun de ces trois réservoirs de glace continentale (Antarctique, Groenland et glaciers de montagne, voir figure 5.6).

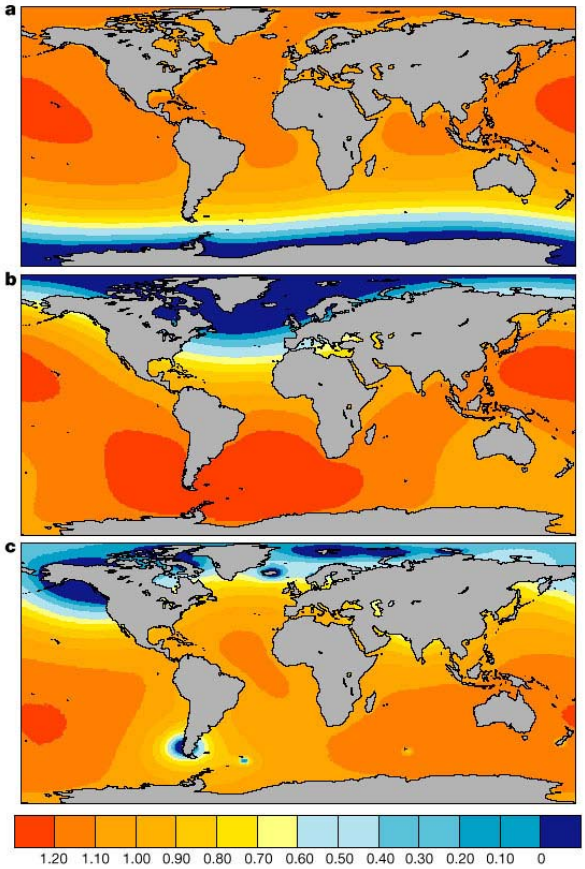

FIG. 5.6 – Distribution géographique des variations du niveau de la mer consécutives à une fonte a) de l'Antarctique, b) du Groenland et c) des glaciers de montagne, prédite par *Mitrovica et al.* [2001, 2009] et *Milne et al.* [2009]. Les variations du niveau de la mer sont normalisées et correspondent à une contribution de chaque masse glaciaire de 1 mm/an de hausse du niveau moyen global de la mer.

- Les changements de la circulation océanique

Des simulations numériques (*Stammer* [2008]) ont montré que l'apport d'eau douce dû à la fonte du Groenland et de l'Antarctique pourrait entraîner des changements majeurs de la circulation océanique globale. *Stammer* [2008] montre que l'apport d'eau douce généré par la fonte du Groenland engendre une réponse localisée du niveau de la mer dans le bassin Atlantique nord en quelques années seulement. A plus longue échelle de temps, cet apport d'eau douce a un effet bien plus global avec une propagation des anomalies vers le

Pacifique et l'Indien avec une échéance de 50 ans. A l'inverse, l'apport d'eau douce induit par la fonte de l'Antarctique a un effet plus régional. En effet, les anomalies du niveau de la mer se localisent principalement autour du continent Antarctique (*Stammer* [2008]).

5.4 La variabilité régionale du niveau de la mer des dernières décennies

Nous venons de voir dans le paragraphe précédent que les observations de la variabilité régionale du niveau de la mer datent de la fin de l'année 1992. Nous n'avons donc pas d'observations du niveau de la mer régional pour les décennies passées. Il est important de connaître et de comprendre cette variabilité régionale du niveau de la mer, ses changements aux échelles interannuelles, décennales et multidécennales afin de pouvoir établir des prévisions futures robustes. Pour cela, nous avons développé une méthode dite de « reconstruction » pour palier ce manque d'information sur les 5 dernières décennies.

5.4.1 Les méthodes de reconstruction

Problématique et motivation

De nombreuses études ont développé ce genre de méthode dans le but de reconstruire des séries temporelles et des champs 2 dimensions de variables océanographiques (la température de surface des océans ou la hauteur du niveau marin) et atmosphériques (la vitesse du vent et la pression atmosphérique à la surface des océans par exemple) dans le passé (*Smith et al.* [1996]; *Chambers et al.* [2002]; *Beckers and Rixen* [2003]; *Church et al.* [2004]; *Alvera-Azcarate et al.* [2005]).

Récemment, *Church et al.* [2004] ont reconstruit le signal du niveau de la mer dans le passé en combinant un nombre variable de marégraphe au cours du temps (signal à 1 dimension, 1-D) et 8 années de données altimétriques (signal à 2 dimensions, 2-D) permettant d'extraire les modes de variabilité principaux sur 1993-2000. Or, nous avons souligné dans le paragraphe 5.1 que les structures spatiales ne sont pas stationnaires au cours du temps et, reconstruire le niveau de la mer sur le XX^{ème} siècle avec la variabilité calculée sur 8 ans de données altimétriques n'est pas forcement une bonne représentation de la réalité. C'est pour cette raison que nous nous sommes orientés vers la modélisation numérique de circulation générale des océans en considérant les sorties d'un modèle forcé pour en extraire les structures spatiales à long terme (supérieures à 10 ans) de l'océan et de reconstruire les tendances régionales du niveau de la mer sur les décennies passées (1950-2003). Comme nous nous intéressons principalement à la variabilité régionale du niveau de la mer, dans

chaque cas nous retirons une tendance uniforme sur l'ensemble du domaine océanique dans le but d'étudier principalement les structures régionales.

Le formalisme mathématique de la reconstruction

Les méthodes de reconstruction combinent des grilles de données à 2 dimensions (2-D), possédant une couverture temporelle limitée, avec des données historiques éparses (1-D) mais bien résolues temporellement (*Smith et al.* [1996]; *Kaplan et al.* [1998, 2000]; *Chambers et al.* [2002]; *Beckers and Rixen* [2003]; *Church et al.* [2004]; *Alvera-Azcarate et al.* [2005]).

Cette méthode se décompose en deux principales étapes.

- La première consiste à décomposer le signal 2-D (de courte période temporelle) en modes principaux de variabilité. Pour ce faire, nous utilisons une analyse de décomposition en composantes principales dite Empirical Orthogonal Functions (EOFs, *Preisendorfer* [1988]; *Toumazou and Cretaux* [2001]). Cette décomposition permet de séparer le signal (matrice $H(x, y, t)$), bien résolu spatialement, en une somme de produits des signaux spatiaux (matrice $U(x, y)$) et temporel (vecteur $\alpha(t)$ des amplitudes correspondantes aux EOFs) selon l'équation qui suit :

$$H(x, y, t) = U(x, y)\alpha(t) \tag{5.1}$$

L'hypothèse de base de la méthode de reconstruction est la stationnarité des modes spatiaux de la matrice $U(x, y)$. Ainsi, nous déduisons que le signal 2-D reconstruit sur la période longue des données en 1-D est le suivant :

$$H_R(x, y, t) = U(x, y)\alpha_R(t) \tag{5.2}$$

Avec $H_R(x, y, t)$ la matrice du signal reconstruit en 2-D sur la plus longue période et $\alpha_R(t)$ le vecteur des amplitudes des nouvelles EOFs sur la période longue.

Lors du calcul de la décomposition en EOF, la matrice H est décomposée en valeurs singulières d'après l'équation suivante :

$$H = USV^t \tag{5.3}$$

Où, U est toujours la matrice des EOFs, S est la matrice diagonale contenant les valeurs propres et V représente le vecteur propre (modes temporels). Ainsi, les amplitudes des EOFs sont équivalentes à $\alpha(t) = SV^t$.

- La seconde étape consiste maintenant à calculer les amplitudes reconstruites sur la plus longue période en ajustant les modes de variabilité aux marégraphes à chaque pas de temps. Ces amplitudes sont calculées à l'aide de la fonction des moindres carrés généralisés :

$$S(\alpha) = (PU_M\alpha - H^0)R^{-1}(PU_M\alpha - H^0) \tag{5.4}$$

Où, H^0 est la matrice du niveau de la mer observé par les marégraphes, P est la matrice de projection égale à 1 pour chaque donnée marégraphique valable, 0 sinon. R représente la matrice de covariance des erreurs. Cette matrice compte pour les erreurs d'instrumentation et les erreurs dûes à la troncature du nombre d'EOFs pour reconstruire la série temporelle sur la longue période. Enfin, U_M représente la matrice des N EOFs (nombre fini de mode) considérées lors du calcul de reconstruction.

Le mouvement uniforme : l'EOF0

Dans le signal du niveau de la mer, il existe un signal basse fréquence (supérieur à 12 mois) correspondant au mouvement uniforme du bassin considéré. Cette partie du signal du niveau de la mer correspond à un signal spatial uniforme et égal à 1 aux points de mesure et d'une partie temporelle représentant la variabilité de la moyenne globale (*Church et al.* [2004]). Lors de la décomposition du signal 2-D afin d'extraire les modes de variabilité, ce signal est projeté sur plusieurs EOFs car ce mode de variabilité n'est pas orthogonal aux autres modes. Cela implique une troncature de ce signal au moment de la recomposition du signal final. Seul un nombre limité d'EOFs du signal 2-D est considéré et, de ce fait, une partie de ce signal uniforme sera perdue. *Church et al.* [2004] proposent de séparer ce signal avant le calcul des EOFs du signal spatial 2-D et de l'ajouter après ce calcul. Nous allons, par la suite, regarder

les résultats en considérant ou non ce mouvement uniforme (ou EOF0) dans le calcul des EOFs du signal spatial 2-D.

La modélisation numérique de circulation générale des océans : le modèle OPA/NEMO

La réanalyse océanique utilisée dans notre reconstruction du niveau de la mer des 50 dernières années a été produite par un schéma d'assimilation de données de type 3-D VAR (*Daget et al.* [2009]) appliqué au modèle de circulation générale des océans OPA/NEMO (*Madec et al.* [1998]). Ce modèle a une résolution de 2° en moyenne avec une grille irrégulière plus fine aux tropiques. Le modèle est forcé par les flux ERA-40 (*Uppala et al.* [2005]). Les profils de température et de salinité sont assimilés tous les 10 jours de janvier 1960 à décembre 2006 à partir de la base de données EN3 (*Ingleby and Huddleston* [2007]). Pour information, les données n'ont pas été corrigées des problèmes instrumentaux découverts très récemment (problèmes des capteurs de pression dans certains flotteurs profilant Argo et biais de profondeur des données XbT).

Le modèle OPA/NEMO est un modèle à surface libre, à volume constant et avec un schéma de conservation du sel (*Roullet and Madec* [2000]). Ainsi, comme le volume des océans reste constant au cours du temps, le niveau global de la mer ne varie pas. Ceci ne permet pas d'étudier l'évolution du niveau moyen mais ne pose pas de problème pour étudier la variabilité régionale.

La figure 5.7 montre les taux de variation du niveau de la mer entre 1960 et 2003 basés sur les sorties de la réanalyse océanique s'appuyant sur le modèle numérique OPA/NEMO. Cette carte nous renseigne sur la variabilité régionale du niveau de la mer (tendance uniforme nulle) sur la période 1960-2003. Il apparaît très clairement que le comportement du niveau de la mer est différent d'une région à l'autre. En effet, les régions des courants de bord ouest montrent de fortes anomalies positives des vitesses d'évolution du niveau de la mer en variabilité régionale (Golf Stream, Kuroshio...). En outre, ces structures spatiales ne sont pas les mêmes que celles du niveau de la mer observé par atimétrie spatiale sur la période 1993-2009 (figure 5.1). Ce résultat confirme bien que les structures spatiales de la variabilité régionale du niveau de la mer ne sont pas stationnaires au cours du temps.

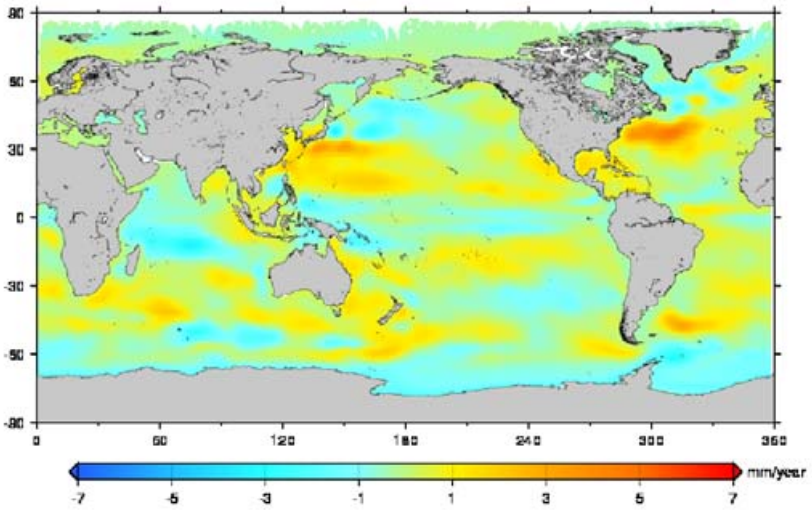

FIG. 5.7 – Cartographie des taux de variation du niveau de la mer entre 1960 et 2003 basée sur les données du modèle numérique OPA/NEMO.

5.4.2 Résultats

Dans ce paragraphe, nous reconstruisons la variabilité régionale du niveau de la mer entre 1950 et 2003. Nous ne considérons pas la tendance du signal de la moyenne globale. Nous prenons en compte les sorties du modèle numérique de circulation générale d'océan OPA et nous calculons les modes principaux de variabilité à l'aide d'une décomposition en EOFs sur la période 1960-2003 (soit 44 ans de données). Puis, nous ajustons ces modes de variabilité aux données marégraphiques, soit 99 enregistrements au total sur la période plus longue de 1950 à 2003. Le choix de ce jeu de marégraphes résulte de plusieurs critères : séries longues de 50 ans de données sans trou et de qualité (ces enregistrements ne présentent pas de comportement douteux dûs aux mouvements de la croûte terrestre). Les cartographies des tendances sur les dernières décennies (1950-2003) du niveau de la mer sont maintenant analysées en détail dans les paragraphes qui suivent.

Méthode A : calcul sans retirer l'EOF0 lors de l'extraction des modes de variabilité du signal 2-D

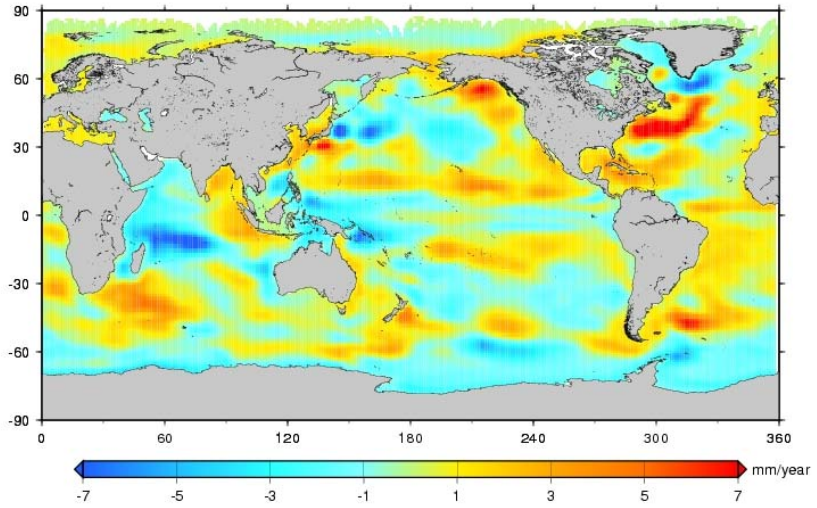

FIG. 5.8 – Cartographie des taux de variation du niveau de la mer reconstruit entre 1950 et 2003 (d'après *Llovel et al.* [2009]).

La figure 5.8 représente les structures spatiales des taux de variation du niveau de la mer sur la période 1950-2003. Nous observons une forte variabilité régionale de ces tendances. Notamment, l'Atlantique nord présente une forte signature d'anomalies positives au niveau du Golf Stream et comporte aussi des anomalies négatives autour du Groenland. L'océan Indien comporte de fortes anomalies de niveau de la mer négatives dans le bassin tropical ouest et des anomalies plutôt positives dans le bassin est ainsi qu'au sud de Madagascar. Pour l'ocan Pacifique, des anomalies de niveau de la mer négatives près de la bande équatoriale et des anomalies positives vers les tropiques (à 15° de latitude) sont visibles. De plus, nous notons un fort signal positif près des côtes de l'Alaska. Cette cartographie des taux de variation du niveau de la mer entre 1950-2003 est comparable avec celle issue de la modélisation numérique (OPA/NEMO) sur 1960-2003, malgré quelques différences notamment dans les valeurs des amplitudes et la position des structures spatiales. En effet, les tendances, en valeurs absolues, du niveau de la mer reconstruit sont plus importantes que celles de la modélisation numérique.

Méthode B : calcul en retirant l'EOF0 lors de l'extraction des modes de variabilité du signal 2-D

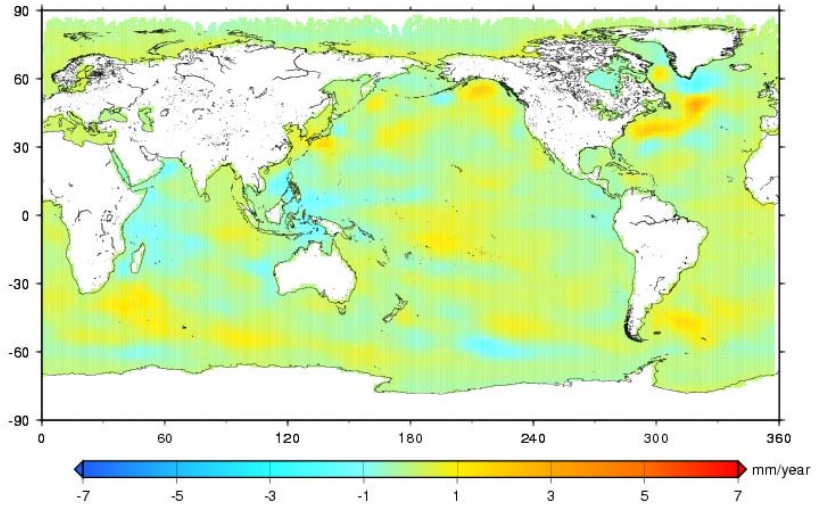

FIG. 5.9 – Cartographie des taux de variation du niveau de la mer reconstruit entre 1950 et 2003 en retirant l'EOF0 lors du calcul de reconstruction.

La figure 5.9 décrit les taux de variation du niveau de la mer sur la période 1950-2003 en retirant, cette fois-ci, le signal uniforme du bassin (signal EOF0 décrit plus haut) lors du calcul des modes de variabilité du signal spatial (2-D). Les amplitudes, en valeurs absolues, sont maintenant plus faibles par rapport à la cartographie des tendances issues de la méthode A. En revanche, dans certaines régions, les mêmes anomalies des tendances persistent, c'est le cas du bassin de l'Atlantique nord avec la forte signature du Golf Stream mais aussi le signal négatif autour du Groenland. Les mêmes structures dans l'océan Indien sont elles aussi à nouveau cartographiées mais avec, cependant, des amplitudes plus faibles.

La comparaison des tendances du niveau de la mer sur 1950-2003 des deux méthodes de reconstruction montre des différences non seulement sur les structures régionales des vitesses d'évolution, mais aussi sur les amplitudes relatives qui sont plus importantes dans le calcul de la méthode A. Il est probable que ces écarts proviennent de la projection de ce mode uniforme sur toutes les autres EOFs qui sont orthogonales, ceci pourrait induire une perte de signal potentiellement responsable des amplitudes importantes observées sur la figure 5.8. Focalisons nous maintenant sur les modes principaux de variabilité de ces deux reconstructions.

5.4.3 Analyses en composantes principales : détermination des principaux modes de variabilité des vitesses du niveau de la mer reconstruit sur 1950-2003

La figure 5.10 représente les trois premiers modes de variabilité du niveau de la mer reconstruit sur la période 1950-2003 (méthode A). Le premier mode de variabilité constitue un signal à long terme dont les structures régionales illustrent la cartographie des tendances du niveau de la mer reconstruit d'après la méthode A sur la période 1950-2003. Ce mode de variabilité traduit un signal multidécennal lié à la variabilité régionale du niveau de la mer reconstruit. Le second mode est lié à la variabilité ENSO avec la signature du dipôle est-ouest de l'océan Pacifique tropical. En effet, la superposition de l'indice SOI (Southern Oscillation Index, courbe rouge) montre la concordance entre le mode temporel de cet EOF et l'index ENSO. Enfin, le troisième mode de variabilité est aussi lié à la variabilité ENSO, mais il traduit les mouvements de la thermocline induisant des transferts de masse/chaleur nord-sud dans le bassin Pacifique tropical (*Delcroix* [1998]).

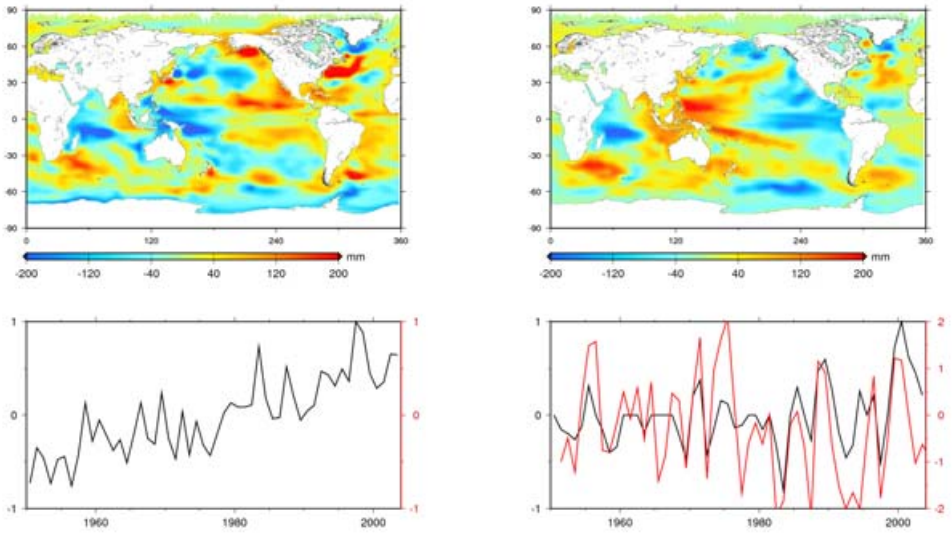

(a) mode 1

(b) mode 2

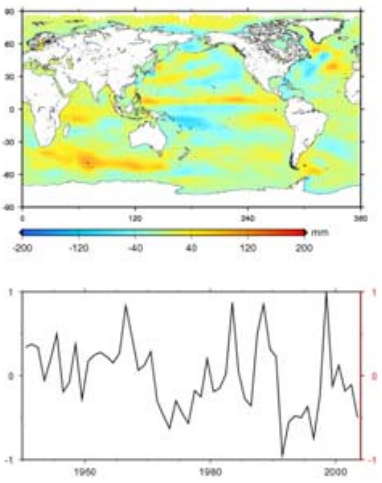

(c) mode 3

FIG. 5.10 – 3 premières EOFs de la reconstruction du niveau de la mer entre 1950 et 2003 (Méthode A) a) mode 1 (50% de variance expliquée), b) mode 2 (25% de variance expliquée), courbe rouge : SOI, c) mode 3 (8% de variance expliquée)

Sur la figure 5.11 figure les trois premiers modes de variabilité du niveau de la mer reconstruit sur la période 1950-2003 (méthode B). Le premier mode de variabilité constitue le signal ENSO caractérisé par la forte signature du dipôle de l'océan Pacifique tropical, confirmé par la forte corrélation de l'index SOI avec le mode temporel correspondant. Ce mode de variabilité est similaire au mode de variabilité 2 de la méthode A (figure 5.10(b)). Le second mode de variabilité lui aussi lié à ENSO avec les mouvements de masse d'eau nord-sud, est similaire au 3ème mode de variabilité de la méthode A. Par contre, le 3ème mode de variabilité correspond à la cartographie des tendances reconstruites du niveau de la mer d'après la méthode B avec une composante temporelle qui suggère une tendance positive sur la période considérée. Or, le signal spatial de cet EOF se compare au même titre que les deux cartes des tendances du niveau de la mer reconstruit (par les deux méthodes) sur la période totale avec des amplitudes plus faibles pour la méthode B. Nous retrouvons assez bien les structures régionales des tendances. Ainsi, la variabilité ENSO est bien présente dans les deux méthodes de reconstruction.

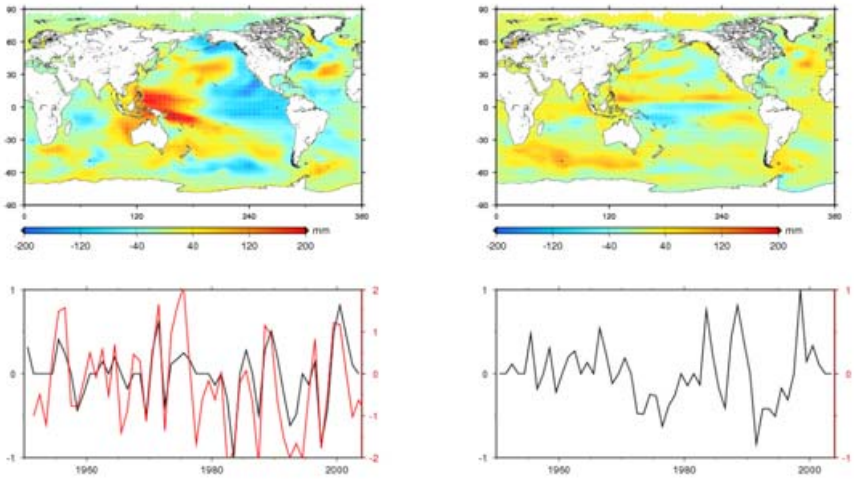

(a) mode 1 (b) mode 2

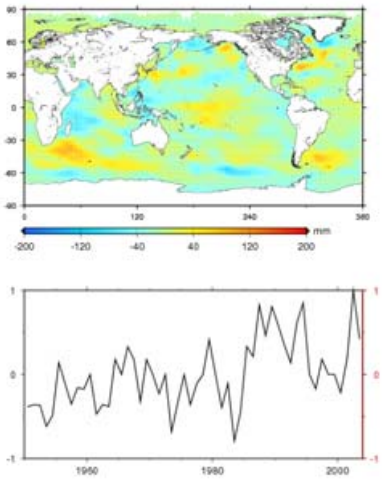

(c) mode 3

FIG. 5.11 – 3 premières EOFs de la reconstruction du niveau de la mer entre 1950 et 2003 (Méthode B) a) mode 1 (45% de variance expliquée), courbe rouge : SOI, b) mode 2 (13% de variance expliquée), c) mode 3 (10% de variance expliquée)

5.4.4 La cartographie régionale du niveau de la mer thermostérique et ses principaux modes de variabilité

Cartographie des vitesses de varition du niveau de la mer thermostérique entre 1955 et 2008

La figure 5.12 montre la cartographie régionale du niveau de la mer thermostérique entre 1955 et 2008. Ces vitesses ont été calculées de la surface jusqu'à 700m de profondeur. Nous observons une forte variabilité régionale des taux de variation du niveau de la mer thermostérique. L'Atlantique nord présente de fortes anomalies positives traduisant un réchauffement de cet océan sur les 5 dernières décennies. Nous trouvons aussi de fortes anomalies positives du niveau de la mer thermostérique au large des côtes de l'Afrique du Sud et entre l'Autralie et la Nouvelle Zélande (mer de Tasmanie). Près des côtes du Japon, nous observons des anomalies positives et des anomalies négatives. Dans ce dernier cas, la couche 0-700m de l'océan s'est refroidie sur les 50 dernières années. Le bassin Pacifique présente des anomalies positives de niveau de la mer thermostérique (bassins Pacifique nord et Pacifique sud). Il apparait très clairement que le comportement du niveau de la mer thermostérique diffère d'une région à l'autre. Nous notons des points communs entre cette cartographie des tendances du niveau de la mer thermostérique et les vitesses du niveau de la mer déduites du modèle numérique OPA/NEMO de la figure 5.7. En effet, nous retrouvons la signature des anomalies positives dans les bassins de l'Atlantique nord, du Pacifique, des anomalies positives et négatives au large des côtes du Japon. Toutefois, les amplitudes sont plus faibles. Nous retrouvons aussi de bonnes ressemblances avec le niveau de la mer reconstruit (voir figures 5.8 et 5.9). Cependant, les amplitudes des vitesses de variation du niveau de la mer reconstruit avec le niveau de la mer stérique sur les 50 dernières années sont plus en accord avec le niveau de la mer reconstruit par la méthode B (en écartant l'EOF0 lors du calcul de reconstruction) que le niveau de la mer reconstruit avec la méthode A (on considère l'EOF0 lors du calcul de la reconstruction).

Principaux modes de variabilité du niveau de la mer thermostérique entre 1955 et 2008

A présent, l'analyse porte sur les modes de variabilité des données *in situ* et tout particulièrement sur le signal du niveau de la mer thermostérique des 50

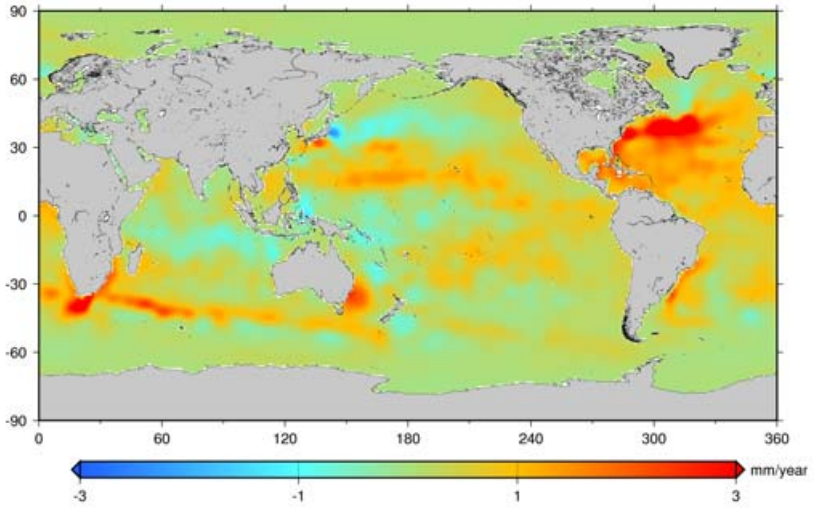

FIG. 5.12 – Cartographie des taux de variation du niveau de la mer thermostérique entre 1955 et 2008 d'après les données de *Levitus et al.* [2009]

dernières années. Pour celâ, les champs de données de température récemment corrigés de biais liés aux sondes XbT (*Levitus et al.* [2009]) sont étudiés.

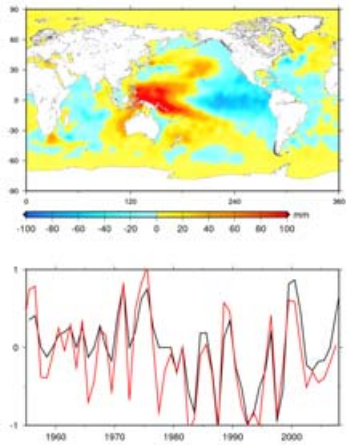

(a) mode 1

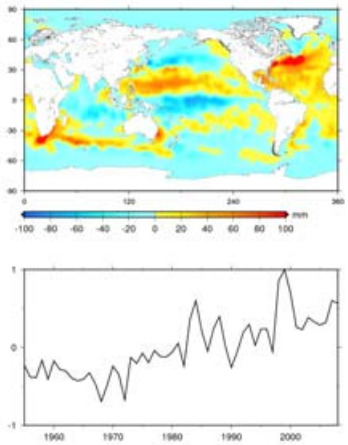

(b) mode 2

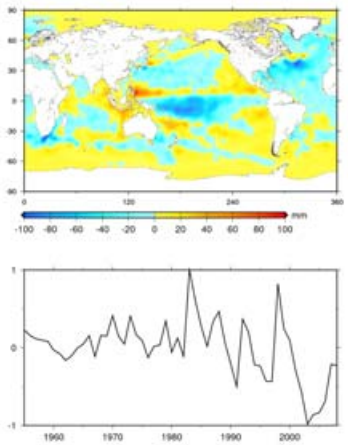

(c) mode 3

FIG. 5.13 – 3 premières EOFs du niveau de la mer thermostérique entre 1955 et 2008 a) mode 1 (21% de variance expliquée), courbe rouge : SOI, b) mode 2 (11% de variance expliquée), c) mode 3 (8% de variance expliquée)

Les trois premiers modes de variabilité de l'expansion thermique des océans d'après les données de *Levitus et al.* [2009] entre 1955 et 2008 sont illustrés sur la figure 5.13. Le premier mode de variabilité représente le signal ENSO avec la signature caractéristique du dipôle de l'océan Pacifique tropical. Le second mode de variabilité constitue le signal multidécennal présentant une tendance positive détecté dans la composante temporelle de l'EOF2. De plus, les structures spatiales sont très semblables au premier mode de variabilité des méthodes A et B de reconstruction (océan Indien, Pacifique tropical mais aussi l'Atlantique nord). Enfin, le troisième mode de variabilité décrit le signal ENSO des flux de masse d'eau nord-sud qui se compare parfaitement avec les modes 3 (méthode A) et 2 (méthode B).

Ainsi, le signal basse fréquence détecté dans le niveau de la mer reconstruit par la méthode A a une signification physique et est traduite par les tendances du niveau de la mer thermostérique. Notons, tout de même que la composante temporelle est bien expliquée par les deux méthodes de reconstruction et, que l'interannualité est mieux représentée par la méthode A. De plus, ce signal illustre l'amplification de la variabilité régionale sur les 50 dernières années.

5.4.5 Résumé de l'article : « Reconstruction à deux dimensions du niveau de la mer passé (1950-2003) à partir de données marégraphiques et d'un modèle de circulation générale d'océan », publié dans le journal « Climate of the Past »

Introduction et résumé de l'article

Lors de cette étude, le niveau de la mer passé a été reconstruit en combinant les enregistrements de 99 marégraphes, couvrant la période 1950-2003 avec les sorties du modèle OPA/NEMO qui couvrent une fenêtre temporelle plus petite 1960-2003. La méthode de reconstruction utilisée dans ce travail est décrite dans le paragraphe 5.4.1 (méthode A).

L'originalité de la démarche réside dans l'utilisation de 44 ans de données spatiales (bien résolues spatialement) au moment du calcul des modes de variabilité du niveau de la mer et ainsi, d'ajuster cette variabilité par moindres carrés aux données des marégraphes dont la distribution spatiale est limitée. Le fait de considérer plus de 40 ans d'information permet de calculer les EOFs sur une période plus longue et ainsi capturer les structures spatiales dominantes de l'océan à une échelle multidécennale (en plus de la variabilité interannuelle). Ceci permet de s'affranchir d'une partie du problème de la non stationnarité de la variabilité régionale des vitesses du niveau de la mer. Avant, les méthodes de reconstruction du niveau de la mer antérieur combinaient l'information 2-D de l'altimétrie spatiale, avec 8 ans de données (*Church et al.* [2004]).

En outre, l'apport considérable des sorties de modèle de circulation générale des océans a été mis en exergue dans ce travail. En effet, nous capturons un signal basse fréquence qui est aussi observé dans le niveau de la mer thermostérique. En considérant plus de 20 ans de données 2-D pour calculer les EOFs, nous capturons ainsi ce signal multidécennal (qui ne pouvait être décelé avec les données altimétrique). Une forte signature de la variabilité interannuelle dont le signal ENSO est dominant (et peut être à moindre degré la signature de la PDO et NAO) est mise en évidence.

Clim. Past, 5, 217–227, 2009
www.clim-past.net/5/217/2009/

Climate of the Past

Two-dimensional reconstruction of past sea level (1950–2003) from tide gauge data and an Ocean General Circulation Model

W. Llovel[1], **A. Cazenave**[1], **P. Rogel**[2], **A. Lombard**[3], **and M. B. Nguyen**[1]

[1]LEGOS, OMP, 18 avenue Edouard Belin, 31401 Toulouse Cedex 09, France
[2]CERFACS/URA1875, 42, Avenue Gaspard Coriolis, 31057 Toulouse Cedex 01, France
[3]CNES, 18 avenue Edouard Belin, 31401 Toulouse Cedex 09, France

Received: 20 February 2009 – Published in Clim. Past Discuss.: 20 March 2009
Revised: 18 May 2009 – Accepted: 2 June 2009 – Published: 23 June 2009

Abstract. A two-dimensional reconstruction of past sea level is proposed at yearly interval over the period 1950–2003 using tide gauge records from 99 selected sites and 44-year long (1960–2003) $2^\circ \times 2^\circ$ sea level grids from the OPA/NEMO ocean general circulation model with data assimilation. We focus on the regional variability and do not attempt to compute the global mean trend. An Empirical Orthogonal Function decomposition of the reconstructed sea level grids over 1950–2003 displays leading modes that reflect two main components: (1) a long-term (multi-decadal), regionally variable signal and (2) an interannual, regionally variable signal dominated by the signature of El Nino-Southern Oscillation. Tests show that spatial trend patterns of the 54-year long reconstructed sea level significantly depend on the temporal length of the two-dimensional sea level signal used for the reconstruction (i.e., the length of the gridded OPA/NEMO sea level time series). On the other hand, interannual variability is well reconstructed, even when only ∼10-years of model grids are used. The robustness of the results is assessed, leaving out successively each of the 99 tide gauges used for the reconstruction and comparing observed and reconstructed time series at the non considered tide gauge site. The reconstruction performs well at most tide gauges, especially at interannual frequency.

1 Introduction

Sea level is an indicator of climate change because it integrates the response of many components of the Earth system: the ocean and its interaction with the atmosphere, land ice, terrestrial waters. Even the solid Earth has some impact on sea level. Since the beginning of the 1990s, sea level is precisely measured by satellite altimetry systems (i.e., Topex/Poseidon, Jason-1 and now Jason-2) with global coverage and short revisit time. The satellite observations have revealed that sea level does not rise uniformly: some regions rise faster than the global mean; in some other regions sea level rise slower (Bindoff et al., 2007). It has been shown that the main cause of regional variability in rates of sea level change is non uniform thermal expansion of the oceans (Cabanes et al., 2001), although other processes may also give rise to regional sea level trends (e.g., the solid Earth response to last deglaciation and gravitational effects of on-going land ice melt). Studies have established that trend patterns in thermal expansion fluctuate both in space and time in response to ENSO (El Nino-Southern Oscillation), NAO (North Atlantic Oscillation) and PDO (Pacific Decadal Oscillation) (Lombard et al., 2005). Thus, it is important to know past regional variability and see how it evolves with time. Climate model projections suggest significant regional variability with respect to the global sea level rise for the end of this century (Meehl et al., 2007). But account for the interannual/decadal variability associated with ENSO and other phenomena by coupled climate models is still imperfect insight into past regional variability over time spans longer than the altimetry record may be helpful to improve the climate models.

Unfortunately, for the last century, information about sea level is sparse and essentially based on tide gauge records along islands and continental coastlines. This data set cannot alone inform on open ocean regional variability. For that reason, a number of previous studies have attempted to reconstruct past decades sea level in two dimensions (2-D), combining sparse but long tide gauge records with global

Correspondence to: W. Llovel
(william.llovel@legos.obs-mip.fr)

Published by Copernicus Publications on behalf of the European Geosciences Union.

gridded (i.e., 2-D) sea level (or sea level proxies) time series of limited temporal coverage (Chambers et al., 2002; Church et al., 2004; Berge-Nguyen et al., 2008). The present study has a similar objective: it expands an earlier work by Bergé-Nguyen et al. (2008) (hereafter denoted as BN08) but makes use of different information for the 2-D fields used for the reconstruction. Previous studies used global sea level grids based on Topex/Poseidon satellite altimetry of limited (10 to 15 years) temporal coverage (e.g., Chambers et al., 2002; Church et al., 2004) or long but spatially inhomogeneous gridded time series of thermal expansion based on in situ hydrographic data (e.g., BN08). In this study, we use global dynamic heights grids from an Ocean General Circulation Model (OGCM), the OPA/NEMO model constrained by data assimilation (Madec et al., 1998). These model outputs, available over a 46-year time span (1960–2005), are combined with tide gauge records (that cover the period 1950–2003). We consider 44-year (1960–2003) time span for the OPA/NEMO outputs to be in line with the tide gauge records length (that ends in 2003). The advantage of using such a long 2-D data set is twofold: (1) the 44-year long coverage minimizes the probably non stationarity of altimetry-based spatial patterns (see BN08 for a discussion), (2) the combination of model-data resulting from an assimilation approach solves the problem of poor geographical and deep ocean coverage of in situ hydrographic data. The resulting sea level reconstruction is presented below for the 1950–2003 time span.

2 Method

Several studies have developed methods for reconstructing past time series of oceanographic (e.g., sea surface temperature, sea surface height) or atmospheric (e.g., surface wind speed, surface pressure) fields by combining 2-D grids of limited temporal coverage (in general available from remote sensing observations over the last 2 decades or less) with historical (several decade-long), sparse 1-D records (e.g., Smith et al., 1994, 1996; Kaplan et al., 1997, 1998, 2000; Church et al., 2004, 2006; Chambers et al., 2002; Beckers and Rixen, 2003; Alvera-Azcarate et al., 2005; Rayner et al., 2003). The general approach uses Empirical Orthogonal Empirical Functions (EOF) decomposition (e.g., Preisendorfer, 1988) of the 2-D time series to extract the dominant modes of spatial variability of the signal. These EOF spatial modes are then fitted to the 1-D records to provide reconstructed multidecade-long 2-D fields. Different computational variants of the method have been developed to estimate the reconstructed long-term 2-D fields depending on the use of a priori information and data errors (e.g., Kaplan et al., 2000; Rayner et al., 2003; Church et al., 2004) or not (Smith et al., 1996). When applied to long-term past reconstruction, an implicit assumption of the method is the temporal stationarity of the spatial patterns recovered from the EOF modes of the short-term 2-D fields. The spatial covariance obtained from the 2-D fields must indeed be able to describe the spatial covariance over the entire period of the reconstruction (e.g., Smith et al., 1996). If the dominant modes of spatial variability have characteristic time scales longer than the time interval covered by the 2-D fields, EOF spatial modes may incompletely capture the relevant long-term signal. In particular the multi-decadal components of the reconstructed signal may be in error.

We briefly summarize below the methodology. Let us call *Fo(x,y,t)* and *Go(x,y,t)* observed global gridded short-term fields and sparse, incomplete long-term sea level data respectively, with x, y and t being Cartesian coordinates and time. The time span T_f covered by the *Fo(x,y,t)* fields is basically shorter than that -called Tg- of the reconstructed fields. Here, *Fo(x,y,t)* corresponds to gridded sea level from the OPA/NEMO models over 1960–2003, while the *Go(x,y,t)* -spatially incomplete- fields correspond to tide gauge records over 1950–2003. The *Fo(x,y,t)* function is expressed as a sum of combined $X_n(x, y)$ spatial modes and $e_n(t)$ principal components using an EOF decomposition (with zero global mean trend). The objective of the reconstruction is to compute 2-D *Go(x,y,t)* fields with global spatial coverage – hereafter denoted as $G_R(x,y,t)$ – over the Tg time span (here 1950–2003). The 2-D reconstructed sea level fields are written as $G_R(x,y,t)=\sum[X_n(x, y)\ Y_n(t)]$ where $Y_n(t)$ are new principal components computed at each time step t and mode n, through a least-squares fit that minimizes the quantity ε expressed by $\varepsilon=[Go(x,y,t)-\sum[X_n(x, y)Y_n(t)]]^2$. For more details, see BN08.

3 Tide gauge data

The tide gauge data used in this study are extracted from the Permanent Service for Mean Sea Level (PSMSL) database (Woodworth and Player, 2003). We use Revised Local Reference (RLR) tide gauge records (annual averages). Detailed descriptions of these time series are available at www.pol.ac.uk/psmsl. From the whole set of records available, we consider stations that have almost complete temporal coverage over 1950–2003. A very careful selection of sites has been realized. Compared to the 118 sites considered in BN08, here we use only 99 sites, deleting from the 118 set a number of tide gauge records with suspect behaviors (e.g., offsets). Search of information on internet about the deleted sites indicates that in almost all cases, tectonic (e.g., co seismic offset or post seismic relaxation of the crust), volcanic or ground subsidence of anthropogenic origin, could be identified as causes of the spurious bias or trends. The tide gauge records are corrected for glacial isostatic adjustment (GIA) using the ICE-5G, VM-2 model (Peltier, 2004). We also correct the tide gauge time series for the inverted barometer response of sea level to atmospheric loading using surface pressure fields from the National Centers for Environmental Project (NCEP) (Kalnay et al., 1996). One problem with tide

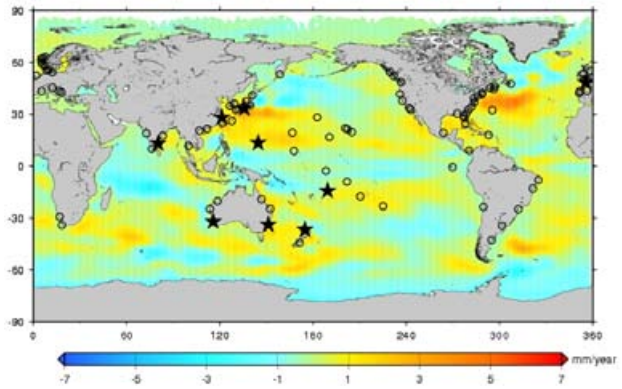

Fig. 1. Location map of the 99 tide gauges (open circles) used in this study. Stars correspond to the comparison sites with records shown in Fig. 10. The background map shows the OPA/NEMO spatial sea level trends computed over 1960–2003 (in mm/yr).

gauge records is that measurements are made in local datum that varies from one site to another. By working with the derivatives, this problem can be overcome (e.g., Holgate and Woodworth, 2004; Holgate, 2007). Here we choose a different approach (e.g., Kuo et al., 2008) consisting of subtracting from each sea level record a mean value computed over the 1950–2003 time span (note that the 99 tide gauge records are almost complete; when small gaps, $<$3 years, are observed, we linearly interpolate missing data). Figure 1 shows the distribution of the tide gauge sites used in this study (superimposed on a map of OPA/NEMO dynamic height spatial trends).

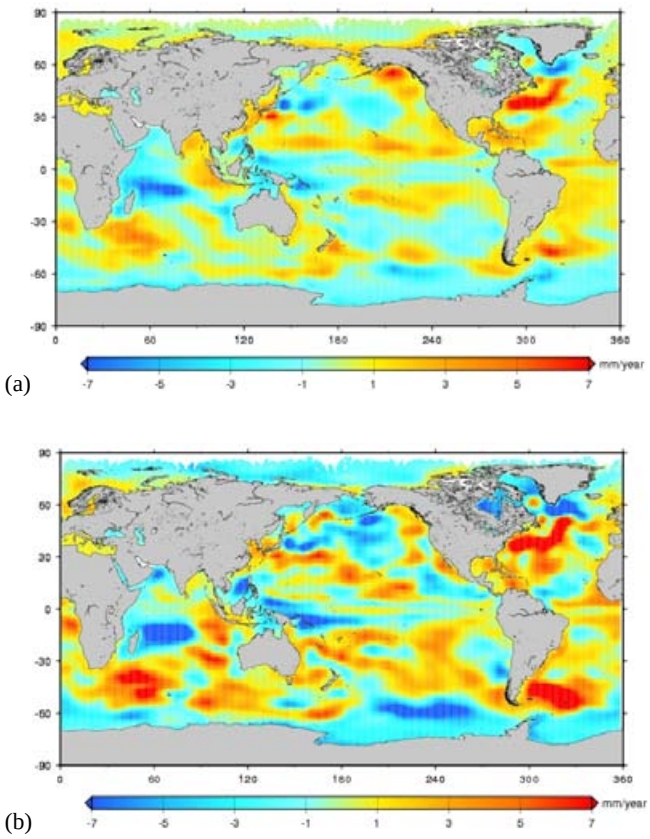

Fig. 2. (a) Spatial trend map over 1950–2003 of reconstructed sea level (with 10 modes for the reconstruction); nominal case (case 1). **(b)** Same as (a) but with 20 modes for the reconstruction. Unit: mm/yr.

4 OPA/NEMO Ocean General Circulation Model outputs

The ocean reanalysis used in this study has been produced with a 3-dimensional variational assimilation system (Daget and Weaver, 2008) applied to the OPA/NEMO OGCM (Madec et al., 1998). The model resolution, 2° on average, with a latitudinal refinement in the tropics, is coarse but appropriate for the multidecadal period of interest here. The model is forced by the standard reanalyse ERA40 heat fluxes (Uppala et al., 2005) and corrected water fluxes (Troccoli and Kalberg, 2004). From September 2002 onwards, when ERA40 terminates, ECMWF (European Centre for Meteorological Forecast) operational surface fluxes are used as forcing. The assimilation system minimizes the discrepancy between model and observations by constraining the model to remain close to the a priori model state. In this iterative procedure, the distance to the observations (respectively to the model state) is taken as the norm defined by the observation error (respectively the model state error). Whilst the observational error is straightforward to characterise, a lot of work has been done to properly define the model state error (Ricci et al., 2005; Weaver et al., 2006). This ensures the propagation of information to the model variables not directly observed (e.g., sea level and velocity) and hence the realism of the analyses. Quality controlled temperature and salinity profiles from the EN3 oceanographic data base (Ingelby and Huddleston, 2007) are assimilated every 10 days from January 1960 to December 2006. Note that these profiles were not corrected for the recently discovered instrumentation problems. The model outputs are on a monthly basis but only annual averages are considered hereafter.

As described in Roullet and Madec (2000), the model is formulated with a prognostic free surface, constant volume and salt preserving scheme, assuming that the mean sea level does not vary. Hence, both forcing and data assimilation have been designed to ensure that no drift in the mean sea level occurs. Water flux balance between precipitation, evaporation and runoff is set to zero in the free surface equation, and assimilation increments (i.e., the model corrections applied every 10 days to the model using temperature and salinity observations) are built under the constraint that the sea level increment is zero on global average. In addition, the model is

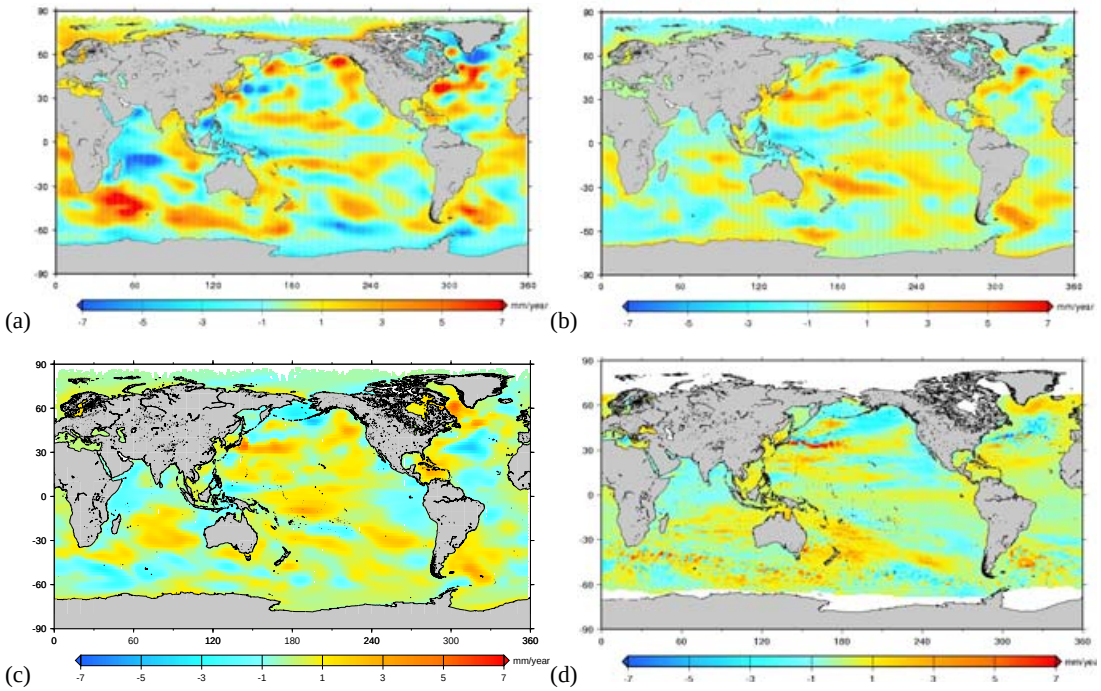

Fig. 3. Spatial trend map over 1950–2003 of reconstructed sea level. **(a)** spatial EOFs from OPA/NEMO over 1973–2003 (case 2); **(b)** spatial EOFs from OPA/NEMO over 1983–2003 (case 3); **(c)** spatial EOFs from OPA/NEMO over 1993–2003 (case 4); **(d)** spatial EOFs from Topex/Poseidon altimetry (case 5). Unit: mm/yr.

relaxed towards a climatology (Levitus et al., 1994) poleward of 60° and in the semi-enclosed seas, so that interannual variations in those regions are almost suppressed. On the other hand, no constraint is applied over open ocean areas.

In Fig. 1 are displayed sea level trends from the OPA/NEMO model with data assimilation over 1960–2003. For the reasons explained above, the map has zero global mean (uniform) trend. Important regional variability is observed, especially in the western parts of the basins. The strongest spatial patterns are located close to the western boundary currents (e.g., Gulf Stream in the Northwestern Atlantic, Kuroshio in the Northwestern Pacific; Malvinas Current in the Southwestern Atlantic).

Here we focus on the regional variation and do not attempt to reconstruct the global mean trend. However, we must pay attention on a possible contamination of any global mean trend to the reconstructed sea level. We first checked that the model EOFs have zero global mean trend (this is expected as the model does not contain any uniform trend signal). We further checked that EOFs of the reconstruction do not contain either significant non-zero global average.

5 Sea level reconstruction

5.1 Reconstructed spatial trend patterns over 1950–2003

We reconstructed 2-D sea level grids at yearly interval over 1950–2003 combining spatial EOFs of the OPA/NEMO grids over 1960–2003 (44 years of gridded data) with 99 tide gauge time series covering the 1950–2003 time span. Most of the variance of the reconstructed sea level is included in the first 10–20 modes. Highest-order modes exhibit essentially noise. In the following, we consider as nominal case (called case 1), the first 10 modes when reconstructing sea level (with 75% of the total signal variance). Corresponding reconstructed spatial trend map over 1950–2003 is presented in Fig. 2a. We note that trend amplitudes are everywhere higher than in the model trend map (Fig. 1) but extrema are located in the same regions (e.g., Gulf Stream, Kuroshio; Malvinas Current, etc.). For comparison we also show the spatial trend map with the first 20 modes used for the reconstruction (Fig. 2b). The 20 modes case contains more energy but is also noisier (as discussed in BN08).

In order to assess the benefit of using multi-decadal gridded OPA/NEMO time series for reconstructing past sea level, we performed tests with shorter model time series. Four cases are considered: 31 years of OPA/NEMO grids (1973–2003) -case 2-, 21 years of OPA/NEMO grids (1983–2003)

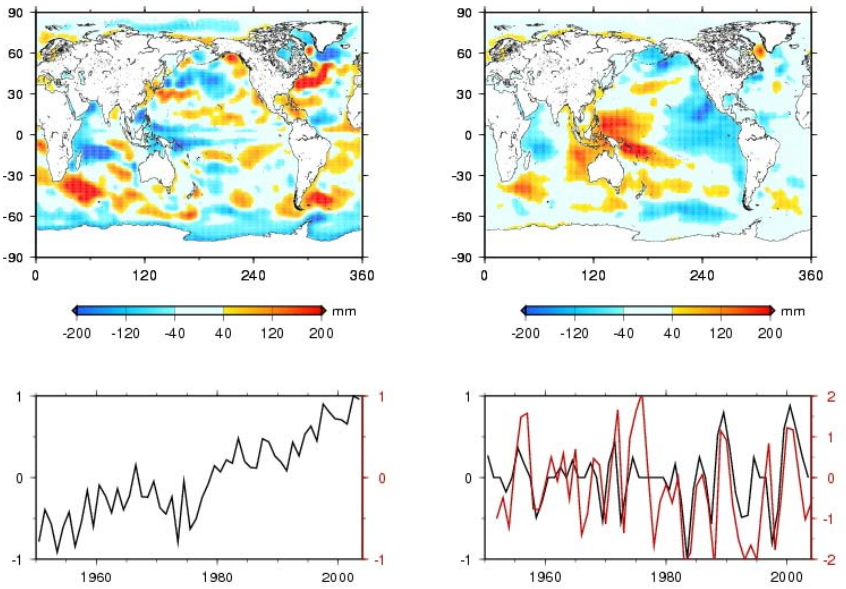

Fig. 4a. EOF decomposition over 1950-2003 for nominal case (case 1): left: mode 1; right mode 2 (with SOI index is superimposed on the temporal curve).

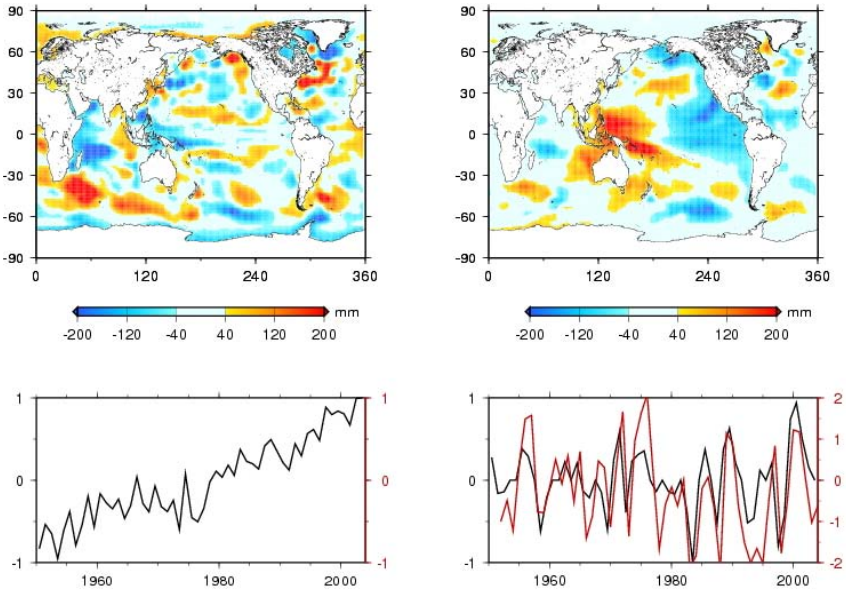

Fig. 4b. Same as **(a)** but for case 2.

-case 3-, and 11 years of OPA/NEMO grids (1993–2003) -case 4. Case 4 can be compared with studies that use decade-long Topex/Poseidon altimetry grids for sea level reconstruction (e.g., Chambers et al., 2002; Church et al., 2004). Corresponding reconstructed spatial trend maps are presented in Fig. 3a, b, c (using for each case, the number of modes that correspond to 75% of the total variance). Significant regional differences are noticed between the first two cases (44 years and 31 years of OPA/NEMO grids, respectively) and cases 3 and 4 (21 years and 11 years of OPA/NEMO grids, respectively) , in particular in the North Atlantic, Indian and Austral oceans, and Northeast Pacific. Spatial trend patterns for cases 1 and 2 give are quite in agreement. A similar observation can be done for cases 3 and 4. We thus observe a transition in reconstructed trends when the temporal coverage of OPA/NEMO grids increases

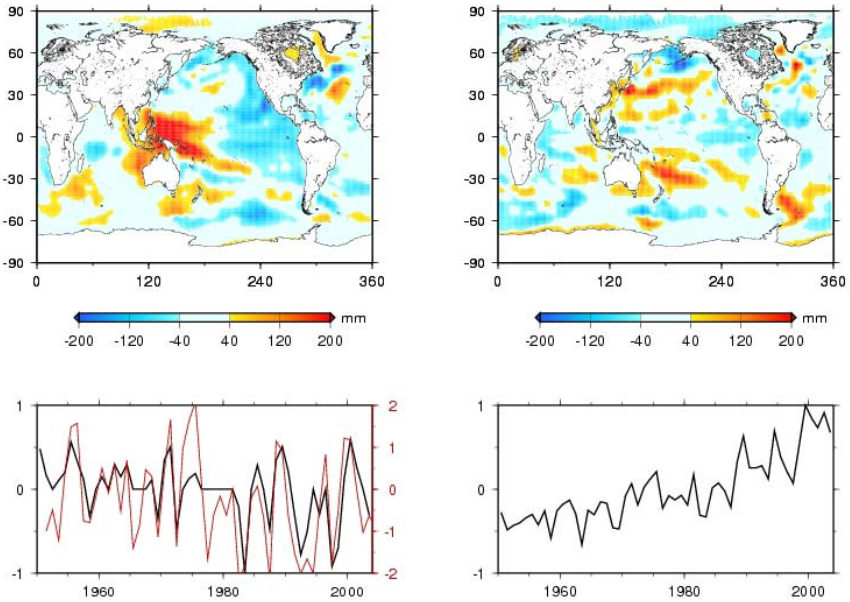

Fig. 4c. Same as **(a)** but for case 3.

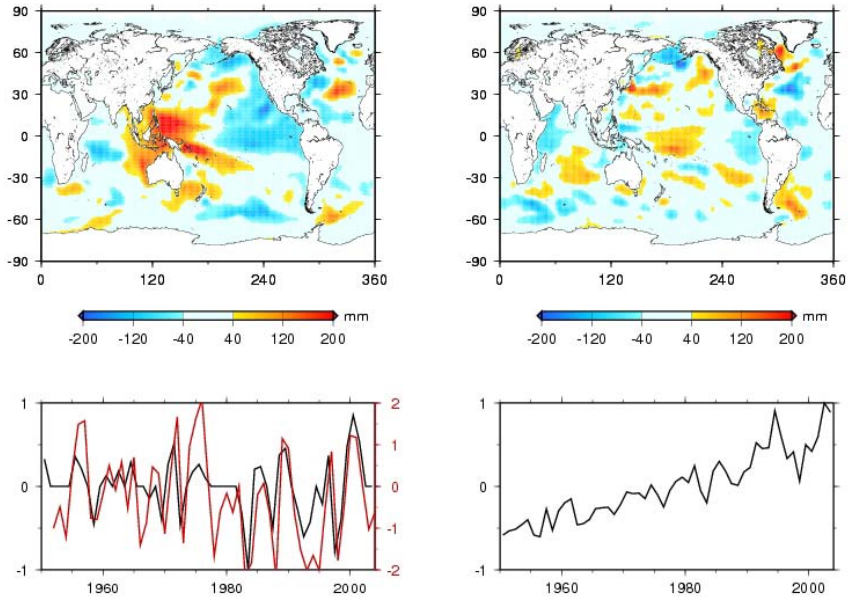

Fig. 4d. Same as **(a)** but for case 4.

from ∼20 years to ∼30 years. As discussed below, the low-frequency sea level signal may not be well captured in cases that use short spatial grids for the reconstruction (cases 3 to 5). In the latter cases, patterns representing interannual variability dominate the reconstructed spatial trends.

To compare with case 4, we also show in Fig.3d reconstructed sea level trends (over 1950–2003) using 11 years (1993–2003) of Topex/Poseidon sea level grids (case 5). The latter case is very similar to Church et al. (2004)'s study. We computed the correlation between case 5 and Church et al. (2004) reconstruction without the uniform global mean trend. The correlation coefficient amounts to ∼60%. Although case 5 contains shorter wavelength signal than case 4, spatial trend patterns show similar large scale features as case 4.

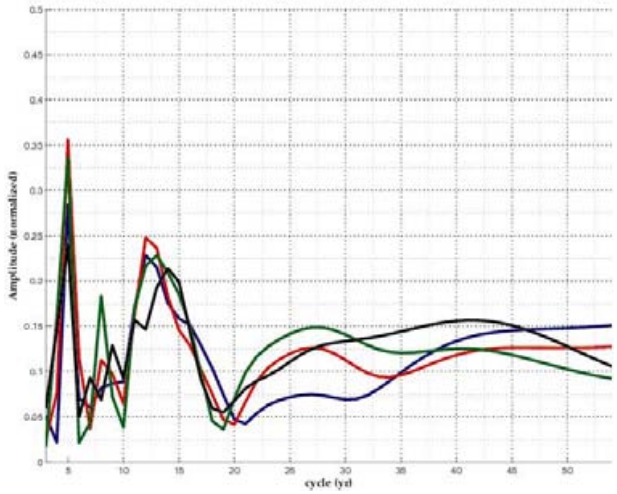

Fig. 5. Energy spectrum of the interannual variability for cases 1 (blue), 4 (red) and 5 (green) and SOI index (black).

We performed EOF decompositions of the reconstructed sea level grids over 1950–2003 for cases 1 to 4. Figure 4 a, b, c, d shows the two leading EOF modes each case. Mode 1 temporal curve (principal component) of nominal case is dominated by a positive slope. Associated mode 1 spatial map closely resembles case 1 reconstructed trend map (Fig. 2), with strong signal in the Austral Ocean (especially southeast of Africa). This suggests that the reconstructed trend map for the nominal case mostly reflects a long-term (multi-decadal), regionally variable signal. Mode 2 of case 1 (Fig. 4a right panel) is dominated by the interannual variability, and displays clear signature of ENSO in the tropical Pacific: the Southern Oscillation Index (SOI) -a proxy of ENSO- is significantly correlated (61%) to the temporal curve on which is it superimposed. It is worth mentioning that the spatial map of mode 2 (case 1) is very similar to the satellite altimetry-based sea level trend map over 1993–2003 (see below). Hence, whilst mode 1 reflects long-term, multidecadal signal, mode 2 mostly reflects ENSO-type interannual variability.

The two leading modes of case 2 (Fig. 4b) closely resemble those of case 1. The first EOF mode of cases 3 and 4 reflects interannual variability (as mode 2 of cases 1 and 2). This is illustrated in Fig. 5 which shows energy spectra of the interannual signal for cases 1, 4 and 5 (i.e., temporal curves spectra of corresponding EOF modes). SOI spectrum is superimposed. The agreement between the four curves is striking. Peaks in the 3–5 yr and 10–15 yr wavebands dominate. They mainly reflect ENSO frequency and associated decadal modulation. On the other hand, looking at the long-term signal (e.g., comparing modes 1 of case 1 and 2 with mode 2 of cases 3 and 4), we note significant difference in the spatial maps, suggesting that multidecadal fluctuations are only partly recovered when using short-term gridded time series for the reconstruction (e.g., cases 3 and 4).

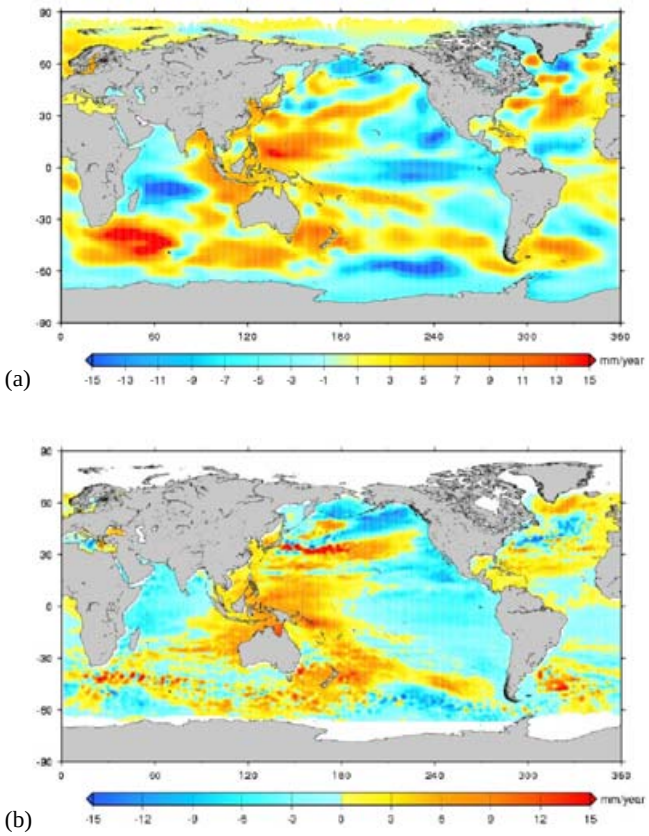

Fig. 6. Spatial sea level trend map over 1993–2003. **(a)** reconstructed sea level for nominal case. **(b)** observed sea level trends from satellite altimetry (uniform trend removed). Unit: mm/yr.

5.2 Robustness of the reconstruction

5.2.1 Sea level reconstruction over the altimetry (1993–2003) period using the OPA/NEMO EOFs

A way to check the validity of the reconstruction is to look at the reconstructed sea level trends over the altimetry period (here 1993–2003) for which we trust the spatial trend patterns. Figure 6a shows the reconstructed spatial trend map over 1993–2003 based on 44-years of OPA/NEMO grids. Comparing with Fig. 6b which shows observed satellite altimetry spatial trend map over 1993–2003 (uniform trend removed) indicate very good agreement, although the reconstructed map is smoother (as expected considering the low resolution of the OPA/NEMO model).

5.2.2 Cross-validation of reconstructed series and tide gauge records

Another way to check the robustness of the reconstruction consists of reconstructing sea level, leaving out successively each one of the 99 tide gauge records (thus each of these 99 reconstructions now uses a set of 98 tide gauges, with

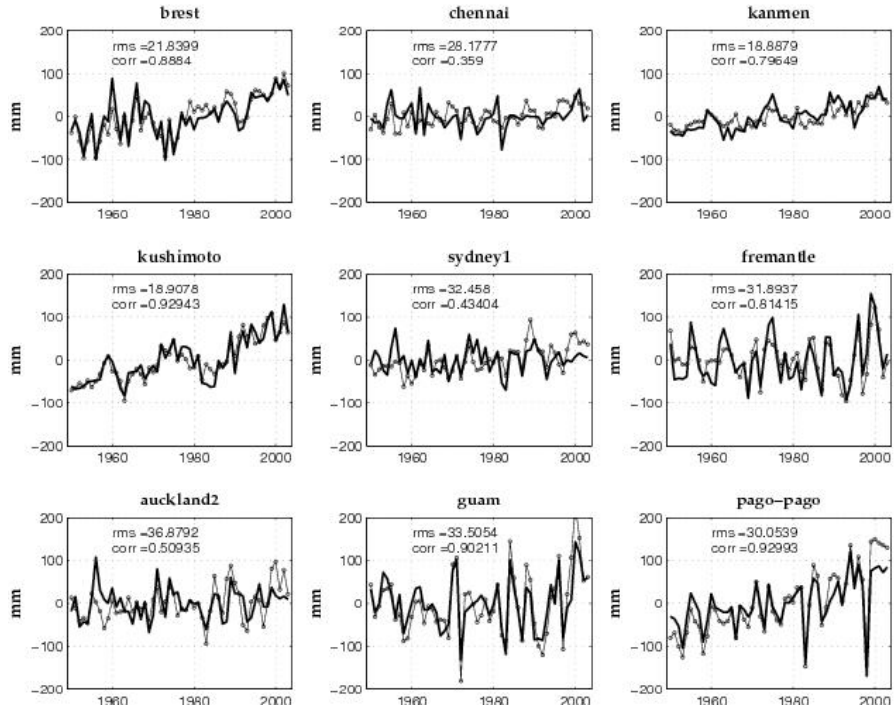

Fig. 7a. Subset of 18 tide gauges not used in the reconstruction; observed record (solid curve); reconstructed sea level curve (thin dotted curve).

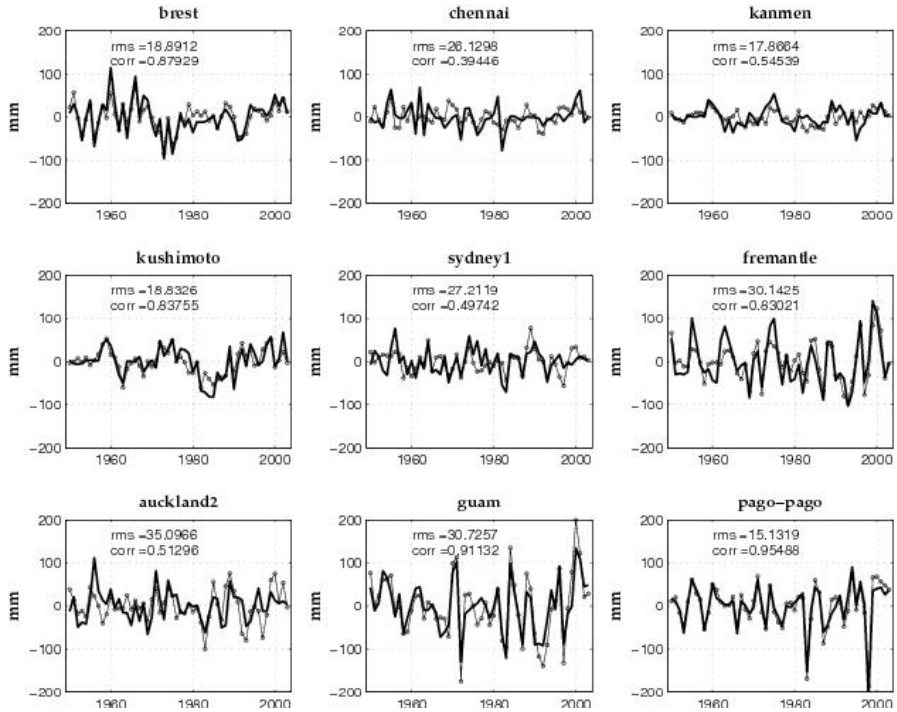

Fig. 7b. Same as **(a)** but with mean trend removed.

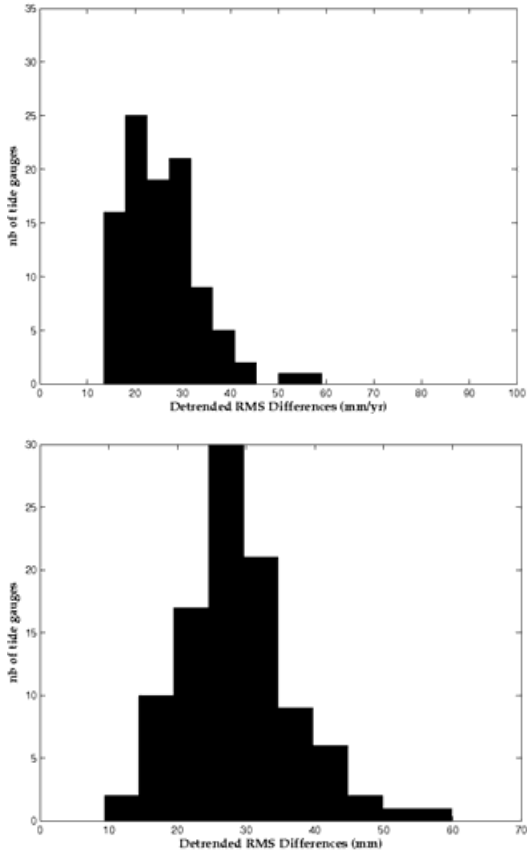

Fig. 8. Histogram of detrended sea level rms differences at the 99 tide gauges (reconstructed minus observed); Upper: case 1; Lower case 5 (reconstruction with Topex/Poseidon). Unit: mm.

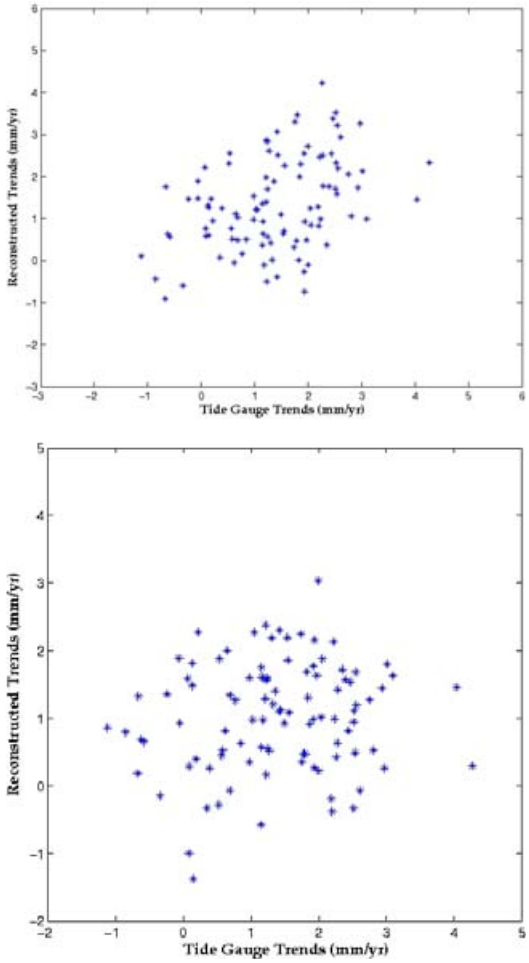

Fig. 9. Reconstructed sea level trends at the 99 tide gauges as a function of observed trends. Upper: case 1; Lower: case 5 (reconstruction with Topex/Poseidon). Unit: mm/yr.

different distribution from one case to another). For each deleted tide gauge, we compare the reconstructed sea level time series at the tide gauge site with the PSMSL data (reconstructed sea level is averaged within 2° around the tide gauge site). For this test we consider two cases: case 1 (reconstruction with 44 years of gridded OPA/NEMO grids) and case 5 (reconstruction with 11 years of Topex/Poseidon gridded data). Figure 7a shows a subset of 18 comparisons (corresponding site locations are enhanced by stars in Fig. 1). Figure 7b is similar to Fig. 7a except for the trend which has been removed. We note that in general interannual to decadal variability is well reproduced (Fig. 7b). The average correlation at the 99 sites amounts to ∼60%. The trends also agree well in most cases, although not everywhere. Sites where trends disagree concern mostly northeast Atlantic areas (e.g., North Shields, Lowestoft, Santander, La Coruna, and Vigo). We suspect that this is due to local underestimated variability in the OPA/NEMO reanalysis, especially in the first 20 years of the period. Similar test performed for case 5 (not shown) shows very similar results for the detrended time series.

To see the above results in another way, we have computed the root mean squared (rms) differences between reconstructed and observed (detrended) sea level time series as well as between trends. Corresponding histograms for the cases 1 and 5 are shown in Fig. 8. Rms (detrended) sea level differences are included in the 15–60 mm but histogram for case 1 is more spread than for case 5. Figure 9 shows plots of reconstructed sea level trends at the 99 tide gauges as a function of observed trends for the two cases (cases 1 and 5). Here we see that case 1 gives better results than case 5, with higher correlation. These comparisons indicate that the reconstruction performs well at the interannual time scale (as previously found by Chambers et al., 2002 and Church et al., 2004), with better results for case 5 than case 1. On the other hand, case 1 gives much better results for the trends (hence at multidecadal time scale) than case 5.

6 Conclusions

We have performed a new 2-D sea level reconstruction over 1950–2003. The main change compared to previous published results (e.g., Chambers et al., 2002; Church et al., 2004; Berge-Nguyen et al., 2008) is the use of 44-year long gridded sea level data set from the OPA/NEMO OGCM with assimilation. This allows us to compute spatial EOFs over a $>$40 yr time span, long enough to capture the multidecadal variability in regional sea level (in addition to the interannual variability). Hopefully, this may prevent from problems due to the use of short-term altimetry grids. Another advantage is the good spatial sampling of the OPA/NEMO outputs compared to in situ-based thermal expansion data (as in BN08). The main conclusion of this study is that using spatial EOFs computed over a short time span (e.g., $\sim$10–20 years) leads to 2-D reconstructed trend patterns significantly different than when 40 years of EOFs are used. The latter case, not only captures the interannual variability (related to ENSO and possibly NAO and PDO) but also the multidecadal variability. Even if they have local deficiencies, such 2-D reconstructed sea level time series based on low resolution ocean reanalysis are able to bring physically consistent large-scale, low-frequency patterns associated with major climatic modes of variability.

As a final remark, we think that the use of OGCM outputs is a step towards better reconstruction of long-term sea level time series (at least waiting for global multidecadal altimetry records). Future improvements is expected by using new generation of eddy-permitting OGCM outputs with higher spatial resolution (e.g., $0.25°\times0.25°$) in which some local misbehaviors can be corrected. This would provide finer description of the spatial trend patterns. Progress in this direction is already underway.

Acknowledgements. We thank Don Chambers, C. K. Shum and an anonymous reviewer for very useful comments.

Nicolas Daget and A. T. Weaver are thanked for their provision of the ocean reanalysis data. These data were produced for the EU FP6 Integrated Project ENSEMBLES (Contract number 505539), whose support is gratefully acknowledged. William Llovel PhD grant is supported by CNRS and Region Midi-Pyrenees.

Edited by: V. Masson-Delmotte

The publication of this article is financed by CNRS-INSU.Ł

References

Alvera-Azcarate, A., Barth, A., Rixen, M., and Beckers, J. M.: Reconstruction of incomplete oceanographic data sets using empirical orthogonal functions: applications to the Adriatic sea surface temperature, Ocean Model, 9(4), 325–346, doi:10.1016/j.ocemod.2004.08.001, 2005.

Berge-Nguyen, M., Cazenave, A., Lombard, A., Llovel, W., Viarre, J., and Cretaux, J. F.: Reconstruction of past decades sea level using thermosteric sea level, tide gauge, satellite altimetry and ocean reanalysis data, Global. Planet. Change, 62, 1–13, 2008.

Bindoff, N., Willebrand, J., Artale, V. , Cazenave, A., Gregory, J., Gulev, S., Hanawa, K., Le Quéré, C., Levitus, S., Nojiri, Y., Shum, C. K., Talley, L., and Unnikrishnan, A.: Observations: oceanic climate and sea level, in: Climate change 2007: The physical Science Basis. Contribution of Working Group I to the Fourth Assessment report of the Intergouvernmental Panel on Climate Change, edited by: Solomon S., Qin, D., Manning, M., Chen, Z., Marquis, M., Averyt, K. B., Tignor, M., and Miller, H. L., Cambridge University Press, Cambridge, UK, and New York, USA, 385–428, 2007.

Cabanes, C., Cazenave, A., and Le Provost, C.: Sea level rise during past 40 years determined from satellite and in situ observations, Science, 294, 840–842, 2001.

Cazenave A. and Nerem R. S.: Present-day sea level change: observations and causes, Rev. Geophys., 42, RG3001, doi:8755-1209/04/2003RG000139, 2004.

Chambers, D. P., Mehlha, C. A., Urban, T. J., and Nerem, R. S.: Analysis of interannual and low-frequency variability in global mean sea level from altimetry and tide gauges, Phys. Chem. Earth, 27, 1407–1411, 2002.

Church, J. A., White, N. J., Coleman, R., Lambeck, K., and Mitrovica, J. X.: Estimates of the regional distribution of sea-level rise over the 1950 to 2000 period, J. Climate, 17(13), 2609–2625, 2004.

Church, J. A., White, N. J., and Hunter, J. R.: Sea-level rise at tropical Pacific and Indian Ocean islands, Global Planet. Change, 53(3), 155–168, 2006.

Daget, N., Weaver, A. T., and Balmaseda, M. A.: Ensemble estimation of background-error variances in a three-dimensional variational data assimilation system for the global ocean, Q. J. Roy. Meteorol. Soc., 135, 1071–1094, 2009.

Holgate, S. J. and Woodworth, P. L.: Evidence for enhenced coastal sea level rise during the 1990s, Geophys. Res. Lett., 31, L07305, doi:10.1029/2004GL019626, 2004.

Holgate, S. J.: On the decadal rates of sea level change during the twentieth century, Geophys. Res. Lett., 31, L01602, doi:10.1029/2006GL028492, 2007.

Ingleby, B. and Huddleston, M.: Quality control of ocean temperature and salinity profiles – historical and real-time data, J. Mar. Sys., 65, 148–175, 2007.

Kalnay, E, Kanamitsu, M., Kistler, R., Collins, W., Deaven, D., Gandin, L., Iredell, M., Saha, S., White, G., Woollen, J., Zhu, Y., Leetmaa, A., Reynolds, B., Chelliah, M., Ebisuzaki, W., Higgins, W., Janowiak, J., Mo, K. C., Ropelewski, C., Wang, J., Roy, J., and Joseph, D.: The NCEP/NCAR 40-year reanalysis project, B. Am. Meteorol. Soc., 77, 437–471, 1996.

Kaplan, A., Cane, M. A., Kushnir, Y., Clement, A. C., Blumenthal, M. B., and Rajagopalan, B.: Analyses of global sea surface temperature 1856–1991, J. Geophys. Res., 103, 18567–18589, 1998.

Kuo, C., Shum, C. K., Braun, A., Cheng, K., and Yi, Y.: Vertical motion determined by combining satellite altimetry and tide gauge records, Terr. Atmos. Ocean. Sci., 19, 21 pp., U201335, doi:10.3319/TAO.2008.19.1-2.21.(SA), 2008.

Levitus, S., Burgett, R., and Boyer, T. P.: World Ocean Atlas (National Oceanic and Atmospheric Administration, Silver Spring, MD), Vols. 3 and 4, 1994.

Lombard, A., Cazenave, A., Le Traon, P. Y., and Ishii, M.: Contribution of thermal expansion to present-day sea level rise revisited, Global Planet. Change, 47, 1–16, 2005.

Madec, G., Delecluse, P., Imbard, M., and Levy, C.: OPA 8.1 Ocean General Circulation Model reference manual. Notes du pôle de modélisation, Institut Pierre Simon Laplace (IPSL), France, 1998.

Meehl, G. A., Stocker, T. F., Collins, W. D., Friedlingstein, P., Gaye, A. T., Gregory, J. M., Kitoh, A., Knutti, R., Murphy, J. M., Noda, A., Raper, S. C. B., Watterson, I. G., Weaver, A. J., and Zhao, Z.-C.: Global Climate Projections, in: Climate Change 2007: The Physical Science Basis. Contribution of Working Group I to the Fourth Assessment Report of the Intergovernmental Panel on Climate Change, edited by: Solomon, S., Qin, D., Manning, M., Chen, Z., Marquis, M., Averyt, K. B., Tignor, M., and Miller, H. L., Cambridge University Press, Cambridge, United Kingdom and New York, NY, USA, 2007.

Peltier, W. R.: Global Glacial Isostasy and the Surface of the Ice-Age Earth: The ICE-5G (VM2) Model and GRACE, Annu. Rev. Earth Pl. Sc., 32, 111–149, 2004.

Preisendorfer, R. W.: Principal component Analysis in Meteorology and Oceanography, Developments in Atmospheric Science, vol. 17, Elsevier, 425 pp., 1988.

Rayner, N. A., Parker, D. E., Horton, E. B., Foll, C. K., Alexer, L. V., Powell, D. P., Kent, E. C., and Kaplan, A.: Global analyses of SST, sea ice, and night marine air temperature since the late nineteenth century, J. Geophys. Res., 108, 4407, doi:10.1029/2002JD002670, 2003.

Ricci, S., Weaver, A. T., Vialard, J., and Rogel, P.: Incorporating state-dependent temperature-salinity constraints in the background-error covariance of variational ocean data assimilation, Mon. Weather Rev., 133, 317–338, 2005.

Roullet, G. and Madec, G.: Salt conservation, free surface and varying volume : a new formulation for Ocean GCMs, J. Geophys. Res., 105, 23927–23942, 2000.

Smith, T. M., Reynolds, R. W., and Ropelewski, C. F.: Optimal averaging of seasonal sea surface temperatures and associated confidence intervals (1860–1989), J. Climate, 7, 949–964, 1994.

Smith, T. M., Reynolds, R. W., Livezey, R. E., and Stockes, D.: Reconstruction of historical sea surface temperature using Empirical Orthogonal Functions, J. Climate, 9, 1403–1420, 1996.

Toumazou, V. and Cretaux, J. F.: Using a Lanczos eigensolver in the computation of Empirical Orthogonal Functions, Mon. Weather Rev., 129, 1243–1250, 2001.

Troccoli, A. and Kallberg, P.: Precipitation correction in the ERA-40 reanalysis, ERA-40 Project Report Series 13, ECMWF, 2004.

Uppala, S. M., da Costa Bechtold, V., Fiorino, M., Gibson, J. K., Haseler, J., Hernandez, A., Kelly, G. A., Li, X., Onogi, K., Saarinen, S., Sokka, N., Allan, R. P., Andersson, E., Arpe, K., Balmaseda, M. A., Beljaars, A. C. M., van de Berg, L., Bidlot, J., Bormann, N., Caires, S., Chevallier, F., Dethof, A., Dragosavac, M., Fisher, L., Fuentes, M., Hagemann, S., Hólm, E., Hoskins, B. J., Isaksen, L., Janssen, P. A. E. M., Jenne, R., McNally, A. P., Mahfouf, J.-F., Morcrette, J. J., Rayner, N. A., Saunders, R. W., Simon, P., Sterl, A., Trenberth, K. E., Untch, A., Vasiljevic, D., Viterbo, P., and Woollen, J.: The ERA-40 re-analysis, Q. J. Roy. Meteorol. Soc., 131, 2961–30128, 2005.

Weaver, A. T., Deltel, C., Machu, E., Ricci, S., and Daget, N.: A multivariate balance operator for variational ocean data assimilation, Q. J. Roy. Meteorol. Soc., 131, 3605–3625, 2005.

Woodworth, P. L. and Player, R.: The permanent service for mean sea level: an update to the 21st century, J. Coastal. Res., 19, 287–295, 2003.

5.4.6 Les modèles climatiques couplés : comparaisons du niveau de la mer reconstruit sur les 5 dernières décennies avec le modèle CNRM-CM3

Dans le chapitre 2 nous avons vu que les projections de la hausse du niveau moyen global de la mer basées sur les modèles climatiques couplés diffèrent fortement selon les modèles considérés. A présent un focus est réalisé sur la cartographie régionale du niveau de la mer pour les 5 dernières décennies à l'aide du modèle climatique couplé CNRM-CM3 (*Salas-Melia et al.* [2005]).

Description du modèle

Le modèle climatique couplé CNRM-CM3 (*Salas-Melia et al.* [2005]) est la troisième version du modèle initialement développé au CERFACS (Toulouse, France) et régulièrement mis à jour au CNRM (Météo France, Toulouse). Ce modèle est composé d'un modèle de circulation générale atmosphérique (AGCM) ARPEGE-Climat 3 (CNRM, *Deque et al.* [1994]; *Deque and Piedelievre* [1995]; *Deque et al.* [1998]; *Gibelin and Deque* [2003]) et d'un modèle de circulation océanique (OGCM) OPA8.1 (LOCEAN, CNRM-IPSL, Paris). Ce modèle couplé prend en compte une paramétrisation homogène et hétérogène de chimie atmosphérique. Il comprend aussi un modèle de glace de mer (GELATO2, *Salas-Melia* [2002]) et un schéma de surface hydrologique TRIP (*Oki and Sud* [1998]). La résolution spatiale est de l'ordre de 2° en longitude avec un raffinement de la maille de l'ordre de 0.5° à l'équateur. L'interaction entre les modèles d'océan et d'atmosphère s'opère à l'aide du coupleur OASIS2.2 (CERFACS, *Terray et al.* [1998]). Lors des simulations numériques, seules les concentrations de gaz à effet de serre et les aérosols sont prises en compte (concentrations mesurées) lors du calcul des sorties du modèle qui ont été utilisées lors du dernier rapport de l'IPCC-AR4 (2007). Le flux solaire est constant sur toute la période de calcul et vaut 1370 W/m^2. Les éruptions volcaniques ne sont pas prises en compte.

Résultats

La figure 5.14 établit la cartographie des tendances du niveau de la mer thermostérique sur la période 1950-2000 à partir des données du modèle couplé CNRM-CM3. La tendance moyenne est retirée pour mettre en valeur la variabilité régionale. Cette cartographie des tendances se compare directement avec la cartographie des tendances du niveau de la mer reconstruit (figures 5.8 et 5.9). La carte des tendances du niveau de la mer thermostérique se

compare bien avec la cartographie des tendances du niveau de la mer reconstruit de la figure 5.8 (*Llovel et al.* [2009]) notamment dans le bassins Pacifique nord et dans l'Atlantique nord. Partout ailleurs, des différences importantes existent. De plus, la carte du modèle couplé concorde avec le niveau de la mer thermostérique déduit des données *in situ* (*Levitus et al.* [2009]). Les deux mêmes régions coïncident assez bien avec en plus un meilleur accord avec les tendances dans le bassin de l'océan Indien. Cependant, les fortes anomalies positives de l'océan Austral, issues du modèle climatique couplé, paraissent suspectes.

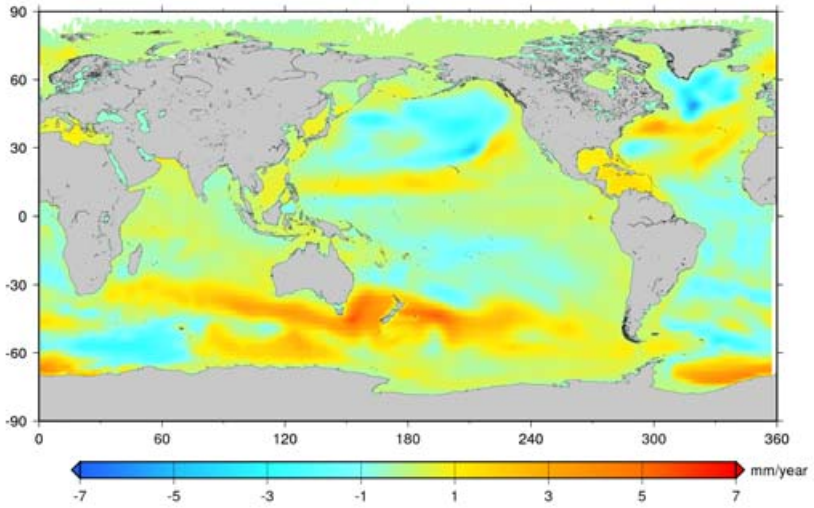

FIG. 5.14 – Cartographie des tendances du niveau de la mer thermostérique (tendance uniforme retirée) entre 1950 et 2000 basée sur les données du modèle couplé CNRM-CM3 (*Salas-Melia et al.* [2005]) de la simulation du XX^{ème} siècle.

Les principaux modes de variabilité des sorties du modèle couplé : analyse en EOF

La figure 5.15 montre les 2 premiers modes de variabilité du niveau de la mer thermostérique calculé avec le modèle climatique couplé CNRM-CM3. La tendance a été retirée avant cette analyse. Le premier mode de variabilité représente le signal ENSO. On s'aperçoit rapidement que ce mode de variabilité est mal simulé dans ce modèle couplé. En effet, le dipôle du bassin Pacifique tropical n'est pas visible dans le mode spatial et, la fréquence des

événements ENSO est de l'ordre de 2 ans dans le mode temporel alors que les observations indiquent une *quasi* périodicité de 3-7 ans. Le second mode de variabilité est plus intéressant car le mode spatial rappelle la cartographie des tendances (figure 5.14) et le mode temporel représente un signal de tendance positive à long terme. Nous avons déjà détecté ce signal dans les modes de variabilité du niveau de la mer reconstruit (*Llovel et al.* [2009]) et dans le niveau de la mer thermostérique (*Levitus et al.* [2009]). Ce signal traduit donc le réchauffement des océans au cours des 50 dernières années qui est probablement lié à l'augmentation des gaz à effet de serre et des aérosols qui sont les seuls forçages du modèle climatique couplé CNRM-CM3. Ce signal a donc probablement une réalité physique et dénote une augmentation des structures spatiales régionales au cours du temps.

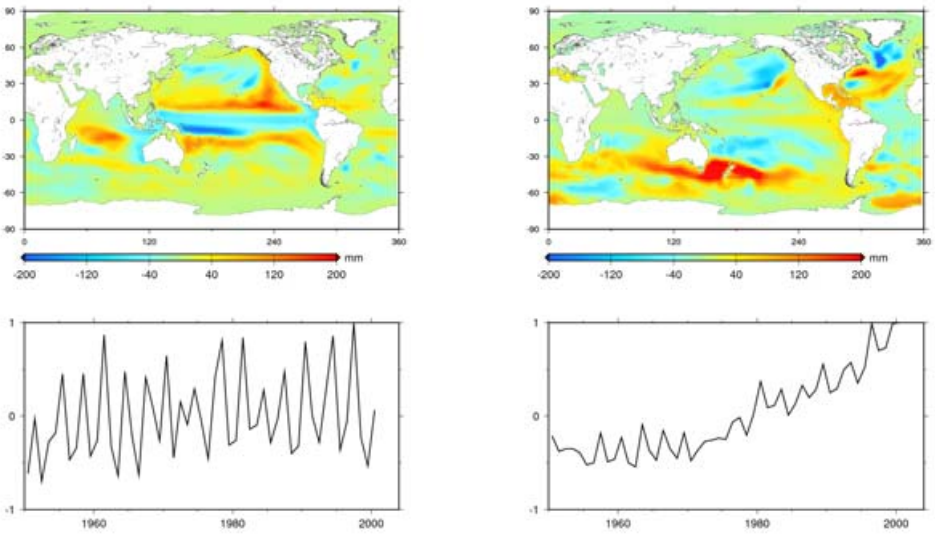

(a) mode 1 (b) mode 2

FIG. 5.15 – 2 premières EOFs du niveau de la mer thermostérique entre 1950 et 2000 déduites du modèle climatique couplé CNRM-CM3 a) mode 1 (18% de variance expliquée), b) mode 2 (15% de variance expliquée)

La variabilité régionale du niveau de la mer prédite par le modèle climatique couplé CNRM-CM3 concorde bien dans certaines régions avec le niveau de la mer reconstruit et le niveau de la mer thermostérique issu des données *in situ* sur les 50 dernières années. Toutefois, il reste encore beaucoup de différence entre ces diverses estimations. A noter que le modèle climatique est

dit « à toit rigide » c'est-à-dire que les variations de la surface libre de l'océan sont considérées comme nulles. Cette approximation allège le temps de calcul numérique. A présent, une nouvelle version est disponible avec le modèle océanique à surface libre. Cette nouvelle version devrait être plus réaliste pour les comparaisons avec le niveau de la mer reconstruit et thermostérique pour les 50 dernières années. Une nouvelle comparaison avec la cartographie régionale du niveau de la mer reconstruit est en cours de réalisation mais les résultats n'ont pu être inclus dans cette thèse.

Chapitre 6

Conclusion

La monté du niveau des mers est une des premières conséquences du changement climatique global. La détermination précise des variations du niveau de la mer est d'une importance capitale notamment, pour les populations vivant dans des endroits à risques et vulnérables tels que les zones côtières basses, les deltas des grands fleuves ou encore les petites îles basses du Pacifique et de l'océan Indien. Nous montrons tout au long de cette thèse les liens étroits entre les fluctuations climatiques et les variations du niveau de la mer dûes aux variations du contenu thermique de l'océan, aux pertes de masse des calottes polaires, à la fonte actuelle des glaciers de montagne et aux variations du stock d'eaux continentales. Nous avons établi différentes estimations des variations du niveau de la mer et des causes climatiques tant en global qu'en variabilité régionale.

Ainsi, en complément des observations des satellites altimétriques qui nous renseignent directement sur les fluctuations absolues du niveau de la mer, nous avons analysé les produits de nouvelles techniques de mesure telles que les données de température et de salinité acquises par les flotteurs profilant de subsurface Argo ou encore, les données de gravimétrie spatiale fournies par la mission GRACE. Avec ces observations géophysiques totalement indépendantes, nous avons estimé la hausse du niveau de la mer et ses principales causes climatiques pour les années récentes (2003-2009) et sur la période altimétrique totale (1993-2009) en termes de tendance, de variabilité interannuelle en moyenne globale et aussi, en terme de variabilité régionale. De plus, le bilan sur deux périodes d'étude (1993-2009 et 2003-2009) a été établi. Un bon accord est trouvé entre la hausse observée du niveau de la mer et les différentes contributions climatiques du niveau de la mer en moyenne globale sur la période altimétrique totale avec, néanmoins, une incertitude plus importante. Pour cela, nous estimons directement le contenu stérique (données

de température et de salinité du projet Argo) et le signal massique des océans (données gravimétriques GRACE au dessus des océans). Les différentes contributions climatiques, c'est-à-dire la perte de masse des calottes polaires à l'aide de GRACE et la fonte actuelle des glaciers de montagne à partir des estimations disponibles dans la littérature ont été estimées. De plus, nous proposons une estimation de la contribution du stock d'eaux continentales des 33 plus grands bassins hydrologiques du monde et leur impact sur la tendance et la variabilité interannuelle du niveau de la mer. La variabilité interannuelle du niveau de la mer observé et corrigé de la composante stérique est expliquée en grande partie par les variations du stock d'eaux continentales sur la période récente 2003-2009. Sur des périodes plus longues, le signal des eaux continentales déduit de la modélisation numérique suggère que la variabilité interannuelle du niveau de la mer observé est responsable d'une partie de la variabilité interannuelle en moyenne globale du niveau de la mer, et notamment lors de l'événement ENSO de 1997-1998.

Nous nous sommes ensuite intéressés plus particulièrement à la variabilité régionale des tendances du niveau de la mer observé et nous avons essayé d'en comprendre les causes. Nous avons aussi établi les tendances régionales du niveau de la mer sur les 50 dernières années déduites de méthodes de reconstruction développées au sein de l'équipe GOHS (Géophysique, Océanographie et Hydrologie Spatiales). Nous avons ainsi mis en évidence un signal multidécennal, de tendance positive, dans la variabilité régionale du niveau de la mer des dernières décennies. Une relation entre ce signal multidécennal et la composante thermostérique issue des mesures hydrographiques *in situ* des bases de données mondiales a été mis en évidence. Nous avons aussi retrouvé ce même signal dans les sorties d'un modèle climatique couplé, prenant en compte les concentrations des gaz à effet de serre et des aérosols atmosphériques.

Ce travail de thèse a répondu à quelques questions mais il reste encore beaucoup de zones d'ombre : Assiste-t-on à une accélération de l'élévation du niveau moyen des mers pour les dernières décennies ? De même, pour la perte de masse des calottes polaires et la fonte actuelle des glaciers de montagne ? Ou bien, est-ce le reflet d'une oscillation décennale/multidécennale ? En plus de la composante stérique du niveau de la mer, quelles sont les autres causes de la variabilité régionale ? Sommes nous en mesure de pouvoir les détecter et de les mesurer ? Peut-on comprendre les variations multidécennales du contenu thermique des océans ? Est-ce un signal physique ou bien un simple artéfact

métrologique ? Quel va être le comportement du stock d'eaux continentales en réponse au changement climatique global ?

Une autre problématique concerne la hausse future du niveau de la mer à l'horizon 2100. De récentes estimations basées sur des méthodes dites « semi-empiriques » relient les variations des vitesses du niveau de la mer à la température moyenne du globe. Ces estimations fournissent une hausse plus importante que celle des modèles climatiques couplés. Mais, ces modèles climatiques couplés ne prennent pas encore en compte les instabilités dynamiques des calottes polaires détectées ces dernières années.

Les prolongements de ce travail de thèse sont nombreux. Ils concernent par exemple l'étude en 3 dimensions de l'histoire des anomalies de température de l'océan au cours des dernières décennies et la mise en évidence du forçage anthropique sur les structures régionales de l'expansion thermique et du niveau de la mer. Ou encore, l'étude des impacts côtiers de la hausse actuelle du niveau de la mer dans le contexte du réchauffement climatique global.

Ces problèmes sont dores et déjà à l'étude au sein de l'équipe GOHS du LEGOS où j'ai effectué ma thèse.

Bibliographie

Ablain, M., A. Cazenave, G. Valladeau, and S. Guinehut, A new assessment of the error budget of global mean sea level rate estimated by satellite altimetry over 1993-2008, *Ocean Sci.*, *5*, 193–201, 2009.

Alkama, R., B. Decharme, H. Douville, M. Becker, A. Cazenave, J. Sheffield, A. Voldoire, S. Tyteca, and P. L. Moigne, Global evaluation of the ISBA-TRIP continental hydrological system. part I : Comparison to GRACE terrestrial water storage estimates and in situ river discharges, *Journal of Hydrometeorology*, *11*, 583–600, 2010.

Allison, I., R. B. Alley, H. A. Fricker, R. H. Thomas, and R. C. Warner, Ice sheet mass balance and sea level, *Antarctic Science*, *21*, 413–426, 2009.

Alvera-Azcarate, A., A. Barth, M. Rixen, and J. M. Beckers, Reconstruction of incomplete oceanographic data sets using empirical orthogonal functions : application to the adriatic sea surface temperature, *Ocean Modelling*, *9*, 325–346, 2005.

Antonov, J. I., Steric sea level variations during 1957-1994 : Importance of salinity, *Journal of Geophysical Research*, *107*, 2002.

Antonov, J. I., S. Levitus, and T. P. Boyer, Thermosteric sea level rise, 1955-2003, *Geophysical Research Letters*, *32*, 2005.

Arendt, A. A., K. A. Echelmeyer, W. D. Harrison, C. S. Lingle, and V. B. Valentine, Rapid wastage of alaska glaciers and their contribution to rising sea level, *Science*, *297*, 382–386, 2002.

Baur, O., M. Kuhn, and W. Featherstone, GRACE-derived ice-mass variations over greenland by accounting for leakage effects, *Journal of Geophysical Research - Solid Earth*, *114*, 2009.

Becker, M., W. Llovel, A. Cazenave, A. Guntner, and J. Cretaux, Recent hydrological behavior of the east african great lakes region inferred from GRACE, satellite altimetry and rainfall observations, *Comptes Rendus Geoscience*, *342*, 223–233, 2010.

Beckers, J. M., and M. Rixen, EOF calculations and data filling from incomplete oceanographic datasets, *Journal of Atmospheric and Oceanic Technology*, *20*, 1839–1856, 2003.

Beckley, B., N. Zelensky, S. Holmes, F. Lemoine, R. Ray, G. Mitchum, S. Desai, and S. Brown, Assessment of the jason-2 extension to the TOPEX/Poseidon, jason-1 Sea-Surface height time series for global mean sea level monitoring, *Marine Geodesy*, *33*, 447–471, 2010.

Berge-Nguyen, M., A. Cazenave, A. Lombard, W. Llovel, J. Viarre, and J. Cretaux, Reconstruction of past decades sea level using thermosteric sea level, tide gauge, satellite altimetry and ocean reanalysis data, *Global and Planetary Change*, *62*, 1–13, 2008.

Berthier, E., E. Schiefer, G. K. C. Clarke, B. Menounos, and F. Remy, Contribution of alaskan glaciers to sea-level rise derived from satellite imagery, *Nature Geoscience*, *3*, 92–95, 2010.

Bettadpur, S., *CSR Level-2 processing standards document for level-2 product release 0004*, GRACE, 2007.

Bindoff, N. L., et al., *Observations : Oceanic Climate Change and Sea Level. In : Climate change 2007 : the physical science basis : contribution of Working Group I to the Fourth Assessment Report of the Intergovernmental Panel on Climate Change*, Cambridge University Press, United Kingdom and New York, NY, USA, 2007.

Boone, A., V. Masson, T. Meyers, and J. Noilhan, The influence of the inclusion of soil freezing on simulations by a soil-vegetation-atmosphere transfer scheme, *Journal of Applied Meteorology*, *39*, 1544–1569, 2000.

Boyer, T. P., S. Levitus, J. I. antonov, R. A. Locarnini, and H. E. Garcia, Linear trends in salinity for the world ocean, 1955-1998, *Geophysical Research Letters*, *32*, 2005.

Bruinsma, S., J. Lemoine, R. Biancale, and N. Vales, CNES/GRGS 10-day gravity field models (release 2) and their evaluation, *Advances in Space Research*, *45*, 587–601, 2010.

Carton, J. A., and B. S. Giese, A reanalysis of ocean climate using simple ocean data assimilation (SODA), *Monthly Weather Review*, *136*, 2999, 2008.

Cazenave, A., and W. Llovel, Contemporary sea level rise, *Annual Review of Marine Science*, *2*, 145–173, 2010.

Cazenave, A., and R. S. Nerem, Present-day sea level change : Observations and causes, *Reviews of Geophysics*, *42*, 2004.

Cazenave, A., K. Dominh, S. Guinehut, E. Berthier, W. Llovel, G. Ramillien, M. Ablain, and G. Larnicol, Sea level budget over 2003-2008 : A reevaluation from GRACE space gravimetry, satellite altimetry and argo, *Global and Planetary Change*, *65*, 83–88, 2009.

Chambers, D. P., Evaluation of new GRACE time-variable gravity data over the ocean, *Geophysical Research Letters*, *33*, 2006.

Chambers, D. P., C. A. Mehlhaff, T. J. Urban, D. Fujii, and R. S. Nerem, Low-frequency variations in global mean sea level : 1950-2000, *Journal of Geophysical Research - Oceans*, *107*, 2002.

Chao, B. F., Y. H. Wu, and Y. S. Li, Impact of artificial reservoir water impoundment on global sea level, *Science*, *320*, 212–214, 2008.

Chen, J. L., C. R. Wilson, D. P. Chambers, R. S. Nerem, and B. D. Tapley, Seasonal global water mass budget and mean sea level variations, *Geophysical Research Letters*, *25*, 3555–3558, 1998.

Chen, J. L., B. D. Tapley, and C. R. Wilson, Alaskan mountain glacial melting observed by satellite gravimetry, *Earth and Planetary Science Letters*, *248*, 368–378, 2006a.

Chen, J. L., C. R. Wilson, D. D. Blankenship, and B. D. Tapley, Antarctic mass rates from GRACE, *Geophysical Research Letters*, *33*, 2006b.

Chen, J. L., C. R. Wilson, and K. W. Seo, Optimized smoothing of gravity recovery and climate experiment (GRACE) time-variable gravity observations, *Journal of Geophysical Research - Solid Earth*, *111*, 2006c.

Chen, J. L., C. R. Wilson, and B. D. Tapley, Satellite gravity measurements confirm accelerated melting of greenland ice sheet, *Science*, *313*, 1958–1960, 2006d.

Chen, J. L., C. R. Wilson, D. Blankenship, and B. D. Tapley, Accelerated antarctic ice loss from satellite gravity measurements, *Nature Geoscience*, *2*, 859–862, 2009.

Church, J., P. L. Woodworth, T. Aarup, and S. Wilson, *Understanding Sea-level Rise and Variability*, John Wiley & Sons Inc, 2010.

Church, J. A., and N. J. White, A 20th century acceleration in global sea-level rise, *Geophysical Research Letters*, *33*, 2006.

Church, J. A., J. M. Gregory, P. Huybrechts, M. Kuhn, K. Lambeck, M. T. Nhuan, D. Qin, and P. L. Woodworth, *Changes in Sea Level, Climate Change*

2001 : The Scientific Basis : Contribution of Working Group I to the Third Assessment Report of the Intergovernmental Panel on Climate Change, Cambridge University Press, New York, 2001.

Church, J. A., N. J. White, R. Coleman, K. Lambeck, and J. X. Mitrovica, Estimates of the regional distribution of sea level rise over the 1950-2000 period, *Journal of Climate*, *17*, 2609–2625, 2004.

Cogley, J. G., Geodetic and direct mass-balance measurements ; comparison and joint analysis, *Annals of Glaciology*, *50*, 96–100, 2009.

community members, E., Eight glacial cycles from an antarctic ice core, *Nature*, *429*, 623–628, 2004.

Conkright, M. E., et al., *NOAA Atlas NESDIS 42, World Ocean Atlas 2001 Volume 1 : Introduction*, U.S. Gov. Printing Office, Wash., DC, USA, 2002.

Daget, N., A. Weaver, and M. Balmaseda, Ensemble estimation of background-error variances in a three-dimensional variational data assimilation system for the global ocean, *Quaternary Journal of the Royal Meteorological Society*, *135*, 1071–1094, 2009.

Decharme, B., Développement et validation d'une modélisation hydrologique globale incluant les effets sous maille et la représentation des zones inondés, Ph.D. thesis, Université Toulouse III - Paul Sabatier, 2005.

Decharme, B., H. Douville, A. Boone, F. Habets, and J. Noilhan, Impact of an exponential profile of saturated hydraulic conductivity within the ISBA LSM : simulations over the rhone basin, *Journal of Hydrometeorology*, *7*, 61–80, 2006.

Decharme, B., R. Alkama, H. Douville, M. Becker, and A. Cazenave, Global evaluation of the ISBA-TRIP continental hydrological system. part II : uncertainties in river routing simulation related to flow velocity and groundwater storage, *Journal of Hydrometeorology*, *11*, 601–617, 2010.

Delcroix, T., Observed surface oceanic and atmospheric variability in the tropical pacific at seasonal and ENSO timescales : A tentative overview, *Journal of Geophysical Research*, *103*, 18,611–18,633, 1998.

Deque, M., and J. P. Piedelievre, High-resolution climate simulation over europe, *Climate Dynamics*, *11*, 321–339, 1995.

Deque, M., C. Dreveton, A. Braun, and D. Cariolle, The arpege/ifs atmosphere model - a contribution to the french community climate modeling, *Climate Dynamics*, *10*, 249–266, 1994.

Deque, M., P. Marquet, and R. G. Jones, Simulation of climate change over europe using a global variable resolution general circulation model, *Climate Dynamics*, *14*, 173–189, 1998.

Douglas, B. C., *Sea level change in the era of the recording tide gauges, in Sea Level Rises, History and Consequences, edited by B.C. Douglas, M.S. Kearney, and S.P. Leatherman*, Academic, San Diego, California, 2001.

Douglas, B. C., and W. R. Peltier, The puzzle of global sea-level rise, *Physics Today*, *55*, 35–40, 2002.

Douville, H., J. Royer, and J. Mahfouf, A new snow parametrization for the météo-france climate model .1. validation in stand-alone experiments, *Climate Dynamics*, *12*, 21–35, 1995.

Dyurgerov, M. B., and M. F. Meier, *Glaciers and the changing Earth system : A 2004 snapshot*, Inst. of Arct. and Alp. Res., Univ. of Colo., Boulder, 2005.

Emiliani, C., Pleistocene temperature, *Journal of Geology*, *63*, 538–578, 1955.

Fleming, K., P. Johnston, D. Zwartz, Y. Yokoyama, K. Lambeck, and J. Chappell, Refining the eustatic sea-level curve since the last glacial maximum using far- and intermediate-field sites, *Earth and Planetary Science Letters*, *163*, 327–342, 1998.

Gibelin, A., and M. Deque, Anthropogenic climate change over the mediterranean region simulated by a global variable resolution model, *Climate Dynamics*, *20*, 327–339, 2003.

Gill, A. E., *Atmosphere-ocean dynamics*, Elsevier, 1982.

Gouretski, V., and K. P. Koltermann, How much is the ocean really warming?, *Geophysical Research Letters*, *34*, 2007.

Guinehut, S., C. Coatanoan, A. Dhomps, P. L. Traon, and G. Larnicol, On the use of satellite altimeter data in argo quality control, *Journal of Atmospheric and Oceanic Technology*, *26*, 395–402, 2009.

Han, S. C., C. K. Shum, C. Jekeli, C. Y. Kuo, C. Wilson, and K. W. Seo, Non-isotropic filtering of GRACE temporal gravity for geophysical signal enhancement, *Geophysical Journal International*, *163*, 18–25, 2005.

Hock, R., M. de Woul, V. Radic, and M. Dyurgerov, Mountain glaciers and ice caps around antarctica make a large sea-level rise contribution, *Geophysical Research Letters*, *36*, 2009.

Holgate, S. J., On the decadal rates of sea level change during the twentieth century, *Geophysical Research Letters*, *34*, 2007.

Holgate, S. J., and P. L. Woodworth, Evidence for enhanced coastal sea level rise during the 1990s, *Geophysical Research Letters*, *31*, 2004.

Huntington, T. G., Can we dismiss the effect of changes in land-based water storage on sea-level rise ?, *Hydrological Processes*, *22*, 717–723, 2008.

Ingleby, B., and M. Huddleston, Quality control of ocean temperature and salinity profiles - historical and real-time data, *Journal of Marine Systems*, *65*, 158–175, 2007.

Ishii, M., and M. Kimoto, Reevaluation of historical ocean heat content variations with time-varying XBT and MBT depth bias corrections, *Journal of Oceanography*, *65*, 287–299, 2009.

Ivins, E. R., and T. S. James, Antarctic glacial isostatic adjustment : a new assessment, *Antarctic Science*, *17*, 541–553, 2005.

Jevrejeva, S., A. Grinsted, J. C. Moore, and S. Holgate, Nonlinear trends and multiyear cycles in sea level records, *Journal of Geophysical Research - Oceans*, *111*, 2006.

Jevrejeva, S., J. C. Moore, A. Grinsted, and P. L. Woodworth, Recent global sea level acceleration started over 200 years ago ?, *Geophysical Research Letters*, *35*, 2008.

Kaplan, A., M. A. Cane, Y. Kushnir, A. C. Clement, M. B. Blumenthal, and B. Rajagopalan, Analyses of global sea surface temperature 1856-1991, *Journal of Geophysical Research - Oceans*, *103*, 18,567–18,589, 1998.

Kaplan, A., Y. Kushnir, and M. A. Cane, Reduced space optimal interpolation of historical marine sea level pressure : 1854-1992, *Journal of Climate*, *13*, 2987–3002, 2000.

Kaser, G., J. G. Cogley, M. B. Dyurgerov, M. F. Meier, and A. Ohmura, Mass balance of glaciers and ice caps : Consensus estimates for 1961-2004, *Geophysical Research Letters*, *33*, 2006.

Kurtenbach, E., T. Mayer-Gurr, and A. Eicker, Deriving daily snapshots of the earth's gravity field from grace-l1b data using kalman filtering, *Geophysical Research Letters*, *36*, 2009.

Kusche, J., Approximate decorrelation and non-isotropic smoothing of time-variable GRACE-type gravity field models, *Journal of Geodesy*, *81*, 733–749, 2007.

Lambeck, K., T. M. Esat, and E. K. Potter, Links between climate and sea levels for the past three million years, *Nature*, *419*, 199–206, 2002.

Lemke, P., et al., *Observations : Changes in Snow, Ice and Frozen Ground. In : Climate change 2007 : the physical science basis : contribution of Working Group I to the Fourth Assessment Report of the Intergovernmental Panel on Climate Change*, Cambridge University Press, United Kingdom and New York, NY, USA, 2007.

Leuliette, E. W., and L. Miller, Closing the sea level rise budget with altimetry, argo, and GRACE, *Geophysical Research Letters*, *36*, 2009.

Levitus, S., and T. Boyer, World ocean atlas 1994, vol. 4 : Temperature, NOAA atlas NESDIS 4, US gov, *Printing Office, Wash., DC, 117 pp*, 1994.

Levitus, S., T. Boyer, M. Conkright, T. OBrien, J. Antonov, C. Stephens, L. Stathoplos, D. Johnson, and R. Gelfeld, *World Ocean Database 1998, vol. 1, Introduction, NOAA Atlas NESDIS 18*, 346 pp., US Government Printing Office, Washington, DC, 1998.

Levitus, S., J. I. Antonov, T. P. Boyer, H. E. Garcia, and R. A. Locarnini, Linear trends of zonally averaged thermosteric, halosteric, and total steric sea level for individual ocean basins and the world ocean, (1955-1959)-(1994-1998), *Geophysical Research Letters*, *32*, 2005.

Levitus, S., J. I. Antonov, T. P. Boyer, R. A. Locarnini, H. E. Garcia, and A. V. Mishonov, Global ocean heat content 1955-2008 in light of recently revealed instrumentation problems, *Geophysical Research Letters*, *36*, 2009.

Llovel, W., A. Cazenave, P. Rogel, A. Lombard, and M. B. Nguyen, Two-dimensional reconstruction of past sea level (1950-2003) from tide gauge data and an ocean general circulation model, *Clim. Past*, *5*, 217–227, 2009.

Llovel, W., M. Becker, A. Cazenave, J. Cretaux, and G. Ramillien, Global land water storage change from GRACE over 2002-2009 ; inference on sea level, *Comptes Rendus Geoscience*, *342*, 179–188, 2010a.

Llovel, W., S. Guinehut, and A. Cazenave, Regional and interannual variability in sea level over 2002-2009 based on satellite altimetry, argo float data and GRACE ocean mass, *Ocean Dynamics*, *60*, 1193–1204, 2010b.

Llovel, W., M. Becker, A. Cazenave, S. Jevrejeva, R. Alkama, B. Decharme, H. Douville, M. Ablain, and B. Beckley, Terrestrial waters and sea level variations on interannual time scale, *Global and Planetary Change*, *75*, 76–82, 2011.

Lombard, A., A. Cazenave, P. Y. LeTraon, and M. Ishii, Contribution of thermal expansion to present-day sea-level change revisited, *Global and Planetary Change*, *47*, 1–16, 2005.

Lombard, A., A. Cazenave, P. Y. LeTraon, S. Guinehut, and C. Cabanes, Perspectives on present-day sea level change : a tribute to christian le provost, *Ocean Dynamics*, *56*, 445–451, 2006.

Lombard, A., G. Garric, and T. Penduff, Regional patterns of observed sea level change : insights from a 1/4A degrees global ocean/sea-ice hindcast, *Ocean Dynamics*, *59*, 433–449, 2009.

Luthcke, S. B., H. J. Zwally, W. Abdalati, D. D. Rowlands, R. D. Ray, R. S. Nerem, F. G. Lemoine, J. J. McCarthy, and D. S. Chinn, Recent greenland ice mass loss by drainage system from satellite gravity observations, *Science*, *314*, 1286–1289, 2006.

Luthcke, S. B., A. A. Arendt, D. D. Rowlands, J. J. McCarthy, and C. F. Larsen, Recent glacier mass changes in the gulf of alaska region from GRACE mascon solutions, *Journal of Glaciology*, *54*, 767–777, 2008.

Madec, G., P. Delecluse, M. Imbard, and C. Levy, OPA8. 1 ocean general circulation model reference manual, institut pierre simon laplace (IPSL, france), note 11, 91 pp, 1998.

Meier, M., M. B. Dyurgerov, U. K. Rick, S. O'Neel, W. T. Pfeffer, R. S. Anderson, S. P. Anderson, and A. F. Glazovsky, Glaciers dominate eustatic sea-level rise in the 21st century, *Science*, *317*, 1064–1067, 2007.

Miller, K. G., P. J. Sugarman, J. V. Browning, B. P. Horton, A. Stanley, A. Kahn, J. Uptegrove, and M. Aucott, Sea-level rise in new jersey over the past 5000Â years : Implications to anthropogenic changes, *Global and Planetary Change*, *66*, 10–18, 2009.

Millero, F. J., and A. Poisson, International one-atmosphere equation of state of seawater, *Deep-Sea Research Part A - Oceanographic Research Papers*, *28*, 625–629, 1981.

Milly, P. C. D., A. Cazenave, and M. Gennero, Contribution of climate-driven change in continental water storage to recent sea-level rise, *Proceedings of the National Academy of Sciences of the United States*, *100*, 13,158–13,161, 2003.

Milne, G. A., A. J. Long, and S. E. Bassett, Modelling holocene relative sea-level observations from the caribbean and south america, *Quaternary Science Reviews*, *24*, 1183–1202, 2005.

Milne, G. A., W. R. Gehrels, C. W. Hughes, and M. E. Tamisiea, Identifying the causes of sea-level change, *Nature Geosci*, *2*, 471–478, 2009.

Minster, J., A. Cazenave, Y. Serafini, F. Mercier, M. Gennero, and P. Rogel, Annual cycle in mean sea level from Topex-Poseidon and ERS-1 : inference on the global hydrological cycle, *Global and Planetary Change*, *20*, 57–66, 1999.

Mitrovica, J. X., M. E. Tamisiea, J. L. Davis, and G. A. Milne, Recent mass balance of polar ice sheets inferred from patterns of global sea-level change, *Nature*, *409*, 1026–1029, 2001.

Mitrovica, J. X., N. Gomez, and P. U. Clark, The Sea-Level fingerprint of west antarctic collapse, *Science*, *323*, 753, 2009.

Nerem, R. S., E. Leuliette, and A. Cazenave, Present-day sea-level change : A review, *Comptes Rendus Geoscience*, *338*, 1077–1083, 2006.

Ngo-Duc, T., K. Laval, J. Polcher, A. Lombard, and A. Cazenave, Effects of land water storage on global mean sea level over the past half century, *Geophysical Research Letters*, *32*, 2005.

Nicholls, R. J., Rising sea levels : potential impacts and responses, *Global Environment Change*, *17*, 83–107, 2002.

Nicholls, R. J., The impacts of sea-level rise, *Ocean Challenge*, *15*, 13–17, 2007.

Noilhan, J., and S. Planton, A simple parameterization of land surface processes for meteorological models, *Monthly Weather Review*, *117*, 536–549, 1989.

Oki, T., and Y. C. Sud, Design of total runoff integrating pathways (trip) - a global river channel network, *Earth Interactions*, *2*, 1–37, 1998.

Paulson, A., S. Zhong, and J. Wahr, Inference of mantle viscosity from GRACE and relative sea level data, *Geophysical Journal International*, *171*, 497–508, 2007.

Peltier, W., Global glacial isostasy and the surface of the ice-age earth : The ice-5G (VM2) model and grace, *Annual Review of Earth and Planetary Sciences*, *32*, 111–149, 2004.

Peltier, W. R., *Global glacial isostatic adjustment and modern instrumental records of relative sea-level history, in Sea Level Rises, History and Consequences, edited by B.C. Douglas, M.S. Kearney, and S.P. Leatherman*, Academic, San Diego, California, 2001.

Peltier, W. R., Closure of the budget of global sea level rise over the GRACE era : the importance and magnitudes of the required corrections for global glacial isostatic adjustment, *Quaternary Science Reviews*, *28*, 1658–1674, 2009.

Petit, J. R., et al., Climate and atmospheric history of the past 420,000 years from the vostok ice core, antarctica, *Nature*, *399*, 429–436, 1999.

Pirazzoli, P. A., *Sea-level changes : the last 20,000 years*, Wiley, 1996.

Plag, H. P., Recent relative sea-level trends : an attempt to quantify the forcing factors, *Philosophical Transactions of the Royal Society A-Mathematical Physical*, *364*, 821–844, 2006.

Prandi, P., A. Cazenave, and M. Becker, Is coastal mean sea level rising faster than the global mean? a comparison between tide gauges and satellite altimetry over 1993 - 2007, *Geophysical Research Letters*, *36*, 2009.

Preisendorfer, R. W., *Principal component analysis in meteorology and oceanography*, Elsevier, 1988.

Radic, V., and R. Hock, Regional and global volumes of glaciers derived from statistical upscaling of glacier inventory data, *Journal of Geophysical Research - Earth Surface*, *115*, 2010.

Rahmstorf, S., A semi-empirical approach to projecting future sea-level rise, *Science*, *315*, 368, 2007.

Ramillien, G., F. Frappart, A. Cazenave, and A. Guntner, Time variations of land water storage from an inversion of 2 years of GRACE geoids, *Earth and Planetary Science Letters*, *235*, 283–301, 2005.

Ramillien, G., A. Lombard, A. Cazenave, E. R. Ivins, M. Llubes, F. Remy, and R. Biancale, Interannual variations of the mass balance of the antarctica and greenland ice sheets from GRACE, *Global and Planetary Change*, *53*, 198–208, 2006.

Raynaud, D., J. Barnola, R. Souchez, R. Lorrain, J. Petit, P. Duval, and V. Y. Lipenkov, Palaeoclimatology : The record for marine isotopic stage 11, *Nature*, *436*, 39–40, 2005.

Rignot, E., J. L. Bamber, M. R. van den Broeke, C. Davis, Y. Li, W. J. van de Berg, and E. van Meijgaard, Recent antarctic ice mass loss from radar interferometry and regional climate modelling, *Nature Geosci*, *1*, 106–110, 2008.

Roemmich, D., and J. Gilson, The 2004-2008 mean and annual cycle of temperature, salinity, and steric height in the global ocean from the argo program, *Progress In Oceanography*, *82*, 81–100, 2009.

Roullet, G., and G. Madec, Salt conservation, free surface, and varying levels : a new formulation for ocean general circulation models, *Journal of Geophysical Research - Oceans*, *105*, 23,927–23,942, 2000.

Rowlands, D. D., Resolving mass flux at high spatial and temporal resolution using GRACE intersatellite measurements, *Geophysical Research Letters*, *32*, 2005.

Saji, N. H., B. N. Goswami, P. N. Vinayachandran, and T. Yamagata, A dipole mode in the tropical indian ocean, *Nature*, *401*, 360–363, 1999.

Salas-Melia, D., A global coupled sea ice-ocean model, *Ocean Modelling*, *4*, 137–172, 2002.

Salas-Melia, D., F. Chauvin, M. Deque, H. Douville, J. F. Gueremy, P. Marquet, S. Planton, J. F. Royer, and S. Tyteca, Description and validation of the CNRM-CM3 global coupled model, *CNRM working note*, *103*, 2005.

Schmidt, R., F. Flechtner, U. Meyer, K. H. Neumayer, C. Dahle, R. Konig, and J. Kusche, Hydrological signals observed by the GRACE satellites, *Survey in Geophysics*, *29*, 319–334, 2008.

Schott, F. A., S. Xie, and J. P. M. Jr, Indian ocean circulation and climate variability, *Reviews of Geophysics*, *47*, 46 PP., 2009.

Shackleton, N. J., The 100,000-year ice-age cycle identified and found to lag temperature, carbon dioxide, and orbital eccentricity, *Science*, *289*, 1897–1902, 2000.

Slobbe, D. C., P. Ditmar, and R. C. Lindenbergh, Estimating the rates of mass change, ice volume change and snow volume change in greenland from ICESat and GRACE data, *Geophysical Journal International*, *176*, 95–106, 2009.

Smith, T., R. Reynolds, R. Livezey, and D. Stokes, Reconstruction of historical sea surface temperatures using empirical orthogonal functions, *Journal of Climate*, *9*, 1403–1420, 1996.

Stammer, D., Response of the global ocean to greenland and antarctic ice melting, *Journal of Geophysical Research - Oceans*, *113*, 2008.

Swenson, S., and J. Wahr, Methods for inferring regional surface-mass anomalies from gravity recovery and climate experiment (GRACE) measurements of time-variable gravity, *Journal of Geophysical Research - Solid Earth*, *107*, 2002.

Tamisiea, M. E., J. X. Mitrovica, G. A. Milne, and J. L. Davis, Global geoid and sea level changes due to present-day ice mass fluctuations, *Journal of Geophysical Research - Solid Earth*, *106*, 30,849–30,863, 2001.

Terray, L., S. Valcke, and A. Piacentini, OASIS 2.2 ocean atmosphere sea ice soil, user's guide and reference manual technical report TR, *Tech. rep.*, CMGC/98-05 CERFACS, Toulouse, France, 1998.

Toumazou, V., and J. Cretaux, Using a lanczos eigensolver in the computation of empirical orthogonal functions, *Monthly Weather Review*, *129*, 1243–1250, 2001.

Uppala, S. M., et al., The ERA-40 re-analysis, *Quarterly Journal of the Royal Meteorological Society*, *131*, 2961–3012, 2005.

Vail, P. R., R. M. Mitchum, and S. Thompson, *Seismic stratigraphy and global changes of sea level, Part 4 : global cycles of relative changes in sea level. In Seismic stratigraphy - Applications to hydrocarbon exploration*, C.E. Payton (ed.), 1977.

Velicogna, I., Increasing rates of ice mass loss from the greenland and antarctic ice sheets revealed by GRACE, *Geophysical Research Letters*, *36*, 2009.

Velicogna, I., and J. Wahr, Acceleration of greenland ice mass loss in spring 2004, *Nature*, *443*, 329–331, 2006.

Vermeer, M., and S. Rahmstorf, Global sea level linked to global temperature, *Proceedings of the National Academy of Sciences*, *106*, 21,527–21,532, 2009.

Woodworth, P. L., and R. Player, The permanent service for mean sea level : An update to the 21st Century, *Journal of Coastal Research*, *19*, 287–295, 2003.

Woppelmann, G., C. Letetrel, A. Santamaria, M. Bouin, X. Collilieux, Z. Altamimi, S. D. P. Williams, and B. M. Miguez, Rates of sea-level change over the past century in a geocentric reference frame, *Geophysical Research Letters*, *36*, 2009.

Wouters, B., D. Chambers, and E. J. O. Schrama, GRACE observes small-scale mass loss in greenland, *Geophysical Research Letters*, *35*, 2008.

Wunsch, C., R. M. Ponte, and P. Heimbach, Decadal trends in sea level patterns : 1993 - 2004, *Journal of Climate*, *20*, 5889, 2007.

Annexe A

Annexe : Article *Berge-Nguyen et al.* [2008] : « Le niveau de la mer reconstruit sur les 50 dernières années en utilisant le niveau de la mer thermostérique, les données marégraphiques, l'altimétrie spatiale et les sorties d'une réanalyses océanique » , publié dans le journal « Global and Planetary Change »

Introduction et résumé de l'article

Dans un premier temps de cette étude, une méthode de reconstruction est testée en considérant différentes périodes temporelles pour le calcul des modes de variabilité des champs à 2-D (entre 10 et 50 ans). Puis, nous testons l'impact du nombre d'enregistrements marégraphiques considérés lors de l'algorithme de reconstruction. Dans chaque cas, les résultats, en variabilité régionale et en moyenne globale, sont comparés avec des données de référence. Les résultats suggèrent que plus l'on considère d'année lors de l'extraction des modes de variabilité, plus le champ reconstruit s'aproche de la réalité.

Dans un second temps, une reconstruction du niveau de la mer est proposée en considérant les données de 118 marégraphes disponibles depuis 1950 avec (1) les données du niveau de la mer thermostérique sur 1955-2003, (2) les données altimétriques de Topex/Poseidon sur 1993-2003 et (3) les sorties de la réanalyse océanique SODA (Simple Ocean Data Assimilation, *Carton and Giese* [2008]) sur 1958-2001. Nous montrons que le niveau moyen global des mers est bien reconstruit. Dans le cas avec l'extraction des modes de variabilité de l'altimétrie sur 11 ans, le niveau moyen global des mers est bien reconstruit par contre, la variabilité régionale des tendances sur 1950-2003 diffère des cartes obtenues avec le niveau de la mer thermostérique. Enfin, quand on extrait les modes de variabilité de la réanalyse océanique SODA, il en résulte une cartographie des tendances encore différente des deux autres cas. Toutefois, dans les trois cas, les reconstructions sur la période altimétrique, prise comme référence, concordent.

Available online at www.sciencedirect.com
ScienceDirect
Global and Planetary Change 62 (2008) 1 – 13
GLOBAL AND PLANETARY CHANGE
www.elsevier.com/locate/gloplacha

Reconstruction of past decades sea level using thermosteric sea level, tide gauge, satellite altimetry and ocean reanalysis data

M. Berge-Nguyen, A. Cazenave *, A. Lombard, W. Llovel, J. Viarre, J.F. Cretaux

LEGOS-CNES, Toulouse, France

Received 23 March 2007; accepted 1 November 2007
Available online 15 December 2007

Abstract

This study investigates past sea level reconstruction (over 1950–2003) based on tide gauge records and EOF spatial patterns from different 2-D fields. In a first step, we test the influence on the reconstructed signal of the 2-D fields temporal coverage. For that purpose we use global grids of thermosteric sea level data, available over 1950–2003. Different time spans (in the range 10–50 yr) for the EOF spatial patterns, and different geographical distributions for the 1-D thermosteric sea level time series (interpolated at specific locations from the 2-D grids), are successively used to reconstruct the 54-year long thermosteric sea level signal. In each case we compare the reconstructed trend map with the reference. The simulation indicates that the longer the time span covered by the spatial EOFs, the closer to the reference the reconstructed thermosteric sea level trends. In a second step, we apply the method to reconstructing 2-D sea level data over 1950–2003, combining sparse tide gauge records available since 1950, with EOF spatial patterns from different sources: (1) thermosteric sea level grids over 1955–2003, (2) sea level grids from Topex/Poseidon satellite altimetry over 1993–2003, and (3) dynamic height grids from the SODA reanalysis over 1958–2001. The reconstructed global mean sea level trend based on thermosteric EOFs (case 1) is significantly lower than the observed trend, while the interannual/decadal sea level fluctuations are well reproduced. Case 2 (Topex/Poseidon EOFs over 1993–2003) leads to a global mean sea level trend over the 54-year time interval very close to the observed trend. But the spatial trends of the reconstruction over 1950–2003 are significantly different from those obtained with thermosteric EOFs. Case 3 (SODA EOFs over 1958–2001) provides a reconstruction trend map over 1950–2003 that differs significantly from the previous two cases. We discuss possible causes for such differences. For the three cases, on the other hand, reconstructed spatial trends over 1993–2003 agree well with the regional sea level trends observed by Topex/Poseidon.

Keywords: sea level; tide gauges; altimetry; thermal expansion; past sea level reconstruction

1. Introduction

Several studies have developed methods for reconstructing past 2-D time series of oceanographic (e.g., sea surface temperature, sea surface height) or atmospheric (e.g., surface wind speed, surface pressure) fields by combining 2-D grids of limited temporal length (in general available from remote sensing observations over the last 2 decades or less) with historical (several decade-long), sparse 1-D records (e.g., Beckers and Rixen, 2003; Alvera-Azcarate et al., 2004, Chambers et al., 2004, Church et al., 2004, Smith et al., 1996; Kaplan et al., 1998, 2000). The general approach uses Empirical Orthogonal Empirical Functions (EOF) decomposition (e.g., Preisendorfer, 1988) of the 2-D times series to extract the dominant modes of spatial variability of the signal. These EOF spatial modes are then fitted to the 1-D records to provide reconstructed long term 2-D fields. Different computational variants of the method have been developed to estimate the reconstructed long-term 2-D fields depending on the use of a priori information and data errors (e.g. Kaplan et al., 2000, Church et al., 2004) or not (Smith et al., 1996). Alternative methodology based on a cross-validation technique has also been developed, mainly for reconstruction of incomplete data sets (e.g., Beckers and Rixen, 2003, Alvera-Azcarate et al., 2004).

When applied to long-term past reconstruction, an implicit assumption of the method is the temporal stationarity of the spatial patterns recovered from the EOF modes of the short-term 2-D

* Corresponding author. Tel.: +33 561332922; fax: +33 561253205.
E-mail address: anny.cazenave@cnes.fr (A. Cazenave).

0921-8181/$ - see front matter © 2007 Elsevier B.V. All rights reserved.
doi:10.1016/j.gloplacha.2007.11.007

fields. The spatial covariances obtained from the short-term 2-D fields must indeed be able to describe the covariance over the entire period of the reconstruction (e.g. Smith et al., 1996). If the dominant modes of spatial variability are longer than the time interval covered by the 2-D fields, EOF spatial modes may not be able to capture the relevant signal, leading to uncertainty in the reconstructed fields. In particular the long-term component of the reconstructed signal may be in error. A first purpose of this study is to investigate this question using thermosteric sea level fields. We have at our disposal a 54-year time span (1950–2003) of gridded 2-D thermosteric sea level data (Ishii et al., 2006) which are used as reference for reconstruction tests. Thermosteric sea level is the component of the total sea level that results from thermal expansion of ocean waters (the term steric is used when both thermal expansion and salinity effects are considered, which is not the case here). Note that we do not consider the first 5 yr (1950–1954) where the ocean temperature data are noisy. Thus the useful time span of the thermosteric sea level data set is 1955–2003 (i.e., 49 yr). Then we consider different time spans (<49 yr) for the EOF decomposition and different geographical distributions for the incomplete 1-D data (interpolated at specific locations from the 2-D grids) and determine the time span under which the spatial patterns of the reconstructed 2-D fields are not adequately recovered. For that purpose, we focus on spatial trend patterns and global mean sea level reconstructed over 1950–2003. In a second step, we apply the method to reconstructing 2-D sea level data over 1950–2003, combining 1-D long tide gauge records over 1950–2003, from the Permanent Service for Mean Sea Level (PSMSL, Woodworth and Player, 2003), with 2-D steric sea level EOFs computed over 1955–2003. In effect, recent studies have shown that spatial trend patterns observed by satellite altimetry are well correlated to thermal expansion trends over their overlapping time span (1993–2003) (e.g., Cazenave and Nerem, 2004, Lombard et al., 2005, 2006). We also perform the past sea level reconstruction over 1950–2003 using tide gauge records and 2-D sea level grids from Topex/Poseidon satellite altimetry over 1993–2003. Finally, we use EOFs spatial patterns based on the SODA (Simple Ocean Data Assimilation) global reanalysis over 1958–2001 (Carton et al., 2005) and compare the spatial trend patterns of the reconstruction with the two other cases.

Section 2 briefly summarizes the data used in this study. Section 3 presents the simulation test based on thermosteric sea level data alone. In Section 4 past sea level reconstructions using tide gauge records and EOF spatial patterns for three different cases: (1) thermosteric spatial EOFs over 1955–2003, (2) Topex/Poseidon EOFs over 1993–2003, and (3) SODA-based EOFs over 1958–2001. Conclusions are proposed in Section 5.

2. Thermosteric sea level data; source and spatio-temporal variability

The thermosteric sea level data used in this study are based on in situ ocean temperature data from Ishii et al. (2006). The Ishii data set consists of $1° \times 1°$ gridded temperature data, down to 700 m, at monthly interval for the historical period (1950–2003). These gridded temperature data are based on objective analysis method applied to raw temperature profiles collected by ships, buoys and moorings during the past few decades. The objective analysis allows interpolating data, irregularly sampled in time and space, onto 'global' grids at regular time steps. The computation of the thermosteric sea level from ocean temperature data is performed in two step process: (1) gridded temperature anomalies are first expressed in terms of density anomalies at each standard level using the classical expression for the equation of state of the ocean (Gill, 1982), (2) density anomalies are vertically integrated along the water column at each grid point and each time step (see for example Lombard et al., 2005, 2006). Although the Ishii et al. (2006) data set provides ocean temperatures at monthly interval, here we compute annual averages of thermosteric sea level grids. Thus the temporal resolution of the thermosteric data is 1 yr. In Fig. 1a is presented the spatial trend patterns of the thermosteric sea level over 1950–2003. In the following, Fig. 1a will be called the long-term reference trend map. Fig. 1b shows the Topex/Poseidon satellite altimetry-based sea level trend map over 1993–2003. Annual averaged gridded sea level data have been used to construct Fig. 1b, so that some detail differences may exist between this map and published maps based on 10-day averages (e.g., Cazenave and Nerem, 2004). But this is unimportant for the present study.

Several studies have shown that the spatial trend patterns of altimetry-derived sea level are strikingly similar to those of thermal expansion over their overlapping time span (1993–2005) (Cabanes et al., 2001, Cazenave and Nerem, 2004, Willis et al., 2004, Lombard et al., 2005, 2006). Besides, EOF analyses of thermal expansion and altimetry-derived sea level over this time span show comparable leading modes (both in terms of spatial patterns and principal components). Such results may eventually suggest that over longer time intervals (i.e., several decades), non-uniform spatial patterns of sea level change may also closely follow those of thermal expansion (although in some regions, in particular the North Atlantic, halosteric trends partly compensate thermosteric trends so that the correlation between thermal expansion and observed sea level trends is not perfect; e.g., Antonov et al., 2005).

Lombard et al. (2005) analysed the Ishii et al. (2003) thermosteric sea level data over the period 1950–1998, and showed that the spatial trend patterns of thermal expansion present strong decadal variability. The spatial patterns of thermosteric sea level trend maps computed over successive 10-year periods appear highly variable from one period to another. EOF analysis applied to yearly averaged thermal expansion grids over the 1950–1998 period indicated that the leading modes of variability are driven by large-scale ocean–atmosphere perturbations, i.e., ENSO (El Nino-Southern Oscillation), NAO (North Atlantic Oscillation) and PDO (Pacific Decadal Oscillation) (Lombard et al., 2005, Levitus et al., 2005). For example, the first mode is dominated by the ENSO signature and its principal component (or temporal curve) is highly correlated (90%) with SOI (Southern Oscillation Index; a proxy of ENSO). Subsequent modes display combined signatures of NAO and PDO. Because of the interannual/decadal variability of these large-scale ocean–atmosphere perturbations, the spatial trends patterns of thermosteric sea level computed for different time

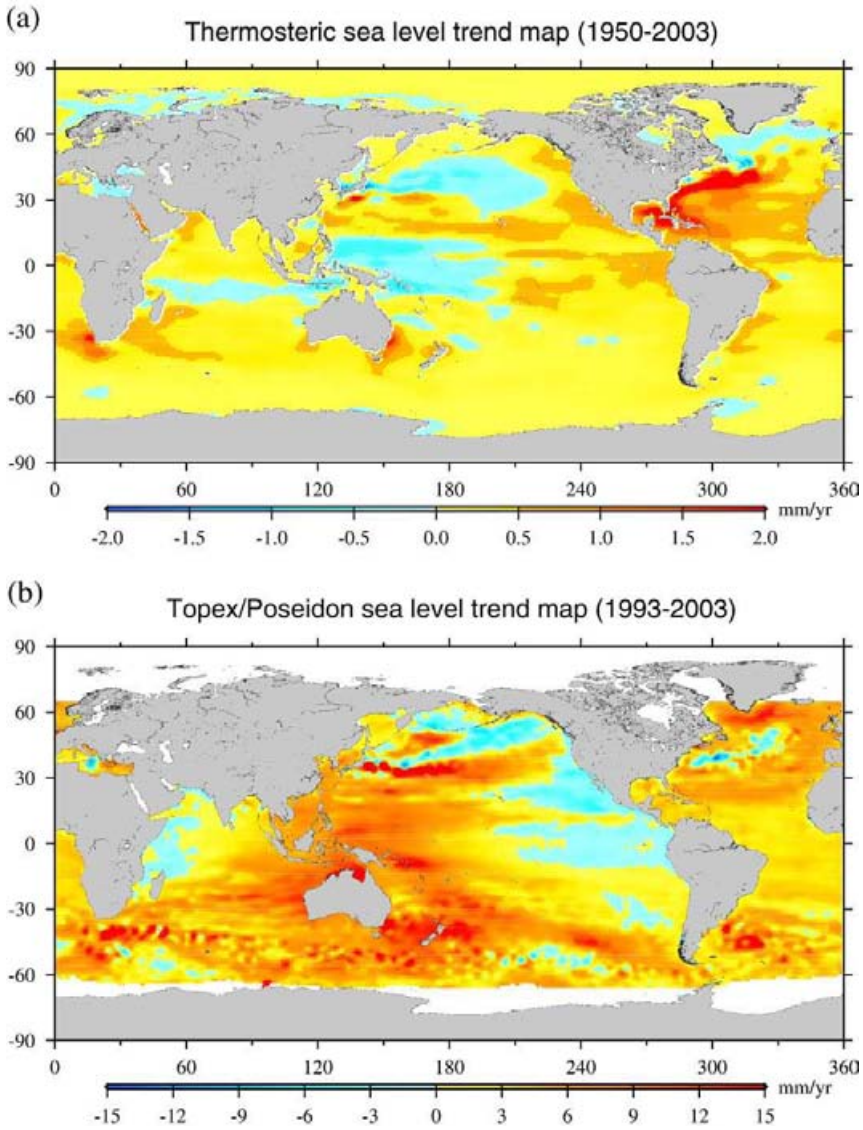

Fig. 1. (a) Spatial thermosteric sea level trends from Ishii et al. (2006) ocean temperature data over 1950–2003. (b) Spatial sea level trends from Topex/Poseidon satellite altimetry over 1993–2003.

spans are expected to be different; and it is indeed what we observe when comparing Fig. 1a and b.

3. Reconstruction tests using thermosteric sea level data

3.1. Method

Here we apply the method developed by Smith et al. (1996) for reconstructing past sea surface temperature. This method assumes that data errors are Gaussian. For the simulation part (first step), this is not a problem since our purpose is to test the influence on the reconstructed long-term fields, of the time length of the short-term 2-D fields considered for computing EOF spatial modes. We briefly summarize below the methodology. Let's call Fo(x,y,t) and Go(x,y,t) observed global gridded short-term fields and sparse, incomplete long-term data respectively, with x, y and t being cartesian coordinates and time. The time span T_F covered by the Fo(x,y,t) fields is basically shorter than that of the reconstructed fields – called T_G – (T_G is the time span covered by the sparse Go(x,y,t) data). For example, Fo(x,y,t) could be the gridded sea level anomalies measured by satellite altimetry since 1993 while Go(x,y,t) could be tide gauges records of several decades length (see for example, Church et al., 2004).

The Fo(x,y,t) function can be decomposed into a series of EOFs modes according to (Preisendorfer, 1988; Toumazou and Cretaux, 2001):

$$F(x,y,t) = \sum [X_n(x,y)e_n(t)]. \quad (1)$$

Where summation is performed from 1 to N. n corresponds to mode rank and is an integer index varying from 1 to N (number

of computed modes). $X_n(x,y)$ are EOF spatial modes and $e_n(t)$ are principal components (temporal functions). The smaller the mode rank n, the larger the variance of the corresponding mode. $X_n(x,y)$ are orthogonal functions. $e_n(t)$ are normalized, with 0–1 as range of variation.

The objective of the reconstruction is to compute global grids of Go(x,y,t) fields over the T_G time interval (with $T_G > T_F$), by combining the spatial information derived from the $X_n(x,y)$ EOF modes (as given by Eq.(1)) and temporal information given by the sparse Go(x,y,t) records. We call $G_R(x,y,t)$ the reconstructed fields, written as:

$$G_R(x,y,t) = \sum [X_n(x,y) Y_n(t)]. \quad (2)$$

In Eq. (2) above, summation is performed from 1 to M, where M is the maximum number of modes considered for reconstructing the 2-D $G_R(x,y,t)$ fields. $Y_n(t)$ are the new principal components computed at each time step t and mode n, through a least-squares fit that minimizes the quantity ε expressed by:

$$\varepsilon = \mathrm{Go}(x,y,t) - \sum [X_n(x,y) Y_n(t)]. \quad (3)$$

Note that $N=(T_F-1)$ and $M \leq N$.

3.2. Simulation; application to thermosteric sea level reconstruction

In this simulation part, we apply the reconstruction method to thermosteric sea level data which cover the period 1950–2003. As mentioned above, the main objective of the thermosteric sea level reconstruction is to test the influence of the temporal coverage of the global gridded data used to compute the EOF spatial patterns (i.e., T_F compared to T_G). To compute the EOF modes, we consider the thermosteric sea level grids over 1955–2003 only. While for this simulation part, we could well have computed the EOF modes over the whole time span covered by the thermosteric sea level grids (1950–2003), for the reconstruction that uses tide gauge data (Section 4), we prefer to exclude the first five years of the thermosteric sea level grids because these are based on incomplete ocean temperature data coverage and thus are more uncertain. The EOF modes computed from the thermosteric sea level grids cover thus the period 1955–2003 (49-year time span, hence 48 modes). In this study, we use the EOF computing code developed by Toumazou and Cretaux (2001).

From the gridded thermosteric sea level fields, we construct two different data sets:

– Data set 1 is a subset of the global gridded data of varying time length T_F (shorter than $T_G=54$ yr). It represents the Fo(x,y,t) data. Different T_F time spans are tested (15, 25, 35, 49 yr).
– Data set 2 represents the sparse Go(x,y,t) data. This data set is constructed by interpolating at specific (x,y) locations the global 1°×1° thermosteric sea level grids over the entire 54-year period to produce 1-D records. Different geographical distributions are tested (see Section 3.3).

As a control test, we first compute reconstructed thermosteric sea level fields assuming $T_F=49$ yr and $T_G=54$ yr, using the total grid meshes of the 2-D (1°×1°) fields (i.e., 41 141 points) and the whole set of computed EOFs modes (equal to 48). There are different ways to assess the reliability of the reconstructed fields, e.g., by comparing annual averages of original and reconstructed fields, by comparing trend maps computed over different time spans, by comparing time series of original and reconstructed fields at specified locations, etc. In this study all these aspects have been considered. But we essentially present results of spatial trend patterns as well as global mean sea level curves. For the control test, we checked that both initial and reconstructed fields are identical. The reconstructed steric sea level trend map computed for the control test over 1950–2003 is almost identical to the long-term reference trend map (Fig. 1a); Thus it is not shown.

3.3. Simulation; Test 1. Influence of the geographical distribution of the sparse Go(x,y,t) data

The first series of tests investigates the influence of the geographical distribution of the sparse Go(x,y,t) data. In this simulation, we do not use tide gauge records. Rather we construct Go(x,y,t) records by interpolating the Fo(x,y,t) global grids at selected locations (x,y) (we construct the Go time series using the Fo data at the grid mesh that includes the x,y point). The length of the Go(x,y,t) time series is 54 yr (1950–2003). The whole set of EOF modes ($M=48$) computed from the Fo(x,y,t) grids are used for the reconstruction. For the geographical distribution of the Go(x,y,t) time series, we consider 4 cases:

(1) : 41141 regularly distributed grid meshes of 1°×1° (control test)
(2) : 10331 regularly distributed grid meshes of 2°×2°
(3) : 175 regularly distributed grid meshes of 16°×16°
(4) : 118 sites irregularly distributed data points. The latter distribution (presented in Fig. 2) corresponds to real tide gauge sites used in Section 4 for past sea level reconstruction.

The spatial trend maps computed from the reconstructed fields over 1950–2003 for each of the four site distributions listed above show very similar results (differences if any are undetectable). It is worth noting that case 4 (real tide gauge site distribution) works as well as cases with more uniform coverage. This is so because, in this test, the lack of spatial information due to the highly non-uniform ‘tide gauge’ distribution is compensated by the long-term (here 49 yr) temporal coverage of the EOF spatial modes. Similarly, the global mean thermosteric sea level curves for the 4 cases show no difference.

3.4. Simulation; Test 2. Influence of the number of EOFs modes used for the reconstruction

A second series of tests consists of determining the optimal number M of EOFs modes used for the reconstruction. For

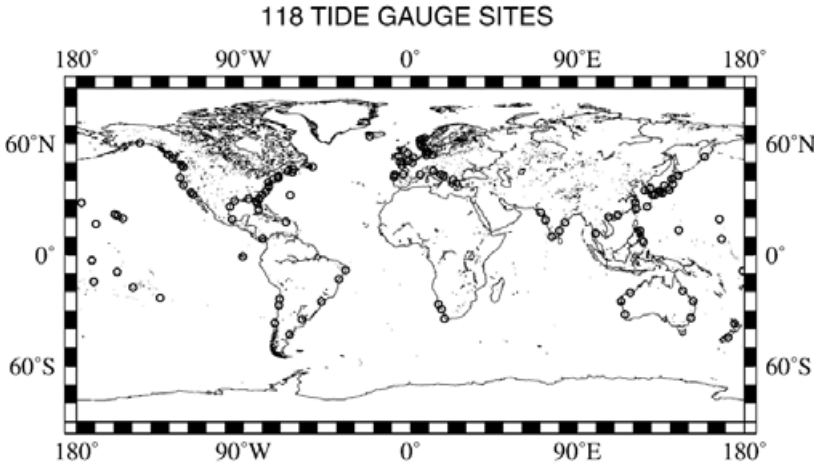

Fig. 2. Distribution of the 118 tide gauge sites considered in this study.

these tests, we consider the Go(x,y,t) geographical distribution of case 4 (118 sites). In this series of tests, the EOF spatial modes are computed with the 49-year long Fo(x,y,t) global grids. The trend maps of the reconstructed fields over 1950–2003 computed with $M=10$, $M=20$ and $M=48$ modes show very little difference between each other and are quite comparable to the long-term reference trend map shown in Fig. 1a. For that reason they are not shown. The global mean reconstructed steric sea level curves for the three M values are also very similar to the reference curve, even if, the larger the number of modes, the closer to the reference the reconstructed trend map and curve.

3.5. Simulation; Test 3. Influence of the temporal coverage TF of the Fo(x,y,t) functions

The most crucial test concerns the length of the 2-D gridded Fo(x,y,t) function used to compute the $X_n(x,y)$ EOF spatial modes, hence the T_F value. This test, we consider the 118 tide gauges sites for the Go(x,y,t) data. The number of modes M used for the reconstruction is dependent on T_F, with $M \leq (T_F - 1)$. A series of tests has been performed in varying the time span T_F for the EOF computation between 15 yr and 49 yr at yearly interval. In Fig. 3a are presented trend maps based on the thermosteric sea level reconstruction over 1950–2003 and computed for different T_F values (16, 30 and 49 yr). Note that here we use the same M value for comparing the different cases. Hence we use $M=15$ (i.e., the first 15 modes for the reconstruction) because this is the maximum number of modes permitted for $T_F=16$ yr. The original (reference) trend map is also shown. Looking at Fig. 3a, we note that cases with $T_F=16$ yr and $T_F=30$ yr poorly reproduce the reference trend map, whereas for $T_F=49$ yr, the agreement is good. To see this differently, Fig. 3b shows the reconstructed global mean steric sea level curves for the 3 cases ($T_F=16$, 30 and 49 yr), as well as the long-term reference curve. We note in particular that for $T_F=16$ yr the reconstructed curve departs significantly from the reference.

3.6. Conclusions of the simulation

The series of tests presented in this section can be interpreted as follow:

(1) The influence of the number of sites is negligible, as far as the time span covered by the 2-D fields used for computing the EOFs is not significantly different from the time interval of the reconstruction
(2) The number of EOF modes considered for reconstructing the fields is not a crucial parameter if the time span covered by the 2-D fields used for computing the EOFs is not significantly different from the time interval of the reconstruction. However, we note that this parameter plays a slightly larger role than the site distribution.
(3) The most crucial parameter for the reconstruction is the relative time intervals covered by the 2-D fields used to compute the EOF spatial patterns (T_F value) and by the reconstruction.

The tests performed in the simulation indicate that the reconstructed fields agree best with the reference data when the EOF spatial patterns are computed over the longest time span. Depending on the level of acceptable error, this constraint may be somewhat relaxed. However from Fig. 3b, we note that the reconstructed global mean steric sea level curve with $T_F=30$ yr and $T_F=16$ yr agree well with the reference curve over the last 30 yr and 16 yr respectively, but show significant discrepancy earlier. Except for the most recent years (well covered by the observations), the interannual/decadal fluctuations of the reconstructed curves are also degraded in the distant past.

4. Reconstruction of past sea level using tide gauges and different sources of spatial EOFs

In this section, we adapt the method discussed above to past sea level reconstruction over the period 1950–2003, taking into account the conclusions of the reconstruction tests presented in Section 3.6

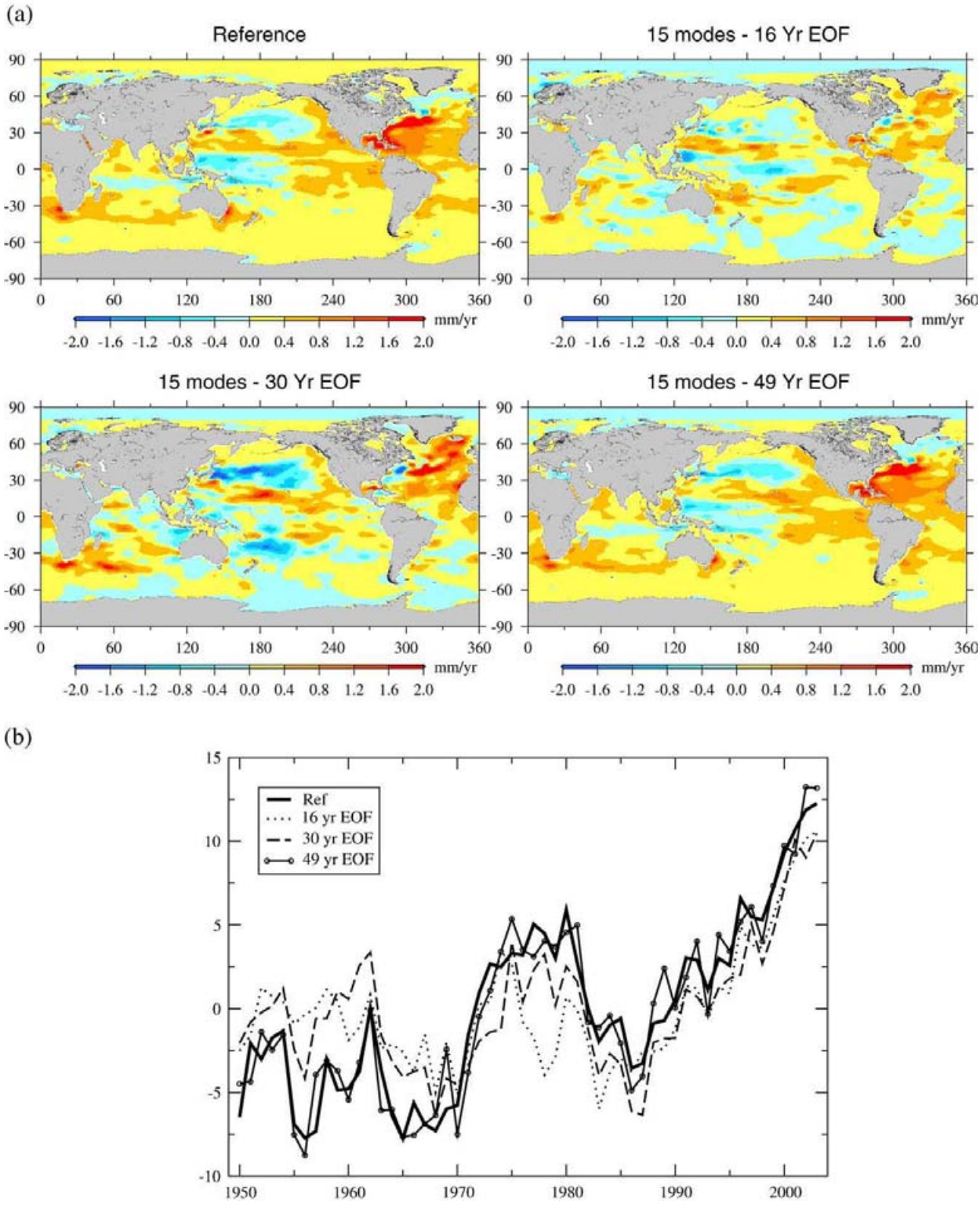

Fig. 3. (a) Influence of the temporal coverage of the EOF spatial patterns (T_F time interval of 16, 30 and 49 yr) on the reconstructed trend patterns computed over 1950–2003. (b) Influence of the temporal coverage of the EOF spatial patterns (T_F time interval) on the reconstructed global mean thermosteric sea level. Reference curve (black). Reconstructed curves with T_F = 16 yr (red), 30 yr (blue) and 49 yr (green).

We use RLR (Revised Local Reference) tide gauge records (annual averages) from the Permanent Service for Mean Sea Level (PSMSL, Woodworth and Player, 2003). From the whole set of records available, we select 118 sites whose distribution is shown in Fig. 2. Criteria considered for the selection are temporal coverage of individual records (gaps larger than 5 yr and total

record lengths shorter than 25 yr lead to rejection) and site stability (sites with known stability problems or located in highly tectonic active areas are rejected). We also reject records with unambiguous discontinuities. Another criteria consist of comparing records of nearby sites. Records presenting significant differences with the regional average are not included. The tide gauges data are corrected for vertical motion of the crust in response to glacial isostatic adjustment (GIA). For that purpose, we use the ICE-4G model of Peltier (2001). No inverted barometer correction is applied (Several studies showed that the inverted barometer trend signal is small; e.g., Ponte, 2006. For the purpose of the present study, neglecting this correction has little consequence).

One problem with tide gauges records is that measurements are made in local datum that vary from one site to another. This problem can be overcome by working with the derivatives (e.g., Holgate and Woodworth, 2004, Holgate, 2007). However this approach cannot be used here. Thus we chose another approach (e.g., Kuo et al., in press), which can be described as follows:

(1) We compute a linear trend for each record using the total record of reliable data.
(2) When a given time series does not cover the whole 54-year time span, missing data are reintroduced through 'virtual' data regularly distributed along a straight line with same linear trend as computed in (1).
(3) A mean reference value is computed for each record. It corresponds to sea level value at the middle of the time span (i.e., 1975). This mean value is thus subtracted to each sea level record.
(4) The above procedure provides complete temporal coverage for each of the 118 records and a common (arbitrary) origin (at mid-epoch of the reconstruction).

4.1. Reconstruction using thermosteric spatial EOFs over 1955–2003

We first perform the reconstruction using the spatial EOFs from the global thermosteric sea level grids over 1955–2003 using thermosteric sea level grids over 1955–2003.

This first reconstruction has the following characteristics:

– Real tide gauge records at the 118 sites presented in Fig. 2.

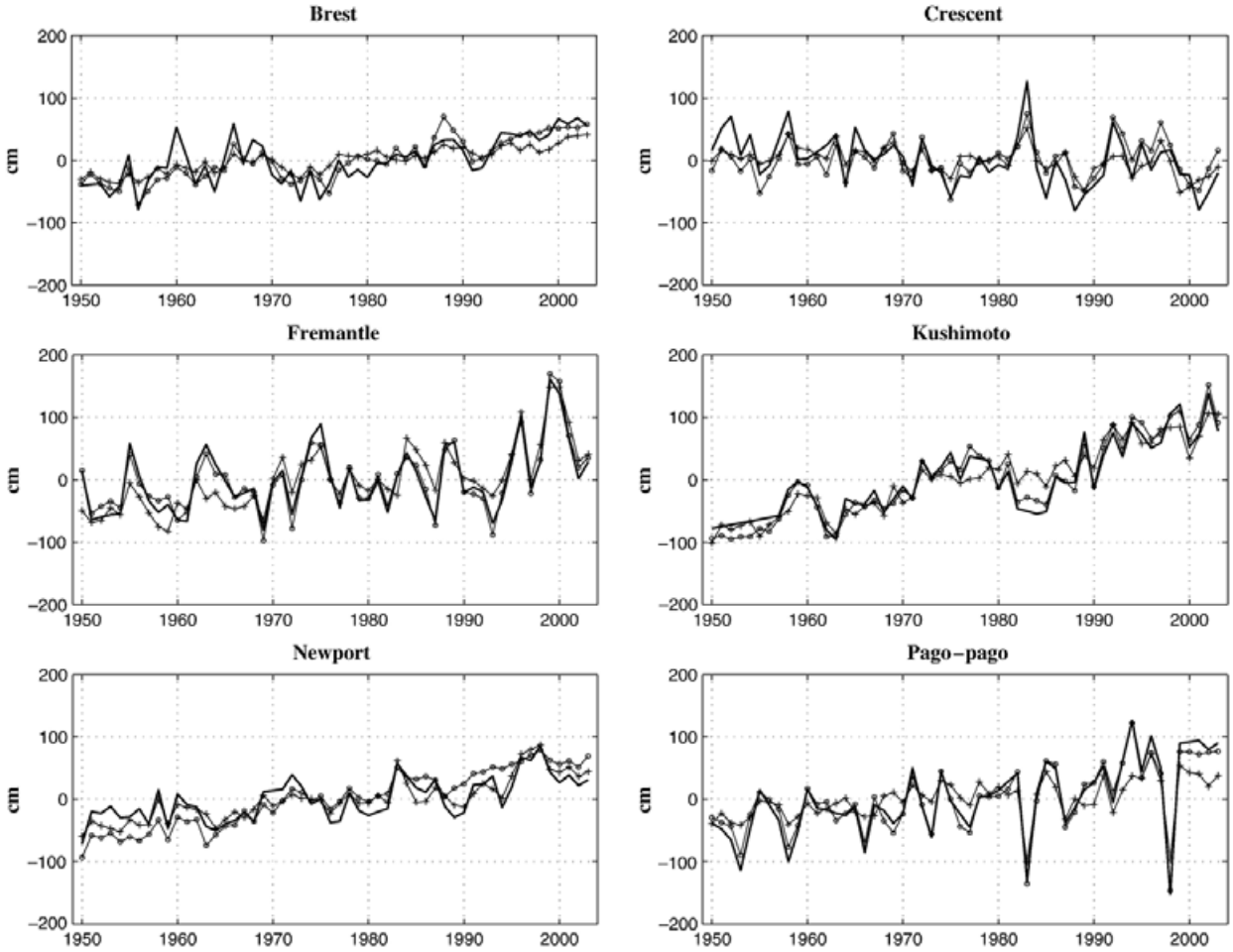

Fig. 4. Reconstructed (using thermosteric EOFs over 1955–2003 and Topex/Poseidon EOFs over 1993–2003) and original sea level curves at 6 tide gauge sites: Brest, Crescent, Fremantle, Kushimoto, Newport and PagoPago. The PSMSL curve is in black. The reconstructed curves with steric EOFs is in green while the reconstructed curve with Topex/Poseidon EOFs is in red. Unit: mm.

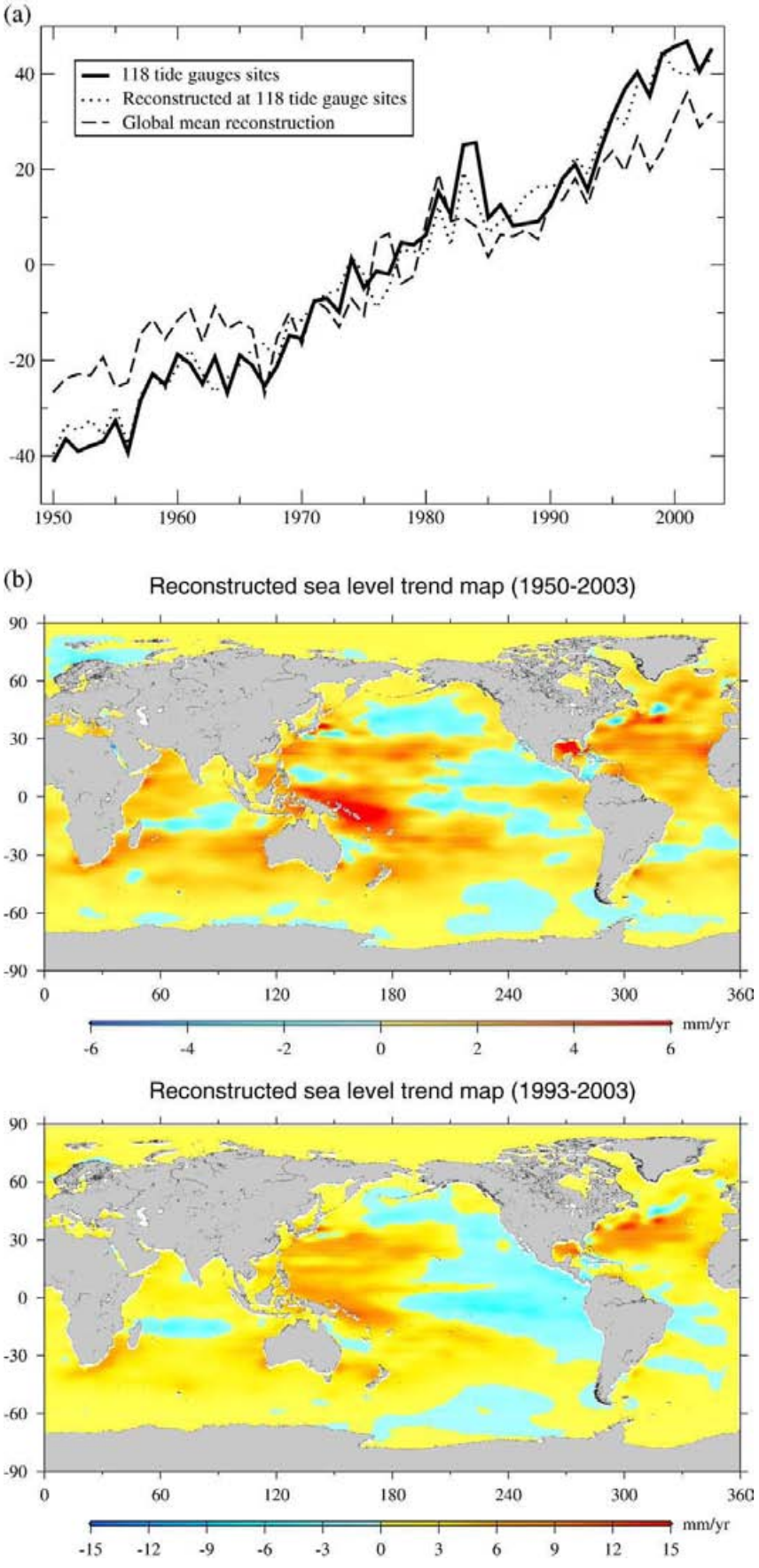
(a)
118 tide gauges sites
Reconstructed at 118 tide gauge sites
Global mean reconstruction
40
20
0
-20
-40
1950
1960
1970
1980
1990
2000
(b)
Reconstructed sea level trend map (1950-2003)
90
60
30
0
-30
-60
-90
0
60
120
180
240
300
360
mm/yr
-6
-4
-2
0
2
4
6
Reconstructed sea level trend map (1993-2003)
90
60
30
0
-30
-60
-90
0
60
120
180
240
300
360
mm/yr
-15
-12
-9
-6
-3
0
3
6
9
12
15

– EOF spatial patterns computed from 49 yr (1955–2003) of 2-D annual thermosteric fields from Ishii et al. (2006) (T_F=49 yr).
– Reconstruction based on 48 modes (M=48, T_G=54 yr).

Fig. 4 shows reconstructed sea level time series (green curves) at six tide gauge sites located in different oceanic regions: Brest (48.4°N, 4.5°W, Northeast Atlantic), Crescent (41.75°N, 124.2°W, Northeast Pacific), Fremantle (32°S, 115.7°E, South Pacific), Kushimoto (33.5°N, 135.8°E, Northwest Pacific), Newport (41.5°N, 71.3°W, Northwest Atlantic) and PagoPago (14.3°S, 170.7°W, Central Pacific). For each site, the original sea level record (from PSMSL) is shown (black curve). We note that the reconstruction reproduces well the sea level interannual/decadal oscillations (also true at all 118 sites). However, for a number of sites, the reconstructed mean trend appears underestimated. We have checked that the underestimation affects essentially southern hemisphere sites and a few sites above 50° north latitude. No doubt that this is due to the lack of thermosteric signal (i.e., lack of in situ hydrographic data) in these remote regions. Thus in regions with large data gaps, the reconstruction appears unable to fabricate the long-term component of the signal.

The reconstructed global mean sea level curve is shown in Fig. 5a. Also shown on this plot, the 'original' curve based on the PSMSL data at the 118 sites and the reconstructed curve at the 118 sites. In the latter two cases, regional averaging has been performed to avoid overweighting of some regions (i.e., North European stations, stations located along the Eastern North American coast and in the Western North Pacific). The global mean reconstructed and original curves agree well on interannual/decadal time scales. However, the rate of rise of the reconstructed global mean sea level (1.1 +/− 0.05 mm/yr) is lower than the PSMSL trend (1.6 +/− 0.05 mm/yr). The reconstructed curve at the 118 tide gauges has a trend of 1.55 +/− 0.04 mm/yr, only slightly lower than the PSMSL curve. The lower trend of the reconstructed global mean sea level is likely a result of the lack of signal in the steric fields as discussed above. However we cannot exclude that the global mean trend really differs from that the average trend at the 118 tide gauge sites, in view of the important regional variability in sea level trends.

We have computed the spatial trend patterns over 1950–2003 from annual fields of the reconstructed sea level (reconstruction with 10, 20, 30 and 48 modes). We note that the lower the M value (e.g., M=10), the smoother the reconstructed trend map. While the large-scale features are comparable in the four cases, large M values introduce small-scale, high-amplitude variability. This result seems in contradiction with the simulation results which showed little difference when M varied. One explanation is that the reconstruction that combines data of different types (tide gauges records and steric spatial patterns) becomes quite sensitive to data noise. In Fig. 5b are presented the trend patterns computed from the whole set of reconstructed grids over two periods: 1950–2003 and 1993–2003 with M=10. The 1950–2003 trend map is significantly different from the reference steric trend map presented in Fig. 1a. But it should be noted that the reconstructed trend map is supposed to represent the total sea level (not the thermosteric contribution alone). Some features present in the thermosteric sea level trend map (Fig. 1a) are also seen in Fig. 5b (e.g., in the Northwest Atlantic, Gulf of Mexico, North Pacific, North Indian ocean). But in some other regions, the patterns are quite different (e.g., central western Pacific, where the thermosteric trend map displays a prominent negative trend while a positive trend is observed in the reconstructed map). The lower panel of Fig. 5b shows the reconstructed trends computed over 1993–2003. Comparing with the Topex/Poseidon trend map (Fig. 1b), we note very good agreement in terms of regional trend distribution, but in general lower amplitude. We note that except for lower amplitudes in general, the long-term (1950–2003) reconstructed trend map (Fig. 5a) is not that different from the short-term (1993–2003) one (Fig. 5b).

4.2. Reconstruction using Topex/Poseidon spatial EOFs over 1993–2003

In a second case, we have performed the reconstruction using the Topex/Poseidon annual grids over 1993–2003 (11 yr) to compute the spatial EOF fields. In this case, the number of 'useful' EOFs is only 10. As above, we reconstruct the global sea level over the 1950–2003 time span, using the 118 tide gauge records. The reconstructed global mean sea level curve (averaged between 65°N and 65°S) is shown in Fig. 6a (the mean tide gauge-based sea level as well as the reconstructed mean curve at the 118 sites are also shown — after geographical averaging). We can see that unlike case 1 (49 yr of thermosteric sea level EOFs), the reconstructed mean curve agrees well with the observed one. The trend of the reconstructed global mean curve is 1.4 +/− 0.05 mm/yr, only slightly lower than the tide gauge trend (1.6 +/− 0.05 mm/yr). In addition the reconstructed sea level trend at the 118 sites (1.7 +/− 0.05 mm/yr) matches well with the observed trend. In Fig. 4 are shown the reconstructed sea level curves (using Topex/Poseidon EOFs) at the 6 tide gauge sites. Compared to the reconstruction using the thermosteric EOFs, the interannual/decennal fluctuations are less well reproduced. This may be an indication that 11 yr of spatial EOFs only partially captures the decadal variability. The spatial trend map of the reconstructed sea level is presented in Fig. 6b for two time spans: 1950–2003 and 1993–2003. The 1993–2003 trend map agrees quite well with the Topex/Poseidon altimetry-based trend map (see Fig. 1b). For the longer period (1950–2003), the trend map differs from the reconstruction trend map based on thermosteric fields over 49 yr

Fig. 5. (a) Reconstruction with thermosteric EOFs over 1955–2003: reconstructed global mean sea level curve (green); 118 tide gauge sites average (red). PSML curve (black). Unit: mm. (b) Upper panel: reconstructed sea level trend map over 1950–2003 with thermosteric EOFs over 1955–2003. Lower panel: reconstructed sea level trend map over 1993–2003 with thermosteric EOFs over 1955–2003. Unit: mm/yr.

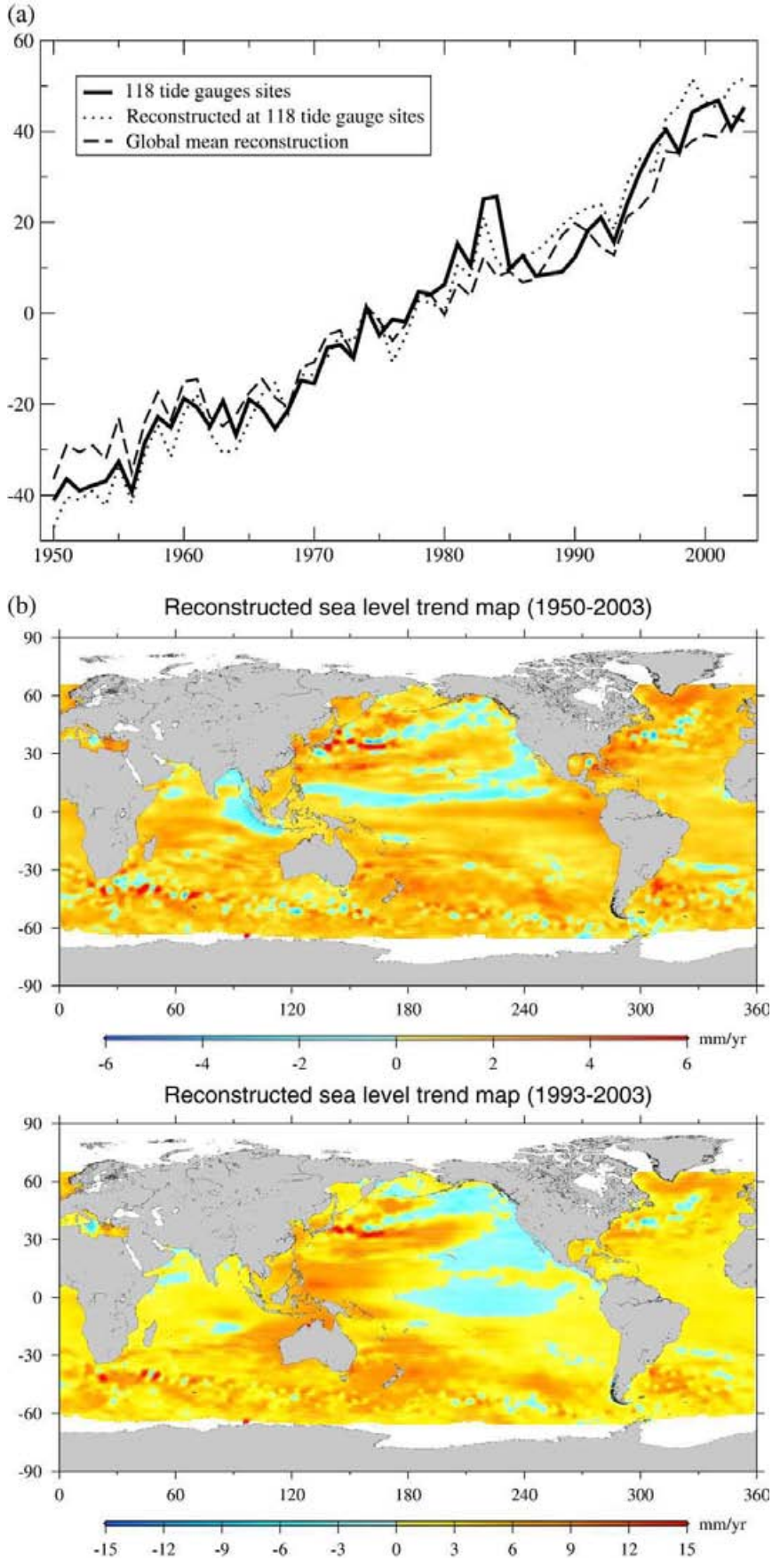
(a)
118 tide gauges sites
Reconstructed at 118 tide gauge sites
Global mean reconstruction
60
40
20
0
-20
-40
1950
1960
1970
1980
1990
2000
(b)
Reconstructed sea level trend map (1950-2003)
90
60
30
0
-30
-60
-90
0
60
120
180
240
300
360
mm/yr
-6
-4
-2
0
2
4
6
Reconstructed sea level trend map (1993-2003)
mm/yr
-15
-12
-9
-6
-3
0
3
6
9
12
15

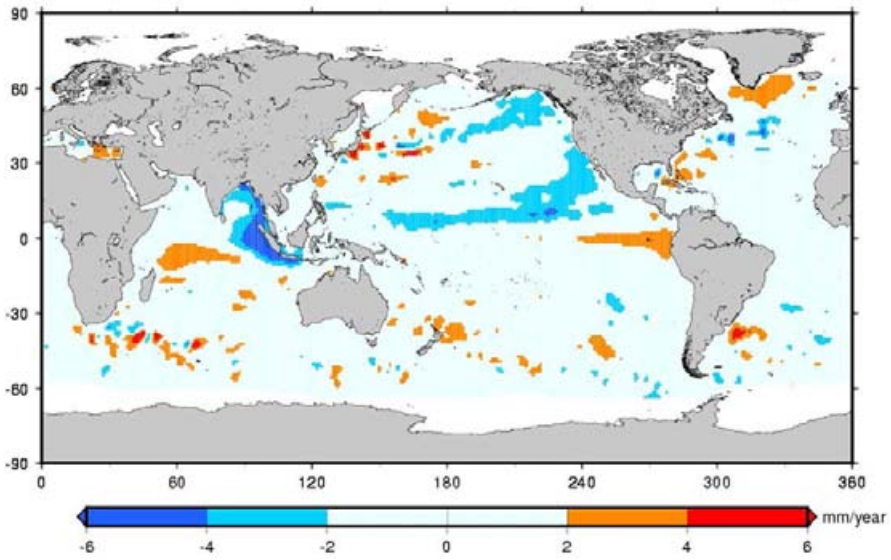

Fig. 7. Difference between the Topex/Poseidon-based reconstruction trend map over 1950–2003 and Church et al. (2004) trend map over 1950–2000. For both maps, an average trend has been removed.

(Fig. 5a), the latter being much smoother. However in some regions (northern Pacific, southern ocean), features are roughly similar (at least in terms of sign). Using the Topex/Poseidon EOFs, we compared reconstructed sea level trend maps over successive time spans: 1993–2003 (shown in Fig. 6b, lower panel), 1983–2003, 1973–2003, 1963–2003 and 1950–2003 (shown in Fig. 6b, upper panel). We found that the trend maps only slightly evolve through time. At this step, it is difficult to say if this is real or if this is due to the inability of the short EOFs time span in capturing the decadal variability. Further studies are needed to clarify this behaviour.

We have compared the Topex/Poseidon-based reconstruction over 1950–2003 with the Church et al.'s (2004) sea level reconstruction over 1950–2000. These authors also used Topex/Poseidon EOFs, but developed a more sophisticated reconstruction method accounting for a priori information and data errors (e.g., Kaplan et al., 2000). Moreover, they use a much larger number of tide gauges records (of variable lengths) than in the present study. At first look, their reconstruction spatial trend map (Fig. 15 of their paper) seems quite different from ours. However, comparing the two trend maps (mean trend removed in each case) shows that the differences are rather localized. The largest differences are noticed in the eastern Indian Ocean (Golf of Bengal and Andaman Sea), eastern equatorial and north Pacific. This is illustrated in Fig. 7 which shows the difference between the two reconstruction trend maps (over the past ~50 yr). It is likely that using more tide gauges and introducing constraints on the solution (as done in Church et al., 2004) may provide better results and may explain the difference with our trend map.

4.3. Reconstruction using SODA reanalysis over 1958–2001

We have used the Simple Ocean Data Assimilation (SODA, version 1.2; Carton et al., 2005) over 1958–2001, to compute spatial EOFs and perform the reconstruction with the same set of tide gauge records as described above. Using dynamic height data from the SODA reanalysis for the spatial EOFs should be superior than to the other two cases discussed above (i.e., thermosteric sea level and Topex/Poseidon). In effect the SODA data set is much longer in time (44 yr) than the Topex/Poseidon data set, and compared to Ishii et al. data set, it includes the halosteric effect in addition to thermal expansion. The reconstruction trend map with SODA EOFs over 1950–2003 is presented in Fig. 8 (left hand side upper panel). Note that the SODA dynamic height data used here do not include any mean trend, so that we only investigate the detrended spatial patterns. We first checked that the reconstructed sea level trend map over 1950–2003 agrees reasonably well with the 'original' trend map computed with the 44-year long SODA sea surface height data (not shown). Then we computed the SODA-based spatial EOFs over different time spans shorter than 44 yr. In Fig. 8 are shown reconstruction trend maps over 1950–2003 based on 21 yr (1981–2001) and 11 yr (1991–2001) of SODA EOFs. In Fig. 8 is also shown, for comparison, the Topex/Poseidon-based reconstructed spatial trend map over 1950–2003 (after removing the mean trend for homogeneity with the SODA-based results). It is interesting to see that the shorter the EOFs time span, the closer the SODA reconstruction trend map to the Topex/Poseidon-based trend map. It is particularly worth

Fig. 6. (a) Reconstruction with Topex/Poseidon EOFs over 1993–2003: reconstructed global mean sea level curve (green); 118 tide gauge sites average (red). PSML curve (black). Unit: mm. (b) Upper panel: reconstructed sea level trend map over 1950–2003 with Topex/Poseidon EOFs over 1993–2003. Lower panel: reconstructed sea level trend map over 1993–2003 with Topex/Poseidon EOFs over 1993–2003. Unit: mm/yr.

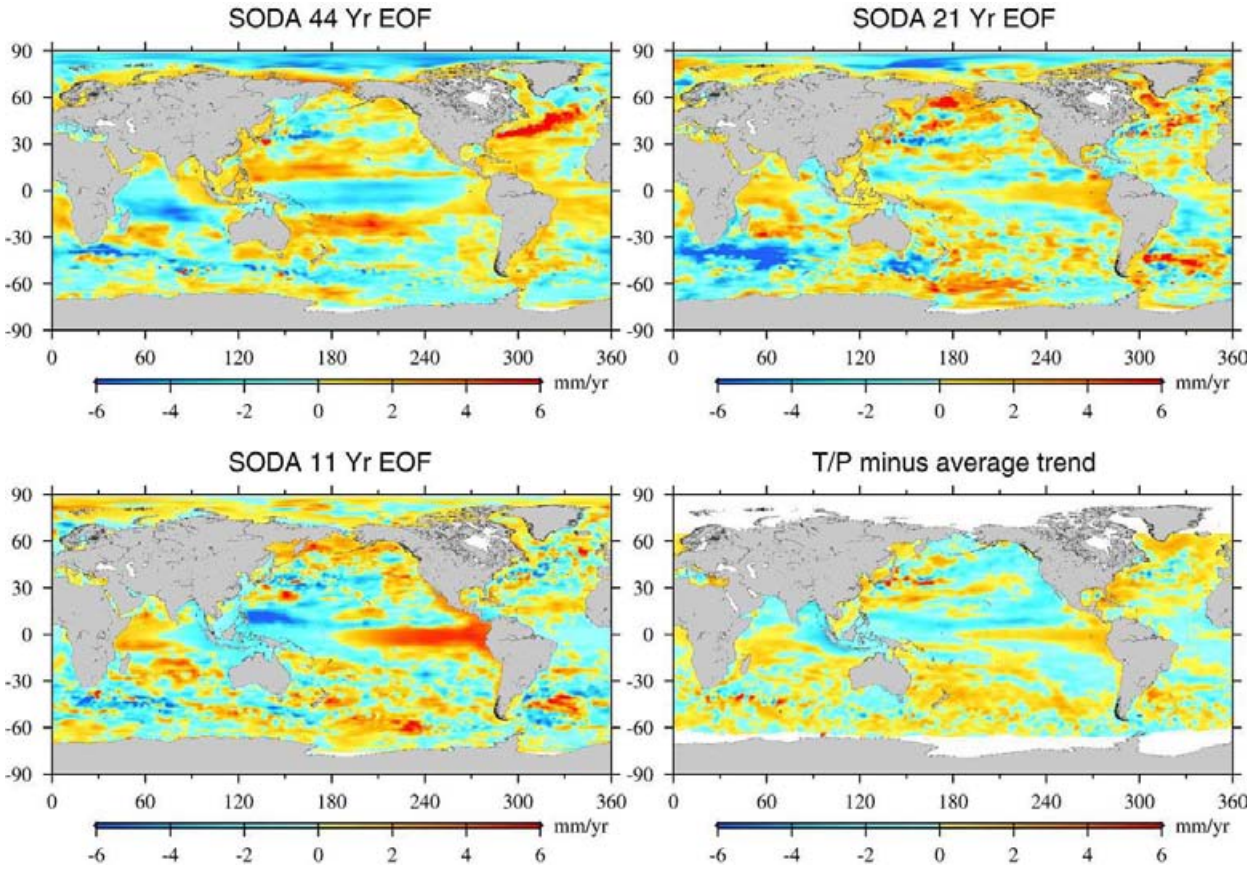

Fig. 8. Reconstruction based on SODA EOFs computed over 44 yr (left upper panel), 21 yr (right upper panel) and 11 yr (left lower panel). The spatial patterns of the Topex/Poseidon reconstruction (mean trend removed) is shown in the right lower panel. Unit: mm/yr.

noticing that with 21 yr of SODA EOFs, the reconstruction poorly agrees with the 44-year EOFs case (left hand side upper panel) while resembling much to the 11-year EOFs case and Topex/Poseidon-based reconstruction trend map.

5. Conclusions

In this study, we have tested the influence of several parameters on reconstructed sea level fields (and their spatial trend patterns) in a simulation that used thermosteric sea level grids available over 1955–2003. The reconstruction has been performed over 1950–2003 for different cases. As expected, the most important parameter is the time length covered by the 2-D fields used to compute the EOF spatial patterns (T_F value). The simulation results indicate that for T_F values shorter than ~30 yr the reconstructed fields (and especially the trend map) does not satisfactorily reproduce the spatial variability. Moreover, the reconstructed global mean trend is significantly lower than the reference trend.

In light of the simulation results, we have first performed a past sea level reconstruction over 1950–2003 using 118 tide gauge records from the PSMSL and EOF spatial patterns computed over 49 yr (1955–2003) from thermosteric sea level grids (Ishii et al., 2006). The global mean reconstructed sea level curve agrees well at interannual/decadal time scales with the observed sea level. But the reconstructed mean curve has a smaller slope than the 'real' slope. One possibility is that the too smooth thermosteric sea level fields (due to sparse data coverage) is responsible for the lower reconstructed signal. The reconstructed trend map (computed over 1950–2003) significantly differs from the reference thermosteric trend map. The use of thermosteric sea level fields for computing the EOFs may not be the best strategy. In effect, the thermosteric sea level data suffer inhomogeneous coverage both in space and time, especially in the southern ocean (e.g., Ishii et al., 2003; Levitus et al., 2005), thus only poorly represent the geographical variability of the 'real' sea level. Moreover, regional variability in sea level results from both thermal expansion and halosteric effects. Thus using only the thermosteric component for the spatial EOFs may bias the reconstruction. We have also reconstructed sea level fields over 1950–2003 using the short Topex/Poseidon altimetry record (over 1993–2003) for computing the spatial EOFs. We note very good agreement between the tide gauge sea level curve and mean rate over 1950–2003. The reconstructed sea level trend map appears somewhat different from the previous case, although in some regions, some features look similar. In both cases (use of thermosteric EOFs over 49 yr and Topex/Poseidon EOFs over 11 yr), the

reconstructed sea level trend map over 1993–2003 agrees well with Topex/Poseidon observed trend map. Finally we used the SODA-based spatial EOFs. The reconstructed spatial trend map (mean trend removed) over 1950–2003 based on 44 yr of SODA EOFs data poorly agrees with the reconstruction based on thermosteric EOFs. These results are somewhat disappointing since the use of different EOFs over different time spans lead to different results. We expected that the use of ~50 yr of quasi global thermosteric sea level fields for computing spatial EOFs would be a good alternative to the still short altimetry data record. However, the local and global mean rates of rise of the reconstructed sea level is clearly too small compared to tide gauge-based estimates, even if the interannual/decadal variability is well reproduced, and the 50-year reconstruction trend map seems poorly constrained. The use of Topex/Poseidon EOFs appears less performant for reproducing past decadal variability but is superior for the global mean sea level trends. The spatial trend patterns of the 50-year reconstruction are suspect as they only marginally differ from the 1993–2003 trend patterns. Possibly the use of ocean circulation model outputs, such as SODA, would be the best alternative as they provide more and more reliable sea level information over the past decades. Future work should explore this possibility as more and more OGCMs results, with and without data assimilation, become available.

Acknowledgements

We thank C.K Shum and another anonymous reviewer for comments that helped us to improve the original manuscript.

References

Alvera-Azcarate, A., Barth, A., Rixen, M., Beckers, J.M., 2004. Reconstruction of incomplete oceanographic data sets using empirical orthogonal functions: applications to the Adriatic sea surface temperature. Ocean Model. doi:10.1016/j.ocemod.2004.08.001.

Antonov, J.I., Levitus, S., Boyer, T.P., 2005. Steric variability of the world ocean, 1955–2003. Geophys. Res. Lett. 32 (12), L12602.

Beckers, J.M., Rixen, M., 2003. EOF calculations and data filling from incomplete oceanographic data sets. J. Atmosph. And Ocean Techn. 20, 1839–1856.

Cabanes, C., Cazenave, A., LeProvost, C., 2001. Sea level rise during past 40 years determined from satellite and in situ observations. Science 294, 840–842.

Carton, J.A., Giese, B.S., Godsky, S.A., 2005. Sea level rise and warming of the oceans in the Simple Ocean Data Assimilation (SODA) ocean reanalysis. J. Geophys. Res. 110, C09006. doi:10.1029/2004JC002817.

Cazenave, A., Nerem, R.S., 2004. Present-day sea level change: observations and causes. Rev. Geophys. 42, RG3001. doi: 8755-1209/04/2003RG000139.

Chambers, D.P., Mehlhaff, C.A., Urban, T.J., Fujii, D., 2004. Low frequency variations in global mean sea level; 1950–2000. J. Geophys. Res. 107 (C4), 3026. doi:10.1029/2001JC001089.

Church, J.A., White, N.J., Coleman, R., Lambeck, K., Mitrovica, J.X., 2004. Estimates of the regional distribution of sea-level rise over the 1950 to 2000 period. J. Climate 17 (13), 2609–2625.

Gill, A.E., 1982. Atmosphere–Ocean Dynamics. Academic Press, San Diego. 662 pp.

Holgate, S.J., Woodworth, P.L., 2004. Evidence for enhanced coastal sea level rise during the 1990s. Geophys. Res. Lett. 31, L07305. doi:10.1029/2004GL019626.

Holgate, S.J., 2007. On the decadal rates of sea level change during the twentieth century. Geophys. Res. Lett. 34, L01602. doi:10.1029/2006GL028492.

Ishii, M., Kimoto, M., Kachi, M., 2003. Historical ocean subsurface temperature analysis with error estimates. Mon. Weather Rev. 131, 51–73.

Ishii, M., Kimoto, M., Sakamoto, K., Iwasaki, S.I., 2006. Steric sea level changes estimated from historical ocean subsurface temperature and salinity analyses. J. Oceanography 62, 155–170.

Kaplan, A., Kushnir, Y., Cane, M.A., 2000. Reduced space optimal interpolation of historical marine sea level pressure: 1854–1992. J. Climate 13, 2987–3002.

Kaplan, A., Cane, M.A., Kushnir, Y., Clement, A.C., Blumenthal, M.B., Rajagopalan, B., 1998. Analyses of global sea surface temperatures 1856–1991. J. Geophys. Res. 103, 18,567–18,589.

Kuo, C., Shum, C.K., Braun, A., Cheng, K., Yi, Y., in press. Vertical motion determined using satellite altimetry and tide gauges, satellite altimetry over land and coastal zones: challenges and applications, special issue Terrestrial, Atmospheric and Oceanic sciences (TAO).

Levitus, S., Antonov, J.I., Boyer, T.P., 2005. Warming of the world ocean, 1955–2003. Geophys. Res. Lett. 32, L02604. doi:10.1029/2004GL021592.

Lombard, A., Cazenave, A., Le Traon, P.Y., Ishii, M., 2005. Contribution of thermal expansion to present-day sea level change revisited. Glob. Planet. Change 47, 1–16.

Lombard, A., Cazenave, A., Cabanes, C., Guinehut, S., Le Traon, P.Y., 2006. Perspectives on present-day sea level change. Ocean Dyn. 56, 445–451. doi:10.10007/s10236-005-0046-x.

Peltier, W.R., 2001. Global glacial isostatic adjustment and modern instrumental records of relative sea level history. In: Douglas, B.C., Kearney, M.S., Leatherman, S.P. (Eds.), Sea Level Rise, History and Consequences. Academic Press, San Diego, pp. 65–95.

Ponte, R.M., 2006. Low frequency sea level variability and the inverted barometer effect. J. Atmos. Ocean. Technol. 23 (4), 619–629.

Preisendorfer, R.W., 1988. Principal Component Analysis in Meteorology and Oceanography. Developments in Atmospheric Science, vol.17. Elsevier. 425 pp.

Smith, T.M., Reynolds, R.W., Livezey, R.E., Stokes, D., 1996. Reconstrution of historical sea surface temperatures using Empirical Orthogonal Functions. J. Climate 9, 1403–1420.

Toumazou, V., Cretaux, J.F., 2001. Using a Lanczos eigensolver in the computation of Empirical Orthogonal Functions. Mon. Weather Rev. 129, 1243–1250.

Willis, J.K., Roemmich, D., Cornuelle, B., 2004. Interannual variability in upper-ocean heat content, temperature and thermosteric expansion on global scales. J. Geophys. Res. 109, C12036. doi:10.1029/2003JC002260.

Woodworth, P.L., Player, R., 2003. The permanent service for mean sea level: an update to the 21st century. J. Coastal. Res. 19, 287–295.

Annexe B

Annexe : Article *Cazenave et al.* [2009] : « Le bilan du niveau de la mer sur la période récente 2003-2008 : une réévaluation à partir des données de gravimétrie spatiale GRACE, d'altimétrie spatiale et des flotteurs Argo », publié dans le journal « Global and Planetary Change »

Cet article traite du bilan du niveau de la mer sur la période récente entre 2003 et 2008 calculé à partir des données d'altimétrie spatiale (Jason-1), de la gravimétrie GRACE et des données des flotteurs Argo.

Le dernier rapport de l'IPCC-AR4 (2007) estime une hausse du niveau de la mer de 3.1 +/- 0.7 mm/an sur la période 1993-2003. Or, depuis 2003, le niveau de la mer stérique montre une pause tandis que le niveau de la mer observé continue à augmenter avec une vitesse de 2.5 +/- 0.4 mm/an entre 2003 et 2008. Cette vitesse d'élévation est plus faible que celle établie lors du dernier rapport de l'IPCC.

Dans cette étude, nous regardons le signal massique des océans en moyenne globale avec les données GRACE fournies par le GFZ sur la période mi-2002 à 2008. Cette estimation est par la suite confrontée à la perte de masse des calottes polaires du Groenland et de l'Antarctique exprimée en équivalent niveau de la mer (calculs réalisés avec les données du GFZ et du GRGS).

Ensuite, le niveau de la mer observé par altimétrie spatiale est analysé à la somme des diverses contributions climatiques : fonte des glaces continentales plus niveau de la mer stérique. Cette étude suggère une accélération dans les apports de masse aux océans dûe à la fonte des glaces continentales au niveau moyen global de la mer entre 2003 et 2008. en outre, ce travail a permis de considérer une correction du GIA proche de 2 mm/an pour estimer le signal massique des océans avec les données de la mission gravimétrique GRACE .

Global and Planetary Change 65 (2009) 83–88

Contents lists available at ScienceDirect

Global and Planetary Change

journal homepage: www.elsevier.com/locate/gloplacha

Sea level budget over 2003–2008: A reevaluation from GRACE space gravimetry, satellite altimetry and Argo

A. Cazenave [a,*], K. Dominh [a], S. Guinehut [b], E. Berthier [a], W. Llovel [a], G. Ramillien [a], M. Ablain [b], G. Larnicol [b]

[a] LEGOS, OMP, Toulouse, France
[b] CLS, Ramonville St Agne, France

ARTICLE INFO

Article history:
Received 2 August 2008
Accepted 12 October 2008
Available online 18 October 2008

Keywords:
sea-level
thermal expansion
ice melt
climate

ABSTRACT

From the IPCC 4th Assessment Report published in 2007, ocean thermal expansion contributed by ~50% to the 3.1 mm/yr observed global mean sea level rise during the 1993–2003 decade, the remaining rate of rise being essentially explained by shrinking of land ice. Recently published results suggest that since about 2003, ocean thermal expansion change, based on the newly deployed Argo system, is showing a plateau while sea level is still rising, although at a reduced rate (~2.5 mm/yr). Using space gravimetry observations from GRACE, we show that recent years sea level rise can be mostly explained by an increase of the mass of the oceans. Estimating GRACE-based ice sheet mass balance and using published estimates for glaciers melting, we further show that ocean mass increase since 2003 results by about half from an enhanced contribution of the polar ice sheets – compared to the previous decade – and half from mountain glaciers melting. Taking also into account the small GRACE-based contribution from continental waters (<0.2 mm/yr), we find a total ocean mass contribution of ~2 mm/yr over 2003–2008. Such a value represents ~80% of the altimetry-based rate of sea level rise over that period. We next estimate the steric sea level (i.e., ocean thermal expansion plus salinity effects) contribution from: (1) the difference between altimetry-based sea level and ocean mass change and (2) Argo data. Inferred steric sea level rate from (1) (~0.3 mm/yr over 2003–2008) agrees well with the Argo-based value also estimated here (0.37 mm/yr over 2004–2008). Furthermore, the sea level budget approach presented in this study allows us to constrain independent estimates of the Glacial Isostatic Adjustment (GIA) correction applied to GRACE-based ocean and ice sheet mass changes, as well as of glaciers melting. Values for the GIA correction and glacier contribution needed to close the sea level budget and explain GRACE-based mass estimates over the recent years agree well with totally independent determinations.

1. Introduction

While global mean ocean heat content (hence thermal expansion) rose regularly since at least the early 1990s as evidenced from in situ ocean temperature data (Guinehut et al., 2004; Willis et al., 2004; Antonov et al., 2005; Levitus et al., 2005; Ishii et al., 2006), new in situ hydrographic observations from the recently deployed Argo system (Roemmich and Owens, 2000) indicate that ocean heat content had a break since 2003 (Willis et al., 2008). If real, this means that, during the last 5 yr, ocean thermal expansion has not contributed to sea level rise, unlike during the previous 10-year period where about 50% of the rate of sea level rise could be attributed to ocean thermal expansion (Bindoff et al., 2007). Yet, satellite altimetry observations indicate that global mean sea level has continued to rise since 2003, at a slightly reduced rate however (of 2.5+/−0.4 mm/yr over 2003–2008, Glacial Isostatic Adjustment – GIA – correction of 0.3 mm/yr applied) compared to the previous decade (see Ablain et al., submitted for publication for details on the satellite altimetry-based sea level data processing and errors assessment). As shown in the IPCC 4th Assessment Report (Bindoff et al., 2007), during the period 1993–2003, altimetry-based rate of sea level rise (of 3.1+/−0.4 mm/yr, GIA applied) can be explained by 1.6+/−0.25 mm/yr steric sea level and 1.2+/−0.2 mm/yr land ice contributions respectively (note that uncertainties quoted here correspond to the 95% errors range). Thus a new question is raised: could the recent rate of sea level rise (since 2003) be explained by fresh water input to the ocean alone as a result of enhanced land ice (and eventually land waters) contribution? In the present study, we try to answer this question by estimating the ocean mass change contribution to sea level using space gravimetry data from the GRACE mission launched in March 2002. GRACE provides spatio-temporal variations of the Earth gravity at monthly or less temporal resolution and ~300–400 km ground resolution (Tapley et al., 2004). Numerous studies published in the recent years have shown that GRACE can offer useful constraints on ocean mass change (e.g., Chambers et al., 2004; Lombard et al., 2007), on the mass balance of the ice sheets (e.g., Velicogna and Wahr, 2006a,b; Chen et al., 2006a,b; Lutchke et al., 2006; Ramillien et al., 2006) and on land water contribution to sea level (Ramillien et al., 2008). Here we analyse GRACE data over a 5.5 year time

* Corresponding author.
E-mail address: anny.cazenave@cnes.fr (A. Cazenave).

0921-8181/$ – see front matter © 2008 Elsevier B.V. All rights reserved.
doi:10.1016/j.gloplacha.2008.10.004

span (August 2002 through February 2008) over oceans, land and ice sheets to estimate the total fresh water mass contribution to past few years sea level rise. We discuss the total fresh water input to the oceans comparing ocean mass change and ice sheet contribution inferred from GRACE with recent independent estimates for the mass balances of the ice sheets and mountain glaciers. In addition as shown by Lombard et al. (2007), comparing the altimetry-derived global mean sea level change with GRACE-based ocean mass change provides an estimate of the steric (i.e., thermal expansion plus salinity effect) contribution to sea level. We also follow this approach here and compare altimetry/GRACE-based steric sea level with Argo-based estimate.

2. Ocean mass variation from GRACE

We have analysed geoid data from the GRACE space mission to estimate the change in mean mass of the oceans since mid-2002. We follow the same procedure as in Lombard et al. (2007), except that we use here the most recent geoid solutions (RL04 Level-2 products) released by the GeoForschungsZentrum – GFZ – (Flechtner, 2007). This data set covers the period August 2002 to February 2008 (~5.5 yr). The geoid solutions consist of spherical harmonics coefficients up to degree and order 120 at monthly interval. To work with geoid anomalies, we remove from each monthly solution, a mean solution averaged over the whole 5.5-year time span. In the geoid solution determination process, an ocean model is removed. As the geoid solution over the oceans represents departure from the ocean model, we add back the initial ocean model. To estimate the ocean mass component, we construct a geographical mask over the whole oceanic domain and compute, at each time step, the convolution product between spherical harmonics of mask and geoid anomalies. We limit the spherical harmonic expansion to degree 50 (corresponding to a ground resolution of ~400 km) to minimize the resonance effects affecting higher harmonic degrees (see Swenson and Wahr, 2006). We next express the results in terms of Equivalent Sea Level, noted ESL (see Lombard et al., 2007 for details about the GRACE data analysis).

The raw GRACE-based ocean mass time series is dominated by an annual cycle caused by the annual exchange of water between land and oceans (Cazenave et al., 2000). As we are interested here in the interannual fluctuations, we remove the annual cycle. The resulting time series, shown in Fig. 1, has a slightly negative slope of ~−0.12+/−0.06 mm/yr over the time span January 2003–December 2007 (we consider this time span – called 2003–2008 – to work with an integer number of years). However, a GIA correction has to be applied to this raw ocean mass time series. In effect, GIA causes a secular change in the mean oceanic geoid that needs to be removed from the GRACE-based raw ocean mass time series to obtain the real water mass change of the oceans. This linear correction is quite large and available from GIA modelling only. It varies from ~1 mm/yr to 2 mm/yr (in ESL unit), depending on modelling assumptions (Willis et al., 2008; Tamisiea et al., in press; Peltier et al., submitted for publication). Lombard et al. (2007) used a GIA correction of 1.7 mm/yr following Tamisiea et al. (in press). Willis et al. (2008) used a value closer to 1 mm/yr. Recently Peltier (submitted for publication) reevaluated, under various modelling assumptions, the GIA corrections that need to be applied to satellite data (satellite altimetry and GRACE) when determining global mean sea level rise and ocean mass change. He shows that Earth rotation effects have strong influence on the ocean mass GIA correction and recommends to use an ocean mass GIA correction of ~2 mm/yr that accounts for the rotational effects. Here we use this value. We will see below that such a value allows us to close the sea level budget. Corresponding GIA-corrected ocean mass time series (annual cycle removed plus 12-month smoothing) is shown in Fig. 1. We note that during the 2003–2008 period, the ocean mass has increased almost linearly, at a rate of 1.9+/−0.1 mm/yr (Table 1). This increase results from fresh water mass input to the oceans as a result of land ice loss and eventually land waters.

Table 1
Sea level rise and the different contributions over 2003–2008 (numbers are from the present study, except for glaciers and ice caps)

Data source	Rate (mm/yr)
Sea level (altimetry; 2003–2008)	2.5+/−0.4
Ocean mass (GRACE; 2003–2008)	1.9+/−0.1
Ice sheets (GRACE; 2003–2008)	1+/−0.15
Glaciers and ice caps (2003–2008; Meier et al., 2007)	1.1+/−0.24
Terrestrial waters (2003–2008)	0.17+/−0.1
Sum of ice and waters	2.2+/−0.28
Steric sea level (altimetry minus GRACE; 2003–2008)	0.31+/−0.15
Steric sea level (Argo; 2004–2008)	0.37+/−0.1

3. Ice sheet contribution from GRACE

We now estimate the ice sheet contribution from GRACE over time span 2003–2008. Two methods are compared:

(1) We average the GRACE signal over the whole Earth surface and remove the ocean contribution using the ocean mask as explained in Section 2. We also average the GRACE signal

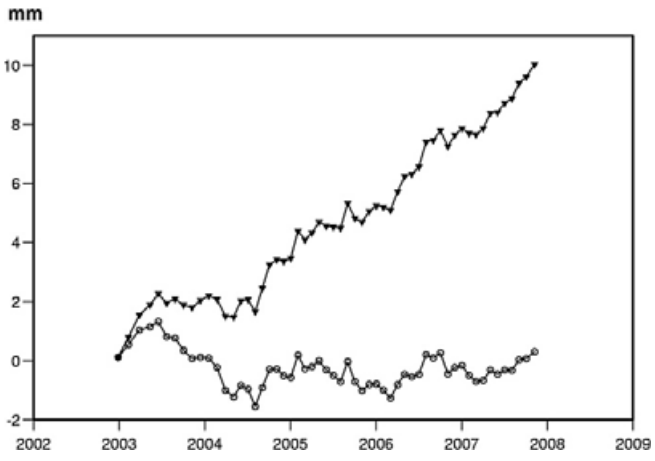

Fig. 1. Ocean mass change from GRACE over 2003–2008. The open circled curve is the raw time series. The black triangles curve corresponds to the GIA corrected time series.

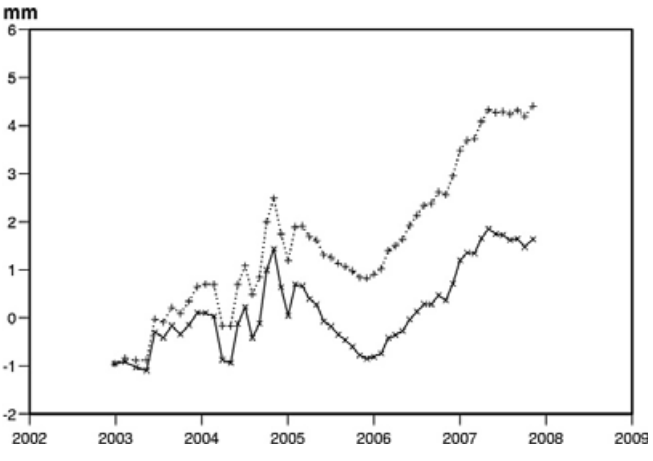

Fig. 2. Total ice sheet contribution to sea level estimated from GRACE over 2003–2008 (method 1; see text). The lower curve (crossed solid line) corresponds to raw data. The upper curve (dotted line with crosses) is the GIA corrected curve.

over the whole land surface using a land mask (excluding the ice sheets). The difference between the two averages provides an estimate of the ice sheet contribution.

(2) We average the GRACE signal using dedicated masks for Greenland and Antarctica as explained in Ramillien et al. (2006).

Although the two calculations are not independent, they provide an upper bound for the so-called leakage effect, i.e., the contamination from far field gravity signals not due to the ice sheets (at a given location, geoid height not only reflects local mass anomalies but also far field anomalies because of the inverse distance relationship between geoid and mass; such a contamination is amplified over small size regions like Greenland because of the low GRACE resolution, of ~400 km). We expect that method 1 minimizes the leakage effects.

Fig. 2 shows the ice sheet contribution expressed in Equivalent Sea Level estimated by method 1. The raw time series exhibits a slightly positive trend of 0.4+/−0.1 mm/yr ESL. To this curve we need to apply the GIA correction over the ice sheets (as over the oceans, GRACE cannot separate climate-related surface mass change from solid Earth mass change related to GIA). For Greenland, this correction is almost negligible (e.g., Ramillien et al., 2006). This is not the case however for Antarctica. In Ramillien et al. (2006), we used a GIA correction for Antarctica of 0.5 mm/yr ESL based on Ivins and James (2005) model. Such a value is also that preferred by Barletta et al. (2008) who investigated a large range of upper and lower mantle viscosities to estimate the GIA correction to be applied to GRACE-derived ice sheet mass balance. We use this value here to compute the GIA-corrected time series shown in Fig. 2. The resulting trend amounts to 1.0+/−0.1 mm/yr ESL. It represents the total ice sheet contribution to sea level as estimated from GRACE over the 2003–2008 time span. In terms of ice mass loss, this corresponds to ~360+/−36 Gigatons/yr.

Results from method 2 are shown in Fig. 3A and B (Greenland and Antarctica contributions expressed in ESL). For Antarctica, we have applied a GIA correction of 0.5 mm/yr (ESL) as discussed above. In both figures, we compared the GFZ GRACE-based time series with another estimate based on another GRACE product (i.e., from the Groupe de Recherche en Geodesie spatiale – GRGS – group, Biancale et al., 2006), to check the consistency of the estimated trend. For each ice sheet, the two sources of data lead to very similar trends (with differences smaller than 0.02 mm/yr). Taking the mean value from the two data sources, we obtain a GRACE-based Greenland contribution to sea level of 0.38+/−0.05 mm/yr (i.e., −136+/−18 Gigatons/yr ice mass loss) over 2003–2008. The Antarctica contribution (GIA correction applied) is 0.56+/−0.06 mm/yr ESL over the same period (i.e., −198+/−22 Gigatons/yr ice mass loss). Summing the two ice sheet contributions leads to 0.95+/−0.08 mm/yr ESL over 2003–2008, in good agreement with the result of method 1. The small difference between the two methods places an upper bound on the leakage effects.

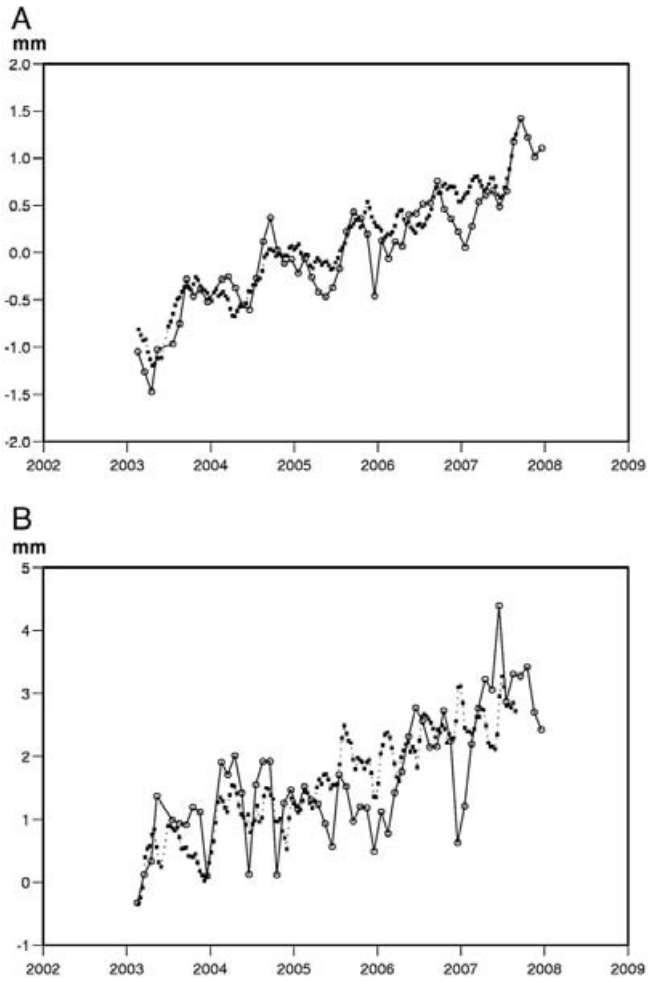

Fig. 3. (A) GRACE-based contribution of Greenland ice loss to sea level (2003–2008). The curve with open circles corresponds to GFZ geoids. The curve with black squares corresponds to GRGS geoids. (B) Same as (A) but for Antarctica. A GIA correction of 0.5 mm/yr ESL has been applied.

4. Total land ice contribution to sea level

4.1. Ice sheets

Several estimates of the ice sheet mass balance from GRACE have been published in the recent years (Velicogna and Wahr, 2006a,b; Chen et al., 2006a,b; Ramillien et al., 2006). Significant uncertainty in trends can be noticed between these different published results. Early results were based on rather short time series. Hence lengthening the time series may lead to different results because of seasonal and interannual variability. As discussed in Cazenave (2006), another cause of discrepancy arises from differences in data processing and methodology developed by the various GRACE project groups when computing the geoid solutions. From most recent published results, including those of the present study, we note that GRACE products from GFZ, GRGS and the 'Mascons' approach (the regional method developed by Lutchke et al., 2006) provide rather converging results, at least for Greenland (see also Forsberg, 2008), with current rates of ice mass loss of ~130–150 Gigatons/yr. Higher rates are found by Velicogna and Wahr (2006a) (210 Gigatons/yr for Greenland; e.g., Witze, 2008) and Chen et al. (2006a) based on Center for Space Research – CSR – geoids. So far, the reason for this discrepancy remains unclear.

From a compilation of published results based on different remote sensing techniques and modelling, Meier et al. (2007) reported for year 2006 contributions (in ESL) of 0.5+/−0.1 mm/yr, 0.32+/−0.04 mm/yr and −0.15+/−0.07 mm/yr for Greenland, West Antarctica and East Antarctica respectively, leading to a total ice sheet contribution of ~0.7+/−0.15 mm/yr for that particular year. Recently Rignot et al. (2008) reassessed Antarctic ice mass balance using radar interferometry and surface mass balance modelling. They conclude that East Antarctica has remained almost in balance since 1992 while accelerated ice mass loss is reported in West Antarctica. The net Antarctica contribution for year 2006 amounts to 0.54+/−0.2 mm/yr. This is three times Meier et al.'s value of 0.17 mm/yr, mainly a result of positive mass balance for East Antarctica in the latter study. It is worth to note that our GRACE-based estimate for Antarctica over the past 5 yr is in good agreement with Rignot et al. (2008) estimate. These results suggest that recent years ice sheet contribution to sea level has increased compared to the 1990s (Lemke et al., 2007). In the following we consider for the total ice sheet contribution, the average of the two methods presented in Section 3, i.e., ~1.0+/−0.15 mm/yr for 2003–2008.

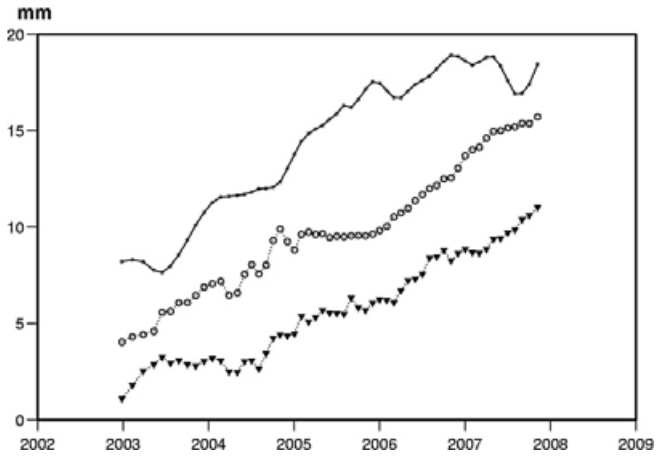

Fig. 4. Upper curve (crossed line): altimetry-based sea level curve; Middle curve (open circles): total land ice contribution using the GRACE-based ice sheet mass balance (this study) and Meier et al. (2007) glaciers contribution; Lower curve (black triangles): GRACE-based ocean mass change (GIA correction applied).

4.2. Glaciers and ice caps

Between 1990 and 2003, the IPCC 4th Assessment Report determined a Glacier and Ice Cap (GIC) contribution to sea level rise of 0.77+/−0.22 mm/yr (Lemke et al., 2007). There are still very few updated estimates of GIC losses for the most recent years (beyond 2003) due to the difficulty to gather mass balance measurements performed worldwide by different research groups. Kaser et al. (2006) reported a contribution to sea level rise of 0.98+/−0.19 mm/yr for 2001–2004, slightly larger than during the previous decade. Using the same data as Kaser et al. (2006) and assuming that ice losses by GIC increased linearly with time since year 2000, Meier et al. (2007) found the GIC contribution to be 1.1+/−0.24 mm/yr ESL for year 2006.

The enhanced mass losses from GIC proposed by Meier et al. (2007) is supported by recent evidences of accelerated ice thinning rates in Alaska (Chen et al., 2006c), Svalbard (Kohler et al., 2007) and in Himalaya (Berthier et al., 2007). The acceleration is also clearly demonstrated by the updated (although not yet complete) glacier mass balance measurements collected by the World Glacier Monitoring Service (WGMS, available at http://www.geo.unizh.ch/wgms/). Analysis of a subset of thirty reference glaciers spread in nine mountain ranges shows that the three years with the strongest ice losses appear after 2002. The mean mass balance for 2002–2006 (the last four hydrological years available) is two to three times more negative than during the previous 10 yr. In the following we consider the value of 1.1+/−0.24 mm/yr ESL from Meier et al. (2007) as representative of the 2003–2008 time span and use it for the sea level budget.

5. Total mass contribution to the sea level budget over 2003–2008

Summing the ice sheet and glacier contributions as discussed above, leads to a total land ice component of 2.1+/−0.25 mm/yr ESL over 2003–2008. To this value should eventually be added a small contribution from land waters. In a previous study (Ramillien et al., 2008), we estimated to ~0.17+/−0.1 mm/yr, the land water contribution to sea level using GRACE data (GFZ geoids, release RL03) over 2003–2006. An updated estimate based on GFZ RL04 GFZ and GRGS GRACE data leads to about the same value over 2003–2008. In the following we use the Ramillien et al. (2008) value.

Comparing the GRACE-based ocean mass trend (1.9+/−0.1 mm/yr; see Section 2) with the total land ice plus land waters contribution estimated independently (2.2+/−0.28 mm/yr; Sections 3 and 4) gives satisfactory agreement for a GIA correction of 2 mm/yr. In a way this provides constraints on the GIA correction, suggesting that the upper range of proposed values is indeed indicated. As mentioned above, this upper range is recommended by Peltier (submitted for publication) because of Earth rotation effects. The comparison also provides constraints on glacier melting contribution, since with GRACE, we can compute separately ocean mass increase (sum of ice sheet mass loss and land waters) and ice sheet mass balance. Comparison of the two results provides constraint on glaciers melting. We note that the latter contribution agrees well with published results based on in situ observations and remote sensing.

Fig. 4 compares for the 2003–2008 period, the observed (from T/P and Jason-1 altimetry) sea level curve (from Ablain et al., submitted for publication) to GRACE-based ocean mass change (with a GIA correction of 2 mm/yr) and total land ice plus land waters contribution discussed above. We note that land ice plus land waters has contributed for 75%–85% to recent sea level rise, i.e., significantly more than during the decade 1993–2003 (Bindoff et al., 2007).

6. Steric sea level inferred from altimetry and GRACE and computed with Argo

As shown in Lombard et al. (2007), it is possible to estimate the steric sea level from the difference between the altimetric (i.e., total) sea level and the GRACE-based ocean mass component. Corresponding steric sea level curve for 2003–2008 is presented in Fig. 5 (assuming a GIA correction of 2 mm/yr for the ocean mass estimate). The steric sea level increased on average since early 2003 through 2006, then shows a slightly decreasing trend. The latter behaviour results from the fact that altimetric sea level flattens since 2006 while the ocean mass continues to increase. If this steric sea level behaviour is real, it could be related to the particularly strong recent La Nina cold phase (Kennedy, 2007). The average slope of the steric sea level curve over 2003–2008 is small, on the order of 0.31+/−0.15 mm/yr. In Fig. 5 is also presented the steric sea level computed from the difference between satellite altimetry and total land ice (i.e., ice sheet contribution estimated in this study plus glacier contribution from Meier et al., 2007) plus land waters curve. It is interesting to note that it closely follows the altimetry minus ocean mass curve.

We now provide an independent estimate of the steric sea level using temperature and salinity data from Argo profiling floats. When available, delayed-mode data are preferred to real-time ones (i.e. for half of the floats) and only measurements with Argo quality control flags at '1' are used. As real-time quality controlled checks applied on the Argo data set are very simple and automated, additional quality

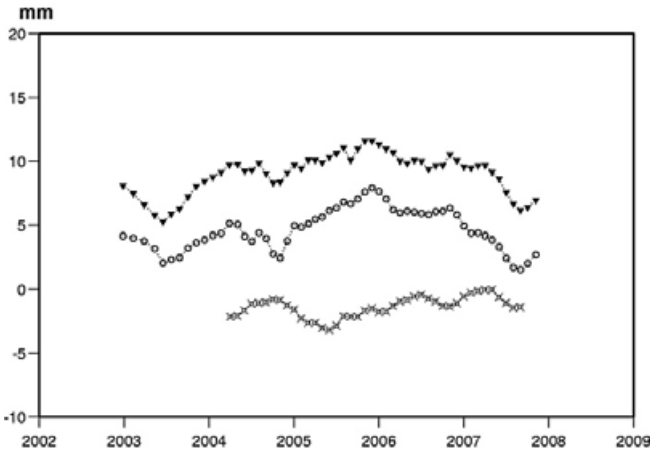

Fig. 5. Steric sea level. Upper curve (black triangles): estimated from the difference between altimetry and GRACE-based ocean mass. Middle curve (open circles): estimated from the difference between satellite altimetry and total land ice plus land waters contribution; Lower curve: ARGO-based estimate (this study).

controls were first performed following the method described in Guinehut et al. (in press). It compares collocated sea level anomalies from altimeter measurements with steric height anomalies calculated from the Argo temperature and salinity profiles. By exploiting the correlation that exists between the two data sets (Guinehut et al., 2006), along with mean representative statistical differences between the two, the altimeter measurements are used to extract random or systematic errors in the Argo float time series (drift, bias, spikes, etc). About 4% of the floats were deleted by this method.

Steric heights at the surface are then computed relative to the 900-m depth from Argo temperature and salinity profiles. The 900-m depth was chosen as a compromise between data coverage and maximum sampled depth to provide optimum spatial and temporal coverage. Steric changes below 900-m do contribute to the sea level budget on multi-decadal time scales but observations and models suggest that major contributions come from the upper ocean (e.g., Antonov et al., 2005, Wunsch et al., 2007).

Argo floats profiles being discrete measurements in time and in space, steric sea level grids at 1/3° resolution are constructed at monthly interval. Mapping is based on an optimal interpolation method (Bretherton et al., 1976), using a temporal correlation scale of 45 days and a spatial correlation scale that varies with latitude, from 1500 km at the equator to 700 km at 50°N (larger values are used in the zonal direction than in the meridional one). In order to take into account errors associated with mesoscale variability aliasing, noise-to-signal ratio is fixed to 2.0 for each in-situ measurement. Besides, a contemporaneous Argo climatology representing the time-mean is removed from the individual steric height prior to mapping. Finally, monthly steric height anomaly grids are globally averaged to produce steric sea level time series.

In order to precisely quantify the impact of Argo data sampling and methodology used to calculate the globally averaged values, the AVISO multi-mission combined sea level products (Ducet et al., 2000) are interpolated at the time and location of each Argo float profile. Sea level maps are then reconstructed using the same mapping technique as for steric maps. This allows us to estimate the impact of the variable Argo coverage. At the beginning of 2002, Argo sampling covers about 40% of the ocean. It reaches around 70% in 2003, then 80% at the beginning of the year 2004. After mid-2006, more than 90% of oceanic areas are sampled. Here we consider Argo data over 2004–2007 only because of the still poor 2003 coverage. The globally averaged steric sea level computed from the gridded data is finally compared altimetry-based sea level (SSALTO/DUACS multi-mission combined products, Ducet et al., 2000). The two curves compare very well over 2004–2008 with a 2.4 mm rms difference, the trend being only slightly reduced by 0.02 mm/yr. Fig. 5 presents the Argo-based steric sea level curve (seasonal cycle removed; as for ocean mass variations, the steric sea level curve for the upper 900-m depth is dominated by an annual cycle due to seasonal heating and cooling of the upper ocean). The curve is rather flat over the 2004–2008 time span. Corresponding linear trend is small and on the order of 0.37+/−0.1 mm/yr. Even if the year to year variability does not match exactly the altimetry/GRACE steric sea level curve (possibly a result of the data processing and deep ocean contribution), it is remarkable to obtain such an agreement. These two independent estimates of steric sea level trend presented in this study are slightly higher than Argo-based values from Willis et al. (2008). Nevertheless, these results strongly indicate a pause in the rate of steric sea level rise in the past few years. The independent estimate based on GRACE and satellite altimetry data indicate that it is not due to any Argo instrumental problem.

7. Conclusion

From the results presented in this study, we see that confronting independent estimates of ocean and land contributions to sea level with altimetry results leads to a rather coherent picture for recent years variations. This can be summarized as follows: since 2003, sea level has continued to rise but with a rate (of 2.5+/−0.4 mm/yr) somewhat reduced compared to the 1993–2003 decade (3.1+/−0.4 mm/yr). Over 2003–2008, the GRACE-based ocean mass has increased at an average rate of ~1.9 mm/yr (if we take the upper range of possible GIA corrections as recommended by Peltier, submitted for publication). Such a rate agrees well with the sum of land ice plus land water contributions (i.e., GRACE-based ice sheet mass balance estimated in this study, GRACE-based land waters plus recently published estimates for the current glacier contribution). These results in turn offer constraints on the ocean mass GIA correction, as well as on the glacier melting contribution.

The steric sea level estimated from the difference between altimetric (total) sea level and ocean mass displays increase over 2003–2006 and decrease since 2006. On average over the 5 year period (2003–2008), the steric contribution has been small (on the order of 0.3+/−0.15 mm/yr), confirming recent Argo results (this study and Willis et al., 2008).

Acknowledgments

The Argo data were collected and made freely available by the international Argo project (a pilot program of the Global Ocean Observing System) and the national programs that contribute to it (http://www.argo.ucsd.edu, http://argo.jcommops.org). The altimeter products were produced by SSALTO/DUACS and distributed by AVISO with support from CNES.

We thank R. Peltier and Luce Fleitout for helpful discussions about the GIA correction.

References

Ablain M., Cazenave A., Guinehut S., Valladeau G., (submitted for publication), A new assessment of global mean sea level from altimeters highlights a reduction of global slope from 2005 to 2008 in agreement with in-situ measurements, submitted to Ocean Sciences.

Antonov, J., Levitus, S., Boyer, T.P., 2005. Thermosteric sea level rise, 1955–2003. Geophys. Res. Lett. 32. doi:10.1029/2005GL023112.

Barletta, V.R., Sabadini, R., Bordoni, A., 2008. Isolating the PGR signal in the GRACE data: impact on mass balance estimates in Antarctica and Greenland. Geophys. J. Int. 172, 18–30.

Berthier, E., Arnaud, Y., Kumar, R., Ahmad, S., Wagnon, P., Chevallier, P., 2007. Remote sensing estimates of glacier mass balances in the Himachal Pradesh (Western Himalaya, India). Remote Sens. Environ. 108 (3), 327–338. doi:10.1016/j.rse.2006.11.017.

Biancale, R., Lemoine, J.-M., Balmino, G., Loyer, S., Bruisma, S., Perosanz, F., Marty, J.-C. and Gégout, P. (2006), 3 years of geoid variations from GRACE and LAGEOS data at 10-day intervals from July 2002 to March 2005, CNES/GRGS product, data available on CD-ROM, also on BGI web page: http://bgi.cnes.fr/.

Bindoff, N., Willebrand, J., Artale, V., Cazenave, A., Gregory, J., Gulev, S., Hanawa, K., Le Quéré, C., Levitus, S., Nojiri, Y., Shum, C.K., Talley, L., Unnikrishnan, A., 2007. Observations: oceanic climate and sea level. In: Solomon, S., Qin, D., Manning, M., Chen, Z., Marquis, M., Averyt, K.B., Tignor, M., Miller, H.L. (Eds.), Climate change 2007: the physical science basis. Contribution of Working Group I to the Fourth Assessment report of the Intergouvernmental Panel on Climate Change. Cambridge University Press, Cambridge, UK.

Bretherton, F.P., Davis, R.E., Fandry, C.B., 1976. A technique for objective analysis and design of oceanographic experiments applied to MODE-73. Deep-Sea Res. 23, 559–582.

Cazenave, A., 2006. How fast are the ice sheets melting? Science 314, 1250–1252.

Cazenave, A., Remy, F., Dominh, K., Douville, H., 2000. Global ocean mass variations, continental hydrology and the mass balance of Antarctica ice sheet at seasonal timescale. Geophys. Res. Lett. 27 (22), 3755–3758.

Chambers, D.P., Wahr, J., Nerem, R.S., 2004. Preliminary observations of global ocean mass variations with GRACE. Geophys. Res. Lett. 31 (L13310).

Chen, J.L., Wilson, C.R., Tapley, B.D., 2006a. Satellite gravity measurements confirm accelerated melting of the Greenland ice sheet. Science 313, 1958.

Chen, J.L., Wilson, C.R., Blankenship, D.D., Tapley, B.D., 2006b. Antarctic mass rates from GRACE. Geophys. Res. Lett. 33. doi:10.1029/2006GL026369.

Chen, J.L., Tapley, B.D., Wilson, C.R., 2006c. Alaskan mountain glacial melting observed by satellite gravimetry. Earth Planet. Sci. Lett. 248 (1–2), 368–378.

Ducet, N., Le Traon, P.-Y., Reverdin, G., 2000. Global high resolution mapping of ocean circulation from TOPEX/Poseidon and ERS-1 and -2. J. Geophys. Res. 105, 19477–19498.

Flechtner, F. (2007), AOD1B product description document for product releases 01 to 04, GRACE 327-750, CSR Publ. GR-GFZ-AOD-001 Rev. 3.1, University of Texas at Austin, 43 pp.

Forsberg, R. (2008), Greenland ice sheet mass balance from GRACE, European Science Foundation workshop on Greeland ice sheet variability.
Guinehut, S., Le Traon, P.-Y., Larnicol, G., Phillips, S., 2004. Combining ARGO and remote-sensing data to estimate the ocean three-dimensional temperature fields. J. Mar. Syst. 46, 85–98.
Guinehut, S., Le Traon, P.-Y., Larnicol, G., 2006. What can we learn from global altimetry/hydrography comparisons? Geophys. Res. Lett. 33 (L10604). doi:10.1029/2005GL025551.
Guinehut, S., Coatanoan, C., Dhomps, A.-L., Le Traon, P.-Y. and Larnicol, G., in press. On the use of satellite altimeter data in Argo quality control, submitted to J. Atmos. Oceanic. Technol.
Ishii, M., Kimoto, M., Sakamoto, K., Iwasaki, S.I., 2006. Steric sea level changes estimated from historical ocean subsurface temperature and salinity analyses. J. Oceanogr. 62 (2), 155–170.
Ivins, E.R., James, T.S., 2005. Antarctic glacial isostatic adjustment: a new assessment. Antarct. Sci. 17 (4), 541–553.
Kaser, G., Cogley, J.G., Dyurgerov, M.B., Meier, M.F., Ohmura, A., 2006. Mass balance of glaciers and ice caps: consensus estimates for 1961–2004. Geophys. Res. Lett. 33 (L19501). doi:10.1029/2006GL027511.
Kennedy, J., 2007. La Nina 2007. Integrated Climate Programme (IPC) 2007–2012, Product E1 (ii), Hadley Center MetOffice (UK).
Kohler, J., James, T.D., Murray, T., Nuth, C., Brandt, O., Barrand, N.E., Aas, H.F., 2007. Acceleration in thinning rate on western Svalbard glaciers. Geophys. Res. Lett. 34 (L18502). doi:10.1029/2007GL030681.
Levitus, S., Antonov, J.I., Boyer, T.P., 2005. Warming of the World Ocean, 1955–2003. Geophys. Res. Lett. 32 (L02604). doi:10.1029/2004GL021592.
Lemke, et al., 2007. In: Solomon, S., Qin, D., Manning, M., Chen, Z., Marquis, M., Averyt, K.B., Tignor, M., Miller, H.L. (Eds.), Climate change 2007: the physical science basis. Contribution of Working Group I to the Fourth Assessment report of the Intergouvernmental Panel on Climate Change. Cambridge University Press, Cambridge, UK.
Lombard, A., Garcia, D., Cazenave, A., Ramillien, G., Fletchner, Biancale, R., Ishii, M., 2007. Estimation of steric sea level variations from combined GRACE and satellite altimetry data. Earth Planet. Sci. Lett. 254, 194–202.
Lutchke, S.B., Zwally, H.J., Abdalati, W., Rowlands, D.D., Ray, R.D., Nerem, R.S., Lemoine, F.G., McCarthy, J.J., Chinn, D.S., 2006. Recent Greenland ice mass loss by drainage system from satellite gravimetry observations. Science 314, 1286–1289.
Meier, M.F., Dyurgerov, M.B., Rick, U.K., O'Neel, S., Pfeffer, W.T., Anderson, R.S., Anderson, S.P., Glazovsky, A.F., 2007. Glaciers dominate eustatic sea-level rise in the 21st century. Science 317 (5841), 1064–1067.
Peltier R., submitted for publication. Closure of the budget of global sea level rise over the GRACE era : the importance and magnitudes of the required corrections for global glacial isostatic adjustment. Quat. Sci. Rev.
Ramillien, G., Lombard, A., Cazenave, A., Ivins, E., Llubes, M., Remy, F., Biancale, R., 2006. Interannual variations of ice sheets mass balance from GRACE and sea level. Glob. Planet. Change 53, 198–208.
Ramillien, G., Bouhours, S., Lombard, A., Cazenave, A., Flechtner, F., Schmidt, R., 2008. Land water contributions from GRACE to sea level rise over 2002–2006. Glob. Planet. Change 60, 381–392.
Rignot, E., Bamber, J.L., Van den Broecke, M.R., Davis, C., Li, Y., Van de Berg, W.J., Van Meijgaard, E., 2008. Recent Antarctic ice mass loss from radar interferometry and regional climate modelling. Nat. Geosci. 1, 106–110.
Roemmich, D., Owens, W.B., 2000. the ARGO project: global ocean observations for understanding for understanding and prediction of climate variability. Oceanography 13 (2), 45–50.
Swenson, S., Wahr, J., 2006. Post-processing removal of correlated errors in GRACE data. Geophys. Res. Lett. 33 (L08402). doi:10.1029/2005GL025285.
Tamisiea, M.E., Mitrovica, J.X., Nerem, R.S., Leuliette, E.W. and Milne, G.A. (in press), Correcting satellite derived estimates of global mean sea level change for glacial isostatic adjustment, Geophys. J. Int., in press.
Tapley, B.D., Bettadpur, S., Ries, J.C., Thompson, P.F., Watkins, M., 2004. GRACE measurements of mass variability in the Earth system. Science 305, 503–505.
Velicogna, I., Wahr, J., 2006a. Revised Greenland mass balance from GRACE. Nature 443, 329.
Velicogna, I., Wahr, J., 2006b. Measurements of time-variable gravity show mass loss in Antarctica. Science 311, 1754–1756.
Willis, J.K., Roemmich, D., Cornuelle, B., 2004. Interannual variability in upper ocean heat content, temperature, and thermosteric expansion on global scales. J. Geophys. Res. 109. doi:10.1029/2003JC002260.
Willis, J.K., Chambers, D.T., Nerem, R.S., 2008. Assessing the globally averaged sea level budget on seasonal to interannual time scales, in press, J. Geophys. Res. 113, C06015. doi:10.1029/2007JC004517.
Witze, A., 2008. Loosing Greenland. Science 452, 798–802.
Wunsch, C., Ponte, R.M., Heimbach, P., 2007. Decadal trends in sea level patterns: 1993–2004. J. Climate 20 (24). doi:10.1175/2007JCLI1840.1.

Annexe C

Annexe : Article *Becker et al.* [2010] : « Le comportement hydrologique récent de la région des grands lacs d'Afrique de l'est déduit des données GRACE, de l'altimétrie spatiale et des précipitations », publié dans le journal « Comptes Rendus Géoscience »

Ce travail analyse la variabilité spatio-temporelle de certains paramètres hydrologiques (stock total d'eau, volume d'eau et précipitation) des Grands Lacs Africains analysée avec les données de gravimétrie spatiale GRACE, de l'altimétrie spatiale et des données de précipitations.

Cette étude suggère que les paramètres hydrologiques (Précipitations, évaporation et ruissellement) présentent un mode de variabilité interannuelle commun. En effet, nous notons un minimum marqué à la fin de l'année 2005 puis, une augmentation vers 2006-2007. Nous montrons que cette élévation est intimement liée au forçage induit par un mode de variabilité de l'océan Indien : le dipôle de l'océan Indien, avec notamment, un fort événement en 2006 (confimé dans une étude récente de *Llovel et al.* [2010b]). Ce mode de variabilité génère des anomalies de précipitations qui vont directement affecter la région des Grands Lacs Africains.

Il s'avère aussi que la variabilité du stock d'eaux continentales des Grands Lacs est aussi liée aux épisodes ENSO. En combinant les variations de volume des lacs nous estimons la variation de l'humidité des sols et des eaux souterraines et, nous comparons ces résultats avec les sorties du modèle numérique hydrologie continentale WGHM (WaterGap Global Hydrological Model).

C. R. Geoscience 342 (2010) 223–233

Contents lists available at ScienceDirect

Comptes Rendus Geoscience

www.sciencedirect.com

Surface geosciences (Hydrology – Hydrogeology)

Recent hydrological behavior of the East African great lakes region inferred from GRACE, satellite altimetry and rainfall observations

Comportement hydrologique récent de la région des grands lacs d'Afrique de l'Est déduit des données GRACE, de l'altimétrie spatiale et des précipitations

Mélanie Becker [a,*], William LLovel [a], Anny Cazenave [a], Andreas Güntner [b], Jean-François Crétaux [a]

[a] *LEGOS/GOHS, UMR5566/CNES/CNRS/UPS/IRD, 18, avenue E. Belin, 31400 Toulouse, France*
[b] *GFZ, German Research Centre for Geosciences, Telegrafenberg, Potsdam, Germany*

ARTICLE INFO

Article history:
Received 15 June 2009
Accepted after revision 10 December 2009
Available online 15 March 2010

Presented by Ghislain de Marsily

Keywords:
GRACE
Altimetry
Lakes
ENSO
Climate change
East Africa

Mots clés :
GRACE
Altimétrie
Lacs
ENSO
Changement climatique
Afrique de l'Est

ABSTRACT

We have jointly analysed space gravimetry data from the GRACE space mission, satellite altimetry data and precipitation over the East African Great Lakes region, in order to study the spatiotemporal variability of hydrological parameters (total water storage, lake water volume and rainfall). We find that terrestrial water storage (TWS) from GRACE and precipitation display a common mode of variability at interannual time scale, with a minimum in late 2005, followed by a rise in 2006–2007. We argue that this event is due to forcing by the strong 2006 Indian Ocean Dipole (IOD) on East African rainfall. We also show that GRACE TWS is linked to the El Niño-Southern Oscillation cycle. Combination of the altimetry-based lake water volume with TWS from GRACE over the lakes drainage basins allows estimating soil moisture and groundwater volume variations. Comparison with the WGHM hydrological model outputs is performed and discussed.

RÉSUMÉ

Nous avons conjointement analysé des données de gravimétrie spatiale de la mission spatiale GRACE, d'altimétrie spatiale et de précipitation au-dessus de la région des Grands Lacs d'Afrique de l'Est, afin d'étudier la variabilité spatiotemporelle de certains paramètres hydrologiques (stock d'eau total, volume d'eau du lac et précipitation) de cette région. Nous trouvons que le stock d'eau total issu de GRACE et les précipitations présentent un mode de variabilité interannuelle commun, avec un minimum marqué fin 2005, puis une augmentation en 2006–2007. Nous montrons que cet événement est dû au forçage du dipôle de l'océan indien de 2006 sur les précipitations de l'Est africain. Nous montrons également que la variation du stock d'eau continentale de cette région est liée à ENSO (El Niño-Southern Oscillation). En combinant les variations de volume des lacs, obtenues par altimétrie, avec celles du stock d'eau continentale de GRACE, nous estimons la variation de l'humidité des sols et des eaux souterraines que nous comparons aux sorties du modèle hydrologique WGHM.

* Auteur correspondant.
E-mail address: melanie.becker@legos.obs-mip.fr (M. Becker).

1631-0713/$ – see front matter
doi:10.1016/j.crte.2009.12.010

1. Introduction

The impact of climate variability on groundwater resources remains poorly known because in situ measurements are very sparse. This is of particular concern in Africa, where approximatively half of its nearly one billion inhabitants rely upon groundwater for their daily water supply (Taylor et al., 2008). Furthermore, future adaptations in response to climate change and rapid population growth are expected to intensify dependence upon groundwater in Africa.

In the recent years, remote sensing observations have been used to study water storage variations in major river basins on time scales from months to decades. For example, satellite altimetry measures water levels of rivers, lakes and flood plains (Birkett, 1995; Birkett, 1999; Calmant et and Seyler, 2006; Calmant et al., 2008; Crétaux and Birkett, 2006; Mercier et al., 2002; Ponchaut and Cazenave, 1998; Zakharova et al., 2006). Over lakes and flood plains, it also provides surface water volume change when combined with surface water area. Since 2002, the gravity recovery and climate experiment (GRACE) space mission measures spatiotemporal change in vertically-integrated water storage (surface water, soil moisture and groundwater, and snow where appropriate). The combination of altimetry and gravimetry gives access to a large range of hydrological products and finds all its interest in remote areas where networks of in situ measurements encounter maintenance problems (Alsdorf et al., 2007; Awange et al., 2008; Frappart et al., 2006; Frappart et al., 2008; Papa et al., 2008; Swenson and Wahr, 2009). Satellite altimetry observations, which are publicly available and of high quality (see below), are a powerful tool for monitoring surface waters of the East Africa region.

In this study, we jointly analysed GRACE and satellite altimetry data over the East African lakes and their drainage basins in order to highlight time-variable hydrological conditions in this region. We analyse also rainfall data as well as thermal expansion of the western Indian Ocean. Finally, we combine altimetry and GRACE data in order to compute soil moisture and groundwater variations and perform comparison with output of a global hydrological model. For simplicity, in the following, we call "soil moisture" the water contained in the pore space of the unsaturated zone, "groundwater" the saturated water zone and "subsurface water" the sum of groundwater and soil moisture.

2. Hydrological characteristics of the study area

In this work, we study the drainage basins of the four largest lakes of the East African Rift Valley: Turkana, Victoria, Tanganyika and Malawi. The study region is shown in Fig. 1. It is crossed by the borders of 11 countries: Ethiopia, Kenya, Sudan, Uganda, Tanzania, Rwanda, Burundi, Republic of Congo, Zambia, Malawi and Mozambique. The contours of the drainage basin (Fig. 1) for each lake are obtained from the drainage network provided by the routing model called Total Runoff Integrating Pathways (TRIP (Oki and Sud, 1998)). The hydrographic network defined by TRIP has a spatial resolution of 1×1

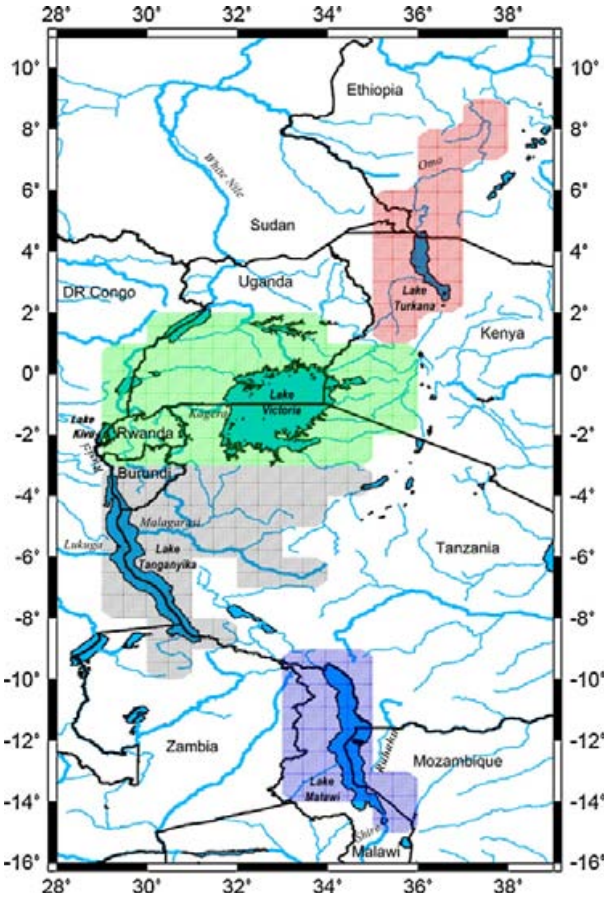

Fig. 1. Boundaries of the East African Great Lakes region. The lakes with their drainage basin selected for the study are: Lake Turkana (red), Lake Victoria (green), Lake Tanganyika (gray) and Lake Malawi (blue). The contours of the drainage basin were obtained from the drainage network provided by the model routing Total Runoff Integrating Pathways (TRIP, (Kundzewicz et al., 2004)).

Fig. 1. Les frontières de la région des grands lacs d'Afrique de l'Est. Les lacs avec leur bassin de drainage sélectionnés pour l'étude sont : le lac Turkana (rouge), le lac Victoria (en vert), le lac Tanganyika (gris) et le lac Malawi (bleu). Les contours des bassins de drainage ont été obtenus à partir de la direction des flux fournie par le modèle de routage *Total Runoff Integrating Pathways* (TRIP, (Kundzewicz et al., 2004)).

and gives for each mesh the direction of the flow. Lake Turkana is located in the arid north-western Kenya. Its drainage basin covers part of Kenya and the Omo River (which supplies about 90% of water to the lake). Lake Turkana loses water mainly by evaporation (Ferguson and Harbott, 1982). Lake Victoria is the largest lake in Africa. The boundaries of the lake cross Kenya, Uganda and Tanzania. Outflow from Lake Victoria contributes most of present-day White Nile River flow. The Kagera River contributes only ~7% of the total water input. In Uganda, where the lake outflow is located, hydropower is the main source of electricity for the country (WWAP, 2006). Lake Victoria's water balance is controlled both by net precipitation, catchment inflow and dam outflow (Yin et and Nicholson, 1998). Lake Tanganyika is the longest lake in the world. It crosses or has on its banks Burundi, the Democratic Republic of the Congo, Tanzania and Zambia.

Lake Tanganyika is fed by many small streams and two major rivers: the river Rusizi, flowing from Lake Kivu to the north and the river Malagarasi, to the south. The only outlet of Lake Tanganyika is the river Lukuga. Lake Malawi is fed by 14 perennial rivers, the largest being the Ruhuhu river. Its unique outlet is the river Shire, a tributary of the Zambezi river.

Fluctuations in lake water volume mainly reflect changes in precipitation and evaporation over the lake and its catchment basin. In that sense, these fluctuations constitute a sensitive indicator of past and present climate changes, at least at local and regional scales. Another important term in the lake water balance is outflow (Awange et al., 2008; Swenson and Wahr, 2009).

The hydrological regime of the East African lakes is primarily dependent on the climatic conditions of the alternating wet and dry seasons. Rainfall over much of East Africa displays a bimodal regime with rainy seasons from March to May and October to December, moderated by coastal and topographic influences (Mutai et al., 1998). The rainfall regimes and the transitional periods show varying degrees of influence from the Atlantic, Indian and Pacific Oceans. Periodic circulation dipole events in the Indian Ocean tend to be associated with above-average and sometimes very extreme rainfall from October to December (Conway et al., 2005).

3. Data sets

In this section, we present the four data sets used in this study.

3.1. Satellite altimetry

Satellite altimetry has been developed and optimized to measure sea surface height (Fu and Cazenave, 2001). However, during the last two decades, it has also been applied to monitor water levels of lakes, floodplains and wetlands (Birkett, 1999; Birkett et al., 1999; Calmant et and Seyler, 2006; Calmant et al., 2008; Crétaux and Birkett, 2006; Frappart et al., 2006; Frappart et al., 2008; Mercier et al., 2002). Water level time series of greater than 15 years length, based on the Topex/Poseidon, Jason-1, ERS-1/2 and ENVISAT altimetry missions are now available for several hundred continental lakes, river stations and man-made reservoirs. These are available on Internet databases (e.g., http://www.pecad.fas.usda.gov/cropexplorer/global_reservoir for large lakes, the HYDROWEB data base http://www.legos.obs-mip.fr/soa/hydrologie/hydroweb for lakes, man-made reservoirs, rivers and floodplains, and the "River and Lakes" database http://earth.esa.int/riverandlake for large lakes and rivers). On rivers and small lakes, conventional nadir-viewing altimetry has limitations because radar waveforms (e.g., raw radar altimetry echoes after reflection from the land surface) are more complex than their oceanic counterparts due to interfering reflections from water, vegetation canopy and rough topography. However, for large lakes (such as those considered in the present study), this technique has proved quite useful to measure surface elevation with good accuracy. Validation studies indicate that water level uncertainty of 3–5 cm RMS (root mean squares) for the largest lakes (Birkett, 1995; Crétaux and Birkett, 2006). A comparison of altimetric lake levels and in situ stage measurements of Lake Victoria near Jinja, Uganda during the period 2000–2004 showed excellent agreement ((Reynolds, 2005), http://www.fas.usda.gov/pecad/highlights/2005/09/uganda_26sep2005/). Fig. 2 presents water volume evolution since 1993 for the four African lakes. Data were smoothed with a 6-month window. To compute the lake water volume at a given date, we simply multiply the spatially averaged water level over the lake area (as given in the HYDROWEB data base) by the lake area given in Table 1. More details on the

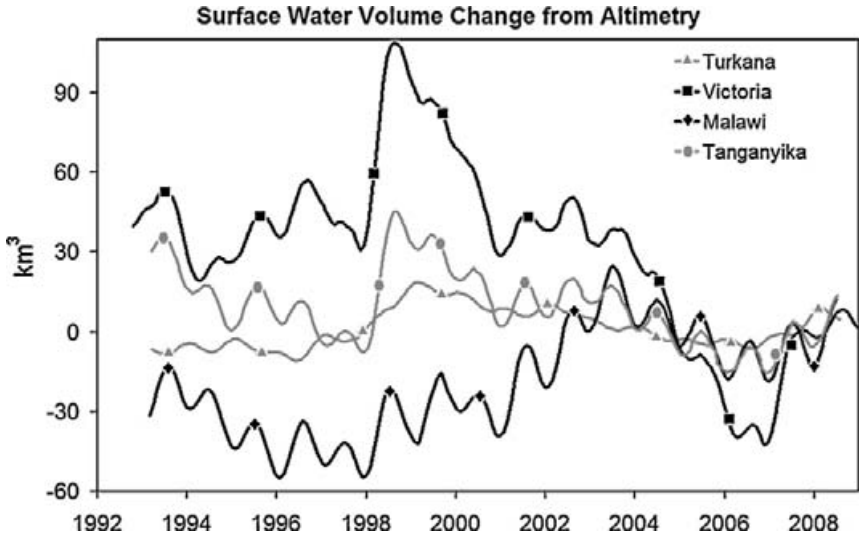

Fig. 2. Mean Lake volume fluctuations (in km^3) from satellite altimetry (1992–2008) for each lake studied: Turkana, Victoria, Malawi and Tanganyika. The data are smoothed, with a 6-month window.

Fig. 2. Moyenne des fluctuations de volume des lacs, (en km^3) à partir des données d'altimétrie spatiale (1992–2008), pour chacun des lacs : Turkana, Victoria, Malawi et Tanganyika. Les données sont lissées avec une moyenne glissante de six mois.

Table 1
Morphometric data for East Africa's largest lakes (Awange, 2006; Bootsma and Hecky, 1993; Spigel and Coulter, 1996; Thieme et al., 2005).

Tableau 1
Données morphométriques des grands lacs de l'Est Africain (Awange, 2006; Bootsma and Hecky, 1993; Spigel and Coulter, 1996; Thieme et al., 2005).

	Turkana	Victoria	Tanganyika	Malawi
Location	3°N – 36°E	1°4S – 33°E	8°5S – 29°5E	11°S – 34°5E
Catchment area (km^2)	130,860	193,000	220,000	126,500
Lake area (km^2)	6750	68,800	32,600	29,500
Total area (km^2)	137,610	261,800	252,600	156,000
Water level control	Unregulated	Regulated	Unregulated	Regulated

method developed for estimating mean lake levels from multiple satellite tracks are given in Crétaux and Birkett (Crétaux and Birkett, 2006). On Fig. 2, we observe a water volume decrease of lakes Tanganyika and Malawi ($\geq 6\,km^3$/year) over 1993–1997. Ponchaut and Cazenave (Ponchaut and Cazenave, 1998) associated this trend, observed from Topex/Poseidon (1993–1997), with recurrent droughts recorded in East and South Africa since the early 1990s. On the other hand, a large water volume increase in late 1997 – early 1998 is noted for lakes Turkana, Victoria and Tanganyika. This major anomalous pattern has been explained by a positive rainfall anomaly occurring in late 1997, related to the equatorial Indian Ocean warming reported during the 1997–1998 ENSO event (Mercier et al., 2002). These lakes exhibit a strong volume decrease between 1998 and 2006, then an increase until 2008. The Malawi lake shows a different pattern. Jury and Gwazantini (Jury and Gwazantini, 2002) showed that the interannual cycles of Malawi lake level are consistent with those found for Zambezi River streamflows, suggesting a degree of regional coherence.

3.2. GRACE space gravimetry

The space gravimetry mission GRACE was launched in March 2002 with the objective of providing spatiotemporal variations of Earth's gravity field. On time scales ranging from months to decades, temporal variations of gravity are mainly due to redistribution of water mass in the surface fluid envelopes of the Earth. On land, GRACE provides measurements of vertically-integrated water storage or terrestrial water storage (TWS) (surface water, soil, groundwater and snowpack) in large river basins (Tapley et al., 2004; Wahr et al., 2004). The GRACE mission is managed by both the US National Aeronautics and Space Administration (NASA) and the German Aerospace Centre (DLR). Monthly gravity field solutions are computed at the University of Texas at Austin Center for Space Research (CSR), the German Research Centre for Geosciences Potsdam (GFZ), the Jet Propulsion Laboratory (JPL), the *Groupe de recherche de geodesie spatiale* (GRGS), and the Delft Institute of Earth Observation and Space Systems (DEOS) as well as at Delft University of Technology, among others. In this study, we use the most recent GRACE data release (RL04) from CSR, JPL and GFZ. This new data set (available at http://grace.jpl.nasa.gov/data/mass/) includes an implementation of the carefully calibrated combination of destriping and smoothing, with different Gaussian filters (Chambers, 2006). Compared to earlier products (contaminated by north-south strips due to orbital resonance induced by aliasing of high-frequency atmospheric perturbations by the GRACE coverage), the latest release is much less noisy because of the destripping procedure applied to the data and needs less spatial smoothing than earlier solutions. The GRACE products are corrected for post-glacial rebound (the solid Earth response to last deglaciation, also sensed by GRACE) using the Paulson et al. (Paulson et al., 2007) model.

Here we consider RL04 GRACE grids from CSR, JPL and GFZ (with 300 km half width Gaussian filter). The data are available as monthly 1×1 grids TWS over land, expressed in units of equivalent water height and cover the period from August 2002 through August 2008. Two months are missing: June 2003 and January 2004. In the following, we use the mean of the three GRACE products: CSR, JPL and GFZ.

3.3. Precipitation data

Monthly grids from August 2002 to August 2008 precipitation ($2.5^\circ \times 2.5^\circ$) used in this study are derived from Global Precipitation Climatology Project database (GPCP, http://lwf.ncdc.noaa.gov/oa/wmo/wdcamet-ncdc.html). GPCP quantify the distribution of precipitation over the global land surface (Adler et al., 2003). We use the Satellite-Gauge Combined Precipitation Data product Version 2 data, whose estimated uncertainties over land range between 10 to 30%. These grids merge infrared and microwave satellite-inferred precipitation with rain gauges data from more than 6000 ground stations.

3.4. WaterGAP Global Hydrological Model

The WaterGAP Global Hydrological Model (WGHM) provides estimates of the TWS globally, with a resolution of $0.5^\circ \times 0.5^\circ$ (Döll et al., 2003). This model has been used to analyse spatiotemporal variations of water storage components globally over large river basins (Güntner et al., 2007). It computes water storage in the snow pack, rooted soil zone, groundwater, on vegetation surfaces, and in surface water reservoirs (rivers, lakes and wetlands). Here, we use the latest WGHM simulations (Hunger and Döll, 2008) forced with precipitation from the Global Precipitation Climatology Centre (GPCC) and air temperature, radiation, and number of rain-days within each month from ECWMF operational forecasts. The conceptual model equations of WGHM are described in detail by Doll et al. (Döll et al., 2003) and Hunger and Doll (Hunger and Döll, 2008). WGHM is based on the best global data sets currently available, and is able to simulate the reduction of river discharge by human

water consumption. In order to obtain a reliable estimate of water availability, it is tuned against observed discharge at 1235 gauging stations, which represent 50% of the global land area and 70% of the actively discharging area. In Africa, most basins north of the equator do not perform well, while the interannual variability of the Central African Congo and the semi-arid to arid Southern African basins of the Zambezi and Orange is captured (Döll et al., 2003).

4. Water storage and climate variation

4.1. GRACE data and precipitation

At a regional scale, total water storage, TWS, measured by GRACE is related to precipitation P through the water budget equation:

$$\frac{d(TWS)}{dt} = P - E - R \quad (1)$$

where E is evapotranspiration and R is river runoff.

In view of the lack of direct information on E and R over the studied region, here we compare TWS and P.

We performed an Empirical Orthogonal Function (EOF) decomposition (Preisendorfer, 1988) of the GRACE data (average from CSR, JPL and GFZ) over the East Africa region (16°S-11°N; 28°E-40°E). EOF analysis decomposes the spatiotemporal data in orthogonal modes of decreasing variance, expressed by spatial patterns and associated variations in time (also called principal component [PC] time series). We removed a composite annual cycle at each data point and the results were smoothed with a 6-month window before the EOF decomposition, in order to emphasize the low frequency signal. Accordingly to North's rule of thumb (North et al., 1982), the first three modes for GRACE TWS were kept. These explain 71, 10 and 9% of the total variance. They are shown on Fig. 3. The first EOF spatial pattern reveals a positive TWS change with a maximum located west of Lake Victoria basin. The

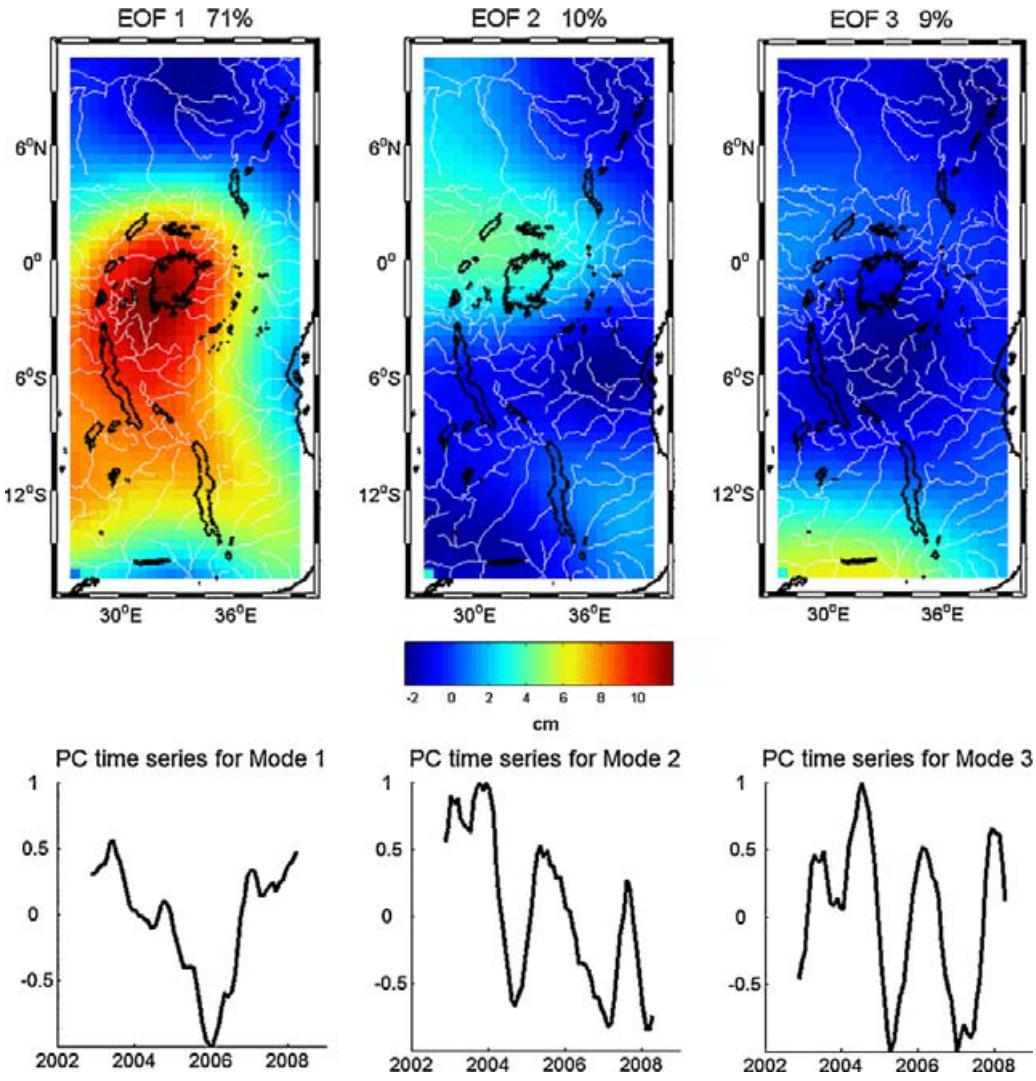

Fig. 3. EOF decomposition of GRACE TWS over East Africa for 2002–2008. The upper panel represents the geographical pattern and the lower panel represents the temporal variation of the GRACE TWS.

Fig. 3. Décomposition en EOF des données de TWS de GRACE sur l'Afrique de l'Est, entre 2002 et 2008. La figure du haut représente la variabilité spatiale et la figure du bas représente la variation temporelle des données de TWS de GRACE.

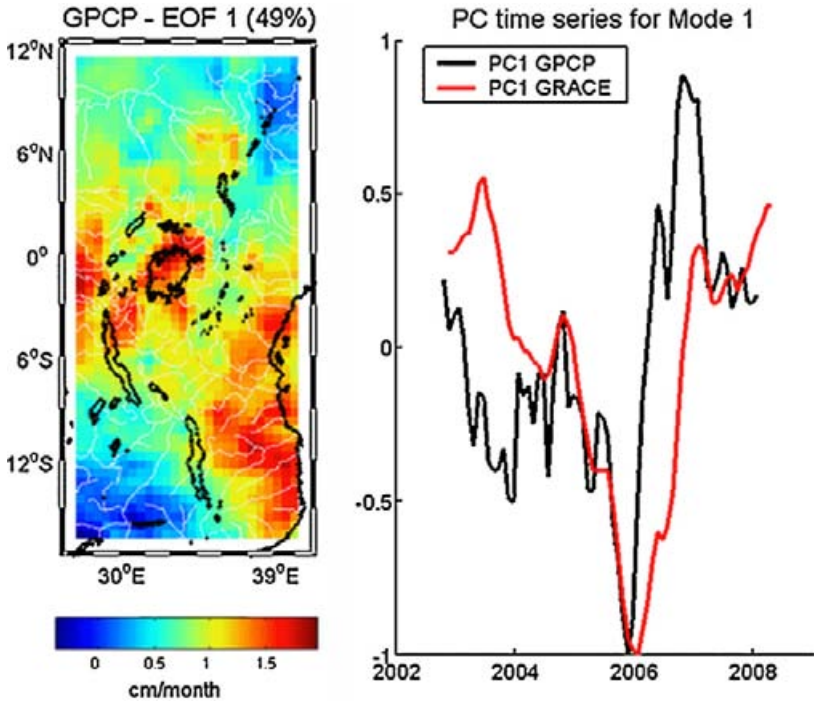

Fig. 4. Mode 1 of the EOF decomposition of precipitation from GPCP over East Africa (2002–2008). The percentage of variance explained by the first mode is 49%. The left panel represents the geographical pattern whereas the right panel represents the temporal variation of the precipitation (black) and the temporal variation of PC1 of GRACE data over East Africa (red) over the same period. The correlation coefficient between the two signals is 0.49, significant at more than 95%.

Fig. 4. Mode 1 de la décomposition en EOF des précipitations GPCP sur l'Afrique de l'Est, (2002–2008). Le pourcentage de variance expliquée par le premier mode est de 49 %. La figure de gauche représente le mode spatial alors que la figure de droite représente la variation temporelle des précipitations (en noir) et la variation temporelle des données GRACE PC1 sur l'Afrique de l'Est (en rouge) sur la même période. Le coefficient de corrélation entre les deux signaux est de 0,49, significatif à plus de 95 %.

corresponding principal component shows a significant negative trend from 2002 to 2006 with a minimum occurring at the end of 2005, then a strong increase until 2008. The mode 2 spatial pattern shows a positive TWS change signal over the north-west part of the area, which includes the Lake Victoria basin. A clear negative trend time evolution is revealed by the corresponding principal component, but also a quasi-periodic oscillation (2-year period). Mode 3 principal component time series shows a quasi-periodic oscillation of period 1.5 to 2 years.

We also performed an EOF decomposition of precipitation data (after removing the annual signal and smoothing with a 6-month window at each grid point). Fig. 4 shows the first leading mode (49% of the total variance) of the EOF decomposition of precipitation data over the studied region. The temporal curve shows a decrease between mid-2003 and the end of 2005, probably related to the 2005 severe drought reported in Equatorial East Africa (Hastenrath et al., 2007). Moreover, a sudden rise occurs in the temporal curve between the end of 2005 and the beginning of 2007. This event will be discussed below in some detail. As indicated by the spatial pattern map, the wettest region is the center of the area that includes the lakes. According to the water budget equation (see Eq. [1] above), we expect that precipitation and TWS show a common mode of variability. Fig. 4 displays the principal component time series of the first mode (PC1) of GRACE and GPCP. The two curves are very similar. The correlation coefficient between the two signals is equal to 0.49, significant at more than 95%. The spatial correlation between PC1 for GRACE and GPCP is −0.46. In a recent study, also based on altimetry and GRACE data over Lake Victoria, Swenson and Wahr (Swenson and Wahr, 2009) showed that increased precipitation over Lake Victoria significantly reduced the TWS deficit accumulated during the previous few years.

4.2. GRACE data and the Indian Ocean Dipole

Several analyses have discussed the relationship between sea surface temperature (SST) of the Indian Ocean and rainfall in East Africa (Birkett et al., 1999; Clark et al., 2003; Goddard and Graham, 1999; Hastenrath, 2007; Latif et al., 1999; Trenberth, 1984; Webster et al., 1999). It is therefore reasonable to assume that SST anomalies associated with Indian Ocean Dipole (IOD) have an influence on adjacent moisture surfaces (Reason, 2002), hence on TWS. The IOD is an ocean-atmosphere interaction, over the Indian Ocean, with alternate positive and negative SST anomalies (Reason, 2002). During the positive phase, there is flooding in East Africa, while the Indian summer monsoon remains above normal, and drought in Indonesia and in several regions of Australia. The IOD usually begins to develop during summer of the northern hemisphere, reaches its maximum during fall and ends in winter as a result of strong seasonal winds (Behera and

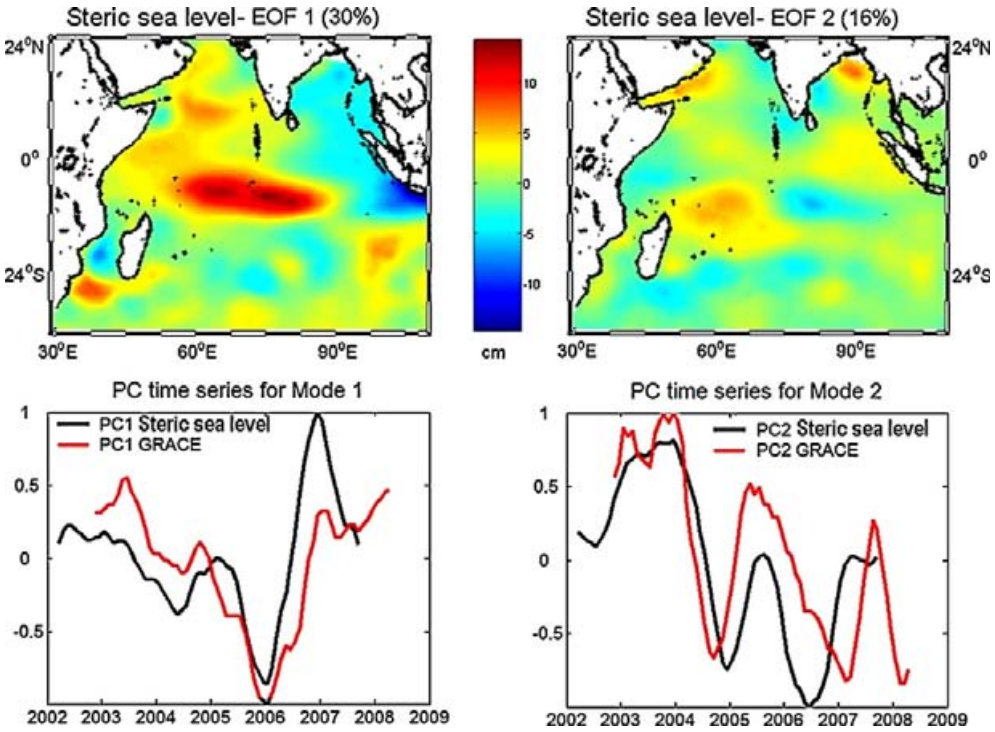

Fig. 5. Mode 1 (left) and mode 2 (right) of the EOF decomposition of steric sea level anomalies from Argo data over the Indian Ocean (2002–2008). The upper panel represents the geographical pattern, the percentage of variance explained by the first mode is 30% and second mode is 16%. Whereas the lower panel represents the temporal variation of the steric sea level (black) and the temporal variation of PC of GRACE TWS over East Africa (red). The correlation coefficient between the PC1 steric sea level and PC1 GRACE TWS is 0.65 and equal to 0.72 between the PC2 steric sea level and PC2 GRACE TWS, both are significant at more than 95%.

Fig. 5. Mode 1 (à gauche) et mode 2 (à droite) de la décomposition en EOF du niveau de la mer d'origine stérique fourni par les données Argo sur l'océan Indien, entre 2002 et 2008. Le panneau supérieur de la figure représente le mode spatial, le pourcentage de variance expliquée par le premier mode est de 30 % et le second mode est de 16 %. Le panneau inférieur représente la variation temporelle du niveau de la mer d'origine stérique PC1/PC2 (noir) et la variation temporelle des données TWS de GRACE PC1/PC2 de l'Afrique de l'Est (en rouge) sur la même période. Les coefficients de corrélation entre le PC1/PC2 du TWS de GRACE et le PC1/PC2 du niveau de la mer d'origine stérique sont de 0,65 et 0,72, significatifs à plus de 95 %.

Yamagata, 2001; Black et al., 2003; Hastenrath, 2007). Horii et al. (Horii et al., 2008) documented the precondition and evolution of the 2006 IOD. The subsurface negative temperature anomalies in the eastern part of the Indian Ocean (1.5°S, 90°E) started in May 2006, about 3 months earlier than the development of surface signatures. The subsurface negative temperature anomalies in the eastern part of the Indian Ocean were associated with unusual westward surface currents and an anomalous easterly wind event in May. These anomalous conditions at the thermocline depth ended between February and March 2007, a few months later than the disappearance of the surface IOD signals. We investigated the steric sea level in the Indian Ocean using temperature data from the Argo profiling floats (Roemmich and Owens, 2000). Steric sea level anomalies have been computed by Guinehut et al. (Guinehut et al., 2009) using ocean temperature and salinity anomalies from the surface down to 900 m depth. We performed an EOF decomposition of the steric sea level grids over the Indian Ocean for the 2002–2007 time span. We removed the annual signal and applied a 6-month smoothing filter as for GRACE and precipitation data. Fig. 5 shows the first leading mode (30% of the total variance) of the steric sea level EOF decomposition. The IOD is clearly evidenced by the geographical pattern associated with the first EOF, confirming observations of Horii et al. (Horii et al., 2008). We observe a decrease of the steric sea level from 2002 to 2006 with a minimum in May 2004, then a sudden increase from late 2005 to 2006, as observed in East Africa precipitation pattern. On Fig. 5, the Argo PC1 (temporal curve) is superimposed on the GRACE TWS PC1 computed over the East African lake region. We note a good agreement between the two curves. The corresponding correlation coefficient is 0.64. Moreover, we note that the correlation coefficient between Argo PC1 and GPCP PC1 is 0.80 (not shown on the figure), confirming the strong link between West Indian Ocean temperature (in fact here, ocean heat content and thermal expansion) and precipitation over East Africa. Fig. 5 shows the second leading mode (16% of the total variance) of the steric sea level EOF decomposition. We observe a quasi-periodic oscillation (2-year period) in the temporal curve. We superimposed the GRACE TWS PC2. As for PC1, a good correlation coefficient (amounting 0.75) is noticed between the two curves. Webster et al. (Webster et al., 1999) reported a 2-year periodicity in SST gradients along the equator, linking two anomalous states: warm in the west and cool in the east, and cool in the west and warm in the east. The cool SST anomalies lead to less evaporation and less rain, while warm SST anomalies lead to enhanced evaporation and

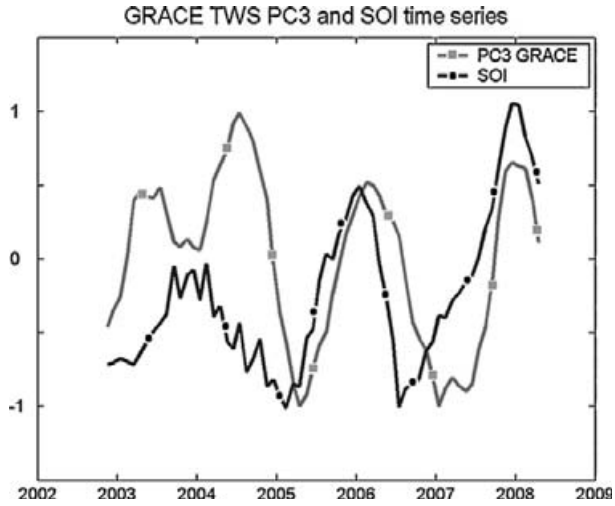

Fig. 6. Mode 3 of the EOF decomposition of GRACE TWS (square) over East Africa and scaled SOI (circle), between 2002 and 2008. The correlation coefficient between the two signals is 0.55, significant at more than 95%.

Fig. 6. Mode 3 de la décomposition en EOF des données TWS de GRACE (carré) sur l'Afrique de l'Est et le SOI redimensionné (cercle), entre 2002 et 2008. Le coefficient de corrélation entre les deux signaux est de 0,55, significatif à plus de 95 %.

more rain. SST anomalies during the IOD events are strongly coupled to surface wind anomalies in the central equatorial Indian Ocean (Saji et al., 1999; Saji and Yamagata, 2003a). In this study, we show that the 2-year periodicity also affects West Indian Ocean heat content and East Africa total water storage.

4.3. GRACE data and ENSO

Several studies have suggested a link between El Niño-Southern Oscillation (ENSO), Indian Ocean temperature and East African rainfall (Birkett et al., 1999; Black et al., 2003; Clark et al., 2003; Goddard and Graham, 1999; Latif et al., 1999; Mercier et al., 2002; Ummenhofer et al., 2009). Recent studies have shown that a significant proportion of the IOD events occurred independently of ENSO and a significant proportion of ENSO events were independent of IOD (Ashok et al., 2003; Behera et al., 2006; Hong et al., 2008; Lau and Nath, 2004; Saji and Yamagata, 2003a; Saji and Yamagata, 2003b). The most recent occurrence of El Niño started in September 2006 and lasted until early 2007 and that of La Niña in 2007/2008, while three IOD events have been reported recently (in 2006, 2007 and 2008; (Cai et al., 2009; Horii et al., 2008; Saji et al., 1999; Vinayachandran et al., 2007)). Consequently, we expect that even a weak ENSO can be correlated with TWS variations over East Africa. To compare GRACE TWS over East Africa with ENSO, we used the Southern Oscillation Index (SOI) defined as the difference in atmospheric pressure anomalies between Tahiti and Darwin (Trenberth, 1984), smoothed with the same 6-month window as for GRACE data. In Fig. 6, are displayed the principal component time series of the third mode (PC3) of GRACE TWS and scaled SOI. The correlation coefficient between the two is equal to 0.55, with variable lag in the range 0 to 6 months. For the 2005–2008 period, the correlation coefficient between the two series is equal to 0.80. This supports the hypothesis that the third EOF mode of TWS (explaining only 9% of the total variance) is related to the ENSO cycle.

Comparison between total water storage from GRACE and surface water volume change from altimetry; inference on soil moisture and groundwater and comparison with outputs of the WGHM hydrological model.

We have combined GRACE TWS with satellite altimetry-derived lake water volume, to estimate soil moisture and groundwater variations over each lake drainage basin. Rodell and Famiglietti (Rodell and Famiglietti, 2001) suggested that the GRACE resolution was insufficient to study basins smaller than 200,000 km^2. For Lake Victoria and Lake Tanganyika, the drainage basin areas are 261,800 and 252,600 km^2 (Table 1). However, Lake Malawi and Lake Turkana basins are considerably smaller, with areas of 156,000 and 137,610 km^2, respectively (Table 1). Nevertheless, latest GRACE data have improved precision and resolution and allow studying smaller basins.

We have averaged GRACE-based water storage over the four lake drainage basins. Their location is shown in Fig. 1 and characteristics summarized in Table 1. To estimate individual lake drainage basin contribution, we simply spatially average, for each month, GRACE equivalent water height over the area included inside the basin, then multiply it by the basin area to estimate water storage (in km^3). A potentially important source of error affecting the basin-averaged water storage time series is the leakage from surrounding basins. Because of the GRACE resolution, water mass signals outside the domain limited by the mask may leak into the considered region, thus polluting the estimated water storage. We have estimated this error as in Ramillien et al. (Ramillien et al., 2008). We consider global monthly grids of total water storage – canopy, surface, soil and underground water plus snow – outputs from WGHM over the time span of analysis. Conceptually, WGHM provides water storage information that is directly comparable to GRACE TWS (whatever the precision of the model). For each month, the global model grid is modified by setting zero values over the considered river basin, keeping the model values outside the basin. This modified data set is then expanded in spherical harmonics up to degree 60 (equivalent to the GRACE resolution). The leakage signal is then estimated by convoluting this spherical harmonic expansion with that of the geographical mask representing the lake drainage basin (see Ramillien et al. (Ramillien et al., 2008), for more details). As noted previously, the leakage signal is mainly seasonal and on the order of 3% of the "model" annual signal on the four lake drainage basins. In terms of interannual variability, the error is negligible. In the following, we do not account for this effect any further.

GRACE data cannot be directly compared to the altimetry-based lake water volume time series, because the GRACE data processing (in particular the smoothing) reduces the TWS signal compared to the "true" signal (Swenson et and Wahr, 2002; Chambers, 2006; Chen et al., 2007). To determine what scaling apply to GRACE data, we

do the flowing: we consider $0.5^\circ \times 0.5^\circ$ outputs from WGHM over the studied region. For each lake drainage basin, we apply the same spatial smoothing to WGHM grids as for GRACE data (Gaussian filter of half-weight radius 300 km) to TWS of WGHM and compute the reduction, time variable, factor compared to unsmoothed data. We focus on the interannual time scale and to estimate the scaling factor, we remove the annual signal. The mean scaling factor obtained for lakes Turkana, Victoria and Tanganyika is 1.1 and for Lake Malawi is 1.2.

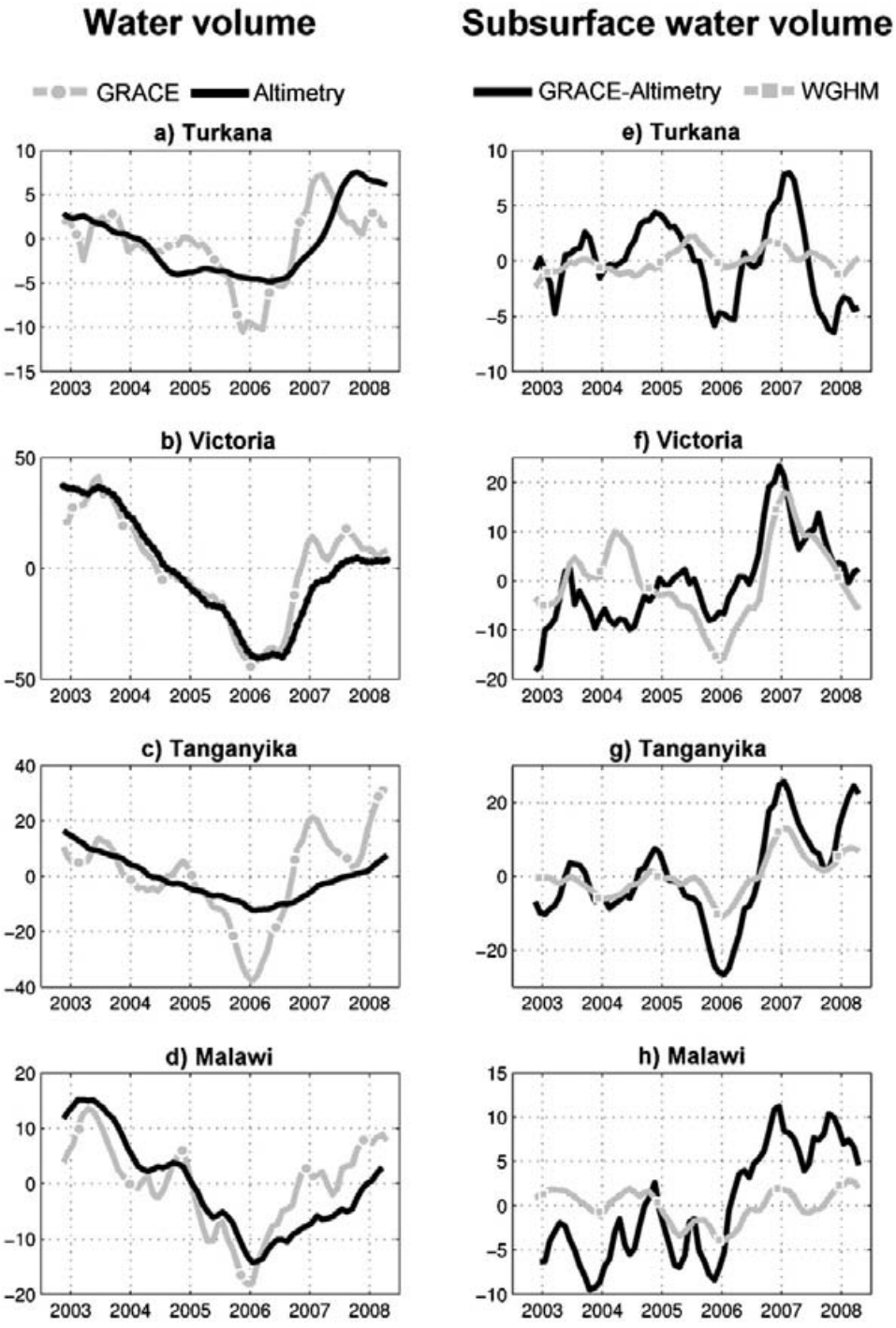

Fig. 7. Left panel: changes in volume (km^3) of the GRACE TWS in the basin (square) and surface water of the lake from altimetry satellite (triangle). Right panel: changes in volume (km^3) of the soil moisture and groundwater: GRACE-Altimetry (diamond) and WGHM outputs (circle). The annual signal is removed and data are smoothed with a 6-month window.

Fig. 7. Figures de gauche : évolution du volume pour chaque bassin (km^3) du TWS de GRACE (carré) et des eaux de surface des lacs à partir de l'altimétrie (triangle). Figures de droite : évolution du volume (km^3) de l'humidité du sol et des eaux souterraines : GRACE-Altimétrie (losange) et WGHM (cercle). Le signal saisonnier a été filtré et les données ont été lissées avec une moyenne glissante de six mois.

Fig. 7 (left panel) shows, for each lake, the lake water volume (from altimetry) superimposed to GRACE TWS (scaling factor applied). In the right panel on Fig. 7, we compare the subsurface water (sum of soil moisture and groundwater) volume change (rescaled GRACE TWS minus altimetry-derived lake volume) with the WGHM outputs (after application of the same Gaussian filter of half-weight radius 300 km). Only soil moisture and groundwater components of the model are considered, because in this semi-arid region: snow, canopy and the surface storage in rivers and reservoirs are insignificant. For Lake Turkana, the total volume of water in the basin is governed by the surface water of the lake (Fig 7a). The correlation coefficient between surface water volume and TWS is 0.60. The subsurface water component has two peaks, which occurred in mid 2005 and late 2006 (Fig. 7e). For Lake Victoria, the volume of water in the basin is also mainly governed by the surface water of the lake (Fig. 7b). The correlation coefficient between surface water volume and TWS is 0.93. TWS and surface water volume show a sharp increase from 2006 to 2007. We note (Fig. 7f) that the subsurface water component increases between 2006 to early 2007, where it reaches its maximum. Lake Tanganyika surface water volume represents a small fraction of TWS variations (Fig. 7c). The correlation coefficient between surface water and TWS is 0.62. A sharp increase in 2006 is observed for Lake Tanganyika. The corresponding subsurface water component (Fig. 7g) shows oscillations, with a minimum in early 2006 and a maximum in early 2007. Therefore, the water volume of Lake Tanganyika drainage basin is mainly governed by the groundwater. For Lake Malawi, surface water volume and TWS (Fig. 7d) are well correlated (0.72). The volume of water in the basin is governed by the surface water of the lake until 2006. The variability of the subsurface water component (Fig. 7h) shows a positive linear trend of 3.7 km^3/year. Abrupt changes in TWS and surface water volumes for all lakes are observed between 2006 and 2007. These are directly correlated with the strong positive and negative episodes of IOD in 2006–2007. In terms of interannual fluctuations of subsurface water, we note a very good correlation coefficient between observations and model results. Especially for Lake Tanganyika (correlation coefficient of 0.93) but the amplitudes appear to differ by about a factor of two, and for Lake Victoria with a correlation coefficient of 0.60 and similar amplitudes.

5. Conclusion

We have investigated TWS and surface water storage changes over the East African Lake region during 2002–2008 and their link with precipitation and IOD. We find that precipitation and TWS from GRACE show a common mode of variability at interannual time scale, with a minimum late 2005 and a sharp rise in 2006–2007. We show that this event is due to forcing by the 2006 IOD on East African rainfall. We also show that GRACE-inferred water storage is related to the El Niño-Southern Oscillation cycle. This study also shows that combining satellite altimetry-based water volumes with TWS from GRACE provides new information on soil moisture and groundwater. This offers interesting perspective, in particular for detecting subsurface water storage changes associated with climate variability and human activities. TWS from GRACE is very helpful as it provides an integrated information on water storage change, not available from in situ measurements (in most regions information on soil moisture and groundwater does not exist and gauging networks on rivers and lakes are drastically decreasing since the early 1980s (Kundzewicz et al., 2004)). It is a valuable tool for hydrological studies and is especially important for separating hydrological components. The combination with other data sources is essential to maximize the benefit of GRACE data.

Acknowledgments

This work is supported by CYMENT project of the RTRA "*Sciences et technologies pour l'aéronautique et l'espace* (STAE)". The altimeter products were produced by SSALTO/DUACS and distributed by AVISO with support from CNES. We thank S. Guinehut from CLS for providing steric sea level grids from Argo. Many thanks go to Professor Pierre Ribstein and the two anonymous reviewers for their helpful comments and suggestions. GRACE data were processed by D. P. Chambers, supported by the NASA Earth Science REASoN GRACE Project, and are available at http://grace.jpl.nasa.gov.

References

Adler, R.F., Huffman, G.J., Chang, A., Ferraro, R., Xie, P.P., Janowiak, J., et al., 2003. The version-2 global precipitation climatology project (GPCP) monthly precipitation analysis (1979–present), J. Hydrometeorol. 4, pp. 1147–1167.

Alsdorf, D.E., Rodríguez, E., Lettenmaier, D.P., 2007. Measuring surface water from space. Rev. Geophys. 45 .

Ashok, K., Guan, Z., Yamagata, T., 2003. A look at the relationship between the ENSO and the Indian Ocean dipole. J. Meteorol. Soc. Japan 81, 41–56.

Awange, J.L., 2006. Lake Victoria: ecology, resources, environment, Springer Berlin Heidelberg.

Awange, J.L., Sharifi, M.A., Ogonda, G., Wickert, J., Grafarend, E.W., Omulo, M.A., 2008. The falling Lake Victoria water level: GRACE, TRIMM and CHAMP satellite analysis of the lake basin. Water Resour. Manage. 22, 775–796.

Behera, S.K., Luo, J.J., Masson, S., Rao, S.A., Sakuma, H., Yamagata, T., 2006. A CGCM study on the interaction between IOD and ENSO. J. Clim. 19, 1688–1705.

Behera, S.K., Yamagata, T., 2001. Subtropical SST dipole events in the southern Indian Ocean. Geophys. Res. Lett. 28 .

Birkett, C., 1995. The contribution of TOPEX/POSEIDON to the global monitoring of climatically sensitive lakes, Oceans. J. Geophys. Res. 100 .

Birkett, C., 1999. Contribution of the TOPEX NASA radar altimeter to the global monitoring of large rivers and wetlands. Water Resour. Res. 34 .

Birkett, C., Murtugudde, R., Allan, T., 1999. Indian Ocean climate event brings floods to East Africa's lakes and the Sudd Marsh. Geophys. Res. Lett. 26 .

Black, E., Slingo, J., Sperber, K.R., 2003. An observational study of the relationship between excessively strong short rains in coastal East Africa and Indian Ocean SST. Mon. Weather Rev. 131, 74–94.

Bootsma, H.A., Hecky, R.E., 1993. Conservation of the African Great Lakes: A Limnological Perspective. Conserv. Biol. 7, 644–656.

Cai, W., Pan, A., Roemmich, D., Cowan, T., Guo, X., 2009. Argo profiles a rare occurrence of three consecutive positive Indian Ocean Dipole events, 2006–2008. Geophys. Res. Lett. 36, pL08701.

Calmant et, S., Seyler, F., 2006. Continental surface waters from satellite altimetry. C. R. Geoscience 338, 1113–1122.

Calmant, S., Seyler, F., Cretaux, J., 2008. Monitoring continental surface waters by Satellite Altimetry. Surv. Geophys. 29, 247–269.

Chambers, D.P., 2006. Evaluation of new GRACE time-variable gravity data over the ocean. Geophys. Res. Lett. 33, pL17603.
Chen, J.L., Wilson, C.R., Famiglietti, J.S., Rodell, M., 2007. Attenuation effect on seasonal basin-scale water storage changes from GRACE time-variable gravity. J. Geodesy 81, 237–245.
Clark, C.O., Webster, P.J., Cole, J.E., 2003. Interdecadal variability of the relationship between the Indian Ocean zonal mode and East African coastal rainfall anomalies. J. Clim. 16, 548–554.
Conway, D., Allison, E., Felstead, R., Goulden, M., 2005. Rainfall variability in East Africa: implications for natural resources management and livelihoods, Philosophical transactions: Mathematical. Phys. Eng. Sci. 49–54.
Crétaux, J., Birkett, C., 2006. Lake studies from satellite radar altimetry. C. R. Geosci. 338, 1098–1112.
Döll, P., Kaspar, F., Lehner, B., 2003. A global hydrological model for deriving water availability indicators: model tuning and validation. J. Hydrology 270, 105–134.
Ferguson, A.J.D., Harbott B.J., 1982. *Geographical, physical and chemical aspects of Lake Turkana*. In: Hopson, A.J. (Ed.). Lake Turkana: A report of the findings of the Lake Turkana Project 1972–1975. London, UK: Overseas Development Administration, pp. 1–107.
Frappart, F., Minh, K.D., L'Hermitte, J., Cazenave, A., Ramillien, G., Le Toan, T., Mognard-Campbell, N., 2006. Water volume change in the lower Mekong from satellite altimetry and imagery data. Geophys. J. Inter. 167, 570–584.
Frappart, F., Papa, F., Famiglietti, J.S., Prigent, C., Rossow, W.B., Seyler, F., 2008. Interannual variations of river water storage from a multiple satellite approach: A case study for the Rio Negro River basin, Atmospheres. J. Geophys. Res. D. 113 .
Fu, L.L., Cazenave, A., 2001. Satellite Altimetry and Earth Sciences. A handbook of Techniques and Applications, Academic Press, San Diego, CA, USA, 463 pp.
Goddard, L., Graham, N.E., 1999. Importance of the Indian Ocean for simulating rainfall anomalies over eastern and southern Africa, Atmospheres. J. Geophys. Res. 104 .
Guinehut, S., Coatanoan, C., Dhomps, A.L., Le Traon, P.Y., Larnicol, G., 2009. On the use of Satellite Altimeter Data in Argo quality control. J. Atmos. Oceanic Technol. 26, 395–402.
Güntner, A., Stuck, J., Werth, S., Döll, P., Verzano, K., Merz, B., 2007. A global analysis of temporal and spatial variations in continental water storage. Water Resour. Res. vol.43 .
Hastenrath, S., 2007. Circulation mechanisms of climate anomalies in East Africa and the equatorial Indian Ocean. Dynam. Atmos. Oceans 43, 25–35.
Hastenrath, S., Polzin, D., Mutai, C., 2007. Diagnosing the 2005 Drought in Equatorial East Africa. J. Clim. 20, 4628–4637.
Hong, C.C., Lu, M.M., Kanamitsu, M., 2008. Temporal and spatial characteristics of positive and negative Indian Ocean dipole with and without ENSO, Atmospheres. J. Geophys. Res. 113, pD08107.
Horii, T., Hase, H., Ueki, I., Masumoto, Y., 2008. Oceanic precondition and evolution of the 2006 Indian Ocean dipole. Geophys. Res. Lett. 35, pL03607.
Hunger, M., Döll, P., 2008. Value of river discharge data for global-scale hydrological modeling. Hydrol. Earth System Sc. 12, 841–861.
Jury, M.R., Gwazantini, M.E., 2002. Climate variability in Malawi, part 2: sensitivity and prediction of lake levels,. Inter. J. Climatol. 22, 1303–1312.
Kundzewicz, Z.W., Graczyk, D., Maurer, T., Przymusinska, I., Radziejewski, M., Svensson, C., Szwed, M., 2004. Detection of change in world-wide hydrological time series of maximum annual flow. GRDC Report 32, p36.
Latif, M., Dommenget, D., Dima, M., Grötzner, A., 1999. The role of Indian Ocean sea surface temperature in forcing east African rainfall anomalies during December–January 1997/98. J. Clim. 12, 3497–3504.
Lau, N.C., Nath, M.J., 2004. Coupled GCM simulation of atmosphere–ocean variability associated with zonally asymmetric SST changes in the tropical Indian Ocean. J. Clim. 17, 245–265.
Mercier, F., Cazenave, A., Maheu, C., 2002. Interannual lake level fluctuations (1993–1999) in Africa from Topex/Poseidon: connections with ocean-atmosphere interactions over the Indian Ocean. Global and Planetary Change vol.32, 141–163.
Mutai, C.C., Ward, M.N., Colman, A.W., 1998. Towards the prediction of the East Africa short rains based on sea-surface temperature-atmosphere coupling. Inter. J. Climatol. 18, 975–997.
North, G.R., Bell, T.L., Cahalan, R.F., Moeng, F.J., 1982. Sampling errors in the estimation of empirical orthogonal functions. Mon. Weather Rev. 110, 699–706.
Oki, T., Sud, Y., 1998. Design of the global river channel network for total runoff integrating pathways (TRIP). Earth Interactions 2 .
Papa, F., Güntner, A., Frappart, F., Prigent, C., Rossow, W.B., 2008. Variations of surface water extent and water storage in large river basins: A comparison of different global data sources. Geophys. Res. Lett. 35, pL11401.
Paulson, A., Zhong, S., Wahr, J., 2007. Inference of mantle viscosity from GRACE and relative sea level data. Geophys. J. Intern. 171, 497–508.
Ponchaut, F., Cazenave A., 1998. Continental lake level variations from Topex/Poseidon (1993–1996), C. R. Acad. Sci. Paris, Ser IIa, 326, pp. 13–20.
Preisendorfer, R.W., 1988. Principal component analysis in meteorology and oceanography. Elsevier science, New York (425 pp).
Ramillien, G., Bouhours, S., Lombard, A., Cazenave, A., Flechtner, F., Schmidt, R., 2008. Land water contributions from GRACE to sea level rise over 2002–2006. Global and Planetary Change 60, 381–392.
Reason, C.J.C., 2002. Sensitivity of the southern African circulation to dipole sea-surface temperature patterns in the South Indian Ocean. Inter. J. Climatol. 22 .
Reynolds, C. Low water levels observed on Lake Victoria. Report published on the Web site for the Production Estimates and Crop Assessment Division of the USDA Foreign Agricultural Service, September 26, 2005. <http://www.fas.usda.gov/pecad/highlights/2005/09/uganda_26sep2005/>.
Rodell, M., Famiglietti, J.S., 2001. An analysis of terrestrial water storage variations in illinois with implications for the gravity recovery and climate experiment (GRACE). Water Resourc. Res. 37, 1327–1340.
Roemmich, D., Owens, W., 2000. *The Argo project: Global ocean observations for understanding and prediction of climate variability*, Oceanography–Washington DC–oceanography society–, vol. 13, pp. 45–50.
Saji, N.H., Goswami, B.N., Vinayachandran, P.N., Yamagata, T., 1999. A dipole mode in the tropical Indian Ocean. Nature 401, 360–363.
Saji, N.H., Yamagata, T., 2003a. Possible impacts of Indian Ocean dipole mode events on global climate. Clim. Res. 25, 151–169.
Saji, N.H., Yamagata, T., 2003b. Structure of SST and surface wind variability during Indian Ocean dipole mode events: COADS observations. J. Clim. 16, 2735–2751.
Spigel, R.H., Coulter G.W., 1996. Comparison of hydrology and physical limnology of the East African Great Lakes: Tanganyika, Malawi, Victoria, Kivu and Turkana (with references to some North American Great Lakes). In: Johnson, T.C., Odada, E.O. (Eds.). The limnology, climatology, and paleoclimatology of the East African lakes. Amsterdam, The Netherlands: Gordon and Breach Publishers, pp. 103–135.
Swenson et, S., Wahr, J., 2002. Methods for inferring regional surface-mass anomalies from Gravity Recovery and Climate Experiment (GRACE) measurements of time-variable gravity, Solid Earth. J. Geophys. Res. 107, p2193.
Swenson, S., Wahr, J., 2009. Monitoring the water balance of Lake Victoria, East Africa, from space. J. Hydrol. 370, 163–176.
Tapley, B.D., Bettadpur, S., Ries, J.C., Thompson, P.F., Watkins, M.M., 2004. GRACE measurements of mass variability in the Earth system. Science 305, 503–505.
Taylor, R., Tindimugaya, C., Aureli, A. Can groundwater meet Africa's demand for water as climates change? Eos. Transactions American Geophysical Union, 2008, 89.
Thieme, M.L., Abell, R., Stiassny, M.L.J., Skelton, P., Lehner, B., Dinerstein, E., Teugels, G.G., Burgess, N., Toham, A.K., Olson, D., 2005. Freshwater ecoregions of Africa and Madagascar: a conservation assessment. Island Press, Washington.
Trenberth, K.E., 1984. Signal versus noise in the Southern Oscillation. Monthly Weather Rev. 112, 326–332.
Ummenhofer, C.C., Gupta, A.S., England, M.H., Reason, C.J.C., 2009. Contributions of Indian Ocean sea surface temperatures to enhanced East African rainfall. J. Clim. 22, 993–1013.
Vinayachandran, P.N., Kurian, J., Neema, C.P., 2007. Indian Ocean response to anomalous conditions in 2006. Geophys. Res. Lett. 34, pL15602.
Wahr, J., Swenson, S., Zlotnicki, V., Velicogna, I., 2004. Time-variable gravity from GRACE: First results. Geophys. Res. Lett. 31, pL11501.
Webster, P.J., Moore, A.M., Loschnigg, J.P., Leben, R.R., 1999. Coupled ocean–atmosphere dynamics in the Indian Ocean during 1997–1998. Nature 401, 356–360.
World Water Assessment Programme (WWAP), 2006. Water, a Shared Responsibility: The United Nations World Water Development Report 2. United Nations Educational, Scientific and Cultural Organization (UNESCO), Paris, France, UN-Water. ISBN/ISSN: 9231040065.
Yin et, X., Nicholson, S.E., 1998. The water balance of Lake Victoria. Hydrological Sci. J. 43, 789–811.
Zakharova, E.A., Kouraev, A.V., Cazenave, A., Seyler, F., 2006. Amazon River discharge estimated from TOPEX/Poseidon altimetry. C. R. Geosci. 338, 188–196.

Global warming and sea level rise

Abstract

Tide gauge records suggest a rise in sea level rise of 1.8 mm/yr over the 20st century. More recently, satellite altimetry data reveal a global mean sea level rise of 3.3 mm/yr over 1993-2010. This rise is attributed to Earth's global warming observed since several decades. In this thesis, we analyze observed global mean sea level and its causes over the entire altimetry era (since 1993). Over the recent years (2002-2009), we estimate the effects of ocean thermal expansion and salinity (called steric effects) on sea level, as well as ocean mass change due to land ice and land waters, using Argo and GRACE space gravimetry data. We discuss the regional variability by comparing several datasets for thermal expansion and ocean mass signal. In another study, we investigate terrestrial land water storage variability of the 33 largest river basins worldwide, using GRACE space gravimetry data. We analyze this contribution to the observed global mean sea level inferred by satellite altimetry. In an extension of this study, we analyze the interannual variability of terrestrial land water storage and its impact on sea level variations over the altimetry era and tide gauge era. Finally, we conclude this chapter by studying the sea level budget over the entire altimetry era and the recent years. In a second part, we study the regional patterns in sea level trends. First, we discuss causes of regional variability, mainly non-uniform ocean warming. We then interpret the residual signal (i.e., observed sea level corrected for thermal effects) for the altimetry era. Thereafter, we analyze regional patterns of past sea level over the last decades (1950-2003). The purpose of this study is to provide 2-D regional past sea level reconstruction and obtain some insight on spatial trend patterns and their dominant modes of variability. The ultimate goal is to constrain coupled climate models used by the IPCC (Intergovernment Panel on Climate Change) to predict sea level rise over the 21st century. Moreover, this study highlights a long term signal detected in the reconstructed sea level. This signal is also observed in in situ data and in coupled climate models.

Keywords : Sea level rise, satellite altimetry, Argo, GRACE, sea level budget, land water contribution, reconstructed sea level.

Hausse du niveau de la mer et impact du changement climatique global

Auteur : William Llovel
Directrice de thèse : Anny Cazenave
Discipline : Océanographie Spatiale
Lieu et date de soutenance : Observatoire Midi-Pyrénées le 6 Décembre 2010
Laboratoire : LEGOS, UMR 5566 CNRS/CNES/IRD/UPS, OMP
14 avenue Edouard Belin, 31400 Toulouse, France

Au cours du 20ème siècle, les enregistrements marégraphiques suggèrent une hausse du niveau de la mer de 1.8 mm/an. Plus récemment, les observations spatiales indiquent une hausse de 3.3 mm/an sur la période 1993-2009. Cette augmentation au cours du temps est attribuée au réchauffement global de la planète enregistré depuis plusieurs années maintenant. Durant cette thèse, nous analysons les observations et les causes de la hausse moyenne globale du niveau de la mer. Nous estimons les variations stériques du niveau de la mer grâce aux données du projet international Argo et, les variations de masse des océans liés aux apports d'eau des continents á l'aide des mesures de la mission GRACE. Une autre étude se concentre sur la variabilité du stock d'eaux continentales des plus grands bassins hydrologiques de la planète, à l'aide des données GRACE, et l'impact de cette composante à la hausse du niveau de la mer. Puis, nous analysons l'impact de la variabilité interannuelle du stock d'eaux continentales aux variations du niveau de la mer sur diverses périodes. Enfin, nous étudions le bilan des contributions climatiques à la hausse observée du niveau de la mer sur la période altimétrique totale et pour les années récentes. Dans une deuxième partie, nous étudions les variations régionales du niveau de la mer. Nous établissons dans un premier temps, les causes de la variabilité régionale du niveau de la mer et nous interprétons le signal résiduel issu de la différence entre le niveau de la mer observé et l'expansion thermique des océans. Nous étudions ensuite les variations passées des structures régionales du niveau de la mer sur les dernières décennies (1950-2003). Le but est de reconstruire les variations passées du niveau de la mer en 2-D et ainsi d'avoir une connaissance plus approfondie de l'évolution régionale du niveau moyen des mers. Ce travail a pour objectif ultime de contraindre les modèles climatiques couplés utilisés par l'IPCC (Intergovernmental Panel on Climate Change) pour prédire l'évolution future du niveau de la mer au cours du 21ème siècle. Cette analyse nous permet de détecter un signal basse fréquence dans la variabilité régionale du niveau de la mer que nous observons non seulement dans les données *in situ* mais aussi dans les modèles climatiques couplés.

Mots clés : Niveau de la mer, altimétrie spatiale, Argo, GRACE, bilan du niveau de la mer, stock des eaux continentales, niveau de la mer reconstruit.